An Investigation of the Geothermal Potential of the Upper Devonian Sandstones Beneath Eastern Glasgow

Sean McFie Watson,

MEng

Submitted in fulfilment of the requirements of the

Degree of Doctor of Philosophy

James Watt School of Engineering

College of Science and Engineering

University of Glasgow

Abstract

The urban development of the city of Glasgow is a consequence of its economic development, in part fuelled by local coalfields which exploited rocks in the same sedimentary basin within which geothermal resources in flooded abandoned mine workings, and deeper hot sedimentary aquifers (HSA), are present. This creates an opportunity to provide geothermal heating to areas of dense urban population with high heat demand. The depth of the target HSA geothermal resource, in Upper Devonian aged sandstones of the Stratheden Group, beneath eastern Glasgow was determined by gravity surveying and structural geological modelling. The estimated depth of the geothermal resource ranged from c.1500-2000 m, in the eastward deepening sedimentary basin. To reliably estimate the temperature of the geothermal resource, rigorous corrections to account for the effects of palaeoclimate and topography on heat flow were applied to boreholes in the Greater Glasgow area. The mean regional corrected heat flow was calculated as 75.7 mW m^{-2}, an increase of 13.8 mW m^{-2} from the uncorrected value of 61.9 mW m^{-2}, emphasising the extent to which heat flow was previously underestimated. Extrapolation of the geothermal gradient, calculated from the mean regional corrected heat flow, results in aquifer temperatures of c. 64-79 °C at depths of c.1500-2000 m beneath eastern Glasgow. The geothermal resource may, therefore, be capable of supporting a wide variety of direct heat use applications if sufficient matrix permeability or fracture networks are present. However, diagenetic effects such as quartz and carbonate cementation were found to restrict the porosity in Upper Devonian sandstones in a borehole and outcrop analogue study. These effects may likewise reduce porosity and intergranular permeability in the target aquifer, although this crucial aspect cannot be fully understood without deep exploratory drilling. To quantify the magnitude of the deep geothermal resource, the indicative thermal power outputs of geothermal doublet wells located in Glasgow's East End were calculated for the first time, with outputs ranging from 1.3-2.1 MW dependent upon the aquifer depth. This, however, is predicated upon an aquifer permeability of c. 40 mD, which if reduced to 10 mD or less due to the effects of diagenesis, significantly reduces the thermal power outputs to 230-390 kW. The lack of assured project-success, given uncertainties related to the aquifer properties at depth, coupled with high capital costs of drilling, pose barriers to the development of deep geothermal energy in Glasgow. Further investigation of the economic viability of geothermal exploration, and alternative technological solutions is therefore required to mitigate the technical and economic risks. However, if sufficient matrix permeability or fracture networks are present at depth in the Upper Devonian sandstone sequence, then the potential contribution that geothermal energy could make to meeting local heat demand, reducing greenhouse gas emissions, and addressing the 'energy trilemma' in Glasgow is significant.

Contents

List of Tables

List of Figures

List of Accompanying Material

Please see the accompanying document "*References and Supplementary Material*".

Figures and Tables from the accompanying material which are referenced within the main body of the thesis are denoted by their relevent Appendix. For example, Table 4.A.1 is from Appendix 4.A, Figure 4.B.1 is from Appendix 4.B, and so on.

Contents

Acknowledgements

First, I would like to pay tribute to Professor Paul Younger and Dr Rob Westaway. Both Paul and Rob had an infectious enthusiasm for geoscience research, an inspiring commitment to conduct research for the benefit of society and the environment, and were incredibly generous with their time, being constantly available to provide the most thorough and meticulous of explanations and guidance. It was a privilege to have had the opportunity to be supervised by both during this PhD.

I am also extremely grateful for the supervision of Professor Fiona Bradley and Dr. Neil Burnside throughout this PhD. I would like to thank Fiona for reading this thesis and for offering such constructive feedback. Likewise, I would like to sincerely thank Neil for his encouragement, direction, and advice throughout this PhD, it is greatly appreciated. Their support has been invaluable in completing this work.

I have also benefitted immensely from working with Professor Gioia Falcone, Dr. Ali McCay, Dr. Cees Willems, Aislinn Williams, Helen Robinson, David Walls, and many others in the research group.

This PhD thesis has also benefitted significantly from guidance from experts in industry and the public sector. I would particularly like to thank Ciaran Higgins for taking time to share his expertise in energy master-planning and GIS software.

Sincere thanks are due for the technical support and assistance that I have received throughout the course of this PhD. I would like to thank Dr. Claire Wilson and Dr. Nicolas Beaudoin for conducting the XRD and X-CT scans, respectively, and their kind assistance with analysing the results. Likewise, John Gilleece and Robert McDonald for their time and effort in preparing thin sections and rock samples for analysis.

I would like to thank Dr. Jon Busby of BGS for kindly providing seismic, temperature, thermal conductivity, and heat flow data, which were made available through the BritGeothermal partnership. Furthermore, I am grateful to Professor Jon Gluyas, Dr. Charlotte Adams, and colleagues from BritGeothermal, for their support.

Thanks also to Markus Ronde, Mark Donaldson, and Dr. Richard Middlemiss, for their assistance with the gravity survey fieldwork and data processing.

I would also like to acknowledge and thank staff at the Glasgow City Archives at the Mitchell Library, National Records of Scotland, and Renfrewshire Heritage Centre for allowing access to archive material. Thanks also to David Lister and staff of the Climatic Research Unit at the University of East Anglia, and staff of the Met Office National Meteorological Archive, for providing historic air temperature data; and the National Geological Repository, BGS, for access to the borehole samples. I should particularly like to thank Tracey Gallagher, Scott Renshaw, and the staff of the Keyworth core store for assistance with the sampling.

This thesis was funded by EPSRC, grant number EP/M508056/1 and EP/M506539/1. X-CT and XRD analyses in Chapter 4 were funded by the European Commission Horizon 2020 research and innovation programme under grant agreement No. 691728 (DESTRESS).

Finally, I would like to thank my family and Emma for their patience, motivation, and encouragement to undertake and complete this work.

This thesis is dedicated to the memory of Anne Watson (2 January 1946 – 21 November 2015), John McFie (29 November 1935 – 18 July 2021), Rob Westaway (25 March 1959 – 13 August 2021) and Paul Younger (1 November 1962 – 21 April 2018) who are greatly missed.

Author's Declaration

I declare that, except where explicit reference is made to the contribution of others, that this thesis is the result of my own work and has not been submitted for any other degree at the University of Glasgow or any other institution.

Sean Watson

Copyright Permissions

Figures containing historical and geological maps are reproduced with permission from Digimap. Where figures contain this data, the copyright statement is stated in the figure caption.

BGS UK Land Gravity data was incorporated into the gravity survey modelling of Chapter 3. This data is available under the Open Government Licence: Open Government Licence v3.0.

Where borehole locations are denoted on figures, this is based upon information from borehole logs available from BGS online borehole viewer. These figures therefore contain British Geological Survey Materials © NERC (2021) available under the Open Government Licence: Open Government Licence v3.0.

Figures which contain Ordnance Survey maps are produced using OS VectorMap® District data. Where figures contain this data, the copyright statement is stated in the figure caption. OS Open Data is free to use under the Open Government License: Open Government Licence v3.0.

Air temperature datasets for the Arrochymore, Dowanhill, Helensburgh, Paisley and Salsburgh weather stations were provided by the Climatic Research Unit, University of East Anglia, Norwich, and the Met Office National Meteorological Archive, Exeter, under the Open Database License (https://opendatacommons.org/licenses/odbl/1-0/).

Figures 3.12-3.15 contain seismic data provided by UKOGL-Beneath Britain, © 2002 Crown Copyright. Reproduced by permission of the Controller of Her Majesty's Stationery Office and the Secretary of State of the Department for Business, Energy & Industrial Strategy. © 2002 UK Onshore Geophysical Library.

Porosity and permeability data detailed in Appendix 4.A and referred to within the main thesis text was supplied by the British Geological Survey under Permit Number CP19/006 British Geological Survey © UKRI 2018. Data from the BGS Aquifer Properties Database.

List of Abbreviations

Table 1. General abbreviations.

	Term		Term
BGS	British Geological Survey	MIS	Marine Isotope Stage
BHT	Bottom Hole Temperature Measurements	MVS	Midland Valley of Scotland
BIIS	British and Irish Ice Sheet	NGRIP	North Greenland Ice Core Project
BNG	British National Grid	SIS	Scottish Ice Sheet
DST	Drill Stem Test	TVD	True Vertical Depth
EQM	Equilibrium Temperature Measurements	TWTT	Two-Way Travel Time
HSA	Hot Sedimentary Aquifer	UKGEOS	UK Geo-Energy Observatories
ka BP	Thousand Years Before Present	WI	Windermere Interstadial
LLR	Loch Lomond Readvance	X-CT	X-Ray Computed Tomography
LOG	Log Temperature Measurements	XRD	X-Ray Diffraction
MD	Measured Depth		

Table 2. Abbreviations of stratigraphic formations.

	Formation Name		Formation Name
ASV	Arthur's Seat Volcanic Formation	MCMS	Middle Coal Measures Formation
BGN	Ballagan Formation	MSS	Mauchline Sandstone Formation
BHV	Bathgate Hills Volcanic Formation	MVL	Mauchline Volcanic Formation
CPV	Clyde Plateau Volcanic Formation	PGP	Passage Formation
CYD	Clyde Sandstone Formation	Q	Quaternary Deposits
FAS	Fairlie Sandstone Formation	ROS	Rosneath Conglomerate Formation
HBC	Highland Border Complex	SAG	Stratheden Group
KBS	Kelly Burn Sandstone Formation	SALV	Salsburgh Volcanic Formation
KNW	Kinnesswood Formation	SCK	Stockiemuir Sandstone Formation
KPF	Knox Pulpit Formation	SKM	Skelmorlie Conglomerate Formation
KRW	Kirkwood Formation	UCMS	Upper Coal Measures Formation
LCMS	Lower Coal Measures Formation	ULGS	Upper Limestone Formation
LLGS	Lower Limestone Formation	WEM	Wemyss Bay Sandstone Formation
LSC	Limestone Coal Formation	WLOS	West Lothian Oil Shale Formation
LWM	Lawmuir Formation	WMVAS	West MVS Westphalian-Early Permian Sills

Table 3. Abbreviations of lithological units.

	Lithology
C	Coal
Cmnst	Cementstone
Fa.Bl	Fakey Blaes
Ist	Ironstone
Lava. Det.	Lava Detritus
Lst	Limestone
M.G.	Made Ground
Mdst	Mudstone
Slst	Siltstone
Sst	Sandstone
Strk	Seatrock
Volc. Det.	Volcanic Detritus

Table 4. Abbreviations of geological features in the MVS.

	Fault Name		Fault Name
BF	Bothwell Fault	MKF	Milngavie Kilsyth Fault
BLF	Blythswood Fault	MLS	Midlothian-Leven Syncline
CF	Castlemilk Fault	NTF	North Tay Fault
CK	Clarkston Fault	OF	Ochil Fault
CMF	Comedie Fault	OTF	Ochil Tree Fault
CPF	Campsie Fault	PF	Possil Fault
CRF	Crookston Fault	PRFZ	Paisley Ruck Fault Zone
DF	Dechmont Fault	RF	Rutherglen Fault
DDF	Dura Den Fault	RWF	Redlawood Fault
DWF	Dusk Water Fault	SA	Salsburgh Anticline
EF	Easterhouse Fault	SCS	South Clackmannan Syncline
EOF	East Ochil Fault	SF	Shettleston Fault
GF	Garnkirk Fault	SLF	Slamannan Fault
GL	Glennifer Fault	SS	Strathmore Syncline
HBF	Highland Boundary Fault	STF	South Tay Fault
LB	Lanarkshire Basin	SUF	Southern Upland Fault
LMF	Lumloch-Muirhead Fault		

Table 5. Abbreviations of coal seams and marine bands.

	Seam/Marine Band Name		Seam/Marine Band Name
AV	Airdrie Virtuewell Coal	Knott	Knott Coal
BDK	Baldernock Limestone	LD	Lower Drumgray Coal
BK	Blackhall Limestone	LGI	Lower Garscadden Ironstone
CM	Calmy Limestone	LIL	Lillie's Shale Coal
DB	Dykebar Limestone	LY	Lyoncross Limestone
EC	Ell Coal	MC	Main Coal
GCI	Garibaldi Clayband Ironstone	MMC	Meiklehill Main Coal
HB	Hollybush Limestone	MNHO	Main Hosie Limestone
HC	Humph Coal	O	Orchard Limestone
HUR C	Hurlet Coal	PC	Pyotshaw Coal
I	Index Limestone	SC	Splint Coal
JCB	Johnstone Clayband Ironstone	TH	Top Hosie Limestone
KC	Kiltongue Coal	UC	Upper Coal
KCC	Kilsyth Coking Coal	VC	Virgin Coal

Units:

Geothermal Gradient (dT/dz): °C km^{-1}

Heat Flow (Q): mW m^{-2} (milli-watts per square metre)

Temperature (T): °C

Thermal Conductivity (k): W m^{-1} $°C^{-1}$

Thermal Diffusivity (κ): mm^2 s^{-1}

Specific Heat Capacity (c): J kg^{-1} $°C^{-1}$

Density (ρ): kg m^{-3}

Bouguer Gravity Anomaly (Δg): mgal (milli-gal)

Two-Way Travel Time (TWTT): msec (milli-seconds)

Permeability (K): mD (milli-Darcy)

Thermal Power (P): W

Chapter 1. Introduction

1.1. Project Overview and Rationale

1.1.1. Geothermal Energy Overview

Geothermal energy is the thermal energy stored within, or discharged from, the Earth's crust, which can be utilised for electricity generation and the provision of direct heating and cooling. Electricity generation generally requires the production of geothermal fluids at temperatures of over 100 °C, however cooler production temperatures can be utilised for direct heating and cooling applications (Lund et al., 2020). Due to the significant contribution that buildings make to global carbon emissions (United Nations Environment Programme, 2020), increasing the use of geothermal energy is an urgent priority, particularly for direct heat use applications such as space heating.

Addressing the 'energy trilemma'; providing a sustainable, equitable and secure energy supply, is becoming increasingly important in the UK. Geothermal energy has the capability to address each of these challenges, and its associated technologies are low carbon, clean, and sustainable and do not suffer from the intermittency issues experienced by other renewable energy sources such as wind and solar (Younger, 2015; Gluyas et al., 2018).

1.1.2. Scotland's Energy Context

In June 2019, in response to recommendations from the Committee on Climate Change (an advisory body to the government) the UK became the first major jurisdiction to legislate for net-zero greenhouse gas emissions by 2050, superseding its previous target for reducing emissions by at least 80% from 1990 levels (Bell et al., 2016).

In Scotland, the Scottish Government has set even more ambitious targets than the UK. The Climate Change (Emissions Reductions Targets) (Scotland) Act 2019 set targets to reduce Scotland's emissions of all greenhouse gases to net-zero by 2045 at the latest, with interim targets for reductions of at least 56% by 2020, 75% by 2030, and 90% by 2040.

To meet the statutory greenhouse gas emissions targets, the Scottish Government's energy strategy is centred around improving energy efficiency, developing local energy systems, and increasing renewable energy generation to meet Scotland's energy consumption (Scottish Government, 2020). The Scottish Government has set domestic targets for the development of renewable energy generating capacity and the uptake of low-carbon technologies. For example, it is planned that 50% of heat, transport, and electricity

consumption will be supplied by renewable sources by 2030 and it is hoped that by 2050 the energy system will be almost completely decarbonised.

Based upon the latest statistics, from 2019, 21.1% of Scotland's energy consumption was provided by renewable sources and 6.5% of all non-electrical heat demand was provided by renewable sources (Scottish Government, 2020). Over recent years, renewable electricity generating capacity has developed significantly, and latest statistics show that renewable electricity generation was equivalent to 90.1% of Scotland's gross electricity consumption in 2019 (Scottish Government, 2020). Developing the renewable heating sector, however, has proved more challenging. This is demonstrated by the fact that from 2012-2019, the proportion of non-electrical heat demand met by renewable sources increased by ~4%, from 2.4% in 2012 to 6.5% in 2019 (Scottish Government, 2020). Based upon the latest statistics (for 2019) it is unlikely that the Scottish Government has achieved its interim target of renewables meeting 11% of Scotland's non-electrical heat demand by 2020.

The majority of both generating capacity and output from renewable heat in 2019 in Scotland was provided by biomass primary combustion and biomass combined heat and power (CHP). Biomethane, heat pumps, and energy from waste accounted for the remainder (Scottish Government, 2020). An increase in the diversification and uptake of renewable heat technologies is therefore required in order to meet the Scottish Government's future statutory targets.

The decarbonisation of Scotland's heat supply would significantly contribute to meeting statutory emissions targets as the majority of Scotland's energy consumption is accounted for by heat, at 50.3%, in comparison to 24.5% for transport and 22.1% for electricity (Scottish Government, 2020). Heat also accounts for significant proportion of Scotland's greenhouse gas emissions, with 20.4% of emissions related to heat in buildings (Scottish Government, 2020).

Furthermore, in 2019, 24.6% of households in Scotland were estimated to be in fuel poverty and 12.4% were living in extreme fuel poverty (Scottish House Conditions Survey, 2020). The Fuel Poverty (Targets, Definitions and Strategy) (Scotland) Act 2019, states that a household is in fuel poverty if, in order to maintain a satisfactory heating regime, total fuel costs necessary for the home are more than 10% (20% for extreme fuel poverty) of the households adjusted net income. The rate of fuel poverty in Scotland, coupled with the greenhouse gas emissions related to heat in buildings, demonstrate the challenge of the energy 'trilemma' and the need to provide sustainable and affordable energy.

As a component of an integrated energy supply strategy, geothermal energy thus has the potential to play a key role in the decarbonisation of energy supply in Scotland, particularly when utilised for direct heat use applications and/or coupled with the development of district heating networks which will provide low carbon geothermal heating to industries and households.

1.1.3. Geothermal Energy in Scotland

The Midland Valley of Scotland (MVS) is host to two potentially significant geothermal resources: insulated groundwater in flooded abandoned mine workings (Watson et al., 2019a; Watson and Westaway, 2020); and Hot Sedimentary Aquifers (HSAs) within deeply buried Upper Devonian sandstones (Browne et al., 1987; Gillespie et al., 2013) such as the Knox Pulpit Formation in Fife (Robinson et al., 2016).

The MVS has an esteemed history of subsurface research and industrial development. In the latter half of the 19th century, Lord Kelvin conducted observations of temperature and thermal resistance in the Blythswood-1 and South Balgray boreholes in what is now suburban Glasgow (Thomson et al., 1868; 1869). These observations were then used by Benfield (1939) and Anderson (1940) to study terrestrial heat flow in central Scotland. The coalfields of central Scotland were extensively worked throughout the 19th and 20th centuries (Watson et al., 2019a), and prospecting for deeper workable seams and potential hydrocarbon reservoirs led to the drilling of a number of deeper boreholes in the MVS in the early-to-mid 20th century. A total of 98 hydrocarbon exploration and appraisal wells were drilled in the MVS between 1919 and 2008 (Monaghan, 2014), and overall, the British Geological Survey (BGS) holds over 215,000 records in its borehole database for the MVS, 56 of which are over 1000 m depth (Monaghan, 2014). Downhole geophysical data and bottom hole temperature measurements were recorded in a number these boreholes expanding the geothermal dataset for the region (Gillespie et al., 2013). However, it was not

until the late 1970's and 1980's that research was undertaken to examine the extent and magnitude of possible geothermal resources beneath central Scotland.

Within these studies, the Upper Devonian aged sandstones of the Stratheden Group and the overlying Kinnesswood Formation were identified as potential geothermal resources beneath the MVS, if the near-surface properties of these sandstones were maintained at depth (Browne et al., 1985, 1987).

In 2013, the Scottish Government commissioned a study into the potential for deep geothermal energy in Scotland (Gillespie et al., 2013). Based upon existing data, policy options and recommendations were set out within this study, outlining the required steps that need to be taken to develop deep geothermal energy in Scotland. In terms of characterisation and quantification of the potential geothermal resource, there were calls for demonstrator projects, physical exploration programmes and extensive data acquisition.

Feasibility studies, funded by the Scottish Government's Geothermal Energy Challenge Fund (GECF) were the next stage of the development of the geothermal energy sector in Scotland (Brownsort and Johnson., 2017). The GECF supported feasibility studies exploring the capacity of Scotland's geothermal resource to meet the energy needs of local communities. The four projects awarded funding were Guardbridge in Fife, Hill of Banchory in Aberdeenshire, Aberdeen Exhibition and Conference Centre, and Fortissat in North Lanarkshire (Brownsort and Johnson., 2017). These feasibility studies targeted different geological and hydrogeological settings. At the time of writing none of the GECF projects have transitioned from a feasibility study to an exploration programme and there are no active deep geothermal projects in the MVS.

There are, however, two schemes in the MVS which utilise heat from flooded, abandoned mine workings; one in Shettleston, Glasgow, and the other in Lumphinnans, Fife (Banks et al., 2009). A number of feasibility studies of the potential resource in flooded mine workings have been conducted since 2010, for projects in Lanarkshire and Midlothian. In the Clyde Gateway Regeneration area of the East End of Glasgow, observational and monitoring boreholes have been drilled at the Glasgow Geothermal Energy Research Field Site (GGERFS), the objective of which is to research and test groundwater in the mine workings beneath Dalmarnock and Rutherglen (Monaghan et al., 2017, 2018). The existing mine water geothermal schemes show that decentralized small-scale low carbon energy generation is a promising and applicable option for the MVS.

1.1.4. Geothermal Energy in Glasgow

Younger et al. (2012) suggested that if the near-surface properties of the Upper Devonian sandstones of the MVS are maintained at depth, as they are in the equivalent strata in the Central North Sea, they may be exploitable as HSA geothermal reservoirs.

In the Glasgow area, a heat flow anomaly is centred over a thick succession of Carboniferous and Devonian sedimentary strata, within which it is postulated that convective groundwater flow brings deep, upward flowing warm water to shallow depths (Wheildon et al., 1985; Browne et al., 1987). Furthermore, over the past decade there has been a recognition of the need to apply corrections to heat flow in the UK to account for the effects of palaeoclimate and topography (Westaway and Younger, 2013). Past systematic neglection or under-appreciation of these effects has resulted in values of heat flow being widely underestimated across the country (Westaway and Younger, 2013; Busby et al., 2015). It is anticipated that these effects are particularly influential in western Scotland due to the combination of shallow temperature measurements in the existing geothermal dataset, proximity to the Gulf Stream, and the severity of cooling during Pleistocene cold stages (Westaway and Younger, 2013). Without applying corrections for these effects, values of heat flow are significantly underestimated in the region, and any extrapolation of shallow geothermal gradient to greater depths underestimates the temperature at depth. It is therefore likely that the temperature, and thus geothermal resource beneath Glasgow, is greater than previously anticipated.

The prospect of targeting the Upper Devonian sandstone aquifer as a geothermal reservoir is further enhanced due to the geological structure of the Glasgow area. At outcrop, Upper Devonian sandstones and Lower Carboniferous sediments are overlain by thick piles of basaltic and andesitic igneous rocks of the Clyde Plateau Volcanic (CPV) Formation. It is hypothesised that this structure also occurs beneath the city at depths suitable for geothermal exploration (c. 2-2.5 km) (Younger et al., 2015). The igneous rocks are impermeable and have relatively low thermal conductivity (Oxburgh, 1982; see Chapter 5), and therefore may act as a seal, trapping both heat and water in the underlying sedimentary rocks.

Despite the previous research of the potential geothermal resource in the Upper Devonian sandstones of the MVS (Browne et al., 1987; Gillespie et al., 2013), and the case study of the Guardbridge project in Fife, as yet there has not been a detailed examination of the potential geothermal resource in the HSA setting beneath Glasgow. The urban development of the city and the surrounding conurbation has been a legacy of its economic development,

in part fuelled from local coalfields which exploited the same sedimentary sequence that contains the geothermal resource. This presents an opportunity to provide geothermal heating to areas of dense urban population and high heat demand.

1.2. General Project Aims and Objectives

The primary aim of this project is to quantify the low to mid enthalpy geothermal resource in the Upper Devonian sandstone sequence in the sedimentary basin beneath the city of Glasgow. This PhD thesis addresses a number of the recommendations and knowledge gaps outlined in several previous studies (Browne et al., 1985, 1987; Gillespie et al., 2013), and investigates the following hypotheses:

(1) The deep geothermal resource beneath Glasgow has been underestimated due to a previous lack of consideration of the effect of palaeoclimate and topography on shallow measurements of temperature and heat flow. **(2)** Upper Devonian sandstones are present at depths sufficient to yield temperatures capable of supporting a variety of direct heat use applications of geothermal heating. **(3)** The estimated geothermal resource in the Upper Devonian sandstones beneath Glasgow could contribute to meeting some surface heat demand.

The key objectives of the thesis were thus defined as:

1. Identify and discuss geothermal research that has taken place in the MVS.
2. Identify key features of the geology of the MVS which inform the quantification of geothermal energy resources.
3. Determine the extent and depth of the Upper Devonian sandstones beneath Glasgow.
4. Determine the geometry of major fault structures in Glasgow which may be potential conduits or barriers to fluid flow.
5. Examine the mineralogical and physical properties of analogous Upper Devonian sandstones to those present beneath Glasgow to identify target aquifers.
6. Appraise existing measurements of heat flow and geothermal gradient.
7. Identify perturbations to Glasgow's subsurface thermal state caused by the anthropogenic effects of historic mining.
8. Re-evaluate existing measurements of heat flow and geothermal gradient to correct for the effects of palaeoclimate and topography.
9. Extrapolate corrected geothermal gradients to determine the temperature beneath Glasgow and to demonstrate the "true" magnitude of the geothermal resource.
10. Identify potential end-users of the produced heat.

11. Quantify the geothermal heat output from a geothermal doublet well sited in Glasgow and assess the contribution that it could make to local heat demand.

1.3. Chapter Summaries

An overview of each chapter is presented below.

Chapter 1: Introduction: An introduction to the project is provided within Chapter 1. It states the rationale behind this project and the overall aims and objectives of the work.

Chapter 2: Literature Review

Chapter 2 first presents details of the theory on the production, transfer, and distribution of heat from the Earth's interior to the Earth's surface and the implications for identifying and quantifying geothermal energy resources. An overview of the classification of geothermal resources and applications for their optimum use is then provided, followed by descriptions of heat flow, geothermal gradient, thermal conductivity, and hydrogeological properties of HSA geothermal projects. Previous geothermal research and exploration within the UK is discussed, with future opportunities identified. The chapter concludes by discussing the geology of the MVS, with particular emphasis placed on aspects of the geology which relate to the quantification of the geothermal resource beneath Glasgow. This includes topics such as, the tectonic history of the MVS, the nature of the crystalline basement, the deep crustal structure, and the geology of Glasgow, specifically the Carboniferous and Devonian stratigraphy of the Lanarkshire Basin and the presence of major faults which traverse the city and the surrounding area.

Chapter 3: Development of a Structural Geological Model of Eastern Glasgow

In Chapter 3, gravity surveying fieldwork was conducted, and 3-D numerical modelling undertaken to develop a structural geological model of eastern Glasgow, constrained by the newly collected and processed Bouguer gravity anomaly dataset. This work addressed recommendations set out in Gillespie et al. (2013) which called for a programme of data acquisition and for a physical exploration programme, to be implemented first as a geophysical survey to identify specific target sources. In doing so, the extent and depth of the Upper Devonian sandstones beneath eastern Glasgow were determined and the geometry of the Dechmont Fault examined, as a potential secondary geothermal exploration target.

Chapter 4: Analyses of the Properties of Upper Devonian Sandstones in the Midland Valley of Scotland

Fieldwork was conducted to collect new data to assess the mineralogical and physical properties of the Upper Devonian sandstones in the western MVS. This was achieved by collecting samples from rock outcrops and borehole core samples, then conducting thin section petrography, X-Ray Diffraction (X-RD), and X-Ray Computed Tomography (X-CT) analyses of the samples to determine values of porosity and to assess the effects of diagenesis and deposition on the aquifer properties.

Chapter 5: Appraisal and Revaluation of Glasgow's Geothermal Datasets

Due to the scarcity of deep boreholes and the reliance on extrapolating temperature measurements from shallow boreholes, there is a limited understanding of the regional thermal state beneath the western MVS. This is addressed in Chapter 5 where existing heat flow and temperature measurements were re-calculated for boreholes in the region. By appraising the existing geothermal datasets, it enabled an assessment of existing subsurface temperature measurements, as a precursor to applying corrections to heat flow measurements to account for palaeoclimate and topography in Chapter 6. Then, based upon the re-calculated geothermal dataset, perturbations to Glasgow's subsurface thermal state caused by the anthropogenic effects of historic mining were identified. Finally, a preliminary analysis of the geothermal resource in flooded abandoned mine workings at a case study site in eastern Glasgow was conducted.

Chapter 6: Palaeoclimate and Topographic Corrections to Heat Flow and the Implications for Geothermal Resource Quantification in Glasgow

Corrections to heat flow and geothermal gradient to account for the effects of palaeoclimate and topography were calculated in Chapter 6. In the absence of obtaining measurements from deep in the subsurface, producing a corrected regional heat flow dataset is a critical step towards reliably estimating the temperature of the geothermal resource beneath Glasgow. By utilising the results of Chapters 5 and establishing a palaeoclimate history for the western MVS, rigorous corrections to account for the effects of palaeoclimate and topography on heat flow and geothermal gradient were calculated for fourteen boreholes in the region. Then, combining the results of Chapters 3-6, DoubletCalc software was used to calculate the indicative thermal power output from geothermal doublet wells located at candidate drilling sites in the East End of Glasgow. The contribution that geothermal heat could make to local heat demand was then assessed.

Chapter 7: Conclusion

Chapter 7 brings together all the elements of the work undertaken in this thesis to form a discussion on the geothermal resource in the Upper Devonian sandstone sequence beneath Glasgow. The principal achievements of the thesis are outlined, and the scope for the development of geothermal energy in Glasgow is discussed with reference to precedents of geothermal projects in sedimentary rocks elsewhere in Britain, and abroad. The wider implications of this research are then discussed, and recommendations for next steps in the development of geothermal energy in Glasgow, and in similar geological settings elsewhere, are proposed.

1.4. Publications Arising from This Thesis

The work of this thesis has contributed to two academic journal publications and two conference proceedings publications. The full references are provided below:

Watson, S.M., Westaway, R. and Burnside, N.M. 2019. Digging deeper: The influence of historic mining on Glasgow's subsurface thermal state to inform geothermal research. *Scottish Journal of Geology*, **55** (2), pp. 107-123, https://doi.org/10.1144/sjg2019-012

Watson, S.M. and Westaway, R. 2020. Borehole temperature log from the Glasgow Geothermal Energy Research Field Site: a record of past changes to ground surface temperature caused by urban development. *Scottish Journal of Geology*, **56**, pp. 134-152, http://dx.doi.org/10.1144/sjg2019-033

Watson, S.M., Westaway, R. and Falcone, G. 2019. A Review of Deep Geothermal Energy and Future Opportunities in the UK. Proceedings, European Geothermal Congress, 2019, Den Haag, The Netherlands, 11-14 June 2019.

Watson, S.M., Westaway, R. and Burnside, N.M. 2021. Revaluating Glasgow's Heat Flow Dataset to Account for Corrections for Palaeoclimate: a Case Study of the Maryhill Borehole. Proceedings, World Geothermal Congress 2021, Reykjavik, Iceland.

Chapter 2. Literature Review

2.1. Introduction

In this chapter, theory on the production, transfer, and distribution of heat from the Earth's interior to the Earth's surface and the implications for identifying and quantifying geothermal energy resources is summarised. An overview of the classification of geothermal resources and applications of their use is then provided, followed by descriptions of heat flow, thermal conductivity, geothermal gradient, and hydrogeological properties which are critical to quantifying the magnitude of the geothermal resource. An overview of geothermal research and exploration within the UK is then provided. Finally, the geology of the MVS is summarised, specifically aspects integral to the assessment of the deep geothermal resource beneath Glasgow.

2.2. Heat Flow Distribution in the Lithosphere

The Earth's natural heat is principally derived from the radioactive decay of uranium, thorium, and potassium, supplemented with heat released during the formation of the Earth's core and interior (Turcotte and Shubert, 2014). The Earth has been slowly cooling since its formation, and this primordial heat moves from the Earth's interior towards the surface, where it dissipates (Jaupart et al., 2007).

There are three mechanisms which transfer heat: conduction, convection, and radiation (Turcotte and Shubert, 2014). Conductive heat transfer occurs through a medium via the net effect of molecular collisions, where kinetic energy is transferred from one molecule to another when they collide (Turcotte and Shubert, 2014). Heat is thus conducted through a medium from a hot region to a cold region, and vice versa. Convective heat transfer, on the other hand, is associated with the motion of a medium. For example, heat is transferred from the flow of a hot fluid into a cold region, and vice versa. Heat is also transferred due to electromagnetic radiation, an example of which is the radiant energy from the Sun (Turcotte and Schubert, 2014).

Understanding the distribution of heat from the Earth's interior to the oceanic and continental lithosphere is important when determining geothermal gradients at any point on the Earth's surface. The geothermal gradient is determined by the amount of heat released at the Earth's surface, known as the heat flow. There is a continuous heat flow at the Earth's surface, which consists of heat flow from the mantle and lower crust, supplemented by heat production from radioactive isotopes largely concentrated in the upper crust (Turcotte and

Shubert, 2014). Heat flow, therefore, provides important information on the amount of heat which is produced and the temperature distribution within the Earth's interior. The distribution of heat flow, however, varies spatially and over time, and differs significantly between the oceanic and continental lithosphere (Figure 2.1). Lucazeau (2019) states that of the 40.8 TW of heat which is dissipated from the Earth's interior, only 14.1 TW is released over the continental lithosphere.

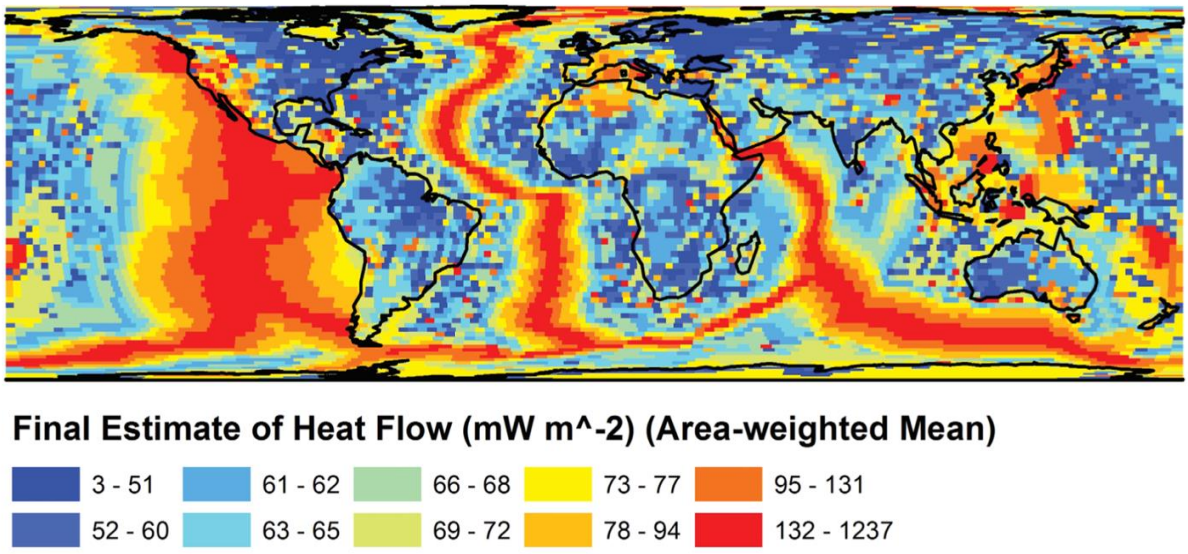

Figure 2.1. Global map of Earth surface heat flow in mW m^{-2} (from Davies, 2013).

Measurements of heat flow at the Earth's surface indicate a variation across continents (Figure 2.1), with areas of the continental crust experiencing enhanced or suppressed geothermal gradients. The variability in the distribution of heat across the continental lithosphere and crust is determined predominantly by conductive heat transfer towards the Earth's surface. This is directly controlled by the thickness, composition, and vertical or horizontal lithological heterogeneity of the continental crust (Ledru and Frottier, 2010). In central areas of continental plates, where the lithosphere is considered to be stabilised and conductive heat transport occurs, the geothermal gradient can vary between 15-25 °C km^{-1}. In this case, the presence of highly radiogenic lithologies such as alkaline and aluminous granites, uranium-bearing sedimentary basins, or highly conductive materials create thermal anomalies (Ledru and Frottier, 2010). Approximately one half of the surface heat flow in the continents can be attributed to the heat production from the radioactive isotopes of uranium, thorium, and potassium in the continental crust (Turcotte and Schubert, 2014).

Convection processes also influence the distribution of heat in the continental crust. These convection processes can result in regions of high heat flow and are predominately located within active zones of magmatism and metamorphism (Ledru and Frottier, 2010; Turcotte and Schubert, 2014). Examples of such are, continental rifting in accretionary systems, active plate margins related to subduction, and convergent plate boundaries. In convection processes, heat is transported via the movement of hot material through the permeable continental crust, bringing magma, for example, close to the surface and enhancing the geothermal gradient (Ledru and Frottier, 2010). At a more local scale, deep sedimentary basins, or fault damage zones, which contain rocks with high primary or secondary porosity and permeability, may allow crustal fluids to freely circulate. In systems such as these, heat from several kilometres depth may be entrained by fluid circulation creating enhanced temperature anomalies (Manning and Ingebritsen, 1999).

2.3. Classification and Utilisation of Geothermal Resources

The geological setting and related conductive and convective heat transfer processes determine the magnitude of a geothermal resource and hence its associated applications. One common classification criterion for describing geothermal resources and their applications is that based upon the temperature and enthalpy of the geothermal fluid.

Enthalpy is a thermodynamic function which is used in geothermal energy to denote the quantity of heat contained in the amount of water or steam produced (Bowen, 1989). Many authors have used this method to classify geothermal resources by applying temperature cut-offs to determine the best economic use of the resource. Muffler and Cataldi (1978) illustrated this as:

Table 2.1. Geothermal resource classification by enthalpy (Muffler and Cataldi, 1978).

Enthalpy	Temperature (°C)	Fluid Phase	End Use
High	>150	Vapour and/or liquid	Primarily electricity generation, then direct heat use of excess/waste heat.
Mid	100-150	Liquid	Electricity generation using an Organic Rankine Cycle (ORC) or binary cycle. Also used for direct heat use.
Low	<100	Liquid	Direct heat use.

However, the categorization of geothermal resources into low and high enthalpy systems is inadequate given the developments in recent years in exploiting “very low enthalpy” systems such as ground source heat pumps or flooded abandoned mine workings, and super-critical geothermal systems such as those in Iceland (Younger, 2015). A more refined categorization

of resources, which corresponds more closely with the optimal domains for application of different energy conversion technologies, was proposed by Younger (2015), illustrated in Figure 2.2.

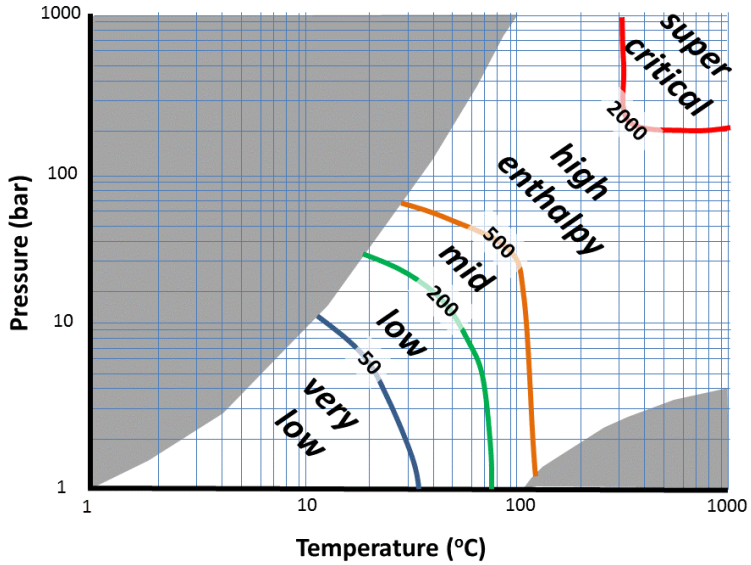

Figure 2.2. Categorization of geothermal resources on the basis of enthalpy. The numbers on the lines dividing the different enthalpy categories are values of enthalpy in kJ/kg (Younger, 2015).

High enthalpy and super critical geothermal resources tend to be located in areas of tectonic activity or active volcanism where the heat flow and geothermal gradient are greatly enhanced. The geothermal fluids extracted from high enthalpy resources are typically under high pressure and high temperature. As a result of this, the fluid changes state to produce steam when it is extracted. This produced steam is then used to turn turbines to produce electricity (DiPippo, 2012).

Mid-enthalpy geothermal resources are mainly exploited for direct heat applications, however, may have the potential for power generation, and thus Combined Heat and Power, through binary cycle power plants (Dickson and Fanelli, 2005; Nusiaputra et al., 2014).

Low and very low enthalpy geothermal resources are typically located in tectonically stable, non-volcanic settings where the heat flow and geothermal gradient are similar to the continental mean values. These resources tend to be located within sedimentary basins where natural, or anthropogenic, permeable formations contain water at temperatures suitable for direct heat utilisation (Younger, 2015; Younger et al., 2012), such as those applications shown in Figure 2.3.

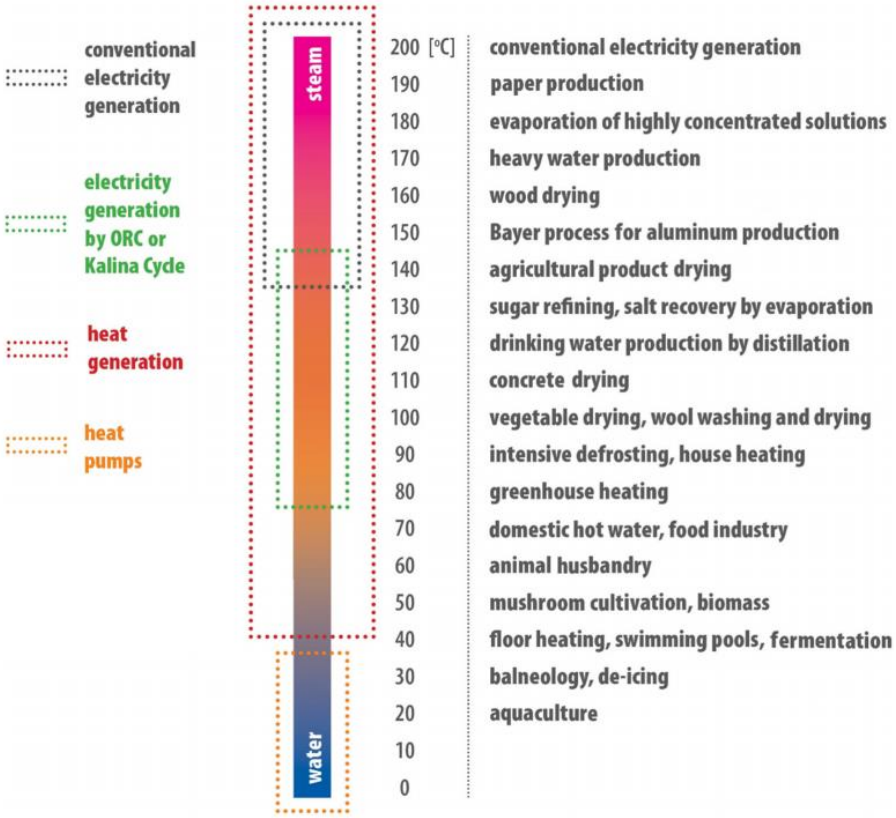

Figure 2.3. Modified Lindal diagram showing applications for geothermal fluids as a function of their temperature. ORC denotes the Organic Rankine Cycle (Kaczmarczyk et al. 2020).

The potential range of applications relevant to this thesis lie at the low-medium temperature end of the spectrum (<80 °C). One such use is the utilisation of geothermal heat by municipal district heating systems (Figure 2.4), with inlet and return temperatures compatible with heat supplied from low-mid enthalpy resources (Figure 2.5).

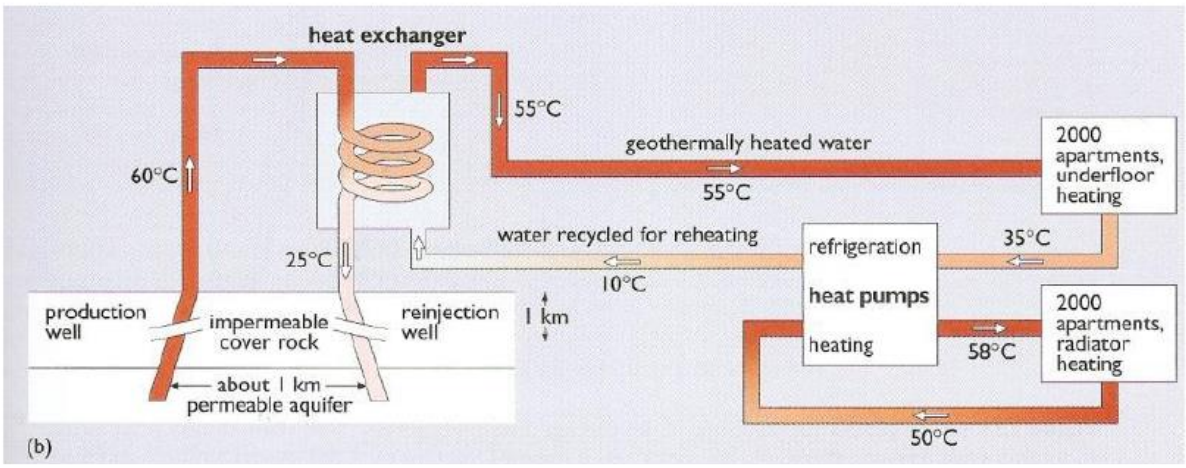

Figure 2.4. Paris Basin geothermal district heating system (Garnish and Brown, 2012).

One benefit of district heating networks is that they can be fed by numerous energy centres (Norden et al., 2011). This is particularly relevant for the utilisation of geothermal heat. With a large area of underlying geothermal resource, each of the production wells, and related energy centres may be located in close proximity to the consumers of the heat. By having a more localised structure of energy supply, the losses which occur when transferring heat through the pipe network are limited (Norden et al., 2011). Figure 2.6 shows that a production temperature of 60-80 °C is suitable for utilisation through the district heating network, however newer designs of district heat networks can operate at lower temperatures (e.g., Lund et al. 2018).

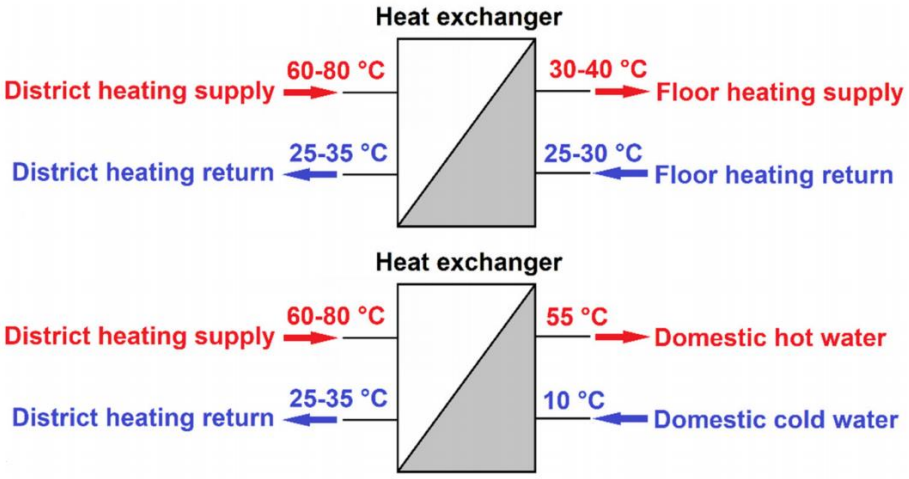

Figure 2.5. Example of low temperatures in a district heating circuit interfaced via heat exchangers to underfloor heating and domestic hot water circuits (Ramboll, 2015).

2.4. Heat Flow, Thermal Conductivity, Geothermal Gradient, and Temperature

Determining subsurface temperature is key to quantifying geothermal resources, appraising exploration targets, and assessing appropriate applications for the utilisation of geothermal energy.

Subsurface temperatures can be measured in boreholes, computed via numerical modelling by solving Fourier's Law, or estimated using the geothermal gradient, the rate at which temperature increases with depth. The geothermal gradient depends upon heat flow, the thermal conductivity of the rocks and the flow of groundwater in the subsurface (Downing and Gray, 1986). Regional variations in heat flow may result from the differences in the radioactive composition of the rocks forming the crust and the dissipation of heat from the Earth's interior. Local variations in heat flow, and hence geothermal gradient, are caused by differences in the thermal conductivity of different rock types and by the redistribution of heat by circulating groundwater (Downing and Gray, 1986), both of which can vary laterally and with depth (Beamish and Busby, 2016).

This section provides an overview of the theory for the calculation of one-dimensional vertical heat flow, including the measurement of thermal conductivity, geothermal gradient, and subsurface temperature.

2.4.1. Heat Flow

Heat flow is the standard measure of the amount of heat travelling through the Earth's crust and is a key parameter in the quantification of geothermal energy resources. The calculation of heat flow is based primarily on the conduction of heat through rock. The basic relationship for conductive heat transport is Fourier's Law which states that heat flow is the product of thermal conductivity and temperature gradient (Turcotte and Schubert, 2014). In one dimension, Fourier's Law takes the form:

$$q = -k \frac{dT}{dz}$$

(Equation 2.1)

Where q is heat flow (mW m^{-2}), $\frac{dT}{dz}$ is the geothermal gradient (°C m^{-1}), k is the coefficient of thermal conductivity (W m^{-1} °C^{-1}) and z is the coordinate in the direction of temperature variation, in this case depth (m). It is standard practise to take the upward surface heat flow

to be a positive quantity, even though in the above equation, with z measured positive downward, it has a negative value (Turcotte and Schubert, 2014).

As described in section 2.2, enhanced heat flow can occur due to heat production from radioactive elements in the crust, crustal thinning, or convective fluid flow in sedimentary basins. For example, in Britain the mean heat flow is 52 mW m^{-2} and the mean geothermal gradient is 26 °C km^{-1}, however in southwest England the mean heat flow is 117 mW m^{-2} and the mean geothermal gradient is 35 °C km^{-1} (Busby, 2014). This is due to the presence of radiogenic granites of the Cornish Batholith underlying this area of the country.

Values of heat flow are determined in boreholes using standard techniques, such as combining measurements of temperature with measurements of thermal conductivity from the geological strata over which temperature was measured, or estimated from heterogeneous media (e.g., in formations that consist of thinly interbedded sandstone, mudstone and siltstone), where the thermal conductivities used in the calculation have to be assumed (Rollin, 1995).

2.4.2. Thermal Conductivity

Thermal conductivity is the capacity of a material to conduct or transmit heat. Rocks with a low thermal conductivity do not transmit heat rapidly, and therefore have a correspondingly high geothermal gradient, and vice-versa. Thermal conductivity varies between different lithologies as it is dependent on the structure and composition of the rock. Thermal conductivity is also influenced by temperature and pressure, and thus the depth of the rock in the subsurface (Waples and Tirsgaard, 2002; Norden et al., 2020). For example, rocks within a sedimentary basin, which are typically porous, experience compaction with increasing depth, which in turn reduces porosity and increases the thermal conductivity (Norden et al., 2020).

The thermal conductivity of a rock is measured on core samples in a laboratory or in-situ within a borehole (Sass et al., 1971, 1984). To measure thermal conductivity the rock sample is exposed to defined and controlled local heating and temperature sensors which measure the temperature response to heating in space and time. The most common method for measurement of thermal conductivity is the divided bar method. The divided bar is a comparative method in which a thermal gradient is applied across samples of known and

unknown thermal conductivity. The sample of known thermal conductivity is used as a reference, and the unknown thermal conductivity is measured in relation to this.

2.4.3. Geothermal Gradient and Temperature

The geothermal gradient is the rate of temperature increase with depth in the Earth's crust. Globally, the mean geothermal gradient is 26 °C km^{-1} (Selley and Sonnenberg, 2015), however this varies between, and within, the continental and oceanic lithospheres. Values of geothermal gradient are determined from measurements of subsurface temperature made within boreholes using wireline downhole logging tools (Prensky, 1992) but prior to the development of this technique, early measurements of temperature were made using hand-operated maximum reading mercury thermometers (Thompson et al., 1868; 1869).

The types of temperature measurement examined in this thesis are bottom hole temperature measurements (BHT), drill stem tests (DST), equilibrium measurements (EQM) and log temperature measurements (LOG). BHT measurements are made when the logging tool is at the bottom of its run, and the temperature is correspondingly at its highest. In the majority of cases, BHT values are representative of the temperature of the circulating drilling fluid and not that of the temperature of the rock formation encountered in the borehole. As such, BHT's are considered an underestimation of the temperature as the drilling fluid is of a lower temperature than that of the rock formation (Deming, 1989). One solution to this is to record an EQM. In this case, the measuring device is allowed to remain in the borehole in order that an equilibrium temperature of the drilling fluid and formation rocks is achieved. However, this can be time consuming as re-equilibration of temperature occurs primarily due to conductive heat transfer as opposed to convective heat transfer (Bullard, 1947; Oxburgh et al., 1972). As it is not always practical to leave boreholes standing for any length of time, it is rare to conduct an EQM and instead, several methods to correct BHTs to mitigate their underestimations have been developed, such as the Horner Correction Method (Deming, 1989). Finally, drill stem testing is a procedure used within hydrocarbon exploration and is used to determine the presence of fluids in a borehole and the rate at which they can be produced from the potential reservoir. Testing involves deploying a series of tools such as a packer, to isolate sections of the well for testing processes, and a downhole valve to open and close the formation to measure reservoir characteristics, such as temperature, which are recorded on downhole measuring tools.

2.5. Hydrogeological Properties of a Geothermal Resource

A detailed understanding of the hydrogeological properties of a geothermal resource is required to quantify the extractable heat output and to ensure that it is efficiently and sustainably designed. Depending on the geological conditions of the target resource, the water-bearing reservoir rock can be an aquifer, a fracture network, or a fault zone. The primary focus of this thesis is to examine the potential geothermal resource in the Hot Sedimentary Aquifer (HSA) setting beneath Glasgow.

HSA systems are located in deep sedimentary basins where aquifers contain water at depths hot enough to be exploited (Garnish and Brown, 2012). These systems are located in porous and permeable sedimentary sequences in tectonically stable regions of either normal or slightly elevated heat flow (Bowen, 1989). The main source of heat resides in the host rocks and the transfer of heat from the host rock to the fluid is conduction dominated (Breede et al., 2015; Mijnlieff, 2020). The most favourable HSA reservoirs exist where a natural system of circulating groundwater yields a high and sustainable flow rate of heated water.

The porosity and permeability of the HSA are crucial parameters in a geothermal project of this type. If the permeability and porosity are too low then poor flow rates will result in low heat extraction, whereas high permeability may result in thermal breakthrough. The challenge in the development of HSA systems, therefore, is in detecting and delineating aquifers with adequate permeability and porosity at depths where temperatures are suitable for the economic and sustainable development of the hot water resources they contain (Downing and Gray, 1986).

2.5.1. Aquifers, Porosity and Permeability

An aquifer is a body of saturated rock that both stores and transmits groundwater (Younger, 2007). Analysis of groundwater systems is dependent on quantifying the factors which govern the ability of the aquifer to store and transmit groundwater. Both storage and transmission properties are controlled by geological factors which for any given rock mass determine; (i) the volume and size of the pores it contains, and (ii) the strength of the rock mass when subjected to compression by the weight of the overlying ground (Beard and Weyl, 1973; Scherer, 1987).

Porosity is the proportion of a given volume of rock that is occupied by pores. Effective porosity is the ratio of the volume of interconnected pores to the total rock volume. The effective porosity of a rock is determined by aspects of the sediment fabric such as grain

shape, grain sorting and grain packing (Beard and Weyl, 1973; Scherer, 1987). For example, the more platy or angular the grains, the closer they can pack together and the lower the effective porosity will be. Sediments composed of grains with a relatively uniform grain size tend to be more porous than those composed of grains of a wide range of sizes. In the latter case the small grains tend to occupy spaces that would be open pores in the uniform sediment. Also, where depositional processes have aligned the long axes of grains parallel to one another, the effective porosity will be lower than if the same sediment were deposited with grains orientated chaotically (Younger, 2007). The relationships between grain size, grain shape and porosity are show in Figure 2.6.

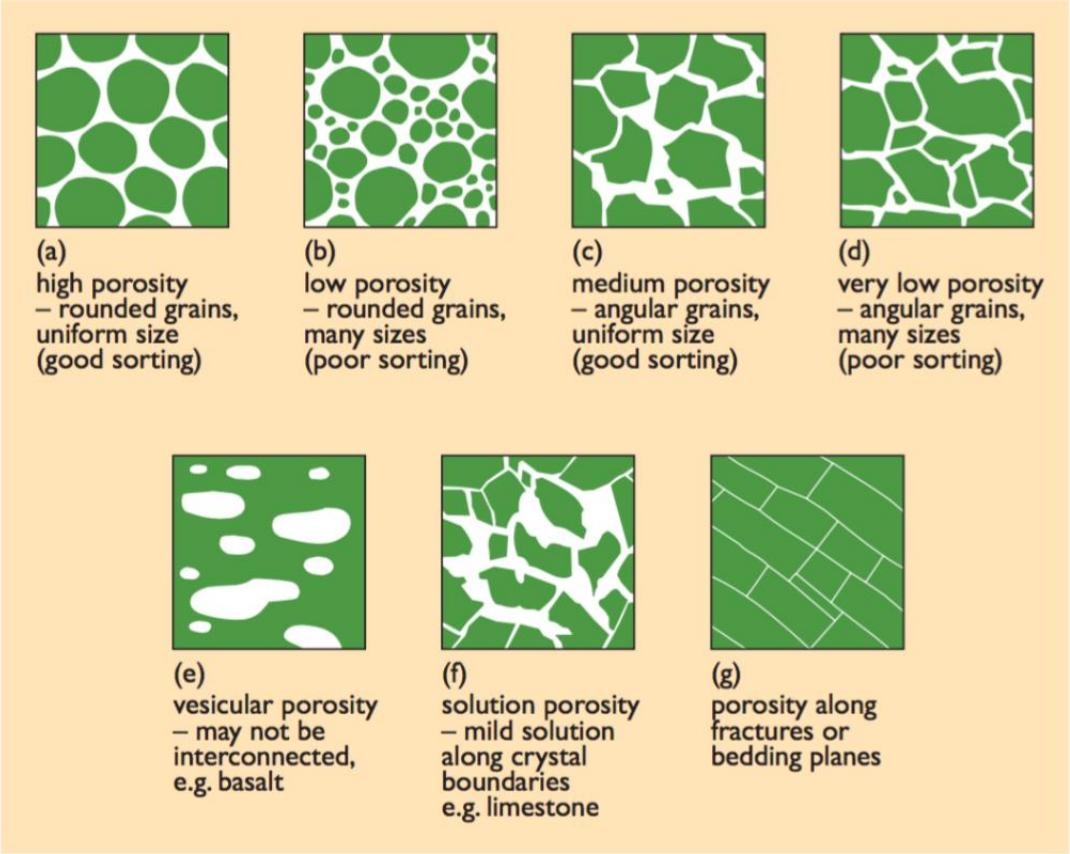

Figure 2.6. Porosity and the sediment fabric (Garnish and Brown, 2012). The relationship between grain size, shape, and porosity in sedimentary rocks (a-d); vesicular porosity in crystallised lava flows (e); solution porosity resulting from rock dissolution, especially where acid groundwaters attack limestone (f); and porosity developing in rocks along original planes of weakness such as bedding planes and fractures (g).

Permeability is the measure of the capacity of a rock to transmit fluid. In an aquifer, the permeability can either be defined as matrix permeability or fracture permeability. Like porosity, variation in the permeability of a rock is recorded with depth as the permeability of an aquifer or fractured crystalline rock decreases with the increasing pressure or effective

stress as a result of overlying strata. A geothermal aquifer must be able to sustain a flow of water, and as such, even highly porous rocks will only be suitable as aquifers if the pores are interconnected (Garnish and Brown, 2012).

The porosity and permeability of sandstones are controlled by the depositional environment and diagenetic processes experienced during burial (Houseknecht, 1987; Gluyas and Cade, 1997).

The effects of deposition and diagenesis are well studied in continental facies deposited under arid conditions (e.g., Olivarius et al., 2015; Tang et al., 2018a; 2018b). At the time of deposition, well-sorted sand has approximately 40% porosity which is then reduced during burial diagenesis by mechanical compaction, intergranular pressure solution, and cementation (Houseknecht, 1987).

The reduction of porosity in sandstones is dominated by mechanical compaction at burial depths of less than 2 km where diagenesis is predominately controlled by stress (Gluyas and Cade, 1997; Paxton et al., 2002; Marcussen et al., 2010). Modelling by Lander and Walderhaug (1999) illustrated that porosity loss in sandstone samples with burial depths of less than 1.5 km was due to compaction and that at this depth, compaction was essentially complete. At greater burial depths, porosity reduction continues due to temperature-induced mineralogical and chemical changes (Weibel et al., 2017). For instance, the development of authigenic quartz cementation is commonly considered as the main controlling factor on the reduction of porosity at burial depths of greater than 2 km (McBride, 1989; Paxton et al., 2002; Aagard and Jahren, 2010), with factors such as chemical compaction, including pressure solution, also contributing to the porosity distribution (Ramm, 1992).

2.5.2. Geothermal Doublet Wells

Geothermal projects which target HSA's typically extract the geothermal fluid through a doublet well system, consisting of a production well and a reinjection well (Figure 2.7). Here, the fluid is extracted from the aquifer via the production well, and then circulated back into the aquifer via the reinjection well once the heat has been utilised. At the surface, the two wells are linked via a heat exchanger, which captures the heat, from the primary salt-water loop and transfers it to the secondary freshwater loop (Mijnlieff, 2020).

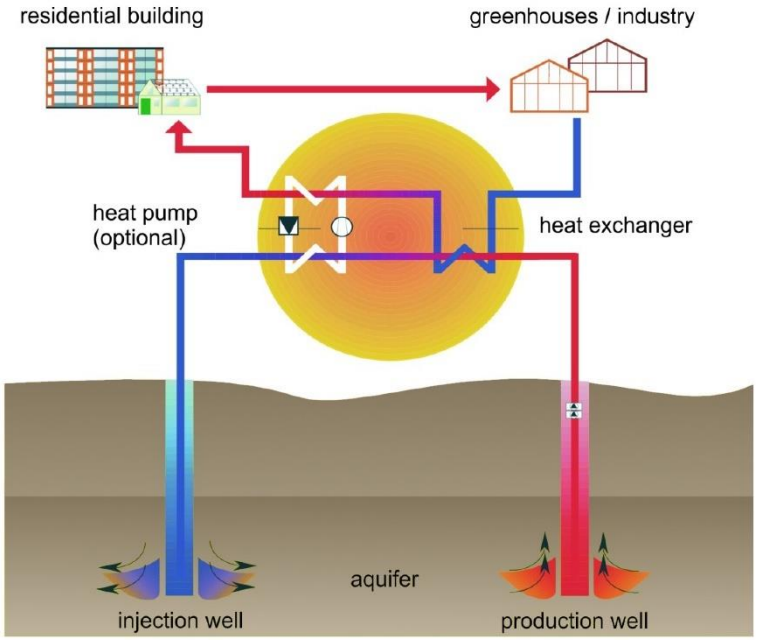

Figure 2.7. Schematic of a geothermal doublet well (Agemar et al., 2014).

The performance of a doublet system is dependent on the permeability and porosity of the aquifer (e.g., Willems et al. 2017a), as there needs to be enough permeability to allow the production well to produce geothermal fluids and to accommodate the re-injected fluid. A critical factor in designing a doublet well system is to ensure that there is enough space between the two wells. If the spacing between the wells is not sufficient, and if the injection and production rates are not reduced, then the production well will start producing the cooler, recently re-injected water. This effect is known as thermal breakthrough and significantly diminishes the performances of the geothermal system (Willems et al. 2017b).

2.6. Geothermal Energy in the UK

To provide context to the investigation of the deep geothermal resource beneath Glasgow, this section describes the geothermal resource base within the UK, the chronology of geothermal research and exploration within the UK, and opportunities for future developments of the sector.

2.6.1. Geothermal Resources in the UK

The UK is located on a tectonically stable portion of the Eurasian tectonic plate. Geothermal resources within the UK consist of very low enthalpy resources within flooded abandoned mine workings, low-mid enthalpy resources within HSAs and mid-high enthalpy resources within buried radiothermal granite plutons. When co-located in areas of high heat demand, the flooded abandoned mine workings and HSAs have the opportunity to provide geothermal heat for direct heat use applications whilst the possibility exists for electricity generation from projects targeted at radiothermal granites.

There are a number of deep onshore sedimentary basins in the UK in which the thickness of sedimentary (and thus, likely, porous, and permeable) water bearing, rock exceeds 2 km which may be host to geothermal reservoirs (Gluyas et al, 2018). The age of these basins is typically older (Upper Palaeozoic) in northern England and Scotland and younger (Mesozoic) in the south of England (Table 2.2; Figure 2.8).

Geothermal research within the UK has predominately focused on reservoirs present within Mesozoic sedimentary basins (Table 2.2). These Triassic and Permian sandstone aquifers, such as the Permian Rotliegend Formation and the Triassic Sherwood Sandstone, or Bunter Sandstone, are proven geothermal reservoirs in Germany, Netherlands, and Denmark (e.g., Agemar et al., 2014; Røgen et al., 2015; Poulsen et al., 2019; Mijnlieff, 2020; Weber et al., 2019). Sedimentary basins of similar depths occur in northern England and central Scotland (Table 2.2; Figure 2.8) where thick sequences of Carboniferous and Devonian strata may contain deep aquifers with suitable reservoir temperatures and aquifer properties for direct heat use applications.

The UK also hosts suites of radiothermal granite batholiths (Figure 2.8). Based upon heat production and heat flow data, the best prospects for exploration are the Cornish and northern England granite batholiths. This has been borne out by exploratory drilling projects (Manning et al., 2007; Cotton et al., 2018; Ledingham et al., 2019).

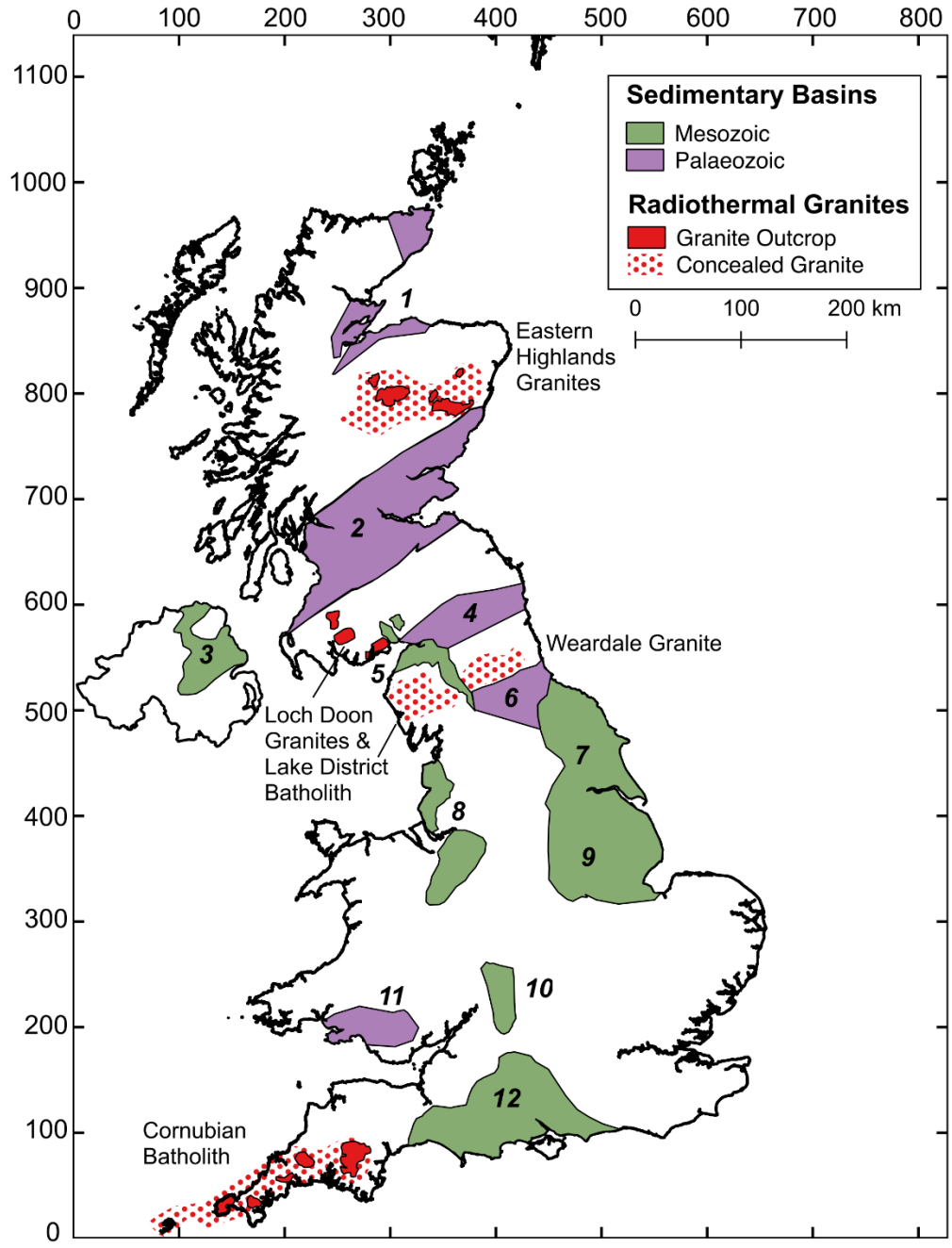

Figure 2.8. Geothermal resource map of the UK adapted from Watson et al. (2020). British National Grid coordinates (north and east) are in 100 km intervals. © Crown copyright and database rights 2021 Ordnance Survey (100025252).

Examination of geochemical data (Younger et al., 2012), correction for the effect of palaeoclimate (Westaway and Younger, 2013; Busby et al., 2015) and gamma-ray spectrometric surveying (McCay and Younger, 2017) identified radiothermal granite plutons that may have geothermal gradients sufficient for direct heat use in the Cairngorms Suite and eastern Highlands of Scotland (Figure 2.8). However, deep drilling is required to confirm greater heat flow at depth, and to assess permeabilities and fracture patterns (Younger et al., 2012).

Table 2.2. The main onshore, sedimentary basins of the UK. Modified from Gluyas et al (2018).

Basin	Basin Thickness (km)	Stratigraphic Age	Reference
Orcadian Basin [1]	3-4	Devonian	Hillier and Marshall, 1992
Midland Valley of Scotland [2]	4 (est.)	Devonian-Carboniferous	Ritchie et al., 2003; Robinson et al., 2016
Northern Ireland [3]	2.5	Triassic to Jurassic	Downing and Gray, 1986
Northumberland Trough [4]	>3	Carboniferous and possibly older	Johnson, 1984; Burnett, 1987; Younger et al., 2016
Carlisle Basin & Solway Trough [5]	1.55-1.9	Permo-Triassic	Downing and Gray, 1986
Stainmore Trough [6]	2.5	Carboniferous and possibly older	Burnett, 1987; Bott et al., 1984
Cleveland & Lincolnshire Basins [7]	3.5	Triassic to Cretaceous	Downing and Gray, 1986; Busby, 2014
Cheshire Basin & West Lancashire Basin [8]	4.7 to base Permian	Carboniferous to Triassic	Plant et al, 1999; Hirst, 2017
East Midlands Basin [9]	2.5	Devonian-Carboniferous	Hirst et al, 2015
Worcester Graben [10]	>3	Permo-Triassic	Busby, 2014
South Wales Basin [11]	2	Devonian-Carboniferous	Downing and Gray, 1986
Wessex Basin [12]	3	Permian to Cretaceous	Busby, 2014

The numbered [n] basins correspond to those shown in Figure 2.8.

2.6.2. Chronology of Geothermal Exploration and Research in the UK

In the UK, the visible manifestation of geothermal activity can be seen at thermal springs, the best-known being at Bath, Bristol, Buxton, and Matlock (Downing and Gray, 1986) which have attracted bathers since Roman times. These waters are meteoric in origin but have been heated by circulation to depths below the surface (Downing and Gray, 1986).

In the latter half of the 19th century, the British Association for the Advancement of Science investigated the thermal state of the subsurface. Numerous measurements of temperature were made in boreholes, particularly those associated with the developing ironstone and coal mining industries, for example in the MVS (Watson et al., 2019).

As Gluyas et al (2018) have summarised, in 1961 it was demonstrated that the hot, radiothermal Weardale Granite exists at depth beneath County Durham when the Department of Geology at Durham University drilled the Rookhope borehole in Weardale. This well proved the eroded top surface of Caledonian (Devonian) granite at a depth of 385 m in a region where there is no outcrop of granite.

The deliberate investigation of geothermal energy in the UK began in the 1970's in response to the global oil crisis and at a time when the petroleum resource offshore of the UK had largely been undiscovered. Following the preliminary studies conducted in the late 1970's, seven deep geothermal exploration boreholes were drilled (Table 2.3), although these were not completed until 1980-1985 by which time the UK had become a petroleum exporter (Gluyas et al., 2018). Three of the boreholes, located at Marchwood and Southampton in southern England, and Larne in Northern Ireland, were drilled and tested to investigate the geothermal potential of the Permo-Triassic sandstones of the respective sedimentary basins. This programme of research was continued in 1984 with the drilling of the Cleethorpes-1 borehole in north-east Lincolnshire. This borehole was drilled to a depth of 2100 m, the primary target being the Basal Permian Sands with a secondary target of the Triassic Sherwood Sandstone Group (Downing and Gray, 1986). In addition to the boreholes drilled in the aforementioned sedimentary basins, three further boreholes were targeted at radiothermal Variscan granite in Cornwall, south-west England. While these boreholes, drilled at Rosemanowes, received much attention as part of the Hot Dry Rock Programme, none made it to production (Richards et al., 1991).

The borehole that can be considered successful, in that it led to an operational geothermal heat project, was that drilled at Southampton (Downing and Gray, 1986; Downing et al., 1984). Since 1987 this borehole has supplied water at 75 °C with thermal power of 2.2 MW, as part of the Southampton District Energy scheme, delivering heat and power to a hospital, university, and commercial premises in central Southampton (Barker et al., 2000).

After a two-decade long hiatus of geothermal exploration in the UK, in 2004 an exploration well was drilled at Eastgate, County Durham, to a depth of 998 m (Table 2.3). The background to this project is summarised by Gluyas et al (2018) and explained in detail by Manning et al (2007). The well encountered naturally fractured Weardale Granite as planned. The bottom hole temperature was 46 °C, indicating a heat flow of 115 mW m^{-2}. This well produced saline water at a temperature of 27 °C from a fractured zone at 411 m depth. The Eastgate-1 borehole proved capable of producing water at a rate of 140 m^3 h^{-1} (39 ls^{-1}) per metre of drawdown. An appraisal well, Eastgate-2, was drilled in 2010 around 700 m from Eastgate-1 to determine whether the fractures were pervasive throughout the granite or were limited to the vicinity of a major fracture in the granite, known as the Slitt Vein. The granite at Eastgate-2 had the same geothermal gradient as at Eastgate-1, but proved to be impermeable, confirming that the fracture permeability at Eastgate-1 is associated with the Slitt Vein.

A further geothermal exploration well was subsequently drilled in the city centre of Newcastle upon Tyne, named the Newcastle Science Central well, now Newcastle Helix (Table 2.3). This reached a depth of 1.8 km and targeted the Lower Carboniferous Fell Sandstone Formation. This well confirmed the high regional geothermal gradient however demonstrated that the Fell Sandstone in this locality is extremely ‘tight’, with no useful rate of water production being feasible (Younger et al., 2016) although it has provided useful information about the mine water geothermics of the area (Westaway and Younger, 2016).

The potential geothermal resource in Cornwall had not been investigated since the 1980’s. However, shown in Table 2.3, at the United Downs project site in Cornwall, drilling was completed in April 2019 for the UD-1 well to a depth of 5275 m MD (5057 m TVD), with a bottom hole temperature of 193 °C, and in June 2019 for the UD-2 well to 2393 m MD (e.g., UDDGP, 2020). This project, located in the Carnmenellis Granite ~7 km from the Rosemanowes site, is for an unconventional well doublet: the aim being generation of

geothermal electricity with an electrical power output of 1-3 MW (e.g., Cotton et al., 2018; Ledingham et al., 2019).

Table 2.3. Summary of deep boreholes drilled in the UK for geothermal exploration.

Location	Completion	Well depth (m)	Bottom hole temperature (°C)	Aquifer depth (m)	Aquifer temperature (°C)
Rosemanowes RH11	December 1981	2175	90	2100	55-70
Rosemanowes RH12	October, 1981	2143	90	Not identified	N/A
Rosemanowes RH15	January 1985	2652	100	Not identified	N/A
Marchwood	February 1980	2609	88	1672-1686	74
Larne	July 1981	2873	91	960-1247	40
Southampton	November 1981	1823	77	1725-1749	76
Cleethorpes	June 1984	2092	69	1093-1490	44-55
Eastgate-1	December 2004	995	46	411	27
Eastgate-2	July 2010	420	-	Not present	No flow
Science Central	July 2011	1821	73	1418.5-1795	No flow
United Downs	2020	2393/5275	193	5275	193

Modified from Younger et al (2012, 2016), and Gluyas et al (2018).

Geothermal projects which target heat stored in flooded, abandoned mine workings are currently in development in the UK. Given the proximity of former coalfields to areas of high urban density and heat demand, and the estimated temperatures of the stored water; flooded, abandoned mine workings present a significant resource and a “low hanging fruit” for the development of geothermal energy sector in the UK (Banks et al., 2019; Farr et al., 2020). However, projects such as these require detailed examination of the connectivity of the flooded mine workings and quantification of the resource prior to development (Walls et al., 2021; Watson and Westaway, 2020).

Furthermore, the realisation by Watson and Westaway (2020) that heat in place in shallow mine workings (~90 m) in Glasgow is anthropogenic, having diffused downward as a result of surface heating effects of urban development, means that this heat is a ‘one off’ resource that might be ‘mined’, not a ‘renewable’ resource that might be utilised sustainably. This indicates that mine water geothermal heat extraction projects should focus on deeper resources, in part because of the greater potential heat outputs due to their higher temperatures and in part due to the resource at these depths being renewable, as a result of basal heat flow from the Earth’s interior, and thus capable of sustainable development. For example, the ‘Seaham Garden Village’ project, in County Durham in north-east England,

will utilise water at 18-20 °C (TCA, 2020), produced from the former Dawdon Colliery (DMM, 2021) whose workings were >500 m deep. The thermal power output from this relatively large, modern colliery will be ~6 MW (TCA, 2020), of which ~2 MW will be used (Evans, 2020).

The boreholes detailed in Table 2.3 are those which have been specifically drilled for geothermal exploration in the UK. In total, there are 2885 boreholes deeper than 500 m in the UK, comprising of oil and gas exploration and production boreholes, and other deep boreholes (Ireland et al., 2021). The Ireland et al. (2021) study highlighted the paucity of borehole data across the onshore UK, stating that of the c. 2600 temperature measurements made in boreholes in the UK, over 90% of the temperature data are from depths less than 2000 m and c. 27% are from depths shallower than 500 m. Whilst acknowledging the significant subsurface uncertainties relating to the quality and accessibility of existing subsurface datasets (Ireland et al., 2021), utilization of the existing borehole infrastructure and the available temperature datasets from deep wells, may provide opportunities for the development of geothermal energy projects in the UK, described below.

2.6.3. Future Opportunities for Developing Geothermal Energy in the UK

Despite the reported potential of geothermal energy in the UK, the high technical and economic risk at the exploration stage currently acts as a significant barrier to development of the sector (Gluyas et al., 2018).

One existing asset which could be utilised to develop the fledgling geothermal sector in the UK is to repurpose onshore hydrocarbon wells for the production and/or storage of geothermal heat. The geothermal potential of hydrocarbon wells has been investigated by several authors, with pilot projects already implemented worldwide and pre-feasibility studies carried out (e.g., Alimonti et al, 2014; Auld et al, 2014; Hirst and Gluyas, 2015; Al-Mahrouqi and Falcone, 2016; Singh et al, 2017; Westaway, 2016; Watson et al., 2020).

One technological option which could be applied in the context of repurposing hydrocarbon is deep geothermal single well (DGSW) heat production (Westaway, 2018; Falcone et al., 2018; Alimonti et al., 2018; 2021). The term DGSW denotes any geothermal project design that utilizes a single borehole rather than a doublet, and which extends into the ‘deep geothermal’ regime, which under the Infrastructure Act 2015, means depths greater than 300 m in the UK. Analytical modelling by Westaway (2018) established that DGSW heat production was found to be cost-effective under the former Renewable Heat Incentive (RHI)

subsidy regime in the UK, provided boreholes are deep enough and in localities where the geothermal gradient is high enough. After a duration of use, if the technology is no longer economic, then the infrastructure might be easily repurposed for seasonal heat storage, offering the potential of making a significant long-term contribution to sustainable future heat supply (Westaway, 2018).

Further opportunities for developing geothermal projects in the UK also exist in settings such as karstified Lower Carboniferous Limestones (Narayan et al., 2018) and in deep Carboniferous-Devonian sedimentary basins, such as that in the western MVS which is the focus of this thesis.

2.7. Geology of the Midland Valley of Scotland

This section describes aspects of the geology of the MVS which are of significance to this thesis, specifically, the tectonic history of the MVS, the geology of the Glasgow area, the crustal structure and nature of the crystalline basement beneath the western MVS, and the depositional environment and sedimentary facies of the Upper Devonian sandstones of the western MVS. An understanding of each aspect is a necessary pre-requisite to investigate the geothermal resource beneath Glasgow.

2.7.1. Overview of the Geology of the Midland Valley of Scotland

The MVS is an elongated WSW-ENE oriented graben of Devonian-Carboniferous age (Figure 2.9) which underlies central Scotland. The basin is bounded to the north and south by the Highland Boundary Fault and Southern Upland Fault respectively, both of which formed important lineaments during the Caledonian Orogeny (Cameron and Stephenson, 1985; Read et al., 2002). Flanked by Dalradian metamorphic rocks of the Scottish Highlands, and Ordovician to Silurian rocks of the Southern Uplands, the MVS is the most extensive area of Scotland which is underlain by sedimentary rocks (Bluck, 2002).

The MVS developed on the eroded and deformed remnants of the Caledonian Mountains, which had formed as a consequence of the closure and suturing of the Iapetus Ocean (the Caledonian Orogeny) at the end of the Early Palaeozoic (Cameron and Stephenson, 1985; Glennie and Underhill, 1998; Read et al., 2002).

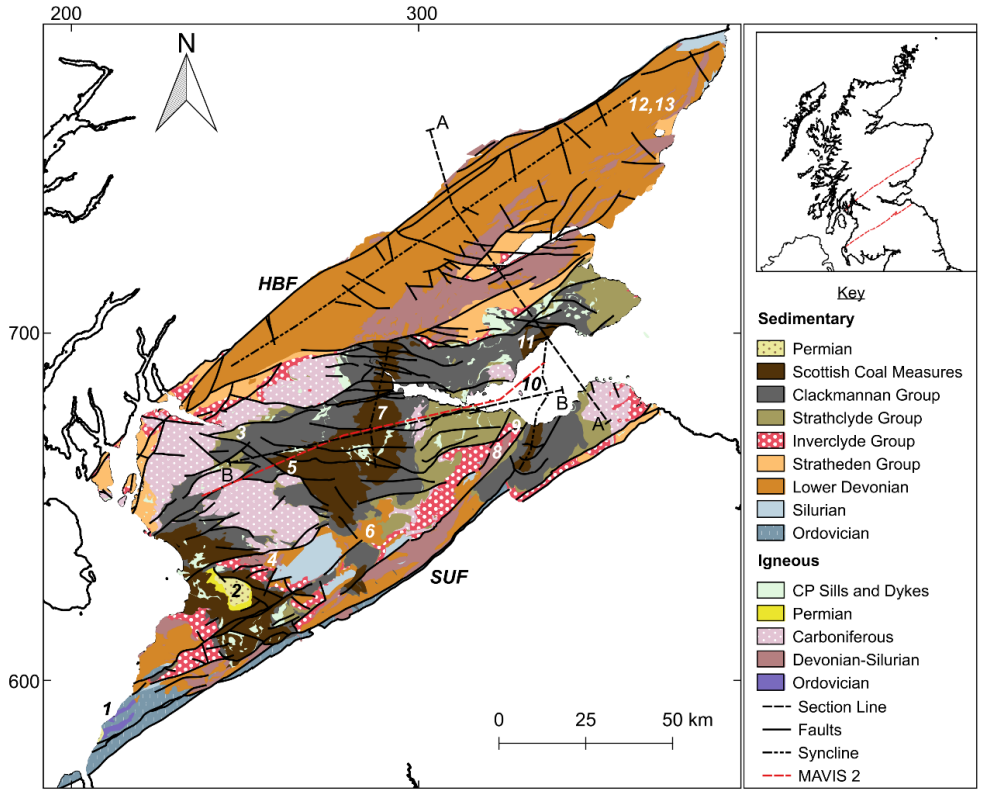

Figure 2.9. Simplified solid geology of the Midland Valley of Scotland. Numbers denote localities and geological features mentioned in the text. These are: (1) Girvan-Ballantrae Complex; (2) Mauchline Basin; (3) Glasgow; (4) Distinkhorn Inlier; (5) Lanarkshire Basin; (6) Lesmahagow Inlier; (7) Clackmannanshire Syncline; (8) Pentland Hills Inlier; (9) Edinburgh; (10) Midlothian-Leven Syncline; (11) Fife-Midlothian Basin; (12) Strathmore Basin; (13) Strathmore Syncline. The location of section lines A-A (Figure 2.10) and B-B (Figure 2.11) are shown. British National Grid coordinates (north and east) are in 100 km intervals. Geological Map Data BGS © UKRI 2021.

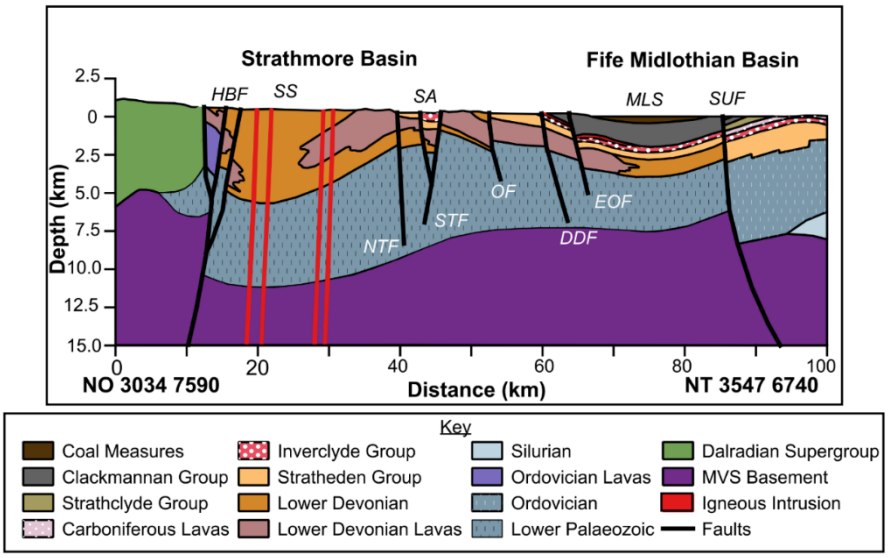

Figure 2.10. North to south trending cross section (A-A) of the MVS showing the deep geological structure of the region. Adapted from Stone (2008). Reproduced with the permission of the British Geological Survey ©UKRI 2021. All rights Reserved.

The MVS terrane has had a prolonged and complex geological history. Monaghan (2014) describes four broad stages to summarise the Palaeozoic to recent basin history of the MVS, (1) Late Devonian to Early Carboniferous basin formation in the Variscan foreland, (2) Mid to Late Carboniferous basin formation to inversion, (3) Latest Carboniferous to Permian tholeiitic magmatism and post-orogenic extension, and (4) Post Carboniferous deposition, uplift, and erosion.

As a result, the MVS is not a simple graben containing a single basin. Instead, the MVS is composed of an internally complex arrangement of fault-bounded Upper Palaeozoic sedimentary basins with synclinal/anticlinal structural styles (Read et al., 2002; Rippon et al., 1996; Ritchie et al., 2003; Underhill et al., 2008), with associated intrusive and extrusive igneous rock, overlying Lower Palaeozoic strata and the crystalline basement (Figure 2.10).

The deepest basin occurs beneath the Firth of Forth, extending northwards into Fife and southwards into the Lothians, and achieves a maximum depth of more than 5 km (Figure 2.11) (Monaghan, 2014). There are also deep sedimentary basins present in Clackmannanshire and in the Lanarkshire Basin at Hamilton, distinguished by marked gravity anomalies, which attain depths of 3 km and 2-2.5 km respectively (Figure 2.11) (Browne et al., 1987; BGS, 1988). Regional gravity anomalies and seismic surveys indicate the presence of a deep sedimentary basin in Glasgow which may have a similar Carboniferous-Devonian stratigraphy to that of the Hamilton basin (Penn et al., 1984).

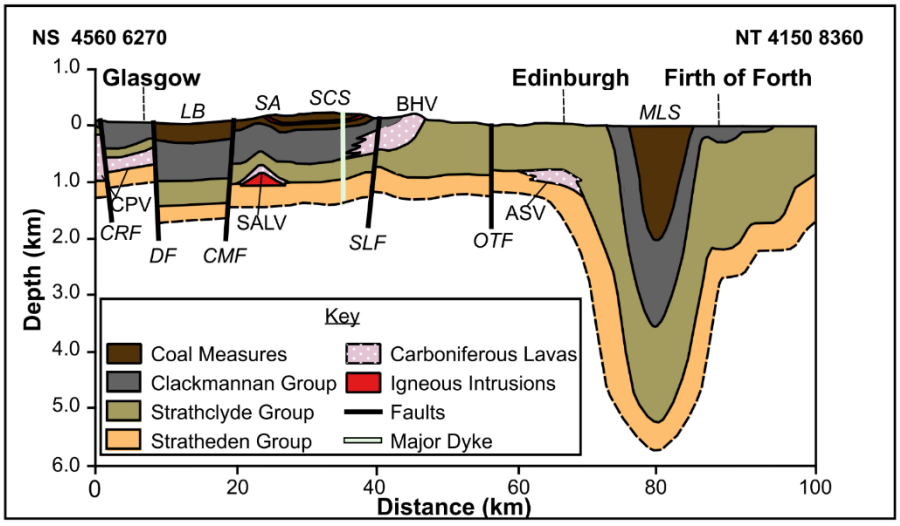

Figure 2.11. East to west trending cross section (B-B) of the MVS showing the deep geological structure of the Upper Palaeozoic sedimentary basins in region. The dashed line indicates continuous thickness of the Stratheden Group and uncertain depth of the base. Adapted from Monaghan (2014) and Heinemann et al. (2018).

2.7.2. Overview of the Geology of Glasgow

The city of Glasgow and its surrounding conurbation are located in a wide, gently undulating plain, flanked to the north and south by the elevated topography of the Campsie Fells, Kilpatrick Hills, Beith-Barrhead Hills, Neilston Block, and the Cathkin Braes. These uplands are in the footwalls of major normal faults of Carboniferous age (Figure 2.12), and are formed by erosion resistant basaltic lava flows, of the Clyde Plateau Volcanic Formation (CPV) (Forsyth et al., 1996; Hall et al., 1998). The lower ground between the uplands is underlain by a deep Carboniferous-Devonian sedimentary basin, dissected by a complex network of lesser faults (Figure 2.12) (Forsyth et al., 1996; Hall et al., 1998). Intrusive igneous rocks of latest Carboniferous and/or Early Permian age also crop out in the Glasgow area, mostly as doleritic sills and dykes (Figure 2.12) (Hall et al. 1998; Browne et al. 1999).

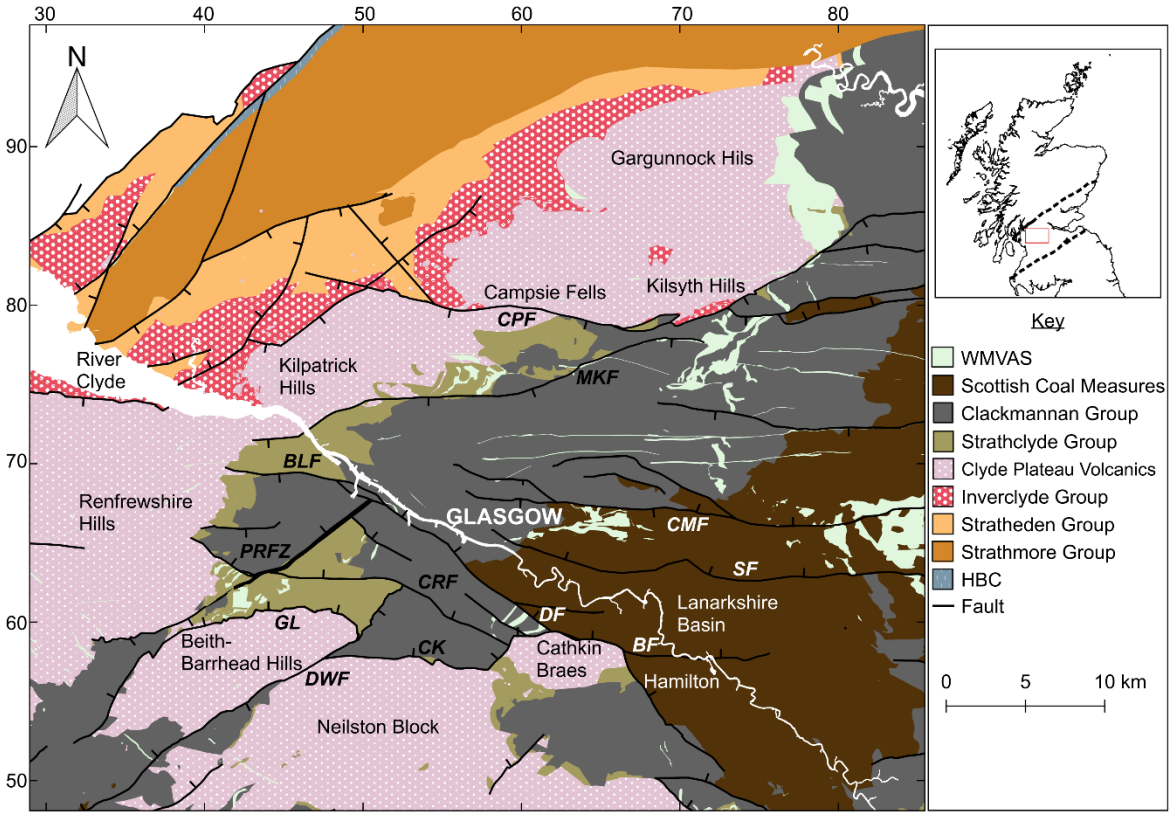

Figure 2.12. Simplified solid geology of Glasgow and the surrounding conurbation. Inset showing location within the Midland Valley of Scotland. The co-ordinates (north and east) are in kilometres within British National Grid 100 km quadrangle NS. Geological Map Data BGS © UKRI 2021.

The basin is bounded to the south by the NW-SE trending Dechmont Fault which downthrows the Lanarkshire Basin to the northeast against Clackmannan Group strata and the CPV in the Cathkin Braes (Figure 2.12). The Dechmont Fault is a major normal fault, believed to date from the late Carboniferous or early Permian but may have been active

intermittently throughout the Carboniferous period (Forsyth et al., 1996; Hall et al., 1998). It is one of the main basin bounding fault structures in the MVS and is considered to have had important controls on the development of Carboniferous sedimentation and volcanicity in the region. This includes controlling the locations of vents from which the lavas of the CPV were erupted, and following erosion of the lavas, local concentrations of detritus were deposited against in the margins of the lava block whilst fluvial sedimentation occurred elsewhere (BGS, 1988; Hall et al., 1998).

Summarised in Table 2.4, the stratigraphy of the Carboniferous-Devonian basin beneath the Glasgow area is dominated by cyclic successions of sedimentary rocks, of the Strathclyde, Clackmannan, and Scottish Coal Measures groups. These strata consist of sandstones and mudstones, with limestones, coals, ironstones and seatrocks, which were laid down in fluvial and fluviodeltaic environments that were established after the submergence of the underlying CPV basaltic lava flows produced during large scale Lower Carboniferous volcanism (Forsyth et al., 1996; Hall et al., 1998).

Stratigraphically below the lavas are the Lower Carboniferous aged Ballagan and Clyde Sandstone Formations and the Upper Devonian sandstones of the Kinnesswood Formation and the Stratheden Group (Table 2.4) (Forsyth *et al.* 1996; Hall *et al.* 1998). As a result of the Acadian Orogeny, there are no rocks of Middle Devonian age present in the MVS (Trewin and Thirlwall, 2002), and Upper Devonian aged sandstones, therefore, overlie the Lower Devonian strata unconformably.

Table 2.4. Generalized stratigraphic column.

Formation	Code	Age	Description	Thickness (m) Glasgow	Airdrie
Scottish Coal Measures Group (CMSC; Carboniferous; Westphalian)					
Upper Coal Measures Fm	UCMS	Bolsovian – Westphalian D	Sst, Slst, Mdst, Strk and C's, mostly reddened	85-100[1]	270[5]
Middle Coal Measures Fm	MCMS	Duckmantian	Sst, Slst, Mdst, Lst, C's and Strk's	160[1]	160-200[5]
Lower Coal Measures Fm	LCMS	Langsettian	Sst, Slst, Mdst, Strk and C's	100[2]	100-160[5]
Clackmannan Group (CKN; Carboniferous; latest Visean and Namurian)					
Passage Fm	PGP	Arnsbergian – Langsettian	Mainly Sst and fireclays	85[3]	75-200[5]
Upper Limestone Fm	ULGS	Pendleian – Arnsbergian	Sst, Slst, Mdst, marine Lst, C's and Strk's	250-285[3]	120-300[6]
Limestone Coal Fm	LSC	Pendleian	Sst, Slst, Mdst, Lst, C's and Strk's	270-340[3]	300-360[5]
Lower Limestone Fm	LLGS	Brigantian – Pendleian	Sst, Slst, Mdst, marine Lst, with thin C's	60-180[3]	100-210[5]
Strathclyde Group (SYG; Carboniferous; Visean)					
Lawmuir Fm	LWM	Brigantian	Mainly Sst, with Slst, Mdst, Lst, C's and Strk's	0-330[3]	0-200[5]
Kirkwood Fm	KRW	Asbian – Brigantian	Tuffaceous Mdst and tuffs	0-35[3]	0-35[5]
Clyde Plateau Volcanic Fm	CPV	Chadian – Asbian	Basalt, with tuffs and volcaniclastic sediments	300-500[3]	400-900[7]
Inverclyde Group (INV; Upper Devonian, Carboniferous; Famennian, Tournaisian and earliest Visean)					
Clyde Sandstone Fm	CYD	Chadian	White Sst, part pebbly, part concretionary	0-60[3]	0-100[5]
Ballagan Fm	BGN	Courceyan – Chadian	Mdst and thin dolomitic Lst (cementstones)	130-245[4]	20-170[5]
Kinnesswood Fm	KNW	Upper Devonian	Red and white Sst, and pedogenic Lst (cornstones)	75-250[3]	150[5]
Stratheden Group (SAG; Upper Devonian)					
Stockiemuir Sandstone Fm	SCK	Upper Devonian	Red and grey-purple cross-bedded Sst	400[3]	35[5]

This table, based on information from Forsyth et al. (1996) and Hall et al. (1998), lists the modern BGS stratigraphic terminology for the study area, which supersedes earlier versions. The Kinnesswood Formation dates from the uppermost Devonian (Famennian stage) (e.g., Marshall et al., 2019). (1) Forsyth & Brand (1986); (2) Forsyth (1979); (3) Hall et al. (1998); (4) Barnhill borehole, IGS (1978); (5) Forsyth et al. (1996); (6) Forsyth (1982); (7) Monaghan (2014).

2.7.3. Upper Devonian Sandstones of the Western Midland Valley of Scotland

This section describes the depositional environment, stratigraphy, and lithology of the primary geothermal targets in this thesis, the Upper Devonian sandstones of the Kinnesswood Formation and underlying Stratheden Group.

In the Devonian period, Scotland was located at subtropical latitudes in the southern hemisphere within the "Old Red Sandstone" continent of Laurussia (Mykura, 1991; Trewin and Thirlwall, 2002). The Caledonian Mountain range transected the continent and was the source of extensive sandy sediments deposited at the time. Lying to the south of the equator, the semi-arid conditions led to the deposition of aeolian desert and fluvial sandstones, which were informally known as the Old Red Sandstone (ORS) facies (Browne et al., 2002; Kendall, 2017).

The Upper Devonian sandstone sequence of the ORS in the MVS consists of the Stratheden Group and the overlying Kinnesswood Formation of the Inverclyde Group (Marshall et al., 2019), which are present at outcrop and in the subsurface in the western MVS (e.g., Figure 2.9-2.12). The stratigraphy of the Upper Devonian sandstone sequence varies throughout the western MVS as a consequence of localised depositional environments, uplift, and erosion (Table 2.5) (Paterson et al., 1990; Browne et al., 2002).

Table 2.5. Stratheden Group Formations in the western MVS (Paterson et al., 1990).

<table>
<tr><td>North of the Clyde Estuary</td><td colspan="2">South of the Clyde Estuary</td></tr>
<tr><td>Helensburgh-Dumbarton</td><td>West of Largs Fault Zone</td><td>East of Largs Fault Zone</td></tr>
<tr><td colspan="3">Kinnesswood Formation</td></tr>
<tr><td rowspan="4">Stockiemuir Sandstone Formation/
Rosneath Conglomerate Formation</td><td>Non-Sequence</td><td>Fairlie Sandstone Formation</td></tr>
<tr><td>Kelly Burn Sandstone Formation</td><td rowspan="3">Kelly Burn Sandstone Formation</td></tr>
<tr><td>Skelmorlie Conglomerate Formation</td></tr>
<tr><td>Wemyss Bay Sandstone Formation</td></tr>
</table>

Detailed in Table 2.6, the Stratheden Group formations in the western MVS consist mainly of cross-bedded sandstones and conglomerates. The majority of these sediments were deposited in braided fluvial river systems draining to the east-north-east (Figure 2.13a) (Bluck, 1978; Mykura, 1991; Ó Dochartaigh, 2004). However, upper sections of the Stockiemuir Sandstone Formation and the Fairlie Sandstone Formation are similar to the Knox Pulpit Formation of the Stratheden Group in Fife, and indicate that they were deposited in an arid, aeolian environment (Figure 2.13b) (Table 2.6).

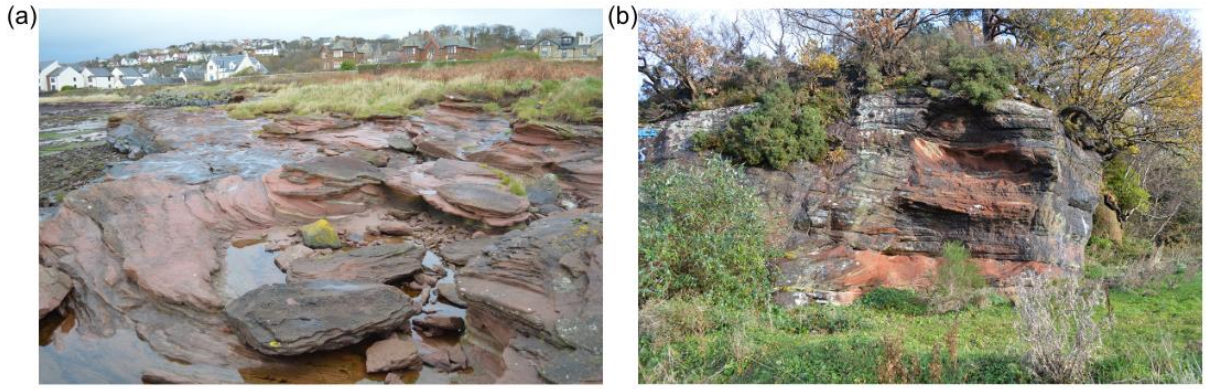

Figure 2.13. Field photograph of the fluvial Kelly Burn Sandstone Formation at Seamill, Ayrshire (a); and of the aeolian Stockiemuir Sandstone Formation at Havoc Hole, Dumbarton (b).

For example, features indicative of fluvial deposition such as mudstone clasts, pebbles, parting lineations, and micaceous films on bedding planes are absent from the upper part of the Stockiemuir Sandstone Formation, and instead fine ‘pin stripe’ laminations are present, characteristic of aeolian deposition (Hall and Chisolm, 1987). Furthermore, at outcrop the upper part of the Fairlie Sandstone Formation is well sorted with occasional well-rounded grains observed in coarser laminae (Chisolm and Dean, 1974), similar to the Knox Pulpit Formation.

Various authors have proposed that these formations are laterally equivalent due to their shared lithological properties and depositional environment, however this remains uncertain (Chisolm and Dean, 1974; Browne et al., 1985; 1987; Hall and Chisolm, 1987; Browne et al., 1999).

Respectively, the Stockiemuir Sandstone, Fairlie Sandstone and Knox Pulpit formations each have a transitional contact with the overlying Kinnesswood Formation, which marked a return to fluvial deposition (Paterson and Hall, 1986; Marshall et al., 2019). Throughout the MVS, the Kinnesswood Formation commonly comprises of fine to medium grained sandstones, arranged in upward fining fluvial cycles. The cross-bedded lower part is considered to have been deposited in fluvial river systems (Figure 2.14), while the fine-grained upper part represents the overbank sediment laid down upon the associated floodplains. This change in depositional environment is indicated by the presence of nodules and thin beds of concretionary carbonate, or cornstones (Paterson et al., 1990; Forsyth et al., 1996; Hall et al., 1998).

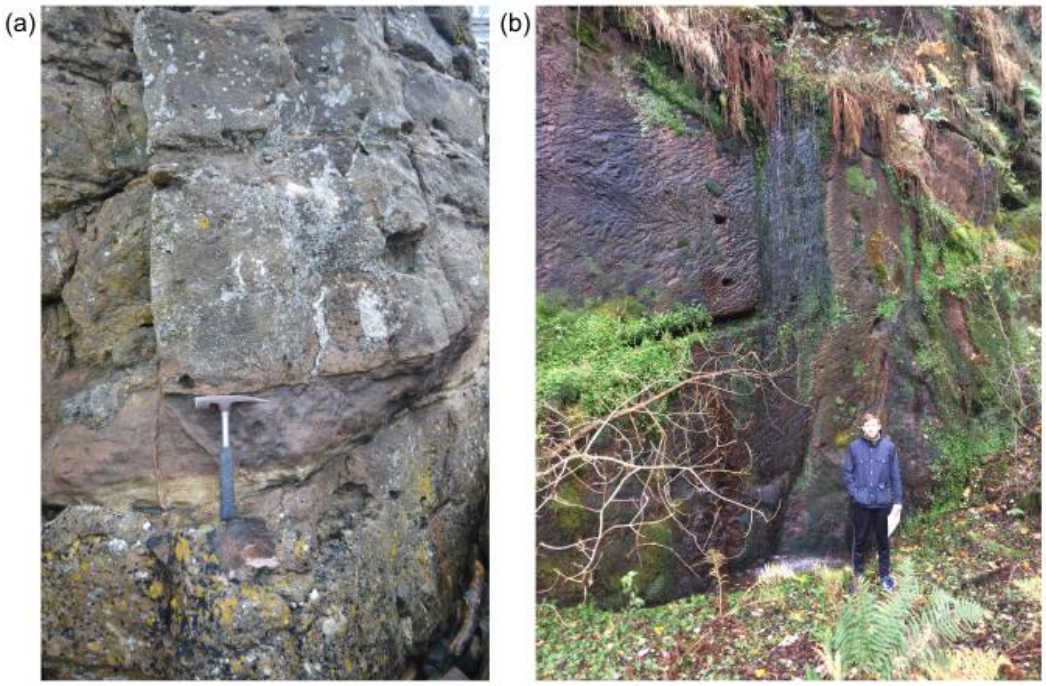

Figure 2.14. Field photograph of the Kinnesswood Formation at Gourock (a); and of the Kinnesswood Formation exposed at a quarry face in the Bonhill Quarry, Dumbarton (b).

The Upper Devonian sandstones of the Kinnesswood Formation and Stratheden Group are encountered in boreholes (generally c. <600 m depth) throughout the MVS. Due to a scarcity of deep boreholes within the western MVS, knowledge of the presence and properties of the Upper Devonian sandstone sequence at depth is limited. However, the presence of Upper Devonian aged sandstones within deep sedimentary basins in the MVS has been inferred from seismic survey interpretations (e.g., Penn et al., 1984; Monaghan et al., 2012) and gravity modelling (BGS, 1988; Hall et al., 1998), and the sequence was encountered at c. 2000 m depth within the Inch of Ferryton 1 borehole [NS 907 901] (Monaghan, 2014).

Table 2.6. Summary of the lithology and depositional environment of Upper Devonian sandstone formations in the western MVS. Includes the Knox Pulpit Formation from Fife, for comparison.

Unit	Lithological Description	Depositional Environment	Thickness
WEM	Cross-bedded, fine grained red-brown sandstone.	Mainly fluvial origin. Deposited in a restricted basin. May contain aeolian deposits.	~50 m
SKM	Conglomerate with clasts of quartz, schist, quartzite and lava, and pebbly sandstone beds.	Mixed alluvial fan and fluvial origin. Deposited from a braided river system flowing to the E-NE.	20-60 m
KBS	Red, medium-coarse grained, cross-bedded, pebbly sandstone with conglomerate beds.	Fluvial. Deposited in a braided river system flowing to the E-NE.	1500 m
FAS	White, fine grained, cross-bedded, and finely laminated sandstones with beds containing quartz pebbles.	Mixed fluvial and aeolian origin.	300 m
RON	Conglomerate with clasts of quartz, quartzite, metamorphic and igneous rock with pebbly sandstone beds.	Fluvial origin.	>1000 m
SCK	Red, fine to coarse grained, cross-bedded sandstone. Lower part contains scattered mudstone clasts and quartz pebbles. Upper part contains fluvial sediments interbedded with aeolian cross bedded sandstones.	Mixed origin. Upper part is aeolian. Lower part is fluvial, deposited from a braided river system flowing to the E-NE.	>400 m
KPF	White, very fine to coarse grained, weakly cemented, feldspathic sandstone.	Aeolian origin.	170 m
KNW	Red, yellow, white, grey-purple, fine to medium grained sandstones with nodules and thin beds of carbonate/limestone (cornstones).	Fluvial origin. Lower part consists of cross-bedded sandstones deposited in river channels. Upper part contains cornstones representing the overbank sediment laid down on the associated floodplain.	<400 m

From Bluck (1978); Paterson et al. (1990); Forsyth et al. (1996); Hall et al. (1998); Monro (1999); Browne et al. (2002). Abbreviations are: WEM; Wemyss Bay Sandstone Formation, SKM; Skelmorlie Conglomerate Formation, KBS; Kelly Burn Sandstone Formation, FAS; Fairlie Sandstone Formation, RON; Rosneath Conglomerate Formation, SCK; Stockiemuir Sandstone Formation, KPF; Knox Pulpit Formation, KNW; Kinnesswood Formation. The stratigraphy and lateral variation of the Stratheden Group of the MVS is illustrated in Figure 8 of Browne et al. (2002).

2.7.4. Crustal Structure of the Western Midland Valley of Scotland

The current understanding of the deep crustal structure of the Glasgow area was derived from a series of Midland Valley Investigation by Seismology (MAVIS) seismic refraction surveys (Davidson et al., 1984; Conway et al., 1987; Dentith and Hall, 1989; 1990). Interpretation of the MAVIS seismic profiles identified three distinct seismic refractors, defining four upper crustal layers beneath the MVS. Beneath Glasgow, the MAVIS interpretation indicates a 2-2.5 km thick Carboniferous and Upper Devonian sedimentary basin, a 1.5 km thick Lower Devonian and Lower Palaeozic sequence and a 3.5 km thick upper crystalline basement, overlying the lower crystalline basement (Figure 2.15).

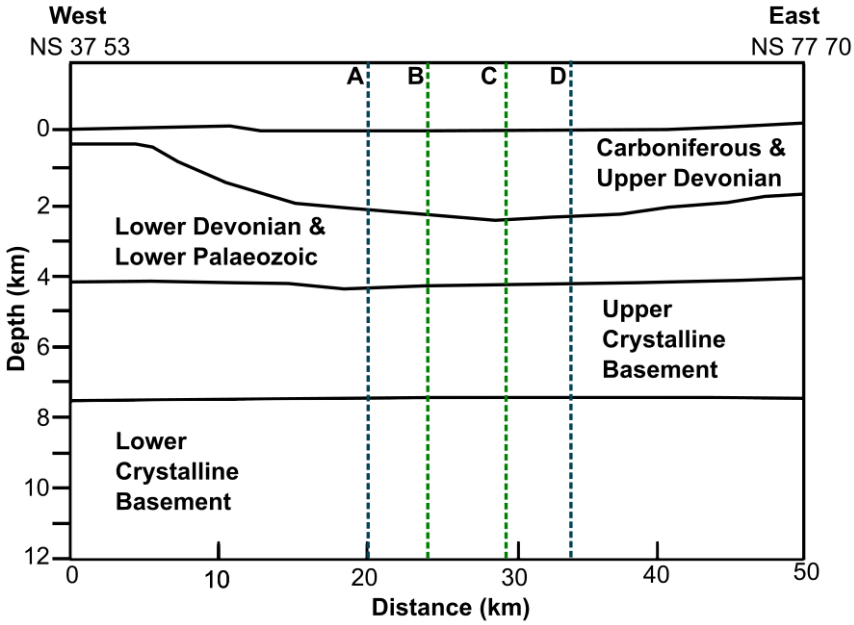

Figure 2.15. Section of the MAVIS 4-Layer crustal model in the western MVS (Dentith and Hall, 1990). A: NS 56 61, B: NS 60 63, C: NS 64 64 and D: NS 68 66. The MAVIS line crosses the regional gravity model at A-D, and the gravity survey area at B-C (see Chapter 3).

The nature of the crystalline basement and Lower Palaeozoic rocks underlying the MVS have been subject to extensive research over recent decades. During the early phase of the Caledonian Orogeny, the MVS terrane is understood to have collided with the continental margin of Laurentia (Figure 2.16) (Bluck et al., 1980), causing the obduction of oceanic crustal rocks. This is proven in the Girvan-Ballantrae area of Ayrshire (Figure 2.9), where sedimentary sequences of Ordovician and Silurian age unconformably overlie an ophiolitic basement (Figure 2.9) (Stone, 2008; Stone and Rushton, 2018). Various authors have proposed that following the collision of the MVS terrane with the Laurentian continental margin, a volcanic arc complex was active within the MVS until at least the Middle Ordovician at c. 455 Ma (Figure 2.16) (Badenzski et al., 2019 and references therein).

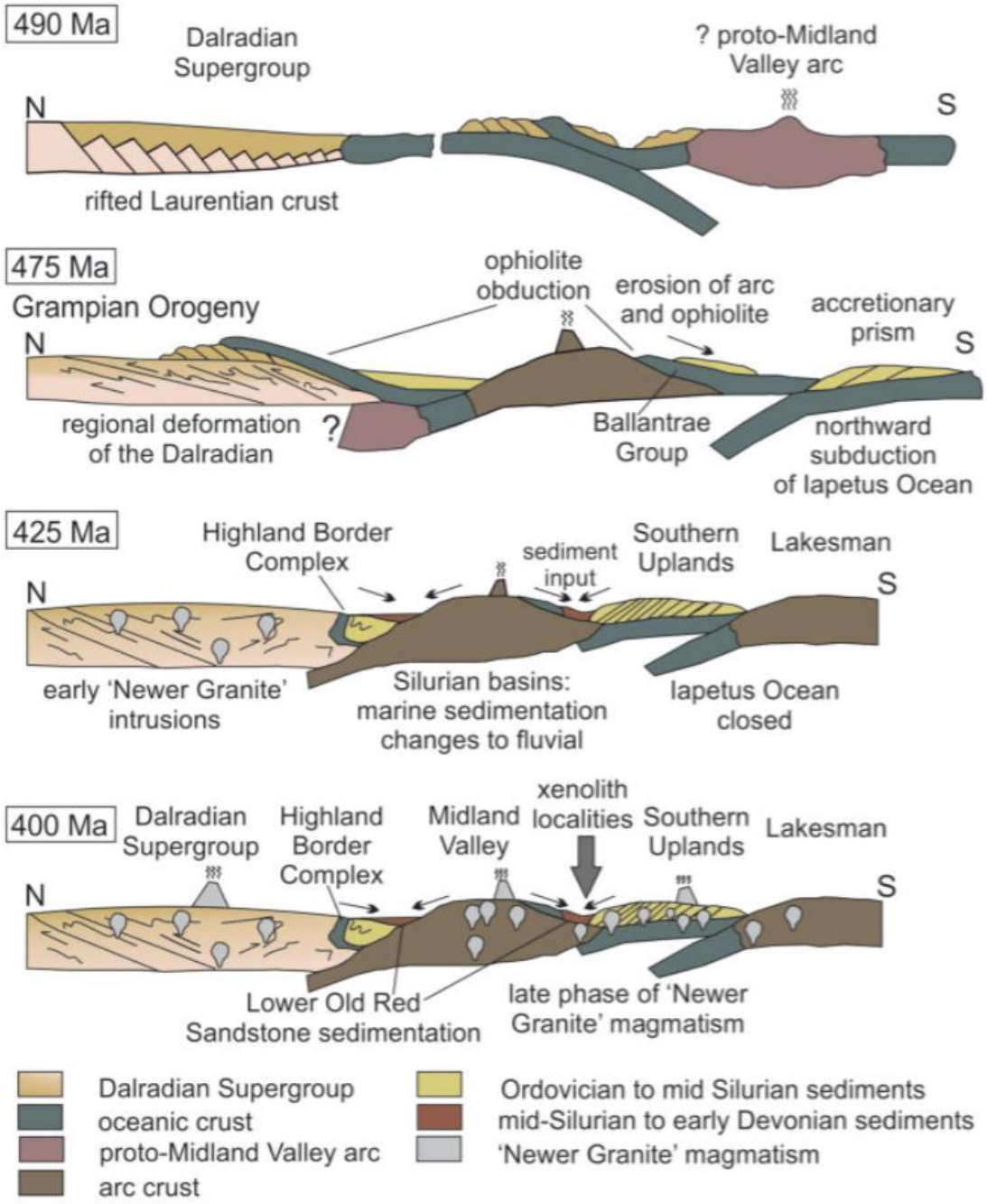

Figure 2.16. Schematic illustrations (after Strachan, 2012; Tanner, 2014) depicting the plate-tectonic setting of southern Scotland from Late Cambrian to Early Devonian. From Badenzski et al. (2019).

Significant fault movement occurred on the Highland Boundary Fault and Southern Upland Fault as a result of the collision of the MVS with Laurentia, displacing rocks in the upland areas adjacent to the MVS terrane. As illustrated in Figure 2.16, during the Silurian and Early Devonian (425-400 Ma), basins were formed in the MVS terrane where sediment input from eroded uplands were deposited in marine and fluvial environments (e.g., the Strathmore Basin shown in Figures 2.9 and 2.10). This period was also characterised by the intrusion of "Newer Granites" over a wide region of Scotland, including latterly in the MVS terrane (Figure 2.14) (Badenzski et al., 2019).

The proposed volcanic arc crust is not exposed within the MVS, however small inliers of Ordovician and Silurian age occur in the Lesmahagow area, the Pentland Hills and in south Ayrshire (Figure 2.9). Deep crustal felsic xenoliths in East Ayrshire and East Lothian, brought to the surface by Permo-Carboniferous volcanism, were proven to include metadiorite and metatonalite protoliths (Badenzski et al., 2019). Based upon U-Pb zircon dating, the metadiorite xenoliths were interpreted as Silurian-Devonian granite plutons, and the metatonalite xenoliths were interpreted as samples of a buried Late Ordovician magmatic arc (Badenzski et al., 2019). Inherited zircons with similar Late Ordovician age were also found to be present in the metadiorites suggesting that the Devonian "Newer Granites" intruded within or through this Late Ordovician MVS arc/crustal structure which possibly underlies much of the MVS (Badenzski et al., 2019).

The presence of radiothermal granite within the basement is one hypothesis for regions of above-average heat flow in the MVS (e.g., Younger et al., 2012; Gillespie et al., 2013). However, measurements of the heat production rate of the Distinkhorn granodiorite intrusion in Ayrshire are reported as 2.0 $\mu W\ m^{-3}$ (Lee et al., 1984; Gillespie et al., 2013). This value is low in comparison to the high heat production rate (3.7 $\mu W\ m^{-3}$) in analogous granite intrusions in the Weardale batholith of north-east England (England et al., 1980).

2.7.5. Synthesis of Literature Review

This literature review has informed the methodology and analysis implemented within this thesis to investigate the geothermal resource within Upper Devonian sandstones beneath Glasgow. In Chapter 3, the bedrock geology of the Glasgow area and the presence of major faults, informs the selection of a new gravity survey fieldwork area. Furthermore, the data shown in Table 2.4, in addition to the interpreted crustal structure and nature of the crystalline basement, provide constraints to input parameters utilised in the development of a structural geological model of the gravity survey area. In Chapter 4, the mineralogical and physical properties of the Upper Devonian sandstones of the western MVS, shown in Table 2.6, were investigated to assess the effects of deposition and diagenesis on porosity. In Chapter 5, the re-evaluation of measurements of heat flow, geothermal gradient, and thermal conductivity within boreholes in the western MVS was undertaken by implementing the theory outlined in section 2.4. The results of this analysis were utilised within Chapter 6, where corrections to heat flow to account for the effects of palaeoclimate and topography were applied. Then, the thermal power output of geothermal doublet wells located at sites in Glasgow's East End was calculated. Direct heat use applications of Glasgow's geothermal resource were then identified such as those discussed in section 2.3.

Chapter 3. Development of a Structural Geological Model of Eastern Glasgow

3.1. Introduction

This chapter investigated the structural geology of eastern Glasgow to determine the geometry of the Dechmont Fault, and the extent and depth of the Upper Devonian sandstones of the Kinesswood Formation and the Stratheden Group. This was achieved by designing and conducting a new gravity survey and developing a 3-D numerical model of the structural geology of the area. This chapter first presents the rationale for conducting this research and the aims of the chapter. The gravity survey fieldwork is then described, reporting its design process and implementation followed by the data analysis and 3-D numerical modelling. Finally, the resulting structural interpretation and implications for geothermal energy in Glasgow are discussed. By developing a structural geological model of the area, the depth and extent of the geothermal resource in the Upper Devonian sandstones beneath Glasgow was determined. The results of this chapter are utilised in subsequent chapters of this thesis to quantify the geothermal resource in the Kinnesswood Formation and Stratheden Group beneath eastern Glasgow, and to identify candidate locations for deep geothermal projects to take place based upon the presence of prospective end-users of the geothermal heat.

3.2. Chapter Aim

One significant barrier to the development of the geothermal sector in Scotland is the current limited knowledge level of the resource (Gillespie et al., 2013). To aid the development of deep geothermal energy in Scotland, Gillespie et al. (2013) recommended that a National Geothermal Exploration Programme should be implemented. It was proposed that this programme would comprise of two parts, first, a research programme to identify deep geothermal prospects, and second, a physical exploration programme consisting of a geophysical survey to identify target resources followed by deep exploratory drilling.

Addressing the recommendation of Gillespie et al. (2013), as a first step in investigating the geothermal resource in the Upper Devonian sandstones of the Kinnesswood Formation and underlying Stratheden Group beneath Glasgow, the aim of this chapter was to conduct a new gravity survey to determine the geological structure and thus the extent and depth of the geothermal resource beneath Glasgow.

The specified target region was eastern Glasgow, where the main structural features include the deep sedimentary basin in the Lanarkshire Basin, and the basin-bounding, north-west trending Dechmont Fault. Specifically, the aims of this chapter were to:

- Collect new gravity data from a high-density gravity survey of eastern Glasgow,
- Develop a 3-D structural geological model of eastern Glasgow using gravity forward modelling based upon the newly collected gravity data,
- Examine seismic survey datasets to constrain the 3-D structural geological model,
- Determine the geometry of the Dechmont Fault and the extent of the buried footwall escarpment,
- Determine the extent and depth of the primary geothermal target in the Upper Devonian sandstones in the deep sedimentary basin in the hanging wall of the Dechmont Fault,
- Identify locations where the Dechmont Fault may intersect the Upper Devonian sandstone sequence, thus creating either a potential secondary geothermal target of fault induced groundwater flow via permeable fractures in the fault damage zone or re-interconnection of intergranular porosity.

The results of this analysis were then utilised within Chapter 6 of this thesis to quantify the geothermal resource in the Upper Devonian sandstones beneath eastern Glasgow, and to select candidate locations for future deep geothermal drilling projects to take place.

3.3. Rationale

3.3.1. Use of Gravity Surveying in Geothermal Exploration

Gravity surveying is an established technique used in geothermal exploration to identify subsurface geological structures. By assessing patterns of Bouguer gravity anomalies, interpretations are made of the location and extent of structural features and potential geothermal reservoirs (Duprat, 1985). Examples of the application of gravity surveying in geothermal exploration include assessing structural controls of thermal springs and geothermal reservoirs (Atef et al., 2016; Nishijima and Naritomi, 2017; Uwiduhaye et al., 2018; Maithya et al., 2020; Njeudjang et al., 2020; Pocasangre et al., 2020), the presence of faults and fault zones (Guglielmetti et al., 2013; Carrier et al., 2020), and the extent of fracture porosity in fault zones (Schill et al., 2010; Altwegg et al., 2015).

3.3.2. Targeting Fault Zones for Geothermal Exploration in the UK

The naturally high permeability of faults and their associated damage zones have been targeted by various geothermal projects in the UK. The Science Central project, now Newcastle Helix, involved drilling adjacent to the Ninety Fathom Fault in the city centre of Newcastle upon Tyne. However, the Dinantian aged sandstone in this locality proved to be extremely tight, and there was no evidence of the upflow of thermal water associated with the fault, so the project ended as a failure (Westaway and Younger, 2016; Younger et al., 2016).

However, as discussed in Westaway et al. (2019), drilling took place in the footwall of the Ninety Fathom fault, some 1.6 km from its footwall cut-off, being determined by the location of the Science Central development site in Newcastle upon Tyne city centre, placing the well bottom c. 3 km from the fault. The drilling of this well was not preceded by any research process, analogous to the present study, concerned with validation of aspects of the structural geology which are critical to the proposed geothermal development.

Another example is the Bishop Auckland geothermal project in County Durham, north-east England. This project planned to target the Butterknowle Fault zone, drilling to intercept the Castle Fault at c. 1.6 km depth beneath Auckland Castle, near the town of Bishop Auckland, where temperatures of >80 °C were estimated (Westaway et al., 2019).

High density gravity surveying and gravity forward modelling were used to validate the conceptual model assumed for this project in order to de-risk the drilling process. The author was directly involved within this project by taking part in the gravity surveying fieldwork in County Durham in October 2015 and processing the gravity survey data. Unfortunately, a subsequent application for funding towards the capital costs of this project did not succeed and as such there are no plans currently for further geothermal investigation at this site.

The availability of in-situ stress data for Britain is very limited (Westaway, 2020), however based upon this limited dataset, in the west of Scotland, the maximum horizontal compressive stress axis is approximately north-north-west to south-south-east (Baptie, 2010). Fractures and faults that are orientated within ± 30 ° of the present-day maximum horizontal compressive stress axis are more likely to display permeably open apertures (Ellis et al., 2014) and may be viable targets for deep geothermal exploration. A fault orientated north-west to south-east, such as the Dechmont Fault in Glasgow, is therefore within 30° of the maximum horizontal compressive stress axis.

The role of the Dechmont Fault as a pathway for deep regional groundwater flow is currently unknown, however given the orientation of the fault, there may be permeably open apertures in the associated fault zone. Furthermore, where post-cementation fracturing has occurred, intergranular porosity within the Upper Devonian sandstone aquifer which was previously lost due to cementation (see Chapter 4) may well have been re-interconnected (Younger et al., 2016), offering scope for significant fluid flow and thus geothermal heat production.

The Dechmont Fault may, therefore, have a significant influence on the magnitude of the geothermal resource in eastern Glasgow and thus both the geometry of the fault and presence of the Upper Devonian sandstone sequence warrant investigation.

3.4. Methodology

This section reports on the design and implementation of the gravity survey and the development of the 3-D geological model. First, the gravity survey fieldwork was designed and carried out to collect new gravity data in eastern Glasgow. Gravity reduction corrections were then applied to this new data to calculate Bouguer gravity anomalies. This new dataset was then gridded using ERDAS ER Mapper GIS software, and input to the 3-D gravity forward modelling software, Noddy. An initial structural geological model of the survey area was constructed, constrained by the newly measured gravity data, borehole data and interpretations of seismic reflection surveys. A sensitivity analysis and iterative modelling procedure was then carried out, resulting in two alternative structural geological model solutions which match the newly measured Bouguer gravity anomalies. By developing these structural geological models of the survey area, the geometry of the Dechmont Fault and upper and lower estimations of the depth to the Upper Devonian sandstone sequence were determined.

3.4.1. Gravity Survey Area and Geological Setting

A ~29 km^2 survey area was chosen from NS 600 575 in the south-west to NS 645 640 in the north-east, spanning the areas of Castlemilk, the Cathkin Braes, Cambuslang, Rutherglen, Dalmarnock, Bridgeton and Parkhead in Glasgow's East End (Figure 3.1).

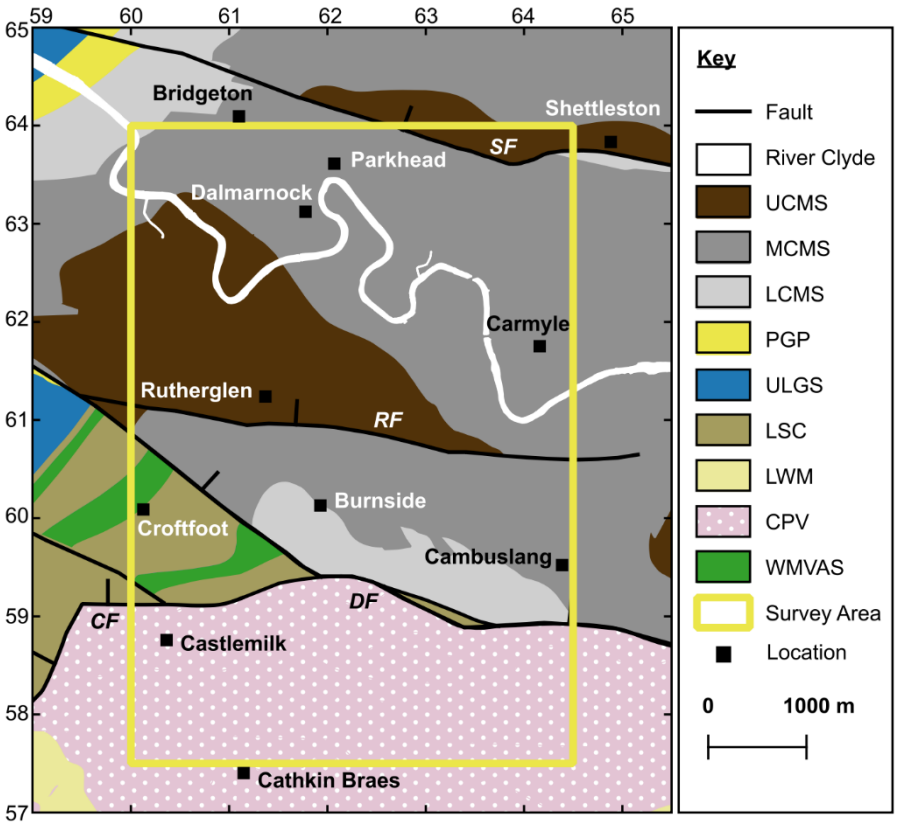

Figure 3.1. Bedrock and structural geology of the survey area. The co-ordinates (north and east) are in kilometres within British National Grid (BNG) 100 km quadrangle NS. Geological Map Data BGS © UKRI 2021.

The geology of the survey area is diverse, with distinct variation in the rocks which outcrop in the footwall and hanging wall of the Dechmont Fault (Figures 3.1-3.3), as well as variation in the geometry and displacement of the fault itself (Figure 3.3). Between NS 553 649 and NS 595 613, the displacement of the Dechmont Fault is 650 m, where the fault offsets the Limestone Coal Formation and Upper Limestone Formation of the Darnley Basin against the Coal Measures within the half-graben of the Rutherglen Basin (Figure 3.1-3.3). The Dechmont Fault extends to NS 619 594 where it adjoins the Castlemilk Fault. At this point the displacement of the Dechmont Fault increases to 1200 m where it offsets the CPV of the Cathkin Braes against the Coal Measures of the Lanarkshire Basin at Rutherglen and Cambuslang (Figure 3.1-3.3).

There are a number of other faults which traverse the survey area. The most significant of these are the W-E trending Shettleston, Easterhouse and Comedie faults, and the SW-NE trending Castlemilk Fault (Figure 3.1-3.3).

Given the difference in density between the igneous and sedimentary rocks, and changes in the thickness of the sedimentary basin within the survey area, clear Bouguer gravity anomaly gradients were anticipated.

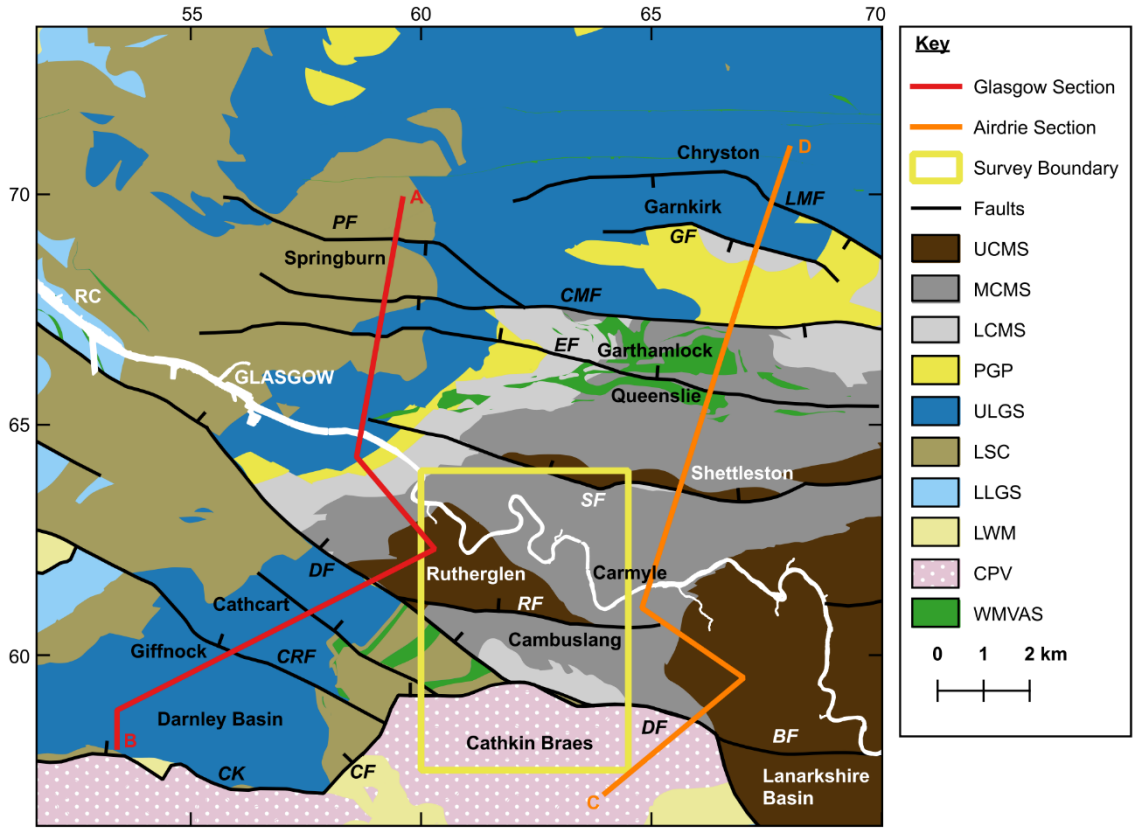

Figure 3.2. Bedrock geology of Glasgow. Survey area, and cross sections from British Geological Survey (1992, 1993) shown, corresponding to Figure 3.3. The co-ordinates (north and east) are in kilometres within BNG 100 km quadrangle NS. Geological Map Data BGS © UKRI 2021.

Figure 3.3. Geological cross sections from British Geological Survey (1993) (A-B) and British Geological Survey (1992) (C-D). Reproduced with the permission of the British Geological Survey ©UKRI 2021. All rights Reserved.

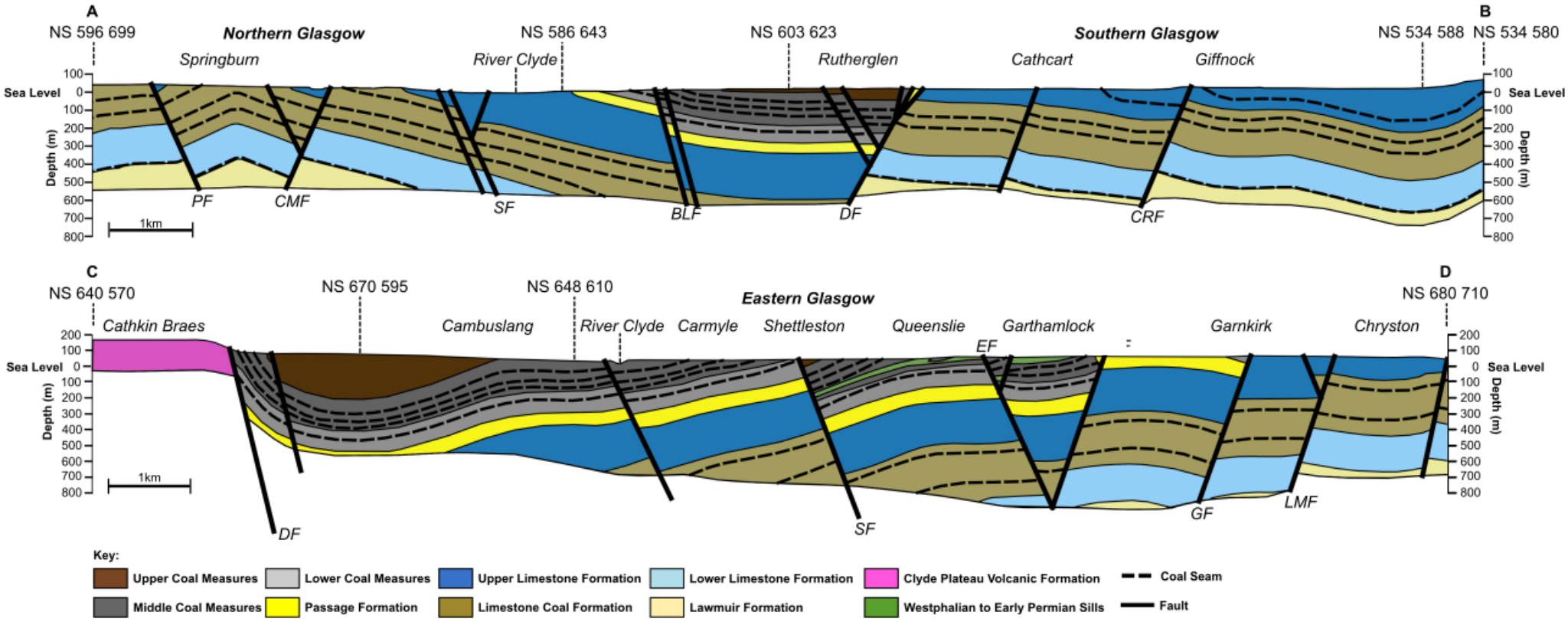

3.4.2. Design of Gravity Survey

To inform the design of the new gravity survey, the publicly available British Geological Survey (BGS) UK Land Gravity dataset was cropped to those data points measured within, and surrounding, the proposed survey area (Figure 3.4).

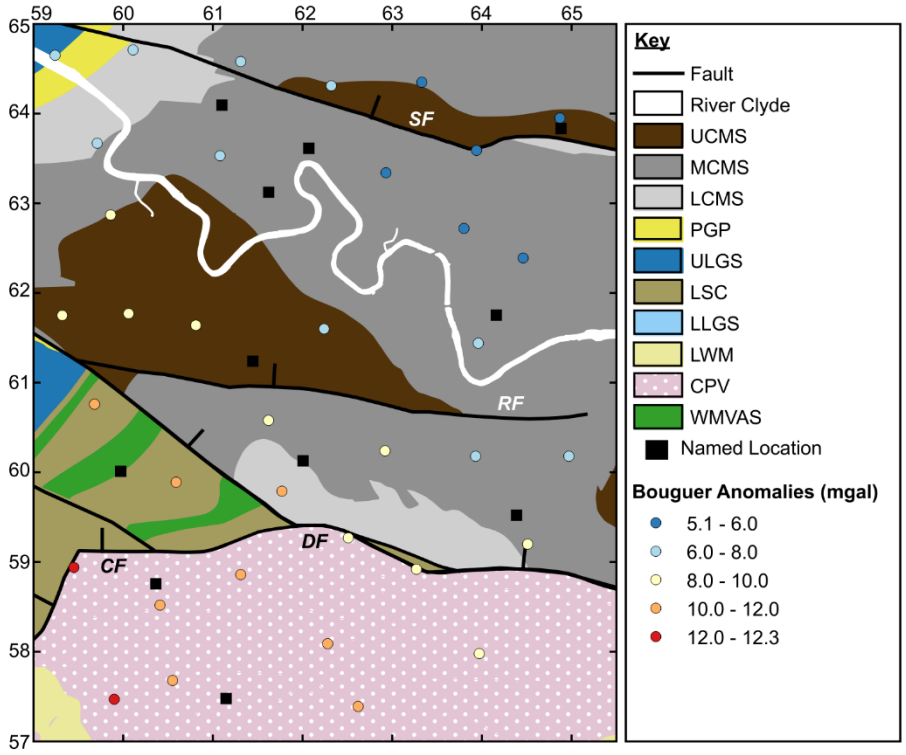

Figure 3.4. Geological map of the survey area with BGS Land Gravity points shown. The 'named locations' correspond to those in Figure 3.1. The co-ordinates (north and east) are in kilometres within BNG 100 km quadrangle NS. Geological Map Data BGS © UKRI 2021. Contains British Geological Survey materials © UKRI 2021.

For each data point, the BNG reference, height (h), free air gravity anomaly (Δg_f), terrain correction (Δg_T), Bouguer correction (Δg_B), and Bouguer gravity anomaly Δg, were provided in the BGS Land Gravity dataset. It was noted that Δg_T and Δg_B had been calculated using a rock density of 2700 kg m^{-3}, however this standard value (used in routine processing of gravity data) was not appropriate for rocks within the study area and the values of Δg_T, Δg_B and Δg were therefore recalculated. The values were recalculated using a density of ~2500 kg m^{-3} for the Coal Measures, 2740 kg m^{-3} for the CPV and 2550 kg m^{-3} for the Clackmannan Group sediments (Hall et al., 1998; Kimbell et al., 2006).

Values of Δg_T and Δg_B were recalculated by multiplying the original value by the ratio of densities, as appropriate for the stratigraphic unit (e.g., for a data point measured in the CPV outcrop of the Cathkin Braes; the revised Δg_B = original Δg_B x 2740/2700). The resulting values of Δg were then recalculated using Equation 3.1:

$$\Delta g = \Delta g_F - \Delta g_B + \Delta g_T$$

Equation 3.1.

These Bouguer gravity anomalies were then mapped across the survey area (Figure 3.4), enabling gaps in the coverage of the data to be examined. There were 28 existing data points within the survey area, typically spaced at one per 1-2 km^2 of land area but were unevenly distributed. The new gravity survey was designed to address this by filling the gaps in the existing coverage with an increased density of data points, thus enabling a more detailed analysis of the pattern of Bouguer gravity anomalies and the development of a more accurate structural geological model of the area, to determine the extent of the geothermal resource.

3.4.3. Gravity Survey Fieldwork and Data Processing

Data Collection

Gravity surveying fieldwork was undertaken by the author, two MSc students and PhD co-supervisor, Dr Rob Westaway, during May-June 2016. While in the field the following procedure was followed to measure new gravity data points and the necessary supplementary terrain, elevation, and location data:

(1) raw gravity measurements were made using a Lacoste-Romberg gravimeter (Figure 3.5),

(2) variations in the height of terrain surrounding each measurement site were noted for use within Hammer's (1939) terrain correction procedure,

(3) the coordinates and elevation of each measurement site were recorded using a differential GPS (dGPS) roving station deployed at each site (Figure 3.5), and a dGPS base station located on the roof of the James Watt South Building in the University of Glasgow (NS 570 666), where its internal batteries were connected to the mains electricity supply to enable continuous recharging during operation,

(4) British National Grid (BNG) coordinates and provisional heights were collected at each site using a handheld GPS receiver,

(5) repeated measurements were made every 3-4 hours at the gravimeter base station (data point TESC at NS 622 606; Figure 3.6) to record gravimeter drift.

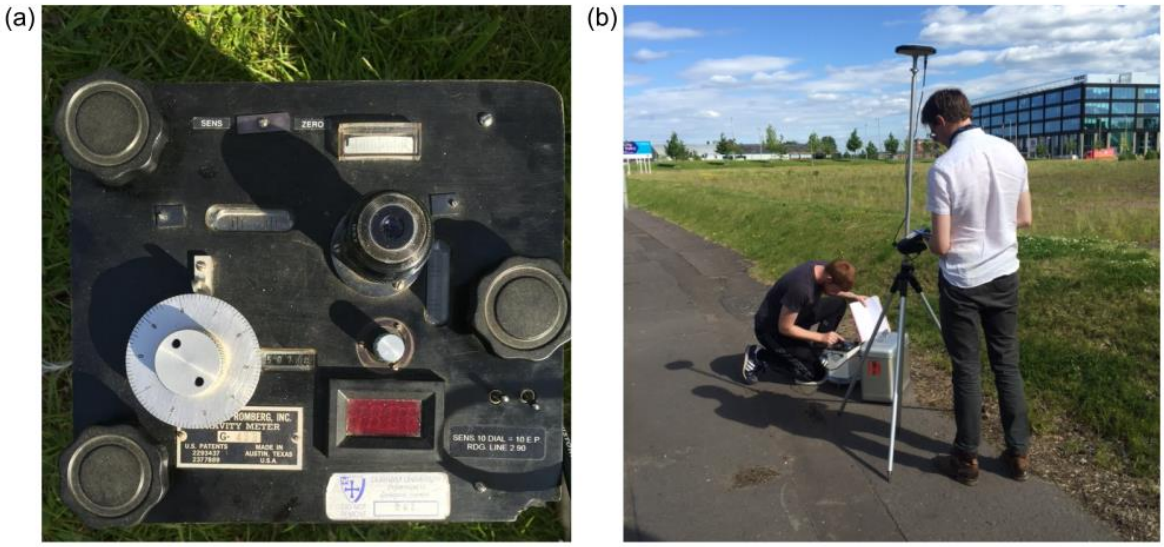

Figure 3.5. Field photograph of the Lacoste-Romberg gravimeter used within the survey (a), and example of field procedure showing dGPS roving station and the author taking a measurement (b).

The survey was not referenced to a measurement of absolute gravity but instead tied directly to the existing BGS Land Gravity dataset. This was possible as a number of the existing BGS gravity measurements were co-located with Ordnance Survey (OS) benchmarks. Unfortunately, most of these benchmarks had been destroyed; the walls on which they had been inscribed having been demolished or were inaccessible. Measurements were taken at two benchmarks where a gravity measurement had been previously made by BGS. Due to incorrect height measurements at one of the benchmarks, which may have been due to limited sky visibility, only one benchmark was suitable for use as a reference. The measurement at this location was made on the 30th of March 2016, at an OS benchmark located on the wall of 161 Brownside Road at NS 62925 60234 (data point 161; Figure 3.6).

In total, 161 new gravity measurements were made across the survey area (Figure 3.6), at a spacing of 300-500 m in residential areas, increasing to 500-1000 m in the Cathkin Braes to the south of the survey area where access issues were encountered on private agricultural land. Thirty-three measurements were made in the footwall of the Dechmont Fault and the remainder at greater density across the surface trace, buried escarpment and hanging wall of

the fault. In anticipation of the 3-D numerical modelling, measurements were made at a grid of points rather than along one or more linear profiles, and Bouguer gravity anomalies were measured to an accuracy of 0.1 mgal.

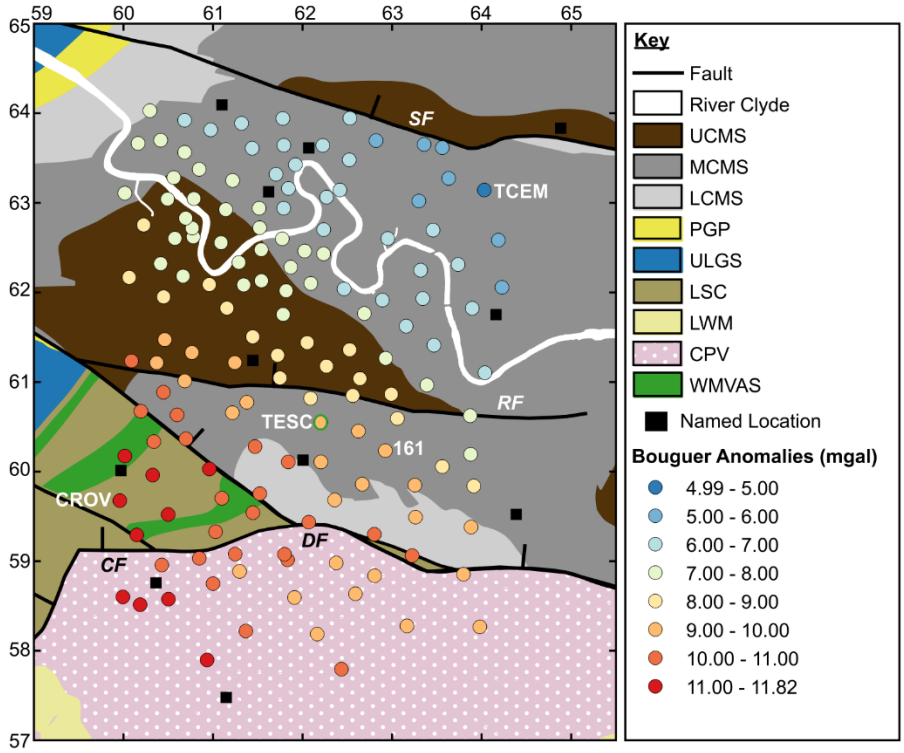

Figure 3.6. Geological map of the survey area with newly measured Bouguer gravity anomalies shown. The named locations correspond to those in Figure 3.1. Abbreviations are given in Figure 3.1. The co-ordinates (north and east) are in kilometres within BNG 100 km quadrangle NS. Geological Map Data BGS © UKRI 2021.

Data Processing

After each day in the field, the GPS signal recordings from the base station and roving station were retrieved. This data was processed using GNSS solutions software to determine accurate heights and coordinates of all points, substituting measurements from topographic contours and Digital Terrain Models (DTM's) mapped in QGIS (Geographic Information System) software for the few points where dGPS did not yield reliable results.

Further data processing was necessary at this stage to convert the GNSS solutions software output from the global Cartesian coordinate system to BNG coordinates. The differential height measurements obtained from dGPS were converted to absolute heights using the height of the aforementioned benchmark at data point '161'. To calculate the height above sea level, this benchmark height of 54.235 m was subtracted from the height of each measurement point. For the majority of points, excluding those where trees or buildings

reduced sky visibility, the GNSS software yielded differential heights accurate to within millimetres.

The raw gravity data were then corrected for the effects of gravimeter drift, latitude, and terrain. These corrections use standard procedures detailed in Appendix 3.A. The tidal corrections to gravity were calculated using the TSoft (Van Camp and Vauterin 2005) and Micro-g LaCoste QuickTide Pro software packages. Due to the inland location, the tidal corrections were small, never larger in magnitude than ~0.1 mgal, and closely consistent between software packages. The values from QuickTide Pro were applied to the raw data.

Then, using accurate heights from the dGPS, the free air and Bouguer corrections were determined (the latter for a density of 2500, 2550 or 2740 kg m^{-3} as appropriate for the surface geology). The standard formulae used for free air and Bouguer corrections are detailed in Appendix 3.A and are widely published in textbooks (e.g., Telford et al. 1990). Finally, the latter corrections were then applied to the gravity data in order to determine the Free Air and Bouguer gravity anomalies.

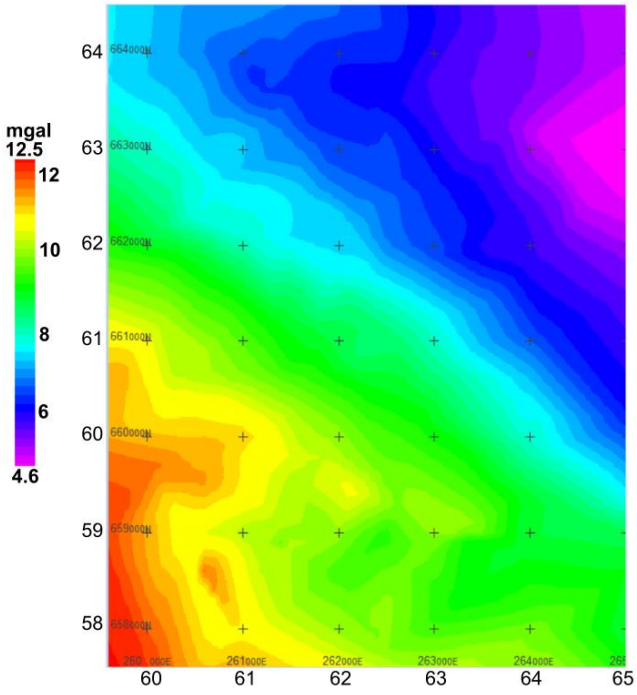

Figure 3.7. Gridded Bouguer gravity anomalies.

The resulting data were merged with those from the re-evaluated BGS Land Gravity dataset, imported into ERDAS ER Mapper software and gridded using a triangulation algorithm with 100 m point spacing. The gridded data were then imported to the 3-D gravity forward modelling software, Noddy, with the results shown in Figure 3.7. The occurrence of gridding

artefacts around the edges of this area was minimised by the inclusion of BGS Land Gravity points located outside of the survey area.

Illustrated in Figure 3.6 and Figure 3.7, the pattern of Bouguer gravity anomalies varies across the footwall, surface trace, buried footwall escarpment and hanging wall of the Dechmont Fault. The highest of the newly measured values was 11.8 mgal at point 'CROV', in the Croftfoot area of Glasgow, and the lowest was 4.99 mgal at point 'TCEM', in Tollcross (Figure 3.6).

The Bouguer gravity high in the footwall of the Dechmont Fault centres over the CPV outcrop in Castlemilk and the Cathkin Braes, and the Namurian-Visean aged sediments of the Croftfoot area (Figure 3.6). This was expected given the presence of higher-density rocks at outcrop such as the CPV lavas and Westphalian-Early Permian igneous intrusions (Figure 3.6). This trend of high Bouguer gravity anomalies extends across the surface trace of the Dechmont Fault into the Coal Measures outcrop at Cambuslang and Burnside and northwards to the Upper Coal Measures basin at Rutherglen (Figure 3.6). The high Bouguer gravity anomalies present here may indicate the presence of the buried footwall escarpment of the Dechmont Fault consisting of high-density strata of the CPV, Lower Devonian and Lower Palaeozoic rocks, and a shallower crystalline basement.

Then, there is a marked transition in the magnitude of Bouguer gravity anomalies from NS 580 630 to NS 650 595, where values drop by 0.5-1.5 mgal, and gradually decrease to a Bouguer gravity low to the north-east of the survey area at Tollcross and Parkhead (Figure 3.6). This may indicate the presence of an eastwards to north-eastwards deepening sedimentary basin containing the deeply buried target geothermal resource within the Upper Devonian sandstone sequence.

These initial interpretations were examined further in section 3.4.5 through the development of a structural geological model, constrained by the new gravity data and existing seismic reflection survey interpretations (section 3.4.5), to determine the geometry of the Dechmont Fault, and the depth and extent of the deep geothermal resource beneath eastern Glasgow.

3.4.4. Creation of a Structural Geological Model using Gravity Forward Modelling

This section describes the workflow involved in developing the 3-D structural geological model of the survey area. To do this, the gravity forward modelling software package, Noddy was used. This former commercial software package is currently supported for academic use by Tectask, the International Union of Geological Sciences (IUGS) commission for structural geology and tectonics.

The aim of the modelling process was to produce a structural geological model which predicts Bouguer gravity anomalies that match those measured in the new gravity survey, thus indicating that the model accurately represents the geology of the survey area. From this, the geometry of the Dechmont Fault and extent and depth of the geothermal resource beneath eastern Glasgow were then determined.

Noddy software requires the user to determine a geological 'history' for the study area, from which the 3-D model is produced, and predicted Bouguer gravity anomalies are calculated. The predicted Bouguer gravity anomalies are then compared to the gridded, measured Bouguer gravity anomalies which are imported from ERDAS ER Mapper to Noddy. This allows the Noddy structural geological model to be validated against the measured data, mismatches between the measured and predicted gravity anomalies identified, and solutions tested.

The Bouguer gravity anomalies predicted by the Noddy structural geological model were dependent upon the modelled stratigraphy, density, and geometry of the geological features of the survey area. Achieving a satisfactory model solution was thus an iterative process which involved the development of an initial model, followed by a sensitivity analysis of the modelled density and stratigraphy which then informed the development of a final model.

A satisfactory model solution was achieved when the discrepancy between the predicted and measured Bouguer anomalies was within the limit of 1 mgal, with such tolerances being the aim of precedents of gravity modelling studies (e.g., Kimbell and Williamson, 2015; 2016; Westaway et al., 2019; Mitjanas et al., 2021). For each model run, the difference between the measured and modelled Bouguer gravity anomalies was recorded at each 1 km interval across the survey area (e.g., at NS 60 61, NS 60 62) and the Root Mean Square (RMS) error of these values was calculated. Various model iterations were produced prior to determining a model which provided the best match to the measured data, with an RMS of less than 1 mgal.

3.4.5. Development of the Initial Structural Geological Model

Initial Modelling Steps and Model Geometry

The Noddy geological history, from which the structural geological model was produced, comprised of a series of model elements (Figure 3.8), designed to capture the essential features of the geological structure of the survey area.

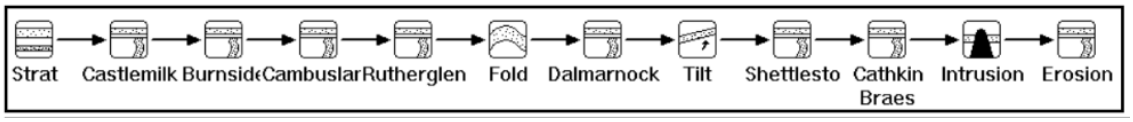

Figure 3.8. Noddy geological 'history'.

The starting point of the model history was to define the dimensions of the model block, in this case 5.5 km by 7.0 km, from NS 595 575 in the south-west to NS 650 645 in the north-east, by 12 km depth. The chosen modelled area was greater than that of the gravity survey area as it included additional existing BGS Bouguer gravity anomalies out with the survey area to minimise gridding artefacts.

A 'Strat' element was then introduced to the model history, which represented the crustal basement and underlying mantle, which was then overlain by a series of layers representing the Lower Crystalline Basement, Upper Crystalline Basement and Lower Palaeozoic rocks.

The scope for developing the Noddy model was limited to the available range of model elements, some of which impose limitations on the choices that the user has to accurately represent the geology of the modelled area. For example, the basic option for defining a fault assumes a planar fault surface with constant dip and displacement. In order to resolve issues such as this and to model the distinctive geological features of the survey area, the model was split into a series of 'unconformity' elements (e.g., Figure 3.9), with each unconformity assigned their own stratigraphy with associated formation densities. The location of each unconformity within the model was derived from the locations of each fault or outcrop boundary within the survey area (see Figure 3.1 compared to 3.9).

Using these unconformity elements, the geometry and throw of each of the faults within the survey area was modelled, with the dip of each fault calculated from those depicted in Figure 3.3 and from seismic survey interpretations (Table 3.1). The geometry of each of the unconformity elements used within the geological model are shown in Table 3.2.

Table 3.1. Geometry of faults in the survey area.

Fault Name	Location	Throw (m)	Glasgow Dip (°)	Airdrie Dip (°)
Dechmont	NS 553 649 to NS 796 497	650-1200	40	60
Castlemilk	NS 579 570 to NS 619 594	400	-	-
Rutherglen	NS 595 613 to NS 652 607	80	-	-
Shettleston	NS 581 658 to NS 731 643	100-200	46	52

Table 3.2. Geometry of the unconformities in the Noddy model.

Unconformity	X (m)	Y (m)	Z (m)	Dip Direction (°)	Dip (°)
Cathkin Braes	2000	1500	0	185	140
Dalmarnock	1763	5048	0	18.6	45
Cambuslang	817.9	3710.1	0	30	40
Burnside	320	3640	0	45	40
Rutherglen	817.9	3710.1	0	7.7	40
Castlemilk	0	1000	0	0	50
Shettleston	3000	6500	0	14	52

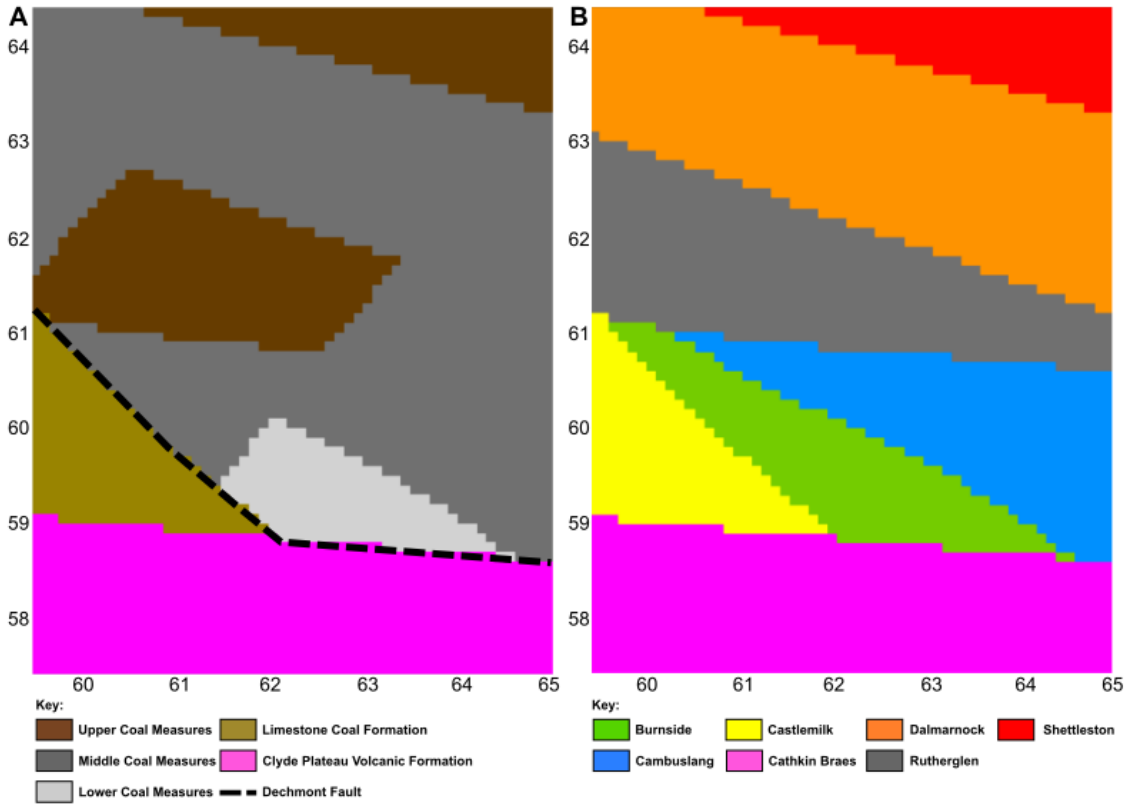

Figure 3.9. Surface geology of Noddy model (A), and unconformities within the Noddy model (B).

Constraining the Stratigraphy of the Initial Structural Geological Model

The thicknesses of the Upper and Lower Crystalline Basement, and the Lower Palaeozoic strata and (which included the Lower Devonian) used within the model were those derived from the MAVIS seismic interpretation (Figure 2.15). For the Devonian and Carboniferous stratigraphy, borehole datasets and seismic reflection surveys were used to inform the thickness of stratigraphic units incorporated into the structural geological model.

A number of seismic surveys were conducted from 1982-1986 in order to prospect for potential hydrocarbons in the West Lothian Oil Shale (WLOS) formation in the Lanarkshire Basin (e.g., Hopkins 1985; Marinex, 1988) and to investigate the crustal structure of northern Glasgow (Penn et al., 1984). Stratigraphic interpretations of the seismic reflection surveys shown in Figure 3.10 have been made by various authors. These include, IGS-MV1 and IGS-MV2 (Penn et al., 1984), SAX-85-06 (Monaghan, 2014), SAX-84-02V (Hopkins, 1985; Marinex, 1988; Hooper, 2003), and SAX-85-01, SAX 85-37, SAX-85-38, SAX-85-40 (Monaghan et al., 2017).

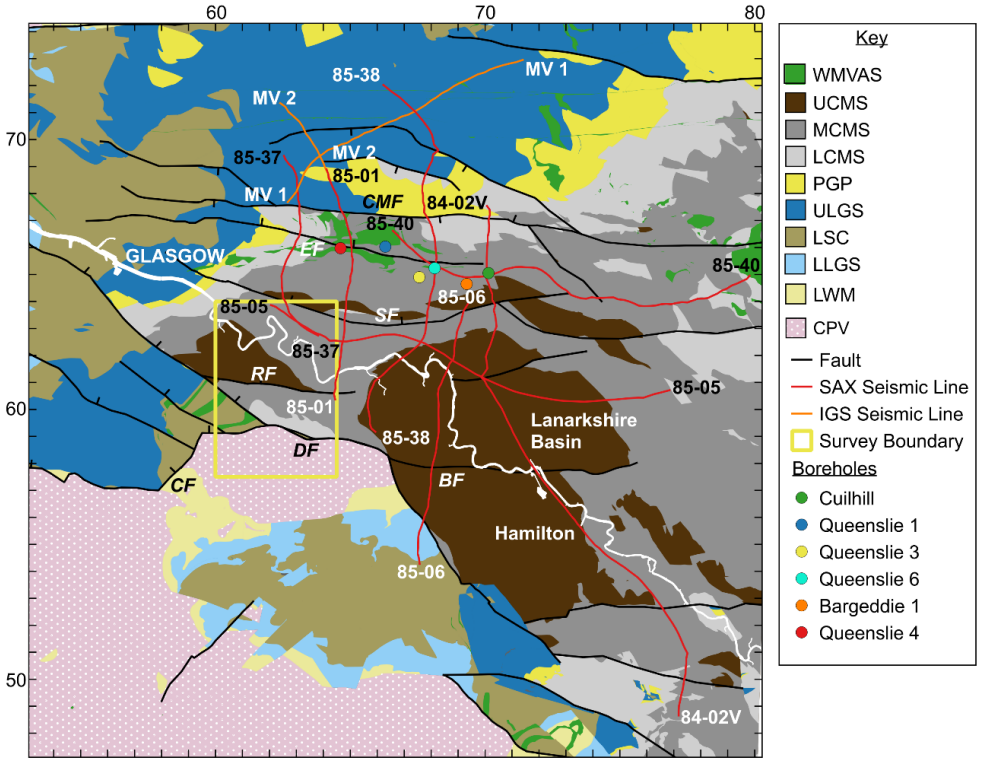

Figure 3.10. Location of seismic survey traves to the north and east of Glasgow which are of interest to the present study. MV1 and MV2 are the IGS seismic surveys from Penn et al. (1984), the remainder are SAXON Oil seismic surveys to prospect for hydrocarbon reservoirs in the WLOS. Geological Map Data BGS © UKRI 2021.

There are three seismic reflection surveys within the gravity survey area: SAX-85-01, SAX-85-05, and SAX-85-37. Two of these; SAX-85-01 and SAX-85-37, show coherent reflectors to c. 700 msec two-way travel time (TWTT) within the survey area, however SAX-85-05 appears to be of poorer quality and reflectors are less coherent. Seismic reflection surveys SAX-85-01 and SAX-85-37 were therefore examined by the author to determine the stratigraphy within the gravity survey area.

First, a velocity model was developed by the author to convert TWTT to depth. This velocity model was established from the seismic dataset measured in the Bargeddie-1 borehole (Teredo Petroleum PLC, 2000), provided by Dr Jon Busby of BGS, which gave interpolated depths (m) and the related TWTT (msec) at 1 m intervals throughout the borehole. The stratigraphic boundaries and associated TWTT measurements from the Bargeddie-1 borehole are shown in Table 3.3. The velocity model equation is shown in Equation 3.2, where *t* is TWTT (msec) and *z* is the depth (m), and Figure 3.11 shows the data points from the Bargeddie-1 dataset which were used to calibrate the model and the model prediction.

$$z = 0 + 1.23t + 0.00051t^2 + 4 \times 10^{-9}t^3$$

Equation 3.2.

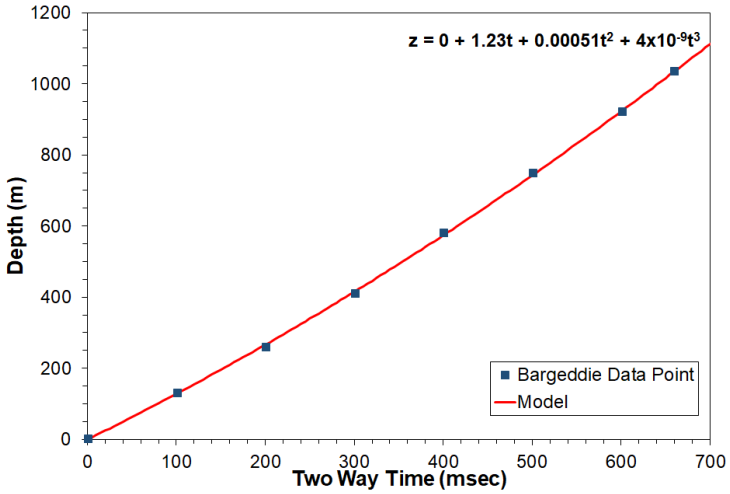

Figure 3.11. Velocity model derived from Bargeddie-1 seismic survey data and logged depths.

Table 3.3. Depth converted seismic reflectors.

Formation	TVDSS (m)	TWTT (s)
Middle Coal Measures	-78	-
Lower Coal Measures	63.5	0.049
Passage Group	211	0.163
Upper Limestone Group	303	0.234
Limestone Coal Group	580	0.402
Lower Limestone Group	601.5	0.415
Upper Oil Shale Group	694	0.471

Interpretations of the SAX-85-01 and SAX-85-37 seismic reflection surveys were then made by author. First, locations where each seismic survey crossed surface traces of faults and geological outcrops were plotted, as shown on local geological maps (e.g., Figure 3.8). Faults were then plotted on to each seismic section based upon the observed discontinuities of the seismic reflectors. Since SAX-85-01 and SAX-85-37 intercept the Penn et al. (1984) seismic reflection surveys (IGS82-MV1 and IGS82-MV2) in the north of Glasgow, seismic reflectors interpreted as key stratigraphic boundaries by Penn et al. (1984) were plotted on to SAX-85-37 from IGS82-MV1, and SAX-85-01 from IGS82-MV2 and traced southward to the survey area. Then, using Equation 3.2, seismic reflectors were converted from two way travel time to depth on SAX-85-01 at the location where the seismic line is in close proximity to the Queenslie-4 borehole. The known stratigraphy of the Queenslie-4 borehole was then used to constrain the seismic interpretation of SAX-85-01.

The resulting interpretations of SAX-85-01 and SAX-85-37 are shown in Figures 3.12 and 3.13, and the Penn et al. (1984) interpretations of IGS82-MV1 and IGS82-MV2 are shown in Figures 3.14 and 3.15.

Equation 3.2 was then used to convert TWTT to depth for each of the reflectors identified on SAX-85-01 and SAX-85-37 to determine the stratigraphy within the survey area. Whilst the deepest reflectors identified by Penn et al. (1984) on IGS82-MV1 and IGS82-MV2 in the north of Glasgow were at c. 900-1100 msec and were interpreted as the base of the Upper Devonian, the deepest reflectors identified on SAX-85-01 and SAX-85-37 within the gravity survey area (S.P c. 100-280 and 100-200 respectively) were at 700 msec and interpreted by the author as the top of the CPV. By applying the velocity model of Equation 3.2, this gives a depth to the top of the CPV as c. 1100 m within the areas of the gravity survey traversed by these seismic reflection lines.

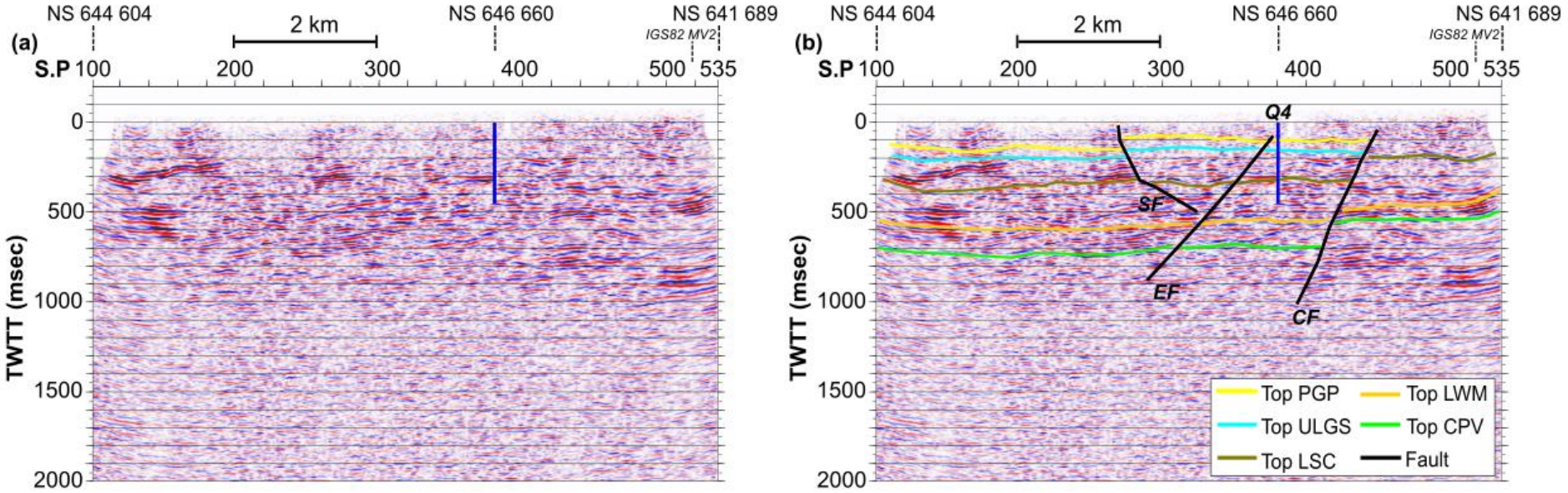

Figure 3.12. (a) Seismic survey SAX 85-01 and (b) interpretation showing the top of each stratigraphic unit and the position of faults. Abbreviations of stratigraphic units are shown in Table 2. Axis show shot points (x axis) and two way travel time (y axis). The location of the Queenslie-4 (Q4) borehole is shown. Faults: CF: Comedie Fault, EF: Easterhouse Fault, SF: Shettleston Fault. UKOGL-Beneath Britain, © 2002 Crown Copyright. Reproduced by permission of the Controller of Her Majesty's Stationery Office and the Secretary of State of the Department for Business, Energy & Industrial Strategy. © 2002 UK Onshore Geophysical Library.

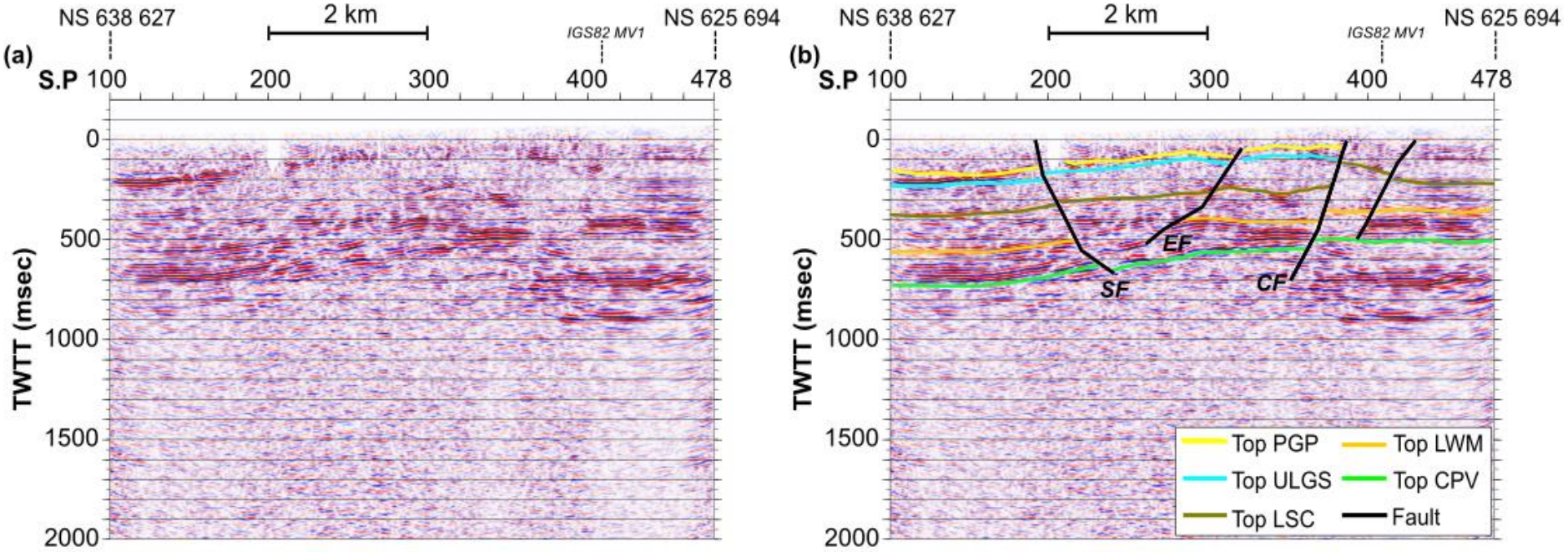

Figure 3.13. (a) Seismic survey SAX 85-37 and (b) interpretation showing the top of each stratigraphic unit and the position of faults. Abbreviations of stratigraphic units are shown in Table 2. Axis show shot points (x axis) and two way travel time (y axis). Faults: CF: Comedie Fault, EF: Easterhouse Fault, SF: Shettleston Fault. UKOGL-Beneath Britain, © 2002 Crown Copyright. Reproduced by permission of the Controller of Her Majesty's Stationery Office and the Secretary of State of the Department for Business, Energy & Industrial Strategy. © 2002 UK Onshore Geophysical Library.

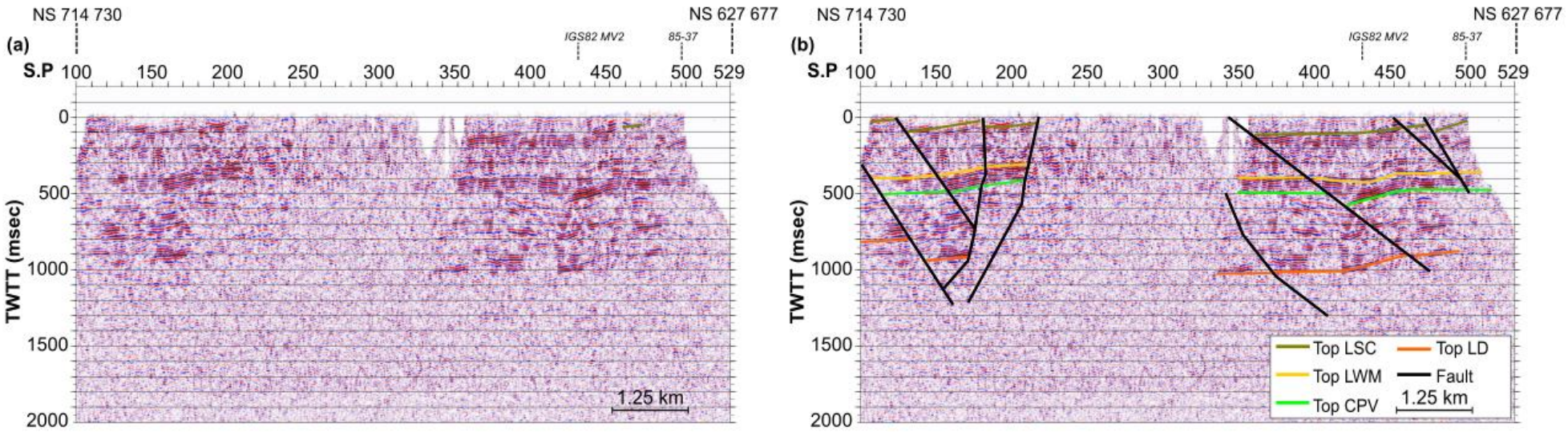

Figure 3.14. (a) Seismic survey IGS82-MV1 and (b) interpretation reproduced from Penn et al. (1984) showing the top of each stratigraphic unit and the position of faults. Abbreviations of stratigraphic units are shown in Table 2. LD: Lower Devonian. Axis show shot points (x axis) and two way travel time (y axis). UKOGL-Beneath Britain, © 2002 Crown Copyright. Reproduced by permission of the Controller of Her Majesty's Stationery Office and the Secretary of State of the Department for Business, Energy & Industrial Strategy. © 2002 UK Onshore Geophysical Library.

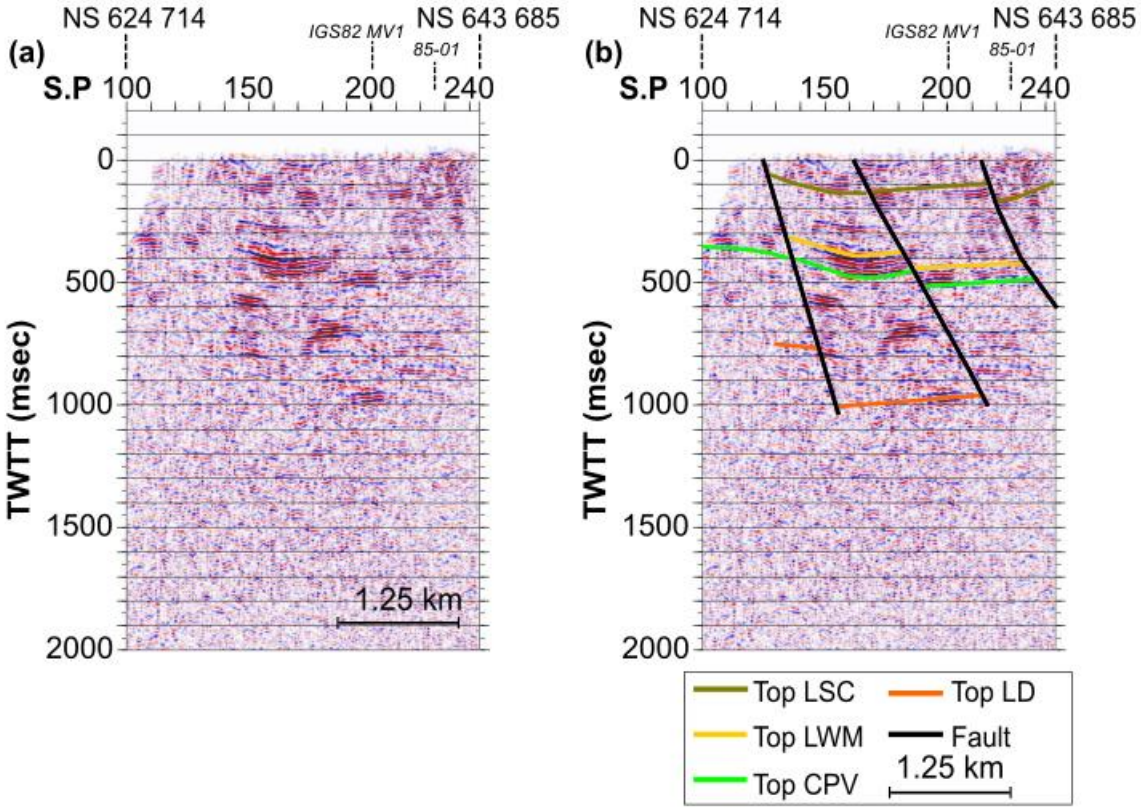

Figure 3.15. (a) Seismic survey IGS82-MV2 and (b) interpretation reproduced from Penn et al. (1984) showing the top of each stratigraphic unit and the position of faults. Abbreviations of stratigraphic units are shown in Table 2. LD: Lower Devonian. Axis show shot points (x axis) and two way travel time (y axis). UKOGL-Beneath Britain, © 2002 Crown Copyright. Reproduced by permission of the Controller of Her Majesty's Stationery Office and the Secretary of State of the Department for Business, Energy & Industrial Strategy. © 2002 UK Onshore Geophysical Library.

This estimated depth to the top of the CPV is supported by modelling of aeromagnetic anomalies within the region (Rollin, 2009), as shown in Figure 3.16, which also indicates that the depth to the top of the CPV reduces to 500-900 m towards the surface trace of the Dechmont Fault and the CPV outcrop in the Cathkin Braes.

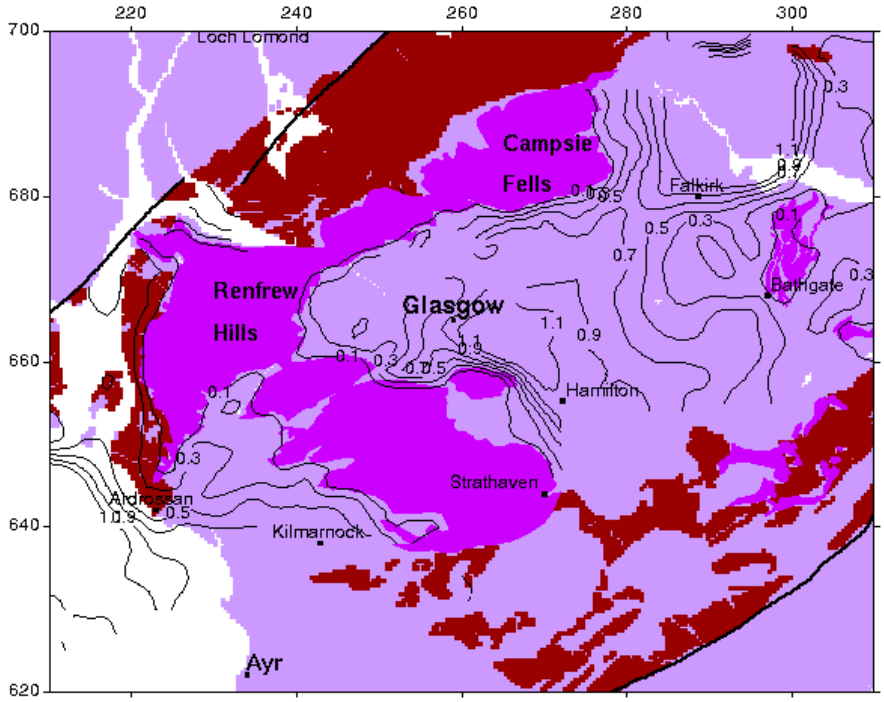

Figure 3.16. Depth to the top of the CPV from modelling of aeromagnetic anomalies, from Rollin (2009). Contours are in 0.2 km intervals.

Guided by the interpretations of SAX-85-01 and SAX-85-37, which placed the top of the CPV at c. 1100 m depth, and the thickness of stratigraphic units encountered in boreholes within the survey area or in the surrounding area in Glasgow's East End (Table 3.4), the stratigraphy of Carboniferous strata to the top of the CPV was determined as input criteria to the structural geological model (Table 3.5).

The thickness of the CPV, and the stratigraphy of the Lower Carboniferous and Upper Devonian sequences could not be constrained by interpretations of SAX-85-01 and SAX-85-37, nor by boreholes in the region. The uncertainty regarding the presence and thickness of these formations was explored during the sensitivity analysis, however as a starting point for the creation of the initial structural geological model, the interpretated thickness of these formations from Penn et al. (1984) were adopted (Table 3.5).

Then, consistent with previous modelling of regional Bouguer gravity anomalies in the western MVS (e.g., Hall et al., 1998), a 1200 m thick Devonian igneous intrusion was modelled to the south-west of the survey area within the Castlemilk unconformity. .

Table 3.4. Thicknesses of formations encountered in selected boreholes in Eastern Glasgow.

		MCMS	LCMS	PGP	ULGS	LSC	LLGS	WLOS	CPV
Borehole	Grid Reference	H (m)	H (m)	H (m)	H (m)	H (m)	H (m)	H (m)	H (m)
Bargeddie 1	NS 69318 64649	141.50	147.50	92.00	277.00	21.50	92.50	264.50	-
Queenslie Bridge	NS 66300 66030	81.38	109.50	92.91	137.46	252.55	-	-	-
Queenslie 2	NS 65895 64900	55.19	106.91	85.27	261.34	250.55	-	-	-
Queenslie 3	NS 67560 64900	89.61	106.07	78.64	246.89	206.65	-	-	-
Queenslie 4	NS 64640 65975	56.69	133.50	49.38	295.35	173.74	-	-	-
Queenslie 6	NS 68130 65235	42.06	112.47	77.72	260.30	121.31	-	-	-
Millholm Paperwork	NS 58605 59645	-	-	-	-	183.16	86.59	20.57	-
GGC01	NS 60915 63109	146.05	20.45	-	-	-	-	-	-
Dalmarnock Pit	NS 61180 62710	145.47	97.49	20.72					

Table 3.5. Thickness of stratigraphic units in the initial Noddy model.

Formation	H (m)
Upper Coal Measures	100
Middle Coal Measures	145
Lower Coal Measures	97
Passage Group	75
Upper Limestone Formation	250
Limestone Coal Formation	220
Lower Limestone Formation	92
Lawmuir Formation	265
Clyde Plateau Volcanics	500 (HW)
Clyde Plateau Volcanics	150 (FW)
Ballagan Formation	100
Kinnesswood Formation	150
Stratheden Group	150
Devonian Lavas	1200
Lower Palaeozoic	1500
Upper Crystalline Basement	3500
Lower Crystalline Basement	7500

Abbreviations: HW: Hanging Wall, FW: Footwall.

Density of Modelled Stratigraphic Units

The densities assigned to the stratigraphic units within the model were a combination of those published for rocks in the MVS and those used within previous modelling of regional Bouguer gravity anomalies (Table 3.6). Each value of density was then converted to $\Delta\rho$, the difference between the density of the stratigraphic unit and the assumed benchmark density of 2.55 Mg m^{-3} used in the gravity reduction calculations.

Table 3.6. Density of stratigraphic units in the Noddy model.

Formation	ρ (Mg m^{-3})	$\Delta\rho$ (Mg m^{-3})	Reference
Upper Coal Measures	2.5	-0.05	Kimbell et al. (2006)
Middle Coal Measures	2.5	-0.05	Kimbell et al. (2006)
Lower Coal Measures	2.5	-0.05	Kimbell et al. (2006)
Passage Group	2.55	0	Kimbell et al. (2006)
Upper Limestone Formation	2.55	0	Kimbell et al. (2006)
Limestone Coal Formation	2.55	0	Kimbell et al. (2006)
Lower Limestone Formation	2.58	0.03	McLean (1961)
Lawmuir Formation	2.58	0.03	McLean (1961)
Clyde Plateau Volcanics	2.74	0.19	McLean (1961)
Clyde Plateau Volcanics	2.74	0.19	McLean (1961)
Ballagan Formation	2.55	0	Kimbell et al. (2006)
Kinnesswood Formation	2.58	0.03	McLean (1961)
Stratheden Group	2.40	-0.15	McLean (1961)
Devonian Lavas	2.83	0.28	Paterson et al (1998)
Lower Palaeozoic	2.77	0.22	Kimbell et al. (2006)
Upper Crystalline Basement	2.8	0.25	Monro (1999)
Lower Crystalline Basement	2.85	0.3	Monro (1999)

Remaining Model Elements and Model Visualisation

The penultimate element introduced to the model was a 'plug', which was used to model an igneous intrusion (Figure 3.14) and high Bouguer gravity anomaly to the south-west of the survey area (Figure 3.7). Finally, an 'erosion' unconformity was applied to the model to remove all rock above sea level, so that the calculation of the modelled Bouguer gravity anomalies was consistent with the gravity reduction procedure.

Combining each of these input parameters, the Noddy 3-D structural model was produced to represent the geology of the survey area. The model is illustrated as a series of oblique views in Figure 3.17. Model input parameters are detailed in their entirety in Appendix 3.B.

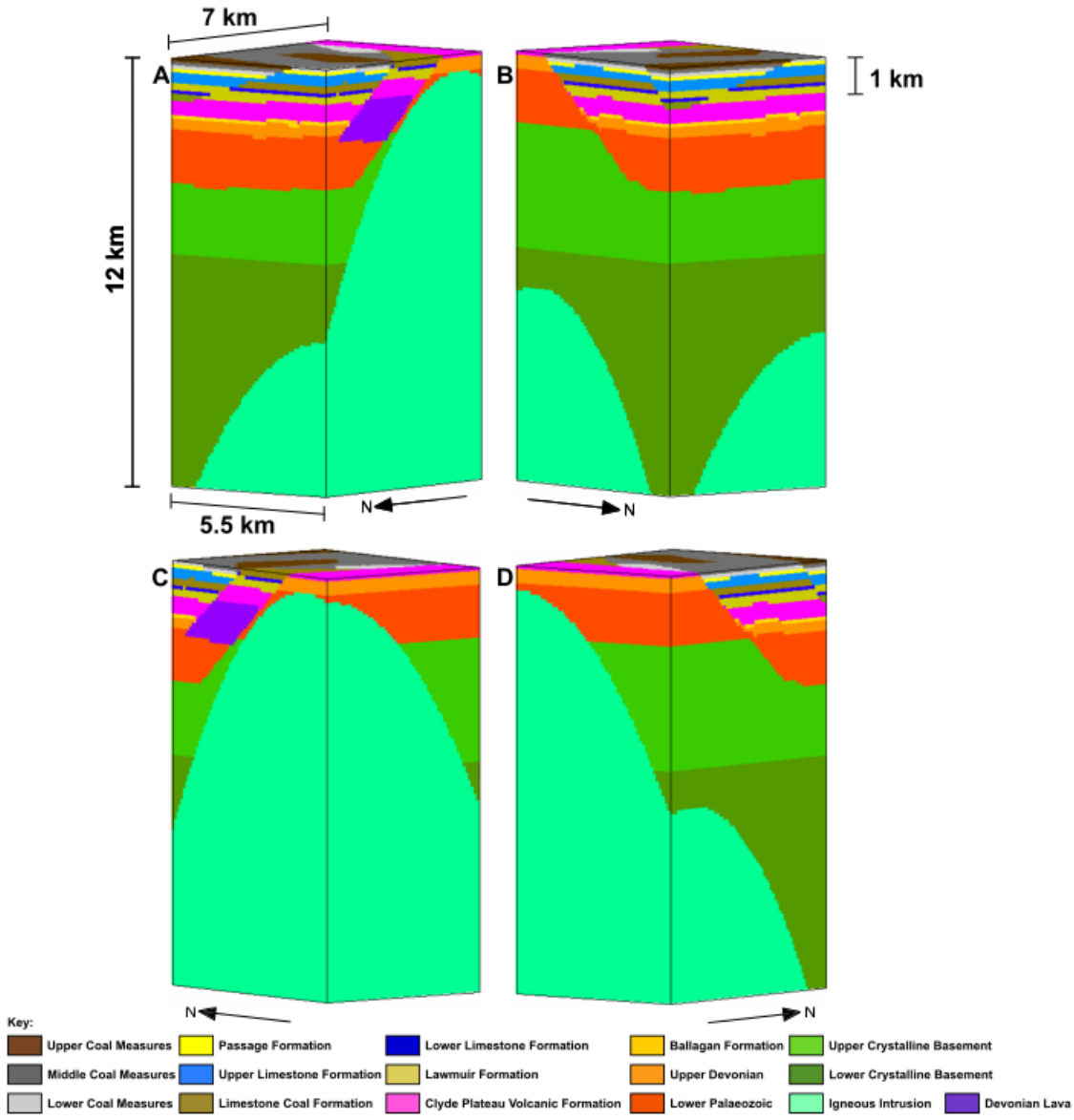

Figure 3.17. Initial Structural Geological Model.

3.5. Gravity Forward Modelling Results

3.5.1. Results of the Initial Structural Geological Model

The Bouguer gravity anomalies predicted by the initial Noddy structural geological model are illustrated in Figure 3.18. This model produced a Bouguer gravity high in the south-west of the Dechmont Fault of 11.2 mgal in the Castlemilk and Croftfoot areas, gradually reducing across the surface trace of the Dechmont Fault, to the Bouguer gravity low in the north-north-east of the survey area, of 4.5 mgal.

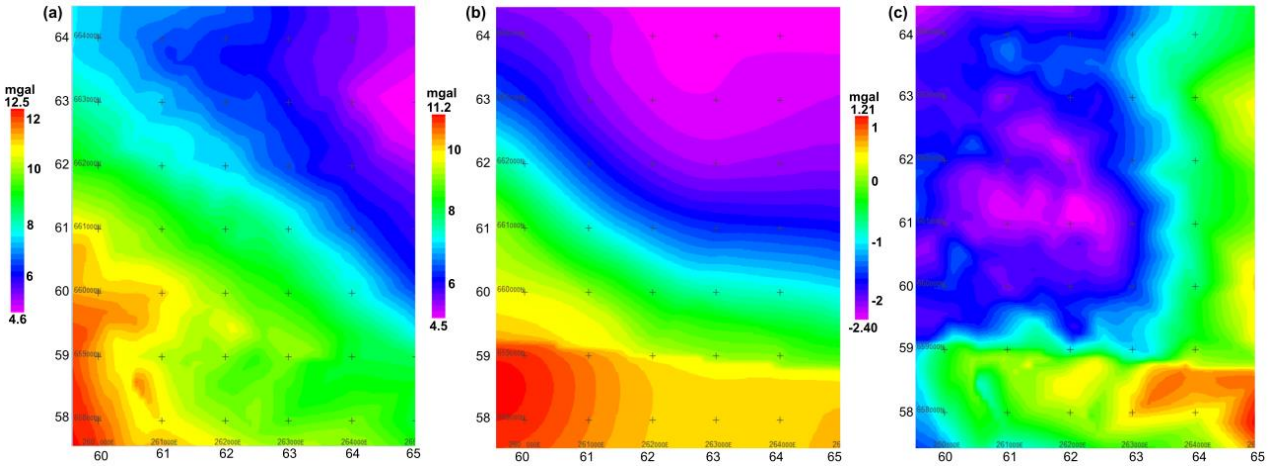

Figure 3.18. Measured Bouguer gravity anomalies (a). Bouguer gravity anomalies predicted by the initial Noddy model b). The discrepancies between the Bouguer gravity anomalies predicted by the model and those measured in the survey (c). Note, the discrepancies are calculated from measured values – modelled values, indicating here that the modelled Bouguer gravity anomalies are too low.

Figure 3.18 (c) shows the difference between the Bouguer gravity anomalies calculated by the model and those from the measured gravity data. The model most accurately matches the measured Bouguer gravity anomalies in the CPV outcrop in the Cathkin Braes and Castlemilk, in the footwall of the Dechmont Fault. The model also matches the Bouguer gravity anomalies in the deep sedimentary basin in the Lanarkshire Basin to the north-east of NS 63 59 in the hanging wall of the Dechmont Fault. Elsewhere, the modelled Bouguer gravity anomalies are a relatively poor match to the measured values. This was particularly true to the north-west of NS 63 59. Overall, the RMS of the difference between the measured and modelled Bouguer gravity anomalies for this initial model was 1.27 mgal.

3.5.2. Improving the Structural Geological Model

Comparison of the Bouguer gravity anomalies predicted by the initial model and those measured in the gravity survey indicated the following points:

- The model matches the CPV outcrop in the footwall of the Dechmont Fault, and the sedimentary basin in the hanging wall of the fault to the north-east of NS 63 59, indicating that the modelled geological structure in these locations is representative.
- A much denser stratigraphic sequence must be present to the north-west of NS 63 59 to produce the pattern of high Bouguer gravity anomalies.
- The sedimentary basin may therefore deepen to the east and north, consistent with the initial interpretation of the measured data and interpretations of seismic surveys to the east and north of the survey area.

To achieve a more representative geological model, a sensitivity analysis was carried out to investigate the effects of varying model input parameters on the resulting Bouguer gravity anomalies. In doing so, those parameters which are most influential were determined and used to achieve an improved match between the modelled and measured results. The scope of the sensitivity analysis was constrained by the range of stratigraphic unit thicknesses shown in Table 2.4 and encountered in boreholes across the Glasgow area (Table 3.4), the range of densities of stratigraphic units shown in Table 3.C.1, and the dip of the faults calculated from seismic interpretations, geological mapping, or discussed in literature. The results of this sensitivity analysis are detailed in Tables 3.7-3.9, showing the minimum and maximum Bouguer gravity anomalies of each model solution, the minimum and maximum difference between the predicted and measured Bouguer gravity anomalies, and the RMS of the difference between the predicted and measured Bouguer gravity anomalies.

Thickness of Stratigraphic Units

Table 3.7 details the results of the sensitivity analysis of varying the thickness of stratigraphic units within the model on the resulting Bouguer gravity anomalies. These results show that reducing the thickness of Carboniferous sediments in the hanging wall of the Dechmont Fault improves the match between the measured and modelled Bouguer gravity anomalies. Indeed, in comparison to the initial model RMS of 1.27 mgal, this sensitivity analysis shows that the most significant improvements to the model solution occurred when the thickness of the ULGS was reduced to 140 m (RMS = 1.13 mgal), the LSC to 100 m (RMS = 1.12 mgal), and the LWM to 130 m (RMS = 1.05 mgal).

Table 3.7. Sensitivity analysis of the modelled thickness of stratigraphic units.

		Model Results		Difference with Measured Data		
Formation	H (m)	g_{min} (mgal)	g_{max} (mgal)	g_{min} (mgal)	g_{max} (mgal)	RMS (mgal)
ULGS	140	4.8	11.2	-2.16	1.21	1.13
ULGS	200	4.7	11.2	-2.29	1.21	1.21
ULGS	295	4.5	11.2	-2.47	1.21	1.32
LSC	100	4.8	11.2	-2.13	1.21	1.12
LSC	300	4.3	11.2	-2.57	1.21	1.36
LLGS	0	4.6	11.2	-2.25	1.21	1.15
LLGS	125	4.5	11.2	-2.45	1.21	1.33
LWM	130	4.9	11.2	-2.15	1.21	1.05
LWM	200	4.7	11.2	-2.29	1.21	1.18
CPV (HW)	350	4.6	11.2	-2.30	1.21	1.32
CPV (HW)	800	4.6	11.2	-2.25	1.21	1.21
CPV (FW)	200	4.5	11.1	-2.4	1.16	1.29
CPV (FW)	400	4.5	12.4	-2.45	1.31	1.36
Intrusion	Absent	4.5	10.3	-2.43	1.27	1.26
LP*	Absent	4.5	12.1	-2.1	3.0	1.31

Abbreviations are shown in Table 2. LP: Lower Palaeozoic.

As discussed in Chapter 2, Hall et al. (1998) state that the Dechmont Fault may have controlled the locations of vents from which the CPV erupted and after Dinantian volcanism had ceased, erosion of the lava block took place and detritus was deposited locally along the margins of the block while fluvial sediments were deposited elsewhere. The LLGS is thickest in the north-east of Glasgow and rapidly thins towards the lava blocks to the north-west in the Campsie Fells and the south-west in the Cathkin Braes, where in the south-west the controlling factor may have been the Dechmont Fault (Browne et al., 1985). The LSC was deposited in a similar pattern (Hall et al., 1998). Seismic reflection surveys SAX-85-01 and SAX-83-37 are limited to areas in the east and north-east of the gravity survey area, and therefore cannot with certainty inform the stratigraphy of the hanging wall to the north-west of NS 63 59. However, if the Carboniferous sediments within the LWM, LLGS, LSC, or ULGS thin towards the Dechmont Fault as suggested by Hall et al. (1998) and Browne et al. (1985), then the cumulative effect of reducing the modelled thickness of these formations would improve the model solution to the north-west of NS 63 59.

This analysis also considered varying the thickness of the CPV, both in the hanging wall and the footwall of the Dechmont Fault as a means of increasing the density of the strata in the buried footwall escarpment of the fault and hence reducing the discrepancy between the measured and modelled Bouguer anomalies north-west of NS 63 59. Possible ponding of the CPV in the hanging wall of the Dechmont Fault, akin to that observed in the hanging wall of the Campsie Fault (Whyte and MacDonald, 1974), was modelled by increasing the

thickness of the CPV from 500 m to 800 m. This had a minor effect on the model solution, reducing the RMS to 1.21 mgal.

Further model iterations, including the removal of the Lower Palaeozoic strata and hence modelling a shallower crystalline basement, and removal of the intrusion in the south-west of the model, both had negligible or adverse effect on the overall match between the measured and modelled Bouguer gravity anomalies.

Presence and Thickness of the Lower Carboniferous and Upper Devonian

Whilst the Upper Devonian sandstone sequence has been interpreted on seismic reflection surveys to the north (Penn et al., 1984) and east of Glasgow (Marinex, 1988), and from gravity modelling of the Hamilton gravity anomaly (Browne et al., 1987), the presence and depth of the Kinnesswood Formation and underlying Stratheden Group beneath the gravity survey area is not known. In this sensitivity analysis, the presence and thickness of the Lower Carboniferous Ballagan Formation, and the Upper Devonian sequence was assessed. Shown in Table 3.8, one model iteration considered the possibility that the Lower Carboniferous and Upper Devonian sequence was absent, reflecting the lack of coherent horizons beneath the CPV on SAX-85-01 and SAX-85-37, and a second iteration modelled the Ballagan Formation and Upper Devonian as a thicker sequence of sediments beneath the CPV, in line with the Brown et al. (1987) interpretation of the Hamilton gravity anomaly. The results shown in Table 3.8 suggest that the Kinnesswood Formation and the Stratheden Group are present in the hanging wall of the Dechmont Fault, albeit as a thinner sequence in comparison to that modelled to the south-east of Glasgow in the Hamilton area.

Table 3.8. Sensitivity analysis of the thickness of the Inverclyde Group and Upper Devonian.

			Model Results		Difference with Measured Data		
	Formation	H (m)	g_{min} (mgal)	g_{max} (mgal)	g_{min} (mgal)	g_{max} (mgal)	RMS (mgal)
Initial Model	BGN KNW SAG	100 150 150	4.5	11.2	-2.4	1.21	1.27
Absent Model	BGN KNW SAG	0 0 0	5.5	13.4	-2.2	3.7	1.54
Browne et al. (1987) Model	BGN KNW SAG	230 150 400	3.7	9.7	-3.7	0.24	2.00

Density of Stratigraphic Units

Table 3.C.1 in Appendix 3.C shows a range of representative densities for each stratigraphic unit included in the structural geological model. Of the Carboniferous formations, those with the largest uncertainty are the Visean sediments of the LLGS and LWM formations, and the CPV lavas. Furthermore, a range of densities are presented in literature for different Lower Palaeozoic lithologies encountered in the MVS and Southern Scotland (Table 3.C.1). Table 3.9 shows the results of the effects of varying the density assigned to each modelled stratigraphic unit.

Table 3.9. Sensitivity analysis of the modelled density of stratigraphic units.

		Model Results		Difference with Measured Data		
Formation	$\Delta \rho$ (Mg m^{-3})	g_{min} (mgal)	g_{max} (mgal)	g_{min} (mgal)	g_{max} (mgal)	RMS (mgal)
UCMS, MCMS and LCMS	0.00	5.1	11.2	-2.09	1.21	1.04
PGP, ULGS and LSC	-0.05	3.8	11.2	-3.21	1.21	1.78
LLGS and LWM	0.00	4.4	11.2	-2.56	1.21	1.41
LLGS and LWM	0.15	5.2	11.2	-1.76	1.27	0.85
CPV	0.25	4.9	11.4	-2.01	1.5	1.01
CPV	0.43	6.0	12.8	-1.39	2.3	0.86
KNW and SAG	0.00	4.7	11.4	-2.36	1.47	1.24
Lower Palaeozoic	0.17	4.2	11	-2.68	0.16	1.53
Lower Palaeozoic	0.25	4.7	11.3	-2.31	1.9	1.22
Lower Palaeozoic	0.28	4.9	11.6	-2.23	2.58	1.25
Crystalline Basement	0.25	4.1	11.2	-2.67	0.6	1.44
Crystalline Basement	0.35	4.9	11.2	-2.13	1.82	1.18
CPV & Lower Palaeozoic	0.25 & 0.28	5.3	11.6	-1.93	2.56	0.9

The results illustrate that varying the density of each of these formations, within the plausible ranges of uncertainty, has a significant impact on the discrepancy between the modelled and measured Bouguer gravity anomalies.

Table 3.9 shows that increasing the density of the Coal Measures to 2.55 Mg m^{-3}, reduces the RMS between the modelled and measured Bouguer gravity anomalies from 1.27 mgal to 1.04 mgal. The most significant improvements to the model solution were achieved, however, when the density of the LLGS and LWM were increased to 2.7 Mg m^{-3} (RMS = 0.85 mgal) or when the density of the CPV was increased to 2.98 Mg m^{-3} (RMS = 0.86 mgal) perhaps reflecting the presence of volcanic detritus within the Visean sediments, or the higher density of unweathered basalt in the CPV subcrop compared to the measured density of 2.74 Mg m^{-3} from outcrop samples in the MVS (Rollin, 2009).

Furthermore, the density of the Lower Palaeozoic strata was varied to represent the presence of denser rocks such as Devonian granite intrusions, in comparison to the density of Silurian-Ordovician greywackes or the Ballantrae Complex (Kimbell et al., 2006) within the initial model. The results show that increasing the density of the Lower Palaeozoic achieved an improved match between the modelled and measured Bouguer gravity anomaly only when combined with an increase in density of the CPV.

Fault Geometry

The geometry of the Dechmont Fault was varied from 40° to 60°. The result of this modelling was that a dip of 40° provides the best fit between the modelled and measured Bouguer gravity anomalies, of an RMS = 1.27 mgal, whereas the RMS increased to 1.56 mgal at 50° and 1.77 mgal at 60°. The modelled dip of 40° was consistent with that calculated from seismic line SAX-84-02V (Marinex, 1988) and Figure 3.3 (Section Line A-B).

Influence of Late Carboniferous-Early Permian Dykes and Sills

One feature of the geology of the survey area which could not be modelled accurately in Noddy was the presence of Late Carboniferous-Early Permian dykes and sills. Attempts were made to include this in the Noddy geological history by using model elements such as ‘plugs’ or ‘dykes’ but no choice of input parameters could model the feature satisfactorily.

As discussed in Westaway et al. (2019), igneous intrusions have a significant effect on Bouguer gravity anomalies as they are much denser than the sediments into which they are intruded (~2900 Mg m^{-3} compared to ~2550 Mg m^{-3}). As illustrated in Figure 3.1, Permian aged igneous intrusions outcrop at Croftfoot and Castlemilk within the survey area. Located to the west of the exposed Permian intrusion in Croftfoot, the Aitkenhead No. 4 borehole (NS 59805 60365) encountered a ~35 m igneous intrusion at a depth of 10 m. Using the standard slab formula in Equation 3.A.5, the presence or absence of a 35 m thick dolerite intrusion will affect the Bouguer gravity anomaly by 0.59 mgal, which is significant given the tolerance of the present study.

An additional complicating factor, not considered in the present analysis, is the potential effect of contact metamorphism accompanying intrusions of Late Carboniferous-Early Permian dykes and sills on the density of surrounding rocks. Devolatilization of coal and baking of coal and other sediments have been reported at distances of up to several hundred metres above and below the Great Whin Sill (Randall, 1995), and might cause sufficient increase in density to influence gravity measurements, given the accuracy tolerances of the

present study. This effect was observed within the Kirkland Neuk borehole in Renfrewshire, where coal was described as “very much burned or charred” by Thomson et al. (1869). This may have been due to the borehole’s proximity to an outcrop of Permian aged sill, related to the Paisley Ruck Fault Zone, lying to the south of the borehole. The presence of high-density igneous intrusions such as those in the shallow subsurface and at outcrop at Croftfoot and Castlemilk, and the associated increase in density of surrounding sedimentary rocks, may therefore, be two contributing factors to the high Bouguer gravity anomalies observed in the south-west of the survey area.

3.5.3 Development of a Final Structural Geological Model

The sensitivity analysis indicated that the most favourable model solutions were obtained when:

(1) the dip of the Dechmont Fault was modelled as 40°,

(2) the Ballagan Formation, Kinnesswood Formation, and Stratheden Group were present with thicknesses of 100 m, 150 m, and 150 m respectively,

(3) the densities of the Coal Measures, LLGS, LWM, CPV or Lower Palaeozoic were increased, or the thicknesses of the ULGS, LSC, LLGS, or LWM were decreased.

Guided by the results of the sensitivity analysis, further model iterations were conducted to assess the impact of combining reductions in the modelled thickness of stratigraphic units with increases in the modelled density.

The most favourable results were obtained when the thickness of the ULGS was reduced to 140 m, the LSC to 100 m, and the LWM to 130 m, and the $\Delta\rho$ of the CPV in the hanging wall of the Dechmont Fault was increased to 0.25 Mg m^{-3}, whilst the remaining model parameters were retained from the initial structural geological model. The input values of density and stratigraphic unit thickness are summarised in Table 3.10 under ‘Lower Model’, and the results are shown in Figure 3.19. Model input parameters are shown in their entirety in Appendix 3.D, Table 3.D.1.

Table 3.10. Model input parameters for the Lower and Upper models.

	Lower Model		Upper Model	
Formation	H (m)	Δρ (Mg m^{-3})	H (m)	Δρ (Mg m^{-3})
Upper Coal Measures	100	-0.05	100	0
Middle Coal Measures	145	-0.05	145	0
Lower Coal Measures	97	-0.05	97	0
Passage Group	75	0	75	0
Upper Limestone Formation	140	0	250	0
Limestone Coal Formation	100	0	220	0
Lower Limestone Formation	92	0.03	92	0.03
Lawmuir Formation	130	0.03	265	0.03
Clyde Plateau Volcanics	500 (HW)	0.25	500 (HW)	0.25
Clyde Plateau Volcanics	150 (FW)	0.19	150 (FW)	0.19
Ballagan Formation	100	0	100	0
Kinnesswood Formation	150	0.03	150	0.03
Stratheden Group	150	-0.15	150	-0.15
Devonian Lavas	1200	0.28	1200	0.28
Lower Palaeozoic	1500	0.22	1500	0.22
Upper Crystalline Basement	3500	0.25	3500	0.25
Lower Crystalline Basement	7500	0.3	7500	0.3

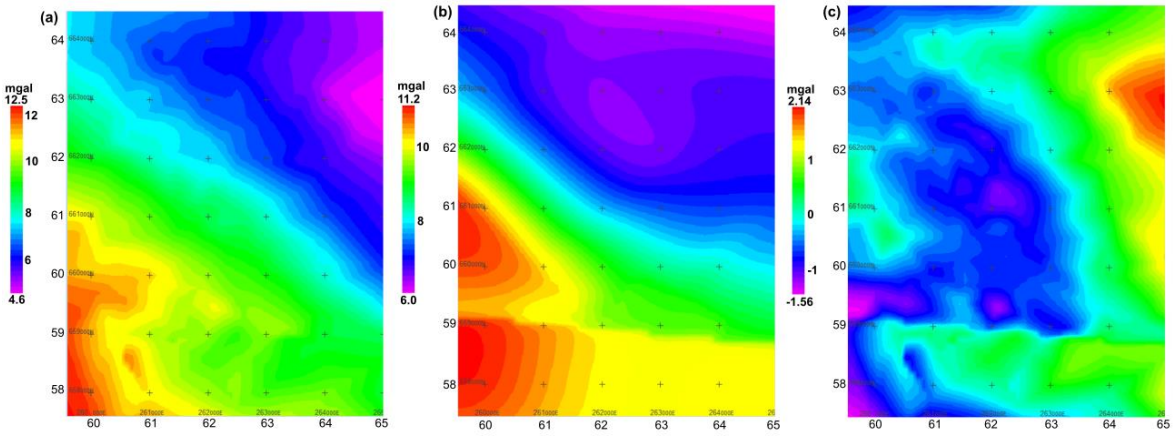

Figure 3.19. Lower Model Output. Measured Bouguer gravity anomalies (a). Bouguer gravity anomalies predicted by the Noddy model b). The discrepancies between the Bouguer gravity anomalies predicted by the model and those measured in the survey (c).

Overall, the RMS of the difference between the measured and modelled Bouguer gravity anomalies for this model was 0.77 mgal. The RMS of the difference between the measured and modelled Bouguer gravity anomalies to the east of NS 63 59 was calculated as 0.75 mgal, and to the west of NS 63 59 was calculated as 0.82 mgal. This illustrates that the modelled Bouguer gravity anomalies are well matched to those measured from the new gravity survey.

However, as shown in Figure 3.19 (c), the model does not suitably match the measured Bouguer gravity anomalies in the north-east of the survey area, indicating that the thicknesses of the stratigraphic units are greater in this area, which would be consistent with the interpreted stratigraphy of the Namurian and Visean sediments from interpretations of SAX-85-01 and SAX-83-37.

Following this, further modelling was undertaken to assess which combination of modelled unit densities produced a best fit between the modelled and measured Bouguer gravity anomalies if the modelled Carboniferous stratigraphy was consistent with the interpretations of SAX-85-01 and SAX-83-37. In this instance, the most favourable results were obtained when the $\Delta\rho$ of the Coal Measures was increased to 0 Mg m^{-3} and the $\Delta\rho$ of the CPV increased to 0.25 Mg m^{-3}. The input values of density and stratigraphic unit thickness are summarised in Table 3.10 under 'Upper Model', and the results are shown in Figure 3.20.

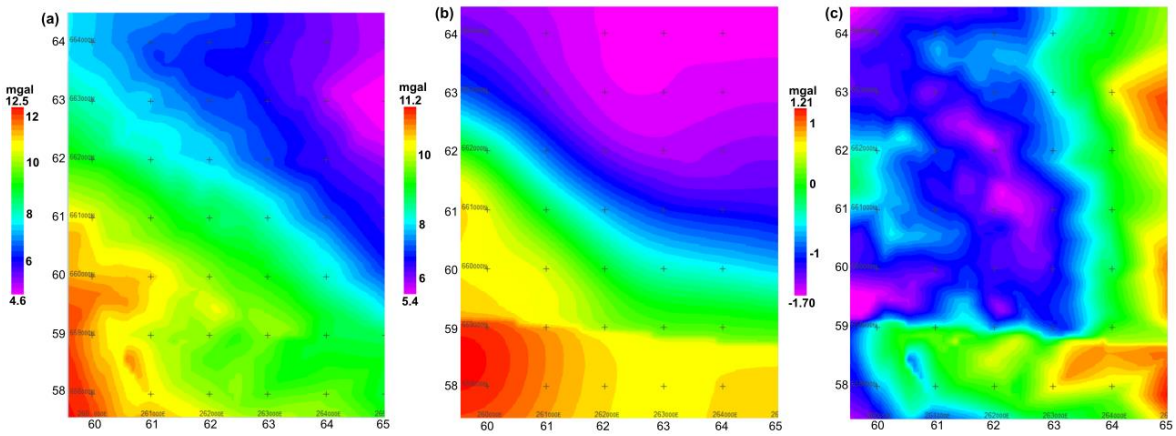

Figure 3.20. Upper Model Output. Measured Bouguer gravity anomalies (a). Bouguer gravity anomalies predicted by the Noddy model b). The discrepancies between the Bouguer gravity anomalies predicted by the model and those measured in the survey (c).

Overall, the RMS of the difference between the measured and modelled Bouguer gravity anomalies for this model was 0.81 mgal. The RMS of the difference between the measured and modelled Bouguer gravity anomalies to the east of NS 63 59 was calculated as 0.66 mgal, and to the west of NS 63 59 was calculated as 0.94 mgal. Of the results presented within this chapter, this model is the only instance whereby the modelled stratigraphy is consistent with the interpretation of SAX-85-01 and SAX-83-37 and the combination of modelled stratigraphy and unit densities has provided a satisfactory match between the modelled and measured Bouguer gravity data.

Synthesis of Results

Based upon the sensitivity analysis and further iterative modelling, the Bouguer gravity anomalies produced by the 'Lower' and 'Upper' structural geological models provide the best matches to the measured Bouguer anomalies from the gravity survey.

Whilst the 'Lower Model' results produced a lower RMS of 0.77 mgal in comparison to 0.81 mgal from the 'Upper Model' results, the modelled stratigraphy of the 'Upper Model' is supported by the interpreted stratigraphy from seismic reflection surveys SAX-85-01 and SAX-83-37 within the survey area.

It is possible that the Namurian and Visean formations are thicker to the east and north-east of the survey area, and that these sediments thin to the south-west towards the Dechmont Fault, following the regional pattern of deposition proposed by Hall et al. (1998), however this lateral variation in thickness could not be resolved within the one structural geological model.

3.6. Implications for Geothermal Energy in Glasgow

For the purpose of quantifying the geothermal resource in the Upper Devonian sandstone sequence beneath Eastern Glasgow, the two alternative structural geological models were each used to determine the extent and depth of the primary geothermal target in the Upper Devonian sandstones of the Kinnesswood Formation and underlying Stratheden Group in the hanging wall of the Dechmont Fault, and the potential secondary geothermal target at locations where the Dechmont Fault may intersect the Upper Devonian sandstones. The 'Lower Model' is considered as the lower estimate of the depth to the top of the Upper Devonian sandstone sequence, and the 'Upper Model', is considered as the upper estimate of the depth to the Upper Devonian sandstone sequence.

3.6.1. Extent of Upper Devonian Sandstones in Eastern Glasgow

The modelled extent of the deeply buried Upper Devonian sequence was output directly from the Noddy modelling software for the two structural geological models and reproduced using QGIS software (Figure 3.21). Then, using the model surface geology and stratigraphy of the 'Lower' and 'Upper' structural geological models, the depth to the Upper Devonian sandstone sequence was determined in the hanging wall of the Dechmont Fault, shown in both Figure 3.22 and 3.23.

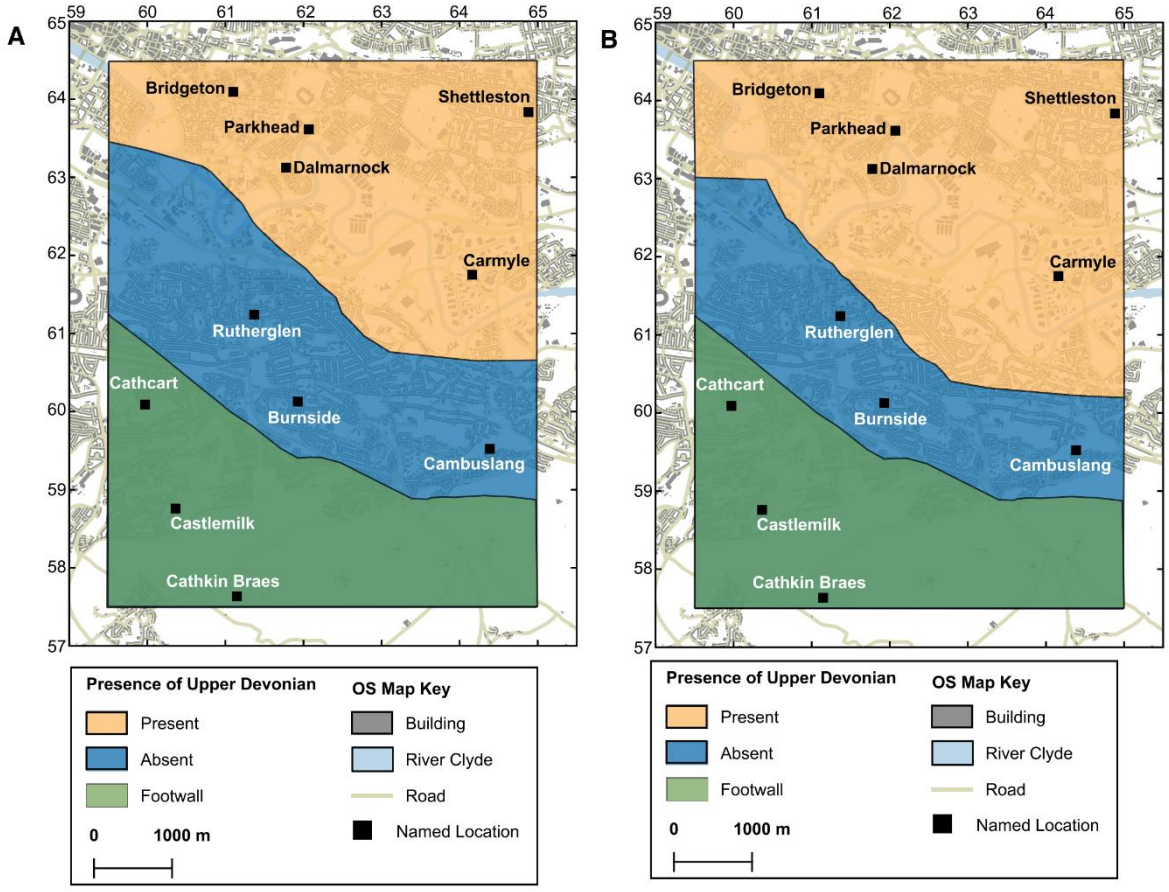

Figure 3.21. Extent of deeply buried Upper Devonian sandstones beneath the survey area shown for the 'Upper Model' (A) and the 'Lower Model' (B).

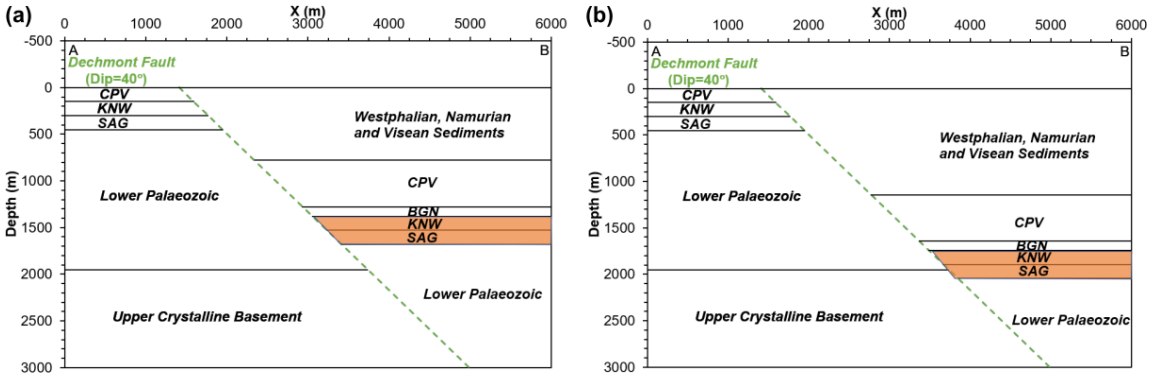

Figure 3.22. Cross section of the 'Lower Model' (a) and the 'Upper Model' (b). This cross section corresponds to section line A-B shown in Figure 3.E.1.

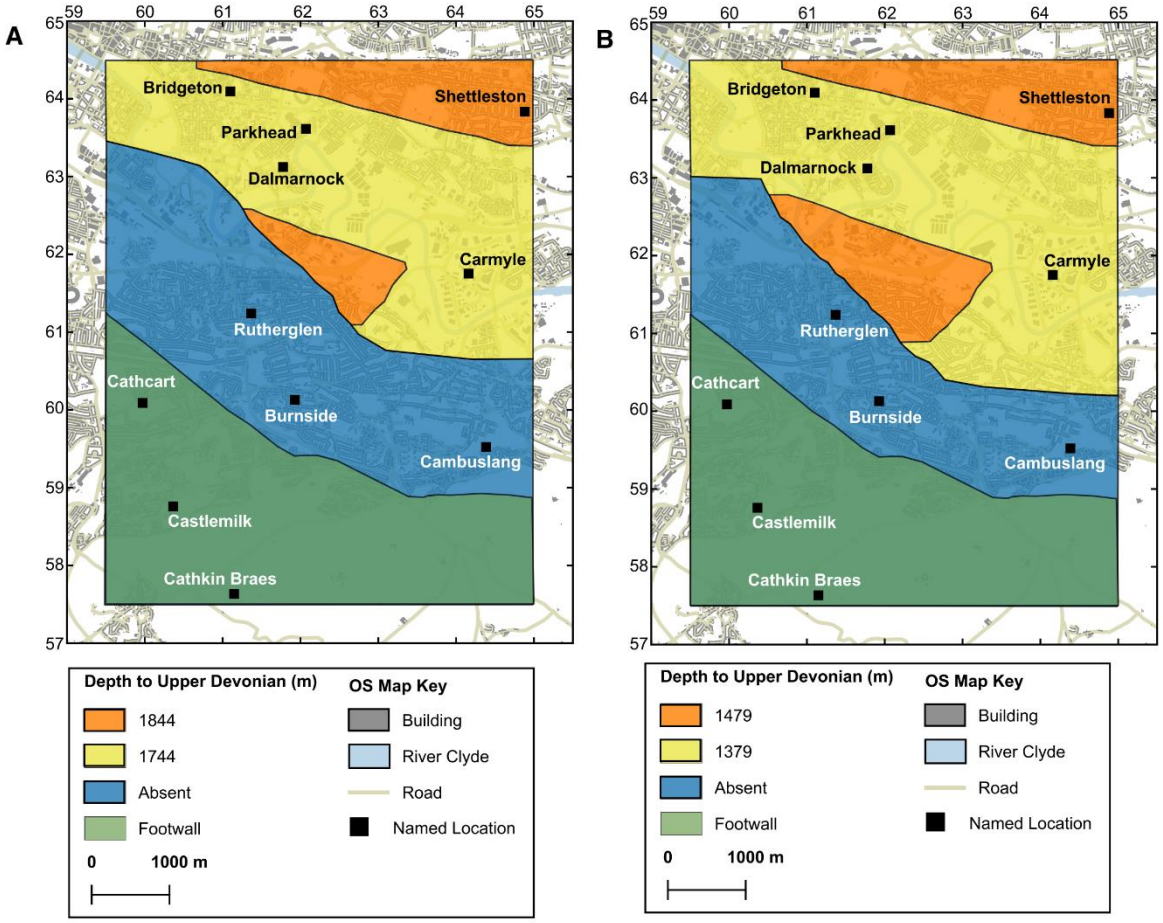

Figure 3.23. Depth to the top of the Kinnesswood Formation in the hanging wall of the Dechmont Fault derived from the stratigraphy of the 'Upper Model' (A) and the 'Lower Model' (B).

Figures 3.22 and 3.23 show that there are areas of the hanging wall of the Dechmont Fault where deeply buried Upper Devonian sandstones are absent, and instead Carboniferous strata are underlain by the buried footwall escarpment, consisting of either (1) the Upper Devonian sandstones at much shallower depth beneath the CPV outcrop, (2) Lower Devonian or Lower Palaeozoic rocks, or (3) a thick sequence of the CPV and underlying igneous intrusion. This encompasses areas such as Burnside, Cambuslang, and Rutherglen which may therefore be ruled out as potential locations for deep geothermal projects due to the absence of the deeply buried Upper Devonian sandstone sequence.

On the other hand, areas such as Bridgeton, Dalmarnock, Parkhead, Carmyle, Tollcross and Shettleston are candidate locations for deep geothermal developments to take place, with an upper estimate of the depth to the top of the Upper Devonian in these locations of 1744-1844 m and a lower estimate of 1379-1479 m (Figure 3.23).

The intersection of the Dechmont Fault and the buried Upper Devonian sandstone sequence may also present possible candidate locations for geothermal exploration in eastern Glasgow. As discussed in section 3.3, given the orientation of the Dechmont Fault in relation to the maximum horizontal compressive stress axis, there may be permeably open apertures in the associated fault zone. Furthermore, where post-cementation fracturing has occurred, intergranular porosity within the Upper Devonian sandstone aquifer which was previously lost due to cementation (see Chapter 4) may well have re-interconnected (Younger et al., 2016), offering scope for significant fluid flow and thus geothermal production. The permeability and porosity of the aquifer may therefore be enhanced where the fault intercepts the Kinnesswood Formation and the underlying Stratheden Group (Figure 3.21 and 3.22). This concept mirrors the original plan for the Science Central borehole, where it was proposed that lateral wells were to be drilled to intersect the Ninety Fathom Fault and associated damage zone in the Fell Sandstone Formation beneath Newcastle city centre (Younger et al., 2016), and the proposed Bishop Auckland geothermal project (Westaway et al., 2019).

To summarise, this study is significant as the newly collected gravity data and the development of the 3-D structural geological model for eastern Glasgow have (1) confirmed the extent and depth of the Upper Devonian sandstones within the Carboniferous-Devonian basin beneath eastern Glasgow, and (2) identified possible locations where the Dechmont Fault may increase the porosity and permeability of the Upper Devonian sandstone aquifer.

Based upon the structural geology and presence of the Upper Devonian sandstones derived from this study, the aquifer properties and temperature of the geothermal resource are investigated further in Chapters 4, 5 and 6 of this thesis. Then, combining these results, the deep geothermal resource beneath Glasgow's East End was quantified.

3.7. Conclusion

As a first step in investigating the geothermal resource in the Upper Devonian sandstones of the Kinnesswood Formation and the underlying Stratheden Group beneath Glasgow, a new gravity survey was conducted to determine the 3-D geological structure of eastern Glasgow and thus the extent and depth of the geothermal resource.

The specified target region was eastern Glasgow, in an area which comprised of a deep sedimentary basin of Carboniferous-Devonian age and the basin-bounding Dechmont Fault. A high-density gravity survey was conducted, measuring new gravity data in both the

footwall, and hanging wall of the Dechmont Fault. In total, 161 new gravity measurements were recorded during the survey fieldwork. Constrained by this new data, gravity forward modelling was carried out using Noddy software to develop a 3-D structural geological model of the survey area. Existing seismic reflection surveys were re-examined, and interpreted seismic reflectors were depth converted to constrain the choice of input parameters to the 3-D gravity modelling. Following a sensitivity analysis and various iterations in the development of the model, two alternative 3-D structural geological model of the survey area were constructed which produce a best-fit between the measured and modelled Bouguer gravity anomalies.

This present study describes the research process required to investigate aspects of structural geology which are critical to any proposed geothermal development in sedimentary rocks in Britain. The results of this study were significant as the creation of this 3-D structural geological model enabled the following features to be determined:

(1) the geometry of the Dechmont Fault,
(2) the extent of the buried footwall escarpment,
(3) the extent and depth of the geothermal resource in the Upper Devonian sandstones of the Kinnesswood Formation and the Stratheden Group in the hanging wall of the Dechmont Fault, and
(4) locations where the Dechmont Fault intersects the deeply buried Upper Devonian sandstone sequence, potentially creating a secondary geothermal target of fault induced groundwater flow in the aquifer.

The results of this investigation were then used to assess candidate locations for deep geothermal exploration to take place in eastern Glasgow. This encompassed areas such as Bridgeton, Dalmarnock, Parkhead, Carmyle, Tollcross and Shettleston, with an upper estimate of the depth to the top of the Upper Devonian in these locations of 1744-1844 m and a lower estimate of 1379-1479 m. Following the work of this chapter, the temperature and aquifer properties of the geothermal resource in the Upper Devonian sandstones beneath Glasgow are investigated further in subsequent chapters of this thesis.

Chapter 4. Analyses of the Properties of Upper Devonian Sandstones in the MVS

4.1. Introduction

This chapter investigated the diagenetic and depositional factors which preserve or restrict porosity in samples of Upper Devonian sandstone to assess the implications for geothermal exploration beneath Glasgow. Fieldwork was conducted by the author to collect representative samples of the Kinnesswood Formation and underlying Stratheden Group samples from outcrop sites surrounding Glasgow and from borehole core archived by the British Geological Survey. Thin section petrography, X-Ray Computed Tomography (X-CT) and X-Ray Diffraction (XRD) analyses were then carried out to determine the effects of diagenesis and deposition on the porosity and properties of each sample. This study did not investigate the permeability of the samples; however, the author acknowledges that the effects of diagenesis and deposition on permeability should be established in future work. The Upper Devonian sandstone formations present in the western MVS with the most favourable properties to be targeted in future geothermal developments in Glasgow were then highlighted. First, the aims and rationale of the chapter are outlined, then the burial history of the western MVS is described. Following this, the approach taken to collect samples of Upper Devonian sandstones from analogue outcrop and borehole sites is detailed. The methodology and the results of the thin section petrography, XRD, and X-CT analyses are then presented. Finally, the effects of diagenesis and depositional environment on the porosity of Upper Devonian sandstones, and the implications for geothermal energy exploration beneath Glasgow, are discussed.

4.2. Chapter Aim

The aim of this chapter was to analyse the depositional and diagenetic effects on the porosity of Upper Devonian sandstones in the western MVS and thus assess the implications for geothermal exploration in Glasgow. As there are currently no boreholes which intercept the Upper Devonian sandstones where they are present at depth beneath Glasgow, an outcrop and borehole (<600 m depth) analogue study of the Upper Devonian sandstones in the western MVS was conducted by the author.

The specific aims of this chapter were to:

- Collect samples of Upper Devonian sandstones from outcrop sites and borehole core,
- Conduct thin section petrography to determine the rock mineralogy, and textural and compositional maturity of each sample,

- Conduct XRD analysis to quantify the mineralogy of the samples with greater accuracy and to identify the presence of authigenic carbonate cement or clay which may inhibit the porosity of the sandstones,
- Conduct X-CT analysis to calculate the sample porosity and examine the physical and mineralogical properties of each sample,
- Combine the results to assess the diagenetic and depositional factors which preserve or restrict porosity,
- Identify the Upper Devonian sandstone formations with the most favourable properties to be targeted in future geothermal developments in Glasgow.

4.3. Rationale

The results of Chapter 3 established that the Upper Devonian sandstones are present at depths exceeding c.1400 m beneath eastern Glasgow. The only borehole in the MVS which has encountered Upper Devonian sandstones at depths equivalent to those beneath Glasgow is the Inch of Ferryton borehole (located at NS 907 901, c. 40 km from Glasgow) which drilled through sandstones of the Stratheden Group at c. 2000 m depth. However, at the time of writing, neither the mineralogical nor hydraulic properties of the Stratheden Group sandstones within this borehole have been analysed or published. There is uncertainty, therefore, regarding the properties of equivalent sandstones at burial depths of c.1400-2000 m beneath Glasgow.

The porosity and permeability of samples of Upper Devonian sandstones from boreholes (<600 m) throughout the MVS were measured by Browne et al. (1985, 1987) (Appendix 4.A). These studies found that the most favourable properties were observed at outcrop in Fife in sandstones of the Knox Pulpit Formation but decreased with depth in the Glenrothes borehole where porosity and permeability was fractured dominated (Browne et al., 1987; Brereton et al., 1988). The physical and mineralogical properties of the sandstones were also examined by Browne et al. (1987), and the findings indicated that porosity is restricted by diagenetic effects such as mineral overgrowth and pressure solution.

An insight to the properties of the Kinnesswood Formation and Stratheden Group sandstones beneath Glasgow is provided by deeply buried sandstones (2.7-3.2 km depth) of the Upper Devonian aged Buchan Formation of the Ardmore Petroleum Field of the Central North Sea. The Buchan Formation is postulated to be laterally equivalent to the Stratheden Group of the MVS (Trewin and Thirlwall, 2002; Kearsey et al., 2015), and is composed mainly of

sandstones deposited in a braided fluvial and aeolian environment (Gluyas et al., 2005). The porosity of sandstones of the Buchan Formation varies between 1% and 28% while permeability varies between <1 mD and >5000 mD (Gluyas et al., 2005; Tang et al., 2020). Tang et al. (2017, 2018a, 2018b) examined the diagenetic and depositional controls on the reservoir quality of aeolian and fluvial facies of the Buchan Formation. Summarised in Table 4.1, these investigations found that aeolian sandstones have a superior reservoir quality to fluvial sandstones, partly due to the higher compositional and textural maturity of aeolian deposits and the differing effects of diagenesis on the aeolian and fluvial deposits.

Table 4.1. Lithological and diagenetic characteristics of aeolian and fluvial facies of the Buchan Formation (Upper Devonian). Summarised from Tang et al. (2018a; 2018b; 2020).

Property	Aeolian Facies	Fluvial Facies
Porosity	5.1-28%	0.1-23.1%
Permeability	0.2-5290 mD	0.2-1240 mD
Reservoir Quality	Higher	Lower
Cementation	Dolomite	Dolomite, quartz overgrowth
Grain Coating	I/S grain coating	I/S grain coating absent
Presence of kaolinite	Limited	Abundant
Compositional Maturity	Higher ($Q_{82}F_2R_{16}$)	Lower ($Q_{76}F_3R_{21)}$
Textural Maturity	Higher	Lower
Grain Size	Fine-medium grained	Fine-medium grained
Grain Sorting	Moderate-well	Poor-moderate
Grain Shape	Sub-rounded to rounded	Sub-angular to sub-rounded
Compaction	Low-moderate	Moderate-high
Contacts	Point and long	Curved and concavo-convex
Influence of Compaction	33% porosity reduction	31% porosity reduction
Influence of Cementation	13-26% porosity reduction	36.4-42.9% porosity reduction

Abbreviations: I/S: Illite/Smectite

In both aeolian and fluvial sandstones, the reduction in porosity and permeability was predominately due to mechanical compaction and dolomite cementation. However, fluvial sandstones exhibited intense quartz overgrowth and quartz cementation which further reduced the reservoir quality. These effects were absent in aeolian sandstones where the presence of grain coating illite/smectite clays inhibited quartz overgrowth and thus preserved the porosity (Tang et al., 2018a, 2018b).

The Buchan Formation therefore provides examples of features which control the quality of deeply buried sandstones aquifers, which could also be present in the Upper Devonian sandstones beneath Glasgow. Specifically, the preservation of porosity due to grain coatings, the reduction in porosity due to compaction and cementation, the heterogeneity of the aquifer

caused by differing depositional environments, and the superior porosity and permeability of aeolian sandstones in comparison to fluvial sandstones.

To provide further insight to the possible properties of Upper Devonian sandstones in the potential geothermal resource beneath Glasgow, further analysis on the effects of deposition and diagenesis on Upper Devonian sandstones in the western MVS was warranted in the context of the preservation of favourable properties at depth in the Buchan Formation.

4.4. Burial History of the Western Midland Valley of Scotland

The reduction of porosity in sandstone is determined by the maximum burial depth rather than the present-day depth, and therefore knowledge of the burial history of the western MVS was used to inform the choice of fieldwork sampling sites and to inform the discussion of the results of the analysis.

Permian and Triassic rocks are largely absent from the MVS, however are preserved locally in the Mauchline Base in Ayrshire (Figure 2.9) (Mykura et al., 1967) and on Arran (Cameron and Stephenson, 1985). Permian and Jurassic rocks up to c. 1500 m thick are also preserved offshore in the outer Firth of Forth and in the Firth of Clyde (Cartwright et al., 2001). This has led to the hypothesis that these younger successions encroached on the MVS and have since been removed by uplift and erosion (Cameron and Stephenson, 1985). Late Palaeozoic and Mesozoic deposition may, therefore, have been substantial across the MVS, with sedimentation likely to have ended in the early Cenozoic at around 60 Ma, coeval with the start of North Atlantic magmatism, uplift, and erosion (Vincent et al., 2010). Thermal history and basin subsidence modelling of the eastern MVS by Vincent et al. (2010) indicated up to 1900 m of additional burial of Carboniferous strata compared to the present-day levels, including up to 660 m deposited by the end of the Carboniferous period subsequently removed by Variscan uplift and erosion, followed by up to 1900 m of burial by sedimentary rocks deposited during the Permian to Palaeogene periods.

Early Cenozoic denudation of western Scotland has been analysed by various authors using low temperature thermochronology techniques, such as Apatite (U-Th)/He and fission track analysis, and thermal modelling (Thompson et al. 1999; Persano et al. 2007; Döpke, 2017; Luszczak et al. 2017). From these studies, the four samples in closest proximity to the western MVS are shown in Table 4.2. One sampled site is located within the MVS, at Distinkhorn in Ayrshire, two in the western Highlands to the north-west of the MVS, and one to the south of the MVS at Crawfordjohn to the south of the Southern Upland Fault.

Table 4.2. Thermochronology samples in western and southern Scotland.

Sample	BNG	Location	Lithology	Z_1 (m)	Z_2 (m)	Ref
6	NM 911 554	Rubha na h-Earba	Sandstone	68	837	1
SCT 2	NS 602 352	Distinkhorn	Granite	240	1226	2
SL-01	NS 919 238	Crawfordjohn	Essexite	310	1464	3
Sgorr Dhonuill	NN 040 555	Sgorr Dhonuill	Granite	195-1001	1037	4

(1) Thompson et al. (1999); (2) Döpke (2017), (3) Luszack et al. (2017), (4) Persano et al. (2017). Cenozoic denudation is calculated relative to the present-day sea level for each site. Z_1 is the site elevation relative to present day sea level (m) and Z_2 is the estimated Cenozoic palaeo-surface relative to present day sea level (m).

Persano et al. (2017) used thermal histories derived from apatite and helium fission track data from samples from 195-1001 m on a traverse of Sgorr Dhonnuil to constrain the early Cenozoic geothermal gradient at 39±9 °C km^{-1} and calculated the maximum amount of denudation relative to present-day sea level to be 1330±230 m. Thompson et al. (1999) stated that the palaeo-temperature of sample '6' in the early Cenozoic was 50±10 °C and estimated that 1429 m of Cenozoic denudation had taken place, meaning that the Cenozoic land surface was 1497 m above the present-day sea level. Whereas Döpke (2017) showed that the palaeotemperature of sample SCT-2 at Distinkhorn was approximately 60 °C during the early Cenozoic, and Luszczak et al. (2017) stated that the palaeotemperature of sample SL-01 at Crawfordjohn was 65 ±15 °C.

The denudation calculated by Persano et al. (2017) was determined based upon a Cenozoic surface temperature of 10 °C and an early Cenozoic geothermal gradient at 39±9 °C km^{-1}, however a higher estimate of the Cenozoic surface temperature was proposed by Green et al., (2012) of 20 °C. Furthermore, the denudation calculated by Thompson et al. (1999) was determined using a Cenozoic geothermal gradient of 35 °C km^{-1} and a Cenozoic surface temperature of 0 °C. The choice of assumed surface temperature and assumed Cenozoic geothermal gradient thus varied significantly between these studies.

For the present study, the author has recalculated estimates of early Cenozoic denudation relative to present day sea level at each of the four sites in Table 4.2 using the palaeo-temperature and palaeo-geothermal gradient data reported by Thompson et al. (1999); Döpke (2017), Luszack et al. (2017), Persano et al. (2017). For these calculations, Equation 4.1 was used where dT/dZ is the Early Cenozoic palaeo-geothermal gradient (°C km^{-1}), T_1 is the Cenozoic surface temperature (°C), T_2 is the Cenozoic palaeo-temperature of the sample

analysed within each study (°C), Z_1 is the present day elevation (m) and Z_2 is the estimated Cenozoic palaeo-surface (m).

$$\frac{dT}{dZ} = \frac{T_2 - T_1}{Z_2 - Z_1}$$

(Equation 4.1)

For these calculations T_1 was assumed to be 20 °C (Green et al., 2012), and dT/dZ assumed to be 39 °C km^{-1} (Persano et al., 2007) were assumed. The results are detailed in Table 4.2.

Luszczak et al. (2017) stated that the palaeotemperature measurement of SL-01 has a range of uncertainty of ±15 °C, therefore if the sample palaeotemperature was as high as 80 °C, then the denudation relative to present day sea level would be 1878 m, and if it was as low as 50 °C, then the this reduces to 1109 m. Similarly, Thompson et al. (1999) stated that the palaeo-temperature of sample '6' in the early Cenozoic was 50±10 °C, therefore at this site if the sample palaeotemperature was as high as 60 °C, then the denudation relative to present sea level would be 1093 m, and if it was as low as 50 °C, then the this reduces to 580 m.

The assumed Cenozoic surface temperature, palaeo-geothermal gradient, and error related to the measured palaeo-temperature, thus have an impact on the resulting estimation of Cenozoic denudation. However, the results shown in Table 4.2 and reported in previous studies (Vincent et al., 2010) demonstrate that early Cenozoic denudation in western and central Scotland was significant and in the range of c. 800-1500 m, or more.

Due to early Cenozoic denudation of western Scotland, Upper Devonian sandstones which presently outcrop close to sea-level or are encountered in boreholes in the western MVS will have experienced maximum burial of c. 1500 m, and thus will have experienced the maximum, or near-maximum, effects of compaction (Lander and Walderhaug, 1999). A sample of Upper Devonian sandstone recovered from c. 1400-2000 m depth beneath Glasgow (see Chapter 3) will therefore not have been compacted significantly more than those encountered at outcrop or in shallow boreholes in the western MVS. The effects of compaction on the porosity of Upper Devonian sandstone samples from this outcrop study are therefore comparable with the effects of compaction on sandstones buried at depths of c. c.1400-2000 m beneath Glasgow. However, the effects of cementation on the porosity of deeply buried sandstones beneath Glasgow, caused by the movement of highly mineralised groundwater, remains uncertain and cannot be resolved without deep exploratory drilling.

4.5. Fieldwork and Preliminary Analysis

This section describes the approach taken to collect samples of Upper Devonian sandstones from analogue outcrop and borehole sites and the selection of samples for further analysis. The selection of sample sites was based upon the need to: (1) sample each formation in Table 2.6, (2) sample representative fluvial or aeolian deposits of the respective formation, and (3) sample similar sedimentary facies to compare outcrop and borehole samples.

4.5.1. Borehole Core Samples

In the 1970's and 1980's a number of boreholes were drilled by the Institute of Geological Sciences (IGS) to investigate the Lower Carboniferous and Upper Devonian stratigraphy of the MVS. Six of the boreholes; Barnhill, Clachie Bridge, Everton, Glenburn, Kipperoch, and Tak Ma Doon, are located in outcrops of the CPV or the Inverclyde Group surrounding Glasgow (Figure 4.1, 4.2), in areas such as the Clyde Muirshiel Regional Park, Kilpatrick Hills, Glenniffer Braes, and Gargunnock Hills.

As the boreholes were drilled to prove the relationship between the Lower Carboniferous to the Devonian strata in these areas, each borehole encounters thick sequences of the Kinnesswood Formation and/or the underlying Stratheden Group sandstones (Table 4.3, Figure 4.2). Furthermore, in the late 1980's the Glenrothes borehole was drilled to conduct geothermal measurements to investigate the potential geothermal aquifer in the Kinnesswood Formation and Knox Pulpit Formation in Fife (Figure 4.2). This borehole, likewise, encountered a thick Upper Devonian sandstone succession (Table 4.3, Figure 4.2).

Table 4.3. Details of sampled boreholes.

Name	BGS SOBI Ref	NGR	Date[1]	Depth[2] (m)	KNW[3] (m)	SAG[4] (m)
Barnhill	NS47NWBJ2	NS 4269 7571	1977	356.40	288.98-350.78	-
Clachie Bridge	NS68SWBJ1	NS 6448 8368	1976	300.30	283.93-300.30	-
Everton	NS27SWBJ5	NS 2145 7104	1977	143.82	50.83-122.33	122.33-143.82
Glenburn	NS46SEBJ164	NS 4783 6065	1980	467.57	43.54-116.17	116.17-467.57
Glenrothes	NO20SEBJ385	NO 2562 0314	1986	567.65	362.43-449.32	449.32-567.65
Kipperoch	NS37NEBJ20	NS 3727 7742	1977	300.57	51.00-220.14	220.14-300.57
Tak-Ma-Doon	NS78SWBJ5	NS 7291 8053	1978	268.19	85.64-231.59	231.59-268.19

(1) date of drilling, (2) depth of well bottom, (3) interval that Kinnesswood Formation was encountered. (4) interval that the Stratheden Group was encountered.

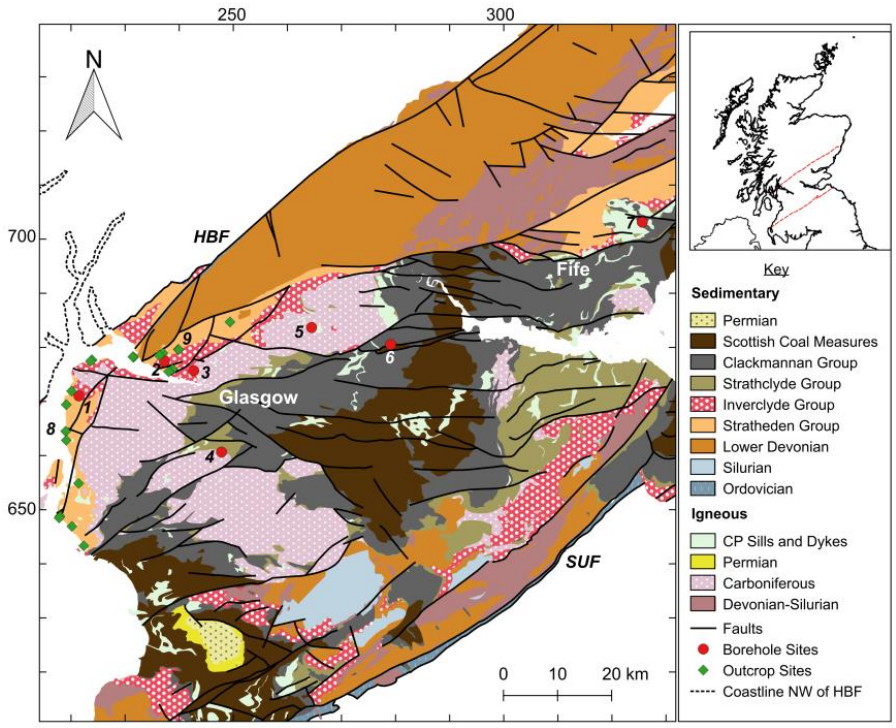

Figure 4.1. Locations of boreholes and outcrop sites in the MVS sampled in this study. Numbered borehole and outcrop sites: (1) Everton, (2) Kipperoch, (3) Barnhill, (4) Glenburn, (5) Clachie Bridge, (6) Tak Ma Doon, (7) Glenrothes, (8) Firth of Clyde Coastline, (9) Dumbarton. Geological Map Data BGS © UKRI 2021.

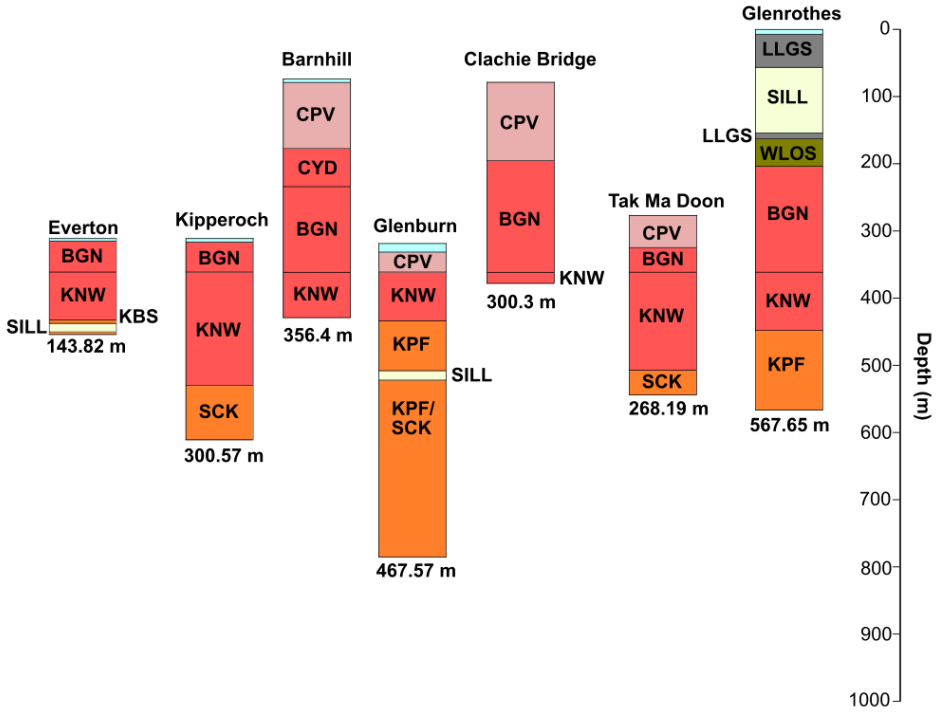

Figure 4.2. Boreholes examined in this study. From (IGS 1976, 1978, 1980, 1982; Brereton et al., 1988). Based upon records provided by British Geological Survey (UKRI).

Sampling of core retrieved from these boreholes therefore provided an opportunity to collect representative specimens of Upper Devonian sandstones from various locations throughout the MVS.

Core samples were collected by the author from each of these boreholes from the BGS Core Archive (e.g., Figure 4.3). This included twenty-five samples of the Kinnesswood Formation and ten samples of the Stratheden Group sandstones. The samples are detailed in Appendix 4.B, Tables 4.B.1 and 4.B.2. The BGS samples are named with the prefix, SSK, followed by the BGS sample number. This differs from the outcrop samples described below, prefixed with an abbreviation of the sampled stratigraphic formation followed by the sample number. This nomenclature is used throughout this chapter when referring to the samples.

4.5.2. Outcrop Samples

To supplement the samples of borehole core, fieldwork was conducted by the author to collect samples from outcrops of Upper Devonian sandstones in the western MVS (Figures 4.3 and 4.4). In total, twenty-six hand specimen samples were collected from outcrop sites (Figure 4.4). Detailed in Tables 4.B.3 and 4.B.4, this consisted of ten samples of the Kinnesswood Formation and sixteen samples from formations of the Stratheden Group.

Figure 4.3. Example of the Kinnesswood Formation outcrop at Gourock where KNW 01 and KNW 02 were sampled (a). Example of the Stockiemuir Sandstone Formation at outcrop at Bonhill Quarry, where SCK 24 was sampled (b). Example of the Knox Pulpit Formation in the Glenrothes borehole (c). Example of the Stockiemuir Sandstone Formation in the Kipperoch borehole (d).

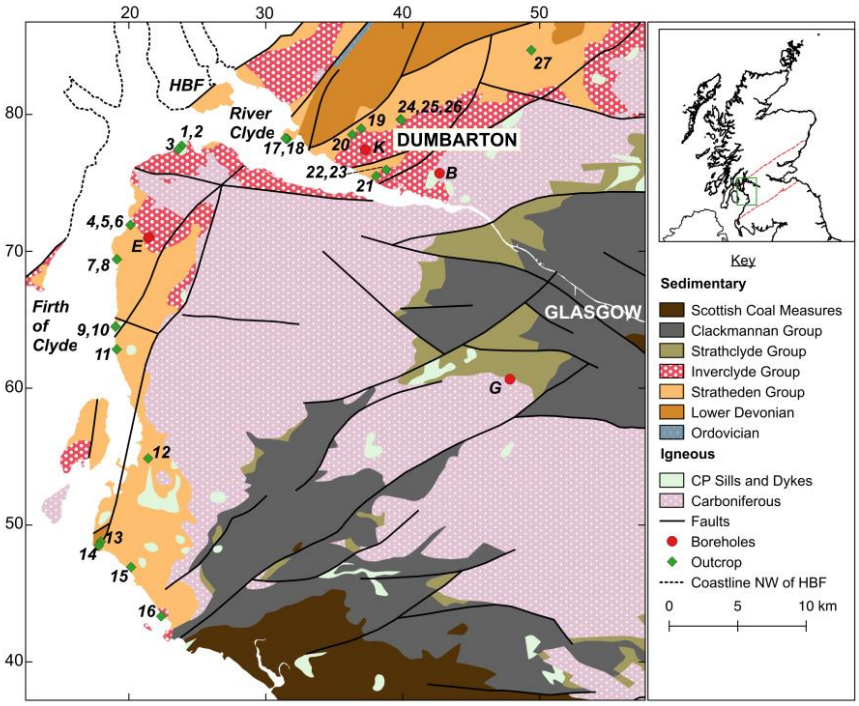

Figure 4.4. Locations of boreholes and outcrop sites in the western MVS sampled in this study. Borehole abbreviations; E: Everton, G: Glenburn, B: Barnhill, K: Kipperoch. Locations 1-27 are outcrop sites and relate to the number of the sample in Appendix 4.B. Geological Map Data BGS © UKRI 2021.

4.5.3. Preliminary Assessment of Samples

Observations were made by the author, both in-situ at outcrop and from hand specimens of the sampled sandstones. Two distinct facies were observed from hand specimens of the Kinnesswood Formation; (1) red or grey-purple laminated sandstones with clasts, mudstone laminae and calcareous bleaching, with varying degrees of cementation (Figure 4.5a), and (2) grey, laminated, cemented sandstones with calcareous concretions (Figure 4.5b).

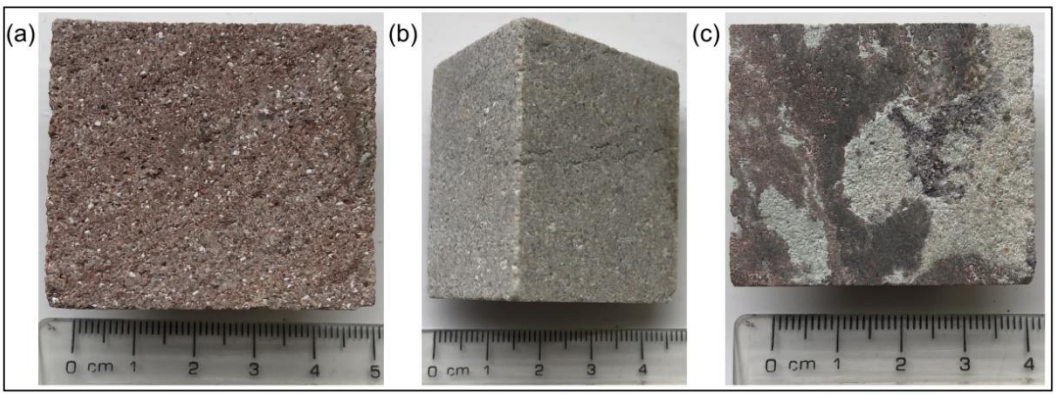

Figure 4.5. Hand specimens of samples SSK 71377 (a), SSK 71496 (b), and SSK 71505 (c).

Samples of the Kinnesswood Formation from the Barnhill, Glenburn and Kipperoch boreholes were representative of facies (1) and were visibly similar to samples obtained from outcrop sites in the Dumbarton area (Figure 4.6a), whereas those from the Glenrothes and Tak Ma Doon boreholes, and from outcrop sites on the Firth of Clyde coastline (e.g., Figure 4.6b) were representative of facies (2). A small number of samples of cornstone horizons were also collected which contained an abundance of carbonate cement (Figure 4.5c). The samples from the Clachie Bridge borehole differed significantly to other samples of the Kinnesswood Formation. This may be due to the proximity of the borehole to an igneous intrusion which thermally altered the rocks (Forsyth et al., 1996).

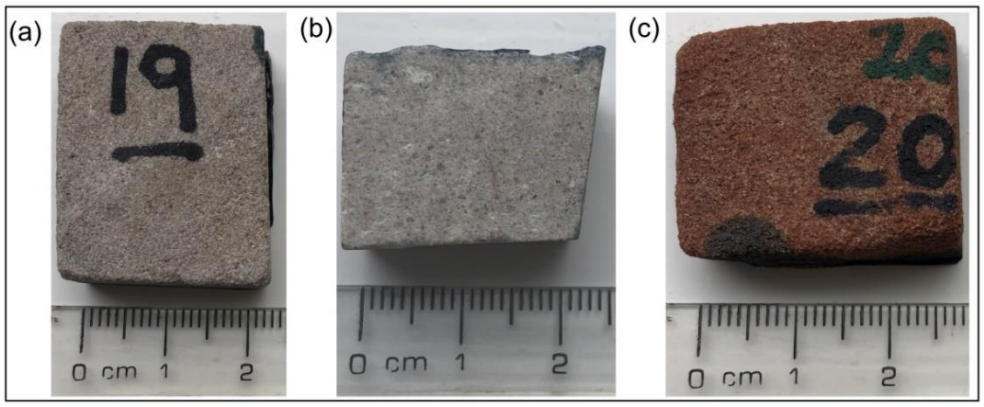

Figure 4.6. Hand specimens of outcrop samples KNW 19 (a), KNW 2 (b), and SCK 20 (c).

Samples of the Skelmorlie Conglomerate and Rosneath Conglomerate Formation were dark red, poorly sorted, and contained abundant metamorphic, quartz and mudstone clasts. The Wemyss Bay Formation ranged from red, poorly sorted, conglomeratic sandstone, to red, cross-bedded, well sorted, fine grained sandstone. Each of these samples visibly lacked porosity and were well cemented and compacted. These sandstones were markedly different to the younger Upper Devonian sandstones sampled in the Kipperoch, Everton, Glenrothes and Glenburn boreholes and from outcrop sites. Samples of the Stockiemuir Sandstone, Knox Pulpit, and Fairlie Sandstone formations from these locations were typically red or pale cream, well sorted sandstones with laminations and minimal cementation (Figure 4.3, Figure 4.6c, 4.7a, and 4.7b). The majority of these samples were distinctly aeolian and lacked the fluvial characteristics of the older Devonian sandstones, however the samples from the Kipperoch borehole may be from aeolian horizons interbedded within fluvial deposits. The samples of the Kelly Burn Sandstone Formation were typical of fluvial deposition and were visibly tighter than the aeolian sandstones, containing clasts, carbonate concretions and carbonate bleaching (Figure 4.7c), although not to the extent of the older fluvial samples.

Figure 4.7. Hand specimen of samples SSK 71508 (a), SSK 71381 (b), and SSK 71523 (c).

Following this preliminary analysis, samples were selected for thin section petrography, XRD and X-CT analyses to determine the porosity of each sample and assess the diagenetic and depositional factors which preserve or restrict porosity. The samples which were selected were those, (1) representative of the three distinct Kinnesswood Formation facies, (2) representative of the aeolian and fluvial facies of the Stratheden Group, and (3) which allowed for comparisons to be drawn between outcrop and borehole core.

Samples which were deemed unrepresentative (i.e., Clachie Bridge borehole samples) or did not meet the criteria (i.e., Rosneath Conglomerate, Skelmorlie Conglomerate, and Wemyss Bay Sandstone Formation samples), were omitted from further analysis. Field and hand specimen observations of these samples are detailed in Appendix 4.B.

4.6. Methodology

4.6.1. Petrographic Analysis Methodology

Thin section petrography was used to determine the rock mineralogy, and the textural and compositional maturity of each sample. By doing so, the depositional and diagenetic controls on the porosity of each sample were examined. Thin sections of thirty-nine samples were prepared, the majority of which were borehole core samples, and the remainder were representative outcrop samples. The samples were impregnated with blue epoxy resin in order to identify porosity, and care was taken to minimise breakage and preserve cements, textures, and fabrics. Petrographic examination was performed on a standard polarizing microscope and photomicrographs were taken using an attached digital camera under plain polarised (PPL) and cross polarised light (XPL). The mineral grain percentage composition of each sample was estimated visually using Folk (1951) and Folk et al. (1970) comparison charts and presented on ternary diagrams to classify each sample. The extent of compaction (stated as low, moderate, and high) was based upon the number and type of grain contacts observed in each sample (e.g., Taylor, 1950).

4.6.2. XRD Methodology

Following the petrographic thin section analysis, representative samples of the Kinnesswood Formation and Stratheden Group were selected for XRD analysis to quantify the mineralogy of the samples with greater accuracy and to identify the presence of authigenic carbonate cement or clay which may inhibit the porosity of the sandstones. In preparation for the XRD analysis, samples were gently crushed to a powder using a pestle and mortar. Twenty-two samples were selected for this analysis, including nine samples of the Kinnesswood Formation and thirteen samples of the Stratheden Group.

XRD patterns were collected using a Rigaku MiniFlex 6G equipped with a D/teX Ultra detector, a 6-position (ASC-6) sample changer and Cu sealed tube (Ka1 and Ka2 wavelengths - 1.5406 and 1.5444 Å respectively) at the University of Glasgow. Patterns were measured as q/2q scans typically over a range of 3>2q>80°. Data collection and analysis were carried out using Rigaku SmartLab Studio II software, and the search match procedure used the Crystallographic Open Database (https://wiki.crystallography.net/cod/citing/). The Reference Intensity Ratio (RIR) method was used to produce a quantitative analysis of the mineralogical composition of each sample.

This analysis identified the main mineral phases which occur in each sample, such as detrital quartz, calcite, and dolomite. Groups of minerals such as micas, 1:1 clay, and 2:1 clay were

also identified; however, the individual mineral could not be distinguished by the analysis. The mica grouping represents possible candidate minerals such as biotite, muscovite or phlogopite; the 1:1 clay grouping represents possible candidate minerals such as kaolinite, and the 2:1 clay grouping represents possible candidate minerals such as chlorite, illite or smectite.

4.6.3. X-CT Methodology

Following the petrographic thin section and XRD analysis, X-CT analysis was conducted to determine, (1) an estimation of the sample porosity, (2) the porosity distribution within the sample, and (3) further evidence of diagenetic or depositional features which reduce or preserve porosity.

X-CT analysis is a non-destructive and non-invasive method which uses contrasts of X-ray attenuation, a function of density and atomic number, to reconstruct the 3D distribution of areas of different densities within a large variety of materials (Hanna and Ketcham, 2017). The 3D reconstruction is based on a series of contiguous 2D radiographs taken with different view angles, by rotation a sample around a single axis in small steps (Hanna and Ketcham, 2017).

The X-CT scans were performed using a Nikon XTH 320/225 system, equipped with a 225 kV reflection gun and a 2000 x 2000 pixel flat panel photodetector (cell size 0.2 x 0.2 mm) at the Advanced Materials Laboratory at the University of Strathclyde. The X-CT operating conditions varied depending upon the target voxel size (resolution) of the respective scan. First, borehole core samples were scanned, achieving an approximate minimal voxel size 20 µm. These core samples were in their original form as half cores of c. 3 cm height and 2-3 cm diameter (Figure 4.8a, Tables 4.C.1 and 4.C.2). However, improved results were achieved when the size of the scanned sample was reduced, and the duration of the scan extended, thereby increasing the resolution of the scan. Smaller sub-samples of the borehole core samples were then produced (Tables 4.C.3 and 4.C.4) and outcrop samples were prepared as 1-2 cm cubes (Figure 4.8b, Tables 4.C.5 and 4.C.6).

For the highest resolution scans, the X-ray source to sample distance was set to achieve an approximate minimal voxel size of 3-5 µm, which allowed pores and grains of c. 9-15 µm to be resolved. For the majority of these scans, the exposure time for each projection was 2829 ms, and the scans consisted of 1600 projections. The accelerating voltage was 137 kV and the current was 20 µA.

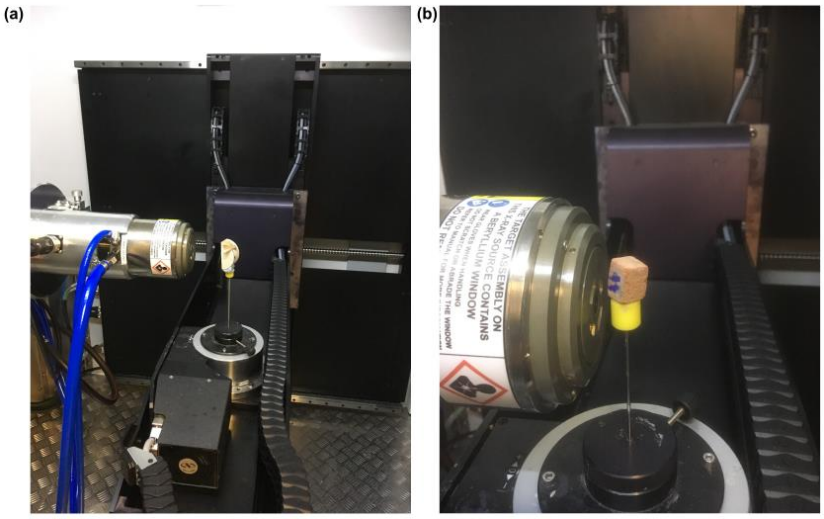

Figure 4.8. Borehole core sample (a) and cubed outcrop sample (b) positioned in the Nikon XTH 320/225 X-CT system.

The 3D volumes of the scanned samples were reconstructed from projections using CT Pro 3D software (© 2004-2016 Nikon Metrology), and beam hardening corrections were applied (Brooks and Di Chiro, 1976). All volumes were reconstructed in 16 bits (65536 grey values). Image processing of reconstructed 3D volumes was then conducted using Dragonfly software (v. 4.1.0.647, © Object Research System (ORS) Inc.), and Avizo software (v.9.2.0, © FEI), both of which are examples of established image processing software packages used in geoscience related X-CT analytical procedures (e.g., Hanna and Ketcham, 2017).

Both software packages were trialled on a number of samples and similar porosity results were achieved. The results presented in this chapter were produced by the Dragonfly software package. Quantitative analysis of sample porosity was undertaken following standard procedures including noise-reduction and segmentation (e.g., Beaudoin et al., 2018; Vasconcelos et al., 2018; Scheffer et al., 2021).

First, noise was reduced by applying an edge-preserving smoothing filter (‘bilateral filter’) which smoothed the intensity of a voxel with that of its neighbours defined by a 3 x 3 x 3 kernel size. Then, a sub-volume within the sample was created using the ‘crop’ tool, reducing discrepancies caused by ring artefacts and beam hardening.

Mineral and pore phases were then segmented using greyscale thresholding and further noise reductions were applied using the ‘remove small spot’ function, which removed all clusters of <10 pixels from the segmented 3D volume. The volumes of the mineral and pore phases

were then computed by counting the voxels in the respective voxel clusters, thereby determining an estimate of the porosity of the sample.

When determining the porosity of each sample, the choice of greyscale value used to segment the pore and mineral phases was critical. A sensitivity analysis was conducted for each sample to assess the variations in porosity caused by the choice of segmented greyscale values. An example of this is shown in Figure 4.9. In this case, the optimal threshold value was 10,500 which satisfactorily captured the pores shown in Figure 4.9a.

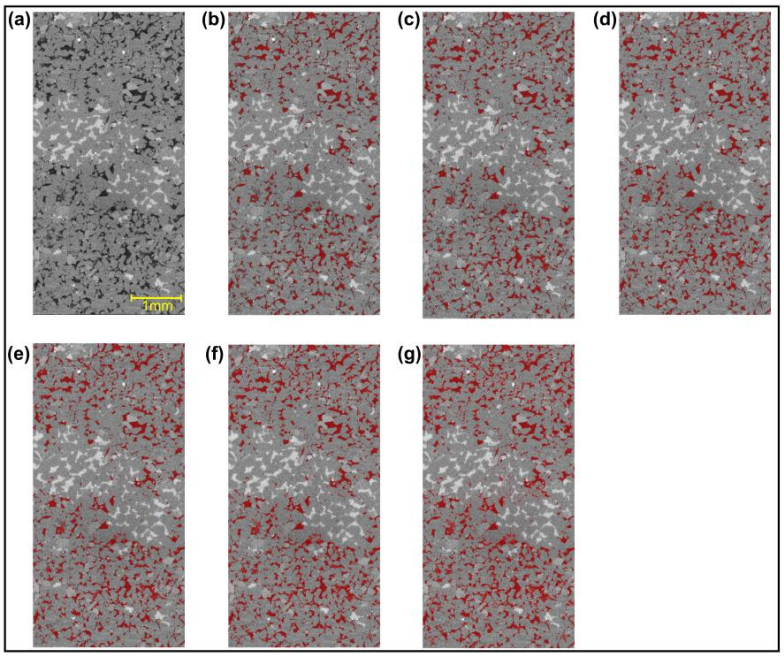

Figure 4.9. Example of thresholding using Dragonfly software to determine the porosity of sample SSK 71508. (a) greyscale X-CT scan (b) Thresholding of 9000; ϕ = 8.22%, (c) Thresholding of 9500; ϕ = 9.32%, (d) Thresholding of 10,000; ϕ = 10.57%, (e) Thresholding of 10,500; ϕ = 12.02% (f) Thresholding of 11,000; ϕ = 13.86%, (g) Thresholding of 11,500; ϕ = 16.54%.

4.7. Results

4.7.1. Petrographic Analysis Results

The textural and compositional results of the thin section petrographic analysis of the Kinnesswood Formation samples are detailed in Table 4.4. and Table 4.D.1, and likewise the Stratheden Group results are detailed in Table 4.4. and Table 4.D.2. The following section discusses key characteristics of the samples and highlights diagenetic and depositional features which influence the porosity of each sample.

Kinnesswood Formation

Samples of the Kinnesswood Formation varied in grain size, shape, and sorting but most commonly the grain shape was angular to sub-rounded, grain sorting tended to be poor to moderate, and grain size was very fine/fine to coarse (Table 4.4). The majority of samples exhibited moderate to high compaction, which was indicated by line and concave contacts with rarer point and dissolution contacts.

Most commonly, the samples were classified as sub-lithic arenites, however the set of samples also included lithic arenites, sub-arkosic arenites and quartz arenites (Table 4.4; Figure 4.10). Generally, the samples were texturally immature but had moderate compositional maturity, with the mean detrital composition calculated as $Q_{76}F_{8}R_{16}$ (respective percentage compositions of quartz, feldspar, and rock fragments). Outcrop and borehole core samples of the Kinnesswood Formation from the Dumbarton area were observed to have a higher compositional maturity ($Q_{82}F_{6}R_{12}$) and a higher textural maturity, exhibiting the most well rounded and well-sorted grains, compared to the remainder of the samples.

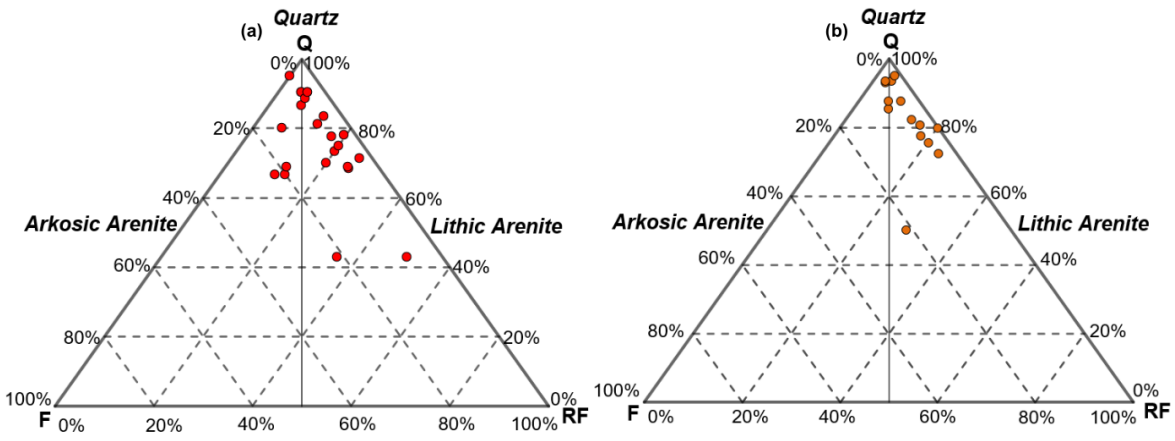

Figure 4.10. Ternary plots of the Kinnesswood Formation (a) and Stratheden Group (b).

Table 4.4. Thin section mineralogical analysis of Kinnesswood Formation samples.

Sample	Location	Description	Grain Shape	Grain Size	Grain Sorting	Compaction
KNW 02	Gourock	Lithic arenite	Angular to sub-rounded	Fine-medium	Moderate	Low
KNW 06	Inverkip	Lithic arenite	Sub-angular to rounded	Medium-coarse	Moderate	Moderate
KNW 16	Ardrossan	Sub-arkosic arenite	Sub-angular to sub-rounded	Fine-coarse	Poor-moderate	Moderate-high
KNW 19	Carmen Q.	Sub-arkosic arenite	Sub-rounded to rounded	Fine	Very well	Low-moderate
KNW 25	Bonhill	Sub-arkosic arenite	Sub-angular to sub-rounded	Fine-medium	Well	Moderate-high
SSK 71377	Glenburn	Lithic arenite	Angular to sub-rounded	Fine-medium	Moderate-well	Moderate
SSK 71378	Glenburn	Sub-arkosic arenite	Sub-angular to rounded	Fine	Poor-moderate	Moderate-high
SSK 71379	Glenburn	Lithic arenite	Angular to sub-rounded	Very fine-coarse	Moderate	Moderate
SSK 71496	Glenrothes	Sub-lithic arenite	Angular to sub-rounded	Very fine-coarse	Poor-moderate	Moderate-high
SSK 71497	Glenrothes	Sub-lithic arenite	Sub-angular to rounded	Very fine-coarse	Poor-moderate	Moderate-high
SSK 71504	Kipperoch	Sub-arkosic arenite	Sub-angular to sub-rounded	Medium	Moderate-well	Moderate-high
SSK 71506	Kipperoch	Sub-lithic arenite	Sub-angular to sub-rounded	Fine-coarse	Poor	Moderate-high
SSK 71507	Kipperoch	Sub-lithic arenite	Angular to sub-rounded	Very fine	Moderate	Moderate
SSK 71510	Barnhill	Lithic arenite	Sub-angular to rounded	Medium-coarse	Poor-moderate	Moderate-high
SSK 71511	Barnhill	Sub-lithic arenite	Angular to sub-rounded	Fine-medium	Poor-moderate	Moderate-high
SSK 71512	Barnhill	Sub-lithic arenite	Sub-rounded to rounded	Fine-medium	Moderate-well	Low-moderate
SSK 71513	Barnhill	Sub-lithic arenite	Angular to sub-rounded	Fine-coarse	Poor-moderate	Moderate
SSK 71514	Barnhill	Sub-lithic arenite	Angular to sub-rounded	Fine-medium	Well	High
SSK 71516	Tak Ma Doon	Sub-lithic arenite	Angular to sub-rounded	Medium-coarse	Poor-moderate	Moderate-high
SSK 71517	Tak Ma Doon	Sub-lithic arenite	Angular to sub-rounded	Fine-medium	Moderate	Low
SSK 71519	Everton	Sub-arkosic arenite	Sub-angular to sub-rounded	Fine-coarse	Poor-moderate	Low-moderate
SSK 71520	Everton	Sub-arkosic arenite	Sub-angular to sub-rounded	Very fine-coarse	Poor-moderate	Low-moderate
SSK 71521	Everton	Quartz arenite	Sub-angular to rounded	Very fine	Moderate-well	Moderate

Shown in Table 4.D.2, detrital quartz was the dominant mineral type (30-80%) in the majority of the samples of the Kinnesswood Formation. Detrital feldspar also occurred in each sample, ranging from 2-15%, and the presence of rock fragments occurred from trace amounts to 35%. Various diagenetic minerals were observed which inhibit porosity, the most prevalent being dolomite cement (0-45%), with lesser amounts of calcite cement (0-20%) and authigenic clay (0-15%) (e.g., Figure 4.11a and 4.11b). Quartz overgrowths were also present, occurring as syntaxial cement which forms as rims around quartz grains and occludes pore space (Figure 4.11a and 4.12).

The blue-epoxy resin highlighted the presence of intergranular porosity and secondary porosity present within the breakdown of detrital grains, which were typically feldspar (e.g., Figure 4.12b). For a number of samples, the syntaxial quartz cement also contained micro-porosity shown by fainter and/or speckled blue epoxy resin (e.g., Figure 4.11a).

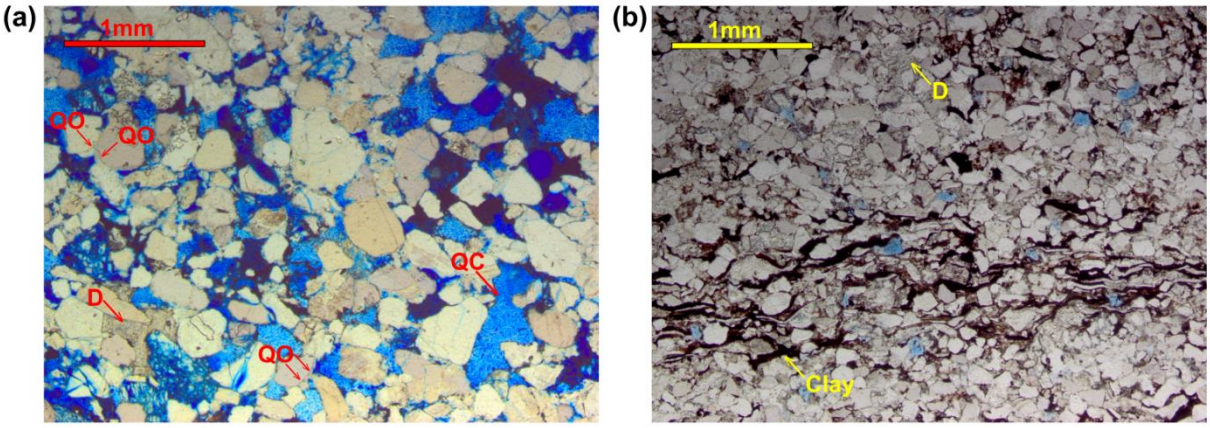

Figure 4.11. Photomicrographs in PPL of samples SSK 71377 (a) and SSK 71478 (b). D: dolomite cement, QC: quartz cement with microporosity, and QO: quartz overgrowth.

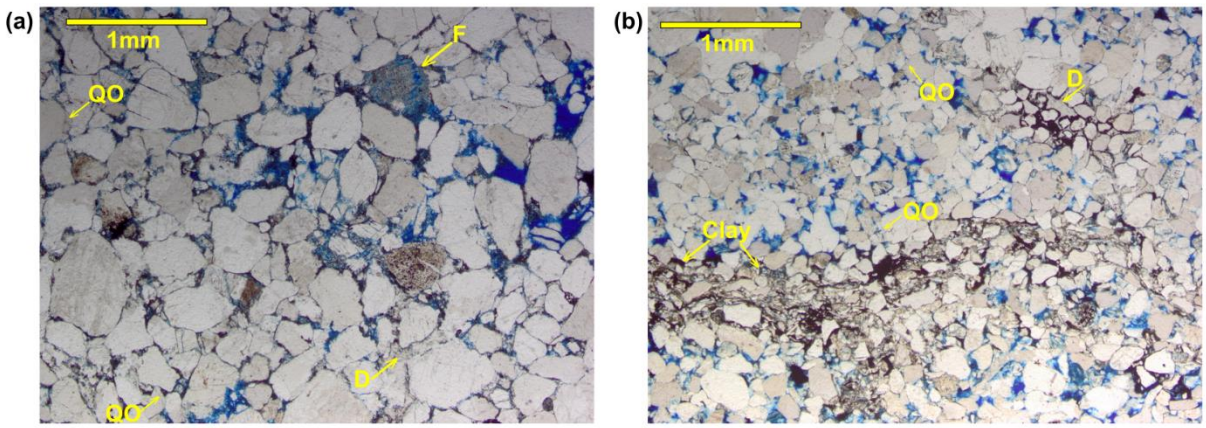

Figure 4.12. Photomicrographs in PPL of samples SSK 71504 (a) and SSK 71507 (b). D: dolomite cement, F: feldspar breakdown exhibiting secondary porosity; QO: quartz overgrowth.

Stratheden Group

The fluvial sandstones of the Kelly Burn Sandstone Formation were classified as sub-lithic and lithic arenites (Figure 4.10; Table 4.5). Samples were moderately compositionally mature, with the mean detrital composition calculated as $Q_{76}F_3R_{21}$, however the grain shape, size, and sorting varied significantly within these samples (Table 4.5). Grains were most commonly angular to sub-rounded. The samples tended to be fine to medium grained however larger clasts were often present, up to 5 mm in size. Given the presence of the larger clasts, grain sorting ranged from poor to well sorted (Figure 4.13). Compaction was moderate to high, indicated by line, dissolution, and concave contacts.

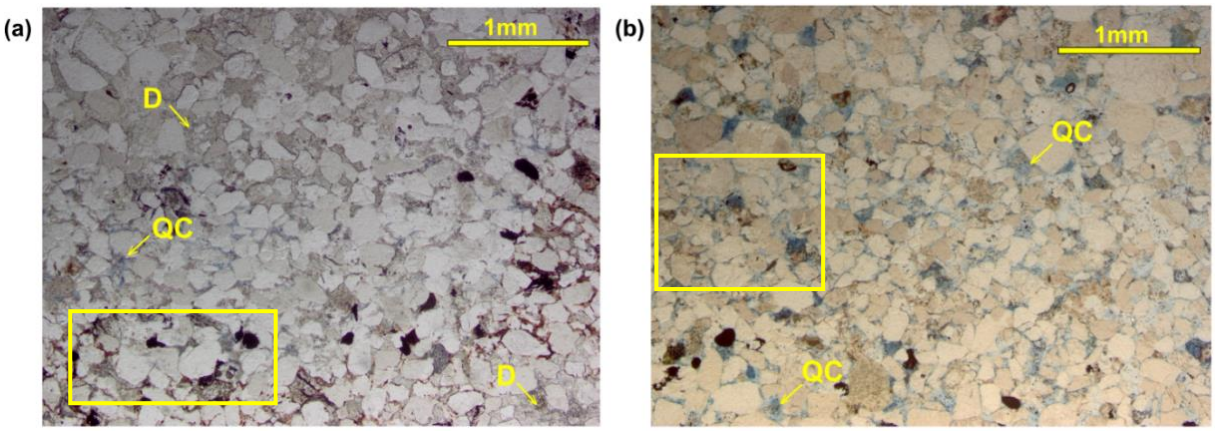

Figure 4.13. Photomicrographs in plane-polarised light of samples SSK 71522 (a) and SSK 71523 (b). Examples of poor grain sorting highlighted. D: dolomite cement, and QC: quartz cement.

Samples SSK 71508 and SSK 71509 (Figure 4.14) of the Stockiemuir Sandstone Formation from the Kipperoch borehole may represent aeolian deposits interbedded within fluvial sandstones. These samples were texturally and compositionally mature, with a mean detrital composition of $Q_{88}F_3R_9$, and lacked the fluvial characteristics shown in the Kelly Burn Sandstone Formation. The samples were fine grained, moderately to well sorted sandstones with sub-angular to rounded grains (Table 4.5), and exhibited low to moderate compaction, with line and point contacts commonly observed.

Table 4.5. Thin section mineralogical analysis of Stratheden Group samples.

Sample	Unit	Location	Description	Grain Shape	Grain Size	Grain Sorting	Compaction
KBS 03	KBS	Gourock	Sub-lithic arenite	Sub-angular to rounded	Fine	Well	Moderate-high
FAS 12	FAS	Fairlie	Sub-arkosic arenite	Sub-angular to sub-rounded	Fine-medium	Moderate-well	Moderate
SCK 20	SCK	Carmen Rd.	Quartz arenite	Sub-rounded to well-rounded	Fine	Very well	Low
SCK 23	SCK	Dalreoch Q.	Sub-lithic arenite	Sub-angular to rounded	Fine	Very well	Moderate
SCK 24	SCK	Bonhill Q.	Quartz arenite	Sub-angular to well-rounded	Fine-coarse	Poor-moderate	Moderate
SSK 71380	KPF	Glenburn	Quartz arenite	Angular to sub-rounded	Very fine	Well	High
SSK 71381	KPF	Glenburn	Sub-arkosic arenite	Sub-rounded to rounded	Very fine	Well	Low
SSK 71382	KPF	Glenburn	Sub-lithic arenite	Angular to sub-rounded	Fine-medium	Well	Moderate-high
SSK 71498	KPF	Glenrothes	Lithic arenite	Angular to sub-rounded	Fine	Moderate-well	Low
SSK 71499	KPF	Glenrothes	Sub-lithic arenite	Sub-angular to rounded	Fine-medium	Moderate-well	Low-moderate
SSK 71508	SCK	Kipperoch	Sub-lithic arenite	Sub-angular to rounded	Fine	Moderate-well	Moderate
SSK 71509	SCK	Kipperoch	Quartz arenite	Sub-angular to rounded	Fine	Well	Low
SSK 71518	SCK	Tak Ma Doon	Lithic Arenite	Angular to sub-rounded	Fine-coarse	Poor-moderate	Low-moderate
SSK 71522	KBS	Everton	Sub-lithic arenite	Angular to sub-rounded	Fine-medium	Poor-moderate	Moderate-high
SSK 71523	KBS	Everton	Lithic arenite	Angular to sub-rounded	Medium	Moderate-well	Moderate

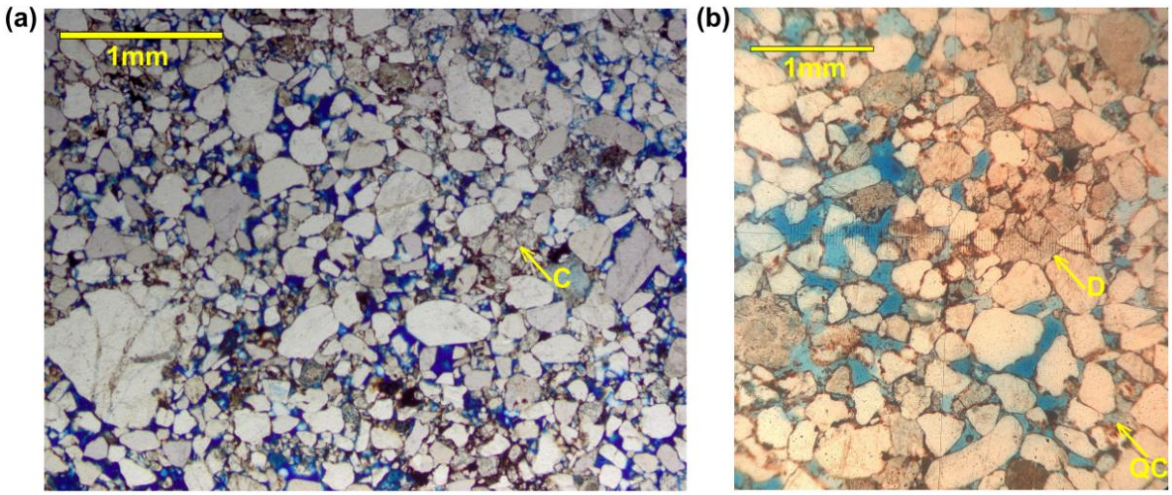

Figure 4.14. Photomicrographs in plane-polarised light of samples SSK 71508 (a) and SSK 71509 (b). C: calcite cement, D: dolomite cement, and QC: quartz cement.

Thin section analysis of aeolian sandstones of the Stratheden Group observed that, in general, the samples exhibited similar textural and compositional properties, and were highly compositionally and texturally mature, with a mean detrital composition of $Q_{84}F_6R_{10}$.

Most commonly, the grain shape was angular to sub-rounded, and samples from the Glenburn borehole and from outcrops of the Stockiemuir Sandstone Formation exhibited the most-well rounded grains (Table 4.5, Figure 4.15). The sandstones were predominately fine to medium grained and well sorted, apart from samples SSK 71518 and SCK 24 where poorer sorting was observed (Table 4.5). Compaction was generally low-moderate, with higher compaction observed in the Glenburn samples. Line and concave contacts were evident, with some rarer point and dissolution compaction also present.

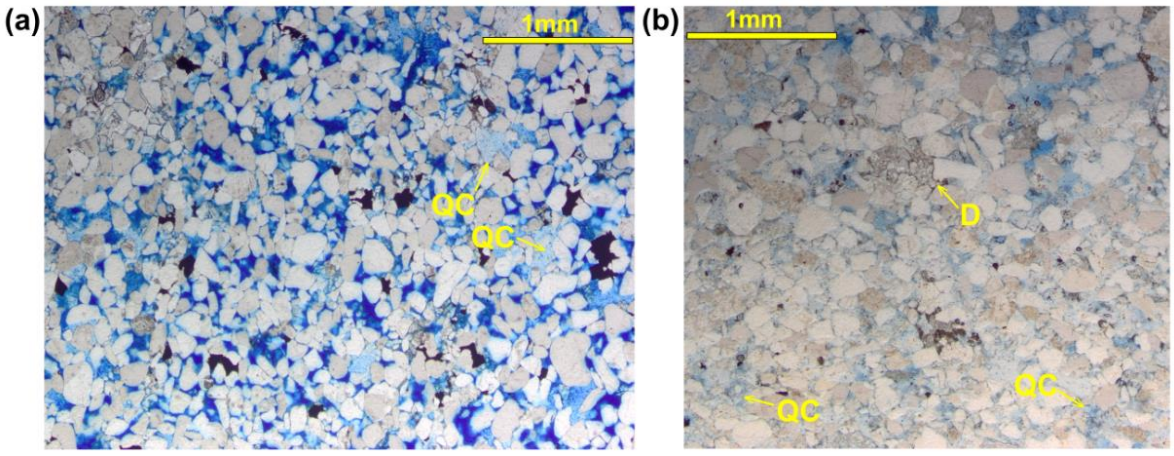

Figure 4.15. Photomicrographs in plane-polarised light of samples SSK 71381 (a) and SSK 71382 (b). D: dolomite cement, and QC: quartz cement.

Detailed in Table 4.D.2, detrital quartz was the dominant mineral type (35-75%) in all samples of the Stratheden Group. Detrital feldspar occurred in trace amounts up to 15%, and similarly the quantity of rock fragments varied from trace amounts to 20%. The rock fragments consisted of mudstone clasts and metamorphic fragments and were most commonly observed in fluvial samples of the Kelly Burn Sandstone.

In general, samples of the Stratheden Group exhibited considerably higher intergranular porosities compared to samples of the Kinnesswood Formation. Dolomite or calcite cementation was largely absent or localised in samples of the Stratheden Group (e.g., Figure 4.14 and 4.15b), however was present in larger quantities in samples SSK 71518 and sample KBS 3. Syntaxial quartz cement and quartz overgrowths were observed in both fluvial and aeolian sandstones of the Stratheden Group (e.g., Figure 4.15), and similar to samples of the Kinnesswood Formation, in a number of the Stratheden Group samples the quartz cement contained micro-porosity. The quartz cement was largely indistinguishable from the pores shown by the blue epoxy resin. This was particularly the case for samples from the Everton and Glenburn boreholes and from outcrop samples (Figure 4.16b).

Illustrated in Figures 4.14 and 4.16, distinctive iron oxide grain coatings were observed in samples of the Stockiemuir Sandstone Formation, both from outcrop and from borehole core samples in samples SSK 71508, SSK 71509, SCK 20 and SCK 24.

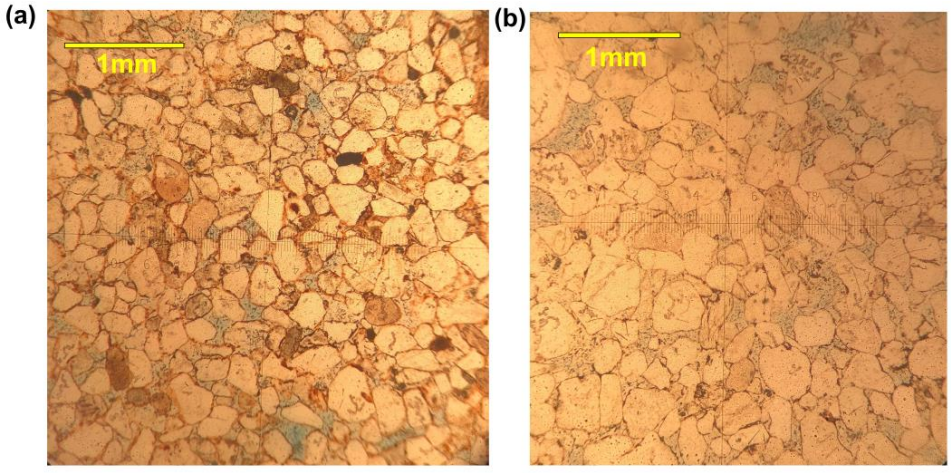

Figure 4.16. Photomicrographs in plane-polarised light of samples SCK 20 (a) and SCK 24 (b).

4.7.2. XRD Results

The results of the quantitative analysis of the mineralogical composition of each sample derived from the XRD patterns are shown in Table 4.6 and Table 4.7.

These results confirm that detrital quartz was the dominant mineral type (54-91.3%) for all samples of the Kinnesswood Formation, excluding that of sample SSK 71520 which was representative the cornstone facies of the Kinnesswood Formation (Figure 4.17).

Diagenetic minerals identified by the XRD analysis in samples of the Kinnesswood Formation included dolomite, calcite, and 1:1 and 2:1 clay. The results illustrate that carbonate cement (10.1-78%) was more prevalent in samples from the Everton borehole and outcrop sites in the Firth of Clyde coastline (SSK 71519, SSK 71520, KNW 02, and KNW 06) compared to those samples obtained from borehole core and outcrops in the Dumbarton area (SSK 71504, SSK 71507, KNW 19 and KNW 25) (Figure 4.17), where carbonate cement was either absent or present in minimal quantities. These results support the thin section petrography observations and indicate consistency in presence of diagenetic minerals in borehole core and analogous outcrop samples.

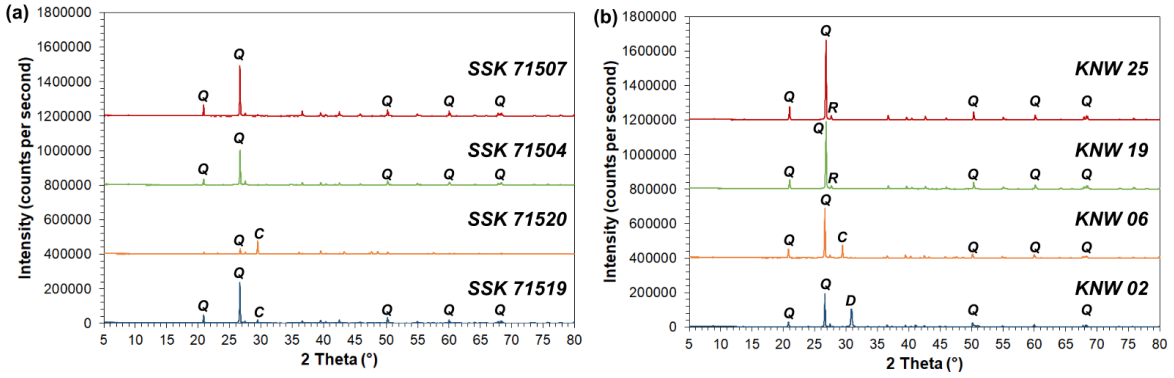

Figure 4.17. XRD patterns of samples of the Kinnesswood Formation from BGS borehole core (a) and outcrop sites (b). Abbreviations: C: Calcite, D: Dolomite, Q: Quartz, R: Rutile.

The results shown in Table 4.7 confirm that detrital quartz was the dominant mineral type (47.9-97%) in all samples of the Stratheden Group sandstones. Iron oxides were identified in sample SCK 20, supporting the identification of grain coatings in the thin section analysis.

The results show that carbonate cement was present in both fluvial and aeolian samples of the Stratheden Group, with the greatest quantities occurring in samples KBS 3, SSK 71382, SSK 71498 and SSK 71509 (Figure 4.18). Carbonate cementation, however, was absent or

found in minimal quantities in the remainder of the boreholes. Authigenic clay was identified in each sample from the Glenburn and Glenrothes boreholes, and 2:1 clay was identified in samples of the Fairlie Sandstone Formation and Kelly Burn Sandstone Formation.

The results support the thin section petrography analysis and emphasise the compositional maturity of the aeolian Stratheden Group formations, which make them favourable targets for geothermal exploration. The results also illustrate the similarities in composition of aeolian samples. This was particularly the case for samples FAS 12, SCK 20, SCK 23, SCK 24, and SSK 71381 with near-identical mineralogical compositions, each with over 90% quartz content, and the absence or minimal presence of carbonate cement or authigenic clay.

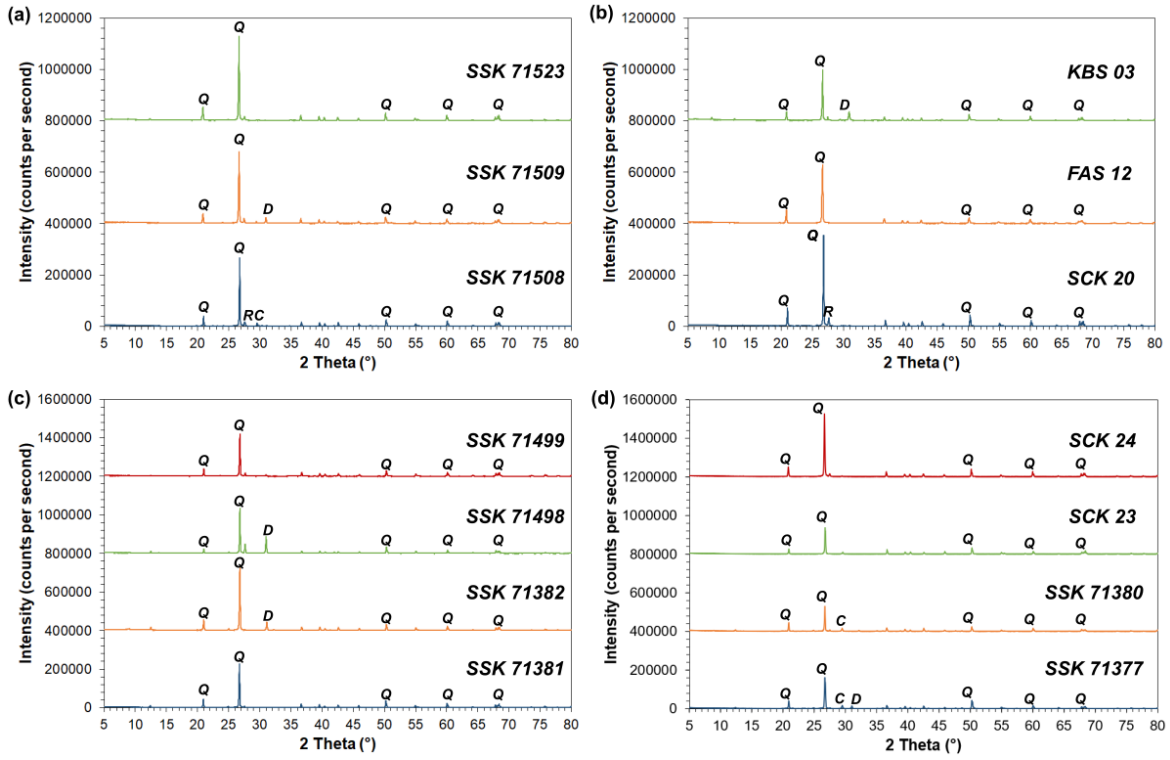

Figure 4.18. XRD patterns of samples of the Stratheden Group from BGS borehole core (a) and (c) and outcrop sites (b) and (d). One sample of the Kinnesswood Formation (SSK 71377) is shown in (d). Abbreviations: C: Calcite, D: Dolomite, Q: Quartz, R: Rutile.

Table 4.6. Mineralogical composition of samples of the Kinnesswood Formation determined by XRD analysis.

Sample	Location	Mineralogical Composition (%)											
		Quartz	Calcite	Dolomite	Micas	Feldspar	1:1 Clay	2:1 Clay	Ilmenite	Rutile	Siderite	Amphibole	Pyroxenes
SSK 71519	Everton	78.7	10.1	-	1.11	5.97	-	-	-	4.09	-	-	-
SSK 71520	Everton	19	78	0.7	0.84	1	-	-	-	0.15	-	-	-
SSK 71377	Glenburn	74	9	3.8	0.6	5.3	7	-	-	-	-	-	-
SSK 71504	Kipperoch	85.3	-	-	8.8	-	-	-	-	1.2	-	3.7	1
SSK 71507	Kipperoch	91.3	2	-	4.1	1.48	-	-	-	1.17	-	-	-
KNW 02	Gourock	54	-	33	4.9	2.7	-	-	-	5.6	-	-	-
KNW 06	Inverkip	69	24	-	2.9	2.4	-	0.5	0.7	1	-	-	-
KNW 19	Carmen Quarry	73	-	-	3.78	9	-	-	-	14	-	-	-
KNW 25	Bonhill	87	-	-	1.9	1.8	-	-	-	7	-	-	1.7

Table 4.7. Mineralogical composition of samples of the Stratheden Group determined by XRD analysis.

Sample	Location	Mineralogical Composition (%)											
		Quartz	Calcite	Dolomite	Micas	Feldspar	1:1 Clay	2:1 Clay	Ilmenite	Rutile	Siderite	Amphibole	Pyroxenes
SSK 71523	Everton	89.1	-	-	5.1	1.8	-	3.37	-	0.3	-	0.3	-
SSK 71380	Glenburn	85	5.8	1	0.35	2.1	5.6	-	-	-	-	-	-
SSK 71381	Glenburn	91.6	-	-	4.1	2.7	1.1	-	-	0.39	-	-	-
SSK 71382	Glenburn	55.1	10	31.2	-	-	0.3	-	0.15	0.3	-	2.9	-
SSK 71498	Glenrothes	70	1.6	12.4	7.2	4.7	1.6	-	-	-	0.9	-	1.7
SSK 71499	Glenrothes	82.4	-	2.8	3.5	2.5	2.6	-	-	-	6.2	-	-
SSK 71508	Kipperoch	79.4	5.4	0.88	2.3	3.17	-	-	-	8.9	-	-	-
SSK 71509	Kipperoch	72.4	1.8	22.9	1.4	0.69	-	-	-	0.4	-	-	0.39
KBS 03	Gourock	47.9	1.5	35.8	8.9	1.21	-	4.5	-	0.18	-	-	-
FAS 12	Fairlie	94.9	-	-	0.65	3.2	-	0.8	-	0.5	-	-	-
SCK 20	Carmen Road	93.4	-	-	-	3.1	-	-	2.2	1.3	-	-	-
SCK 23	Dalreoch Quarry	97	1.2	-	0.5	-	-	-	-	-	-	-	1.2
SCK 24	Bonhill Quarry	93.3	-	-	1.5	3.1	-	-	-	-	-	-	2.1

Micas: e.g., biotite, muscovite or phlogopite; 1:1 Clay Minerals: e.g., kaolinite; 2:1 Clay Minerals: e.g., chlorite, illite or smectite.

4.7.3. X-CT Results

The results of the X-CT analysis of sample porosity are shown in Tables 4.8 and 4.9 for the Kinnesswood Formation and Stratheden Group samples, respectively. The porosity of each sample is presented, along with the range of porosities obtained from the thresholding sensitivity analysis.

Table 4.8. X-CT porosity (Φ) results of Kinnesswood borehole core samples.

Sample	Location	Unit	Depth (m)	Sample Size (mm)	Φ (%)	Φ Range (%)
SSK 71377	Glenburn	KNW	69.3-69.34	2.61 x 2.65 x 5.61	4.38	1.29-9.85
SSK 71378	Glenburn	KNW	89.41-89.44	21.82 x 15.34 x 10.46	7.02	2.28-11.52
SSK 71379	Glenburn	KNW	114.3-114.33	19.54 x 14.30 x 13.52	2.73	0.13-6.77
SSK 71495	Glenrothes	KNW	365.3-365.34	3.36 x 2.56 x 7.27	0.33	0.04-3.94
SSK 71496	Glenrothes	KNW	387.12-387.16	3.08 x 3.85 x 5.83	2.92	1.02-5.74
SSK 71497	Glenrothes	KNW	435.31-435.35	15.35 x 19.05 x 20.33	6.85	2.05-12.18
SSK 71505	Kipperoch	KNW	96.02-96.05	2.28 x 3.83 x 3.78	2.23	0.67-7.86
SSK 71504	Kipperoch	KNW	103.10-103.13	2.57 x 3.20 x 2.64	1.88	0.63-6.18
SSK 71507	Kipperoch	KNW	217.5-217.53	3.00 x 1.87 x 5.87	5.85	4.22-8.91
SSK 71519	Everton	KNW	70.5-70.54	25.07 x 16.36 x 17.90	1.80	0.32-4.07
SSK 71520	Everton	KNW	120.2-120.24	24.38 x 13.60 x 22.18	0.68	0.15-2.53
SSK 71521	Everton	KNW	122.32-122.36	2.80 x 2.11 x 5.71	0.09	0.01-0.51
KNW 01	Gourock	KNW	-	11.08 x 10.58 x 11.88	0.92	0.48-2.12
KNW 02	Gourock	KNW	-	11.45 x 11.61 x 8.78	2.11	1.2-6.77
KNW 06	Inverkip	KNW	-	13.09 x 9.62 x 10.97	1.26	0.41-6.09
KNW 16	Ardrossan	KNW	-	12.84 x 10.48 x 9.51	2.06	0.51-6.62
KNW 19	Carmen Quarry	KNW	-	12.02 x 10.62 x 7.62	7.08	0.81-10.09
KNW 25	Bonhill Quarry	KNW	-	11.85 x 10.25 x 8.59	6.21	3.09-9

The porosities of samples of the Kinnesswood Formation ranged from 0.09-7.08%, with a mean value of 3.13% (Table 4.8). The lowest porosities were computed in samples SSK 71495, SSK 71520 and SSK 71521, two of which were representative of the heavily cemented cornstone facies. The results indicate that samples of the Kinnesswood Formation from the Everton borehole and from outcrop sites on the Firth of Clyde coastline were consistently low. The highest porosities were determined from samples from outcrop sites in Dumbarton (KNW 19 and 25), and samples SSK 71378 and SSK 71497 from the Glenburn and Glenrothes boreholes, respectively.

The porosities of samples of the Stratheden Group are presented in Table 4.9, ranging from 1.01-13.56%, with a mean value of 9.90%. Porosities of samples of the fluvial Kelly Burn Sandstone Formation were the lowest of the Stratheden Group samples, ranging from 1.01-7.61%, with a mean value of 4.71%. For the aeolian samples, the mean porosity was calculated as 11.31%, with values ranging from 9.16%-13.56%. These results show that the

porosities of the aeolian Stratheden Group formations were well constrained, and similar results were observed between borehole core and outcrop samples, as well as between the aeolian sandstones of the Knox Pulpit, Stockiemuir Sandstone, and Fairlie Sandstone formations.

Table 4.9. X-CT porosity (Φ) results of Stratheden Group borehole core samples.

Sample	Borehole	Unit	Depth (m)	Sample Size (mm)	Φ (%)	Φ Range (%)
SSK 71380	Glenburn	KPF	126.42-126.45	12.90 x 10.00 x 11.70	12.34	2.12-19.50
SSK 71381	Glenburn	KPF	159.65-159.68	3.11 x 2.45 x 5.26	13.24	7.72-19.98
SSK 71382	Glenburn	KPF	274.39-274.42	18.41 x 15.39 x 21.95	10.91	0.43-20.41
SSK 71498	Glenrothes	KPF	453.56-453.6	1.41 x 3.35 x 5.41	9.59	7.07-13.75
SSK 71499	Glenrothes	KPF	561.96-562	1.89 x 2.61 x 5.96	9.16	5.18-14.66
SSK 71508	Kipperoch	SCK	237-237.03	3.13 x 2.92 x 6.24	12.02	8.22-16.54
SSK 71509	Kipperoch	SCK	293.55-293.58	12.90 x 26.97 x 27.70	10.69	7.34-15.32
SSK 71522	Everton	KBS	122.5-122.54	22.76 x 16.84 x 24.26	1.01	0.2-4.5
SSK 71523	Everton	KBS	143-143.04	24.52 x 13.90 x 23.18	7.61	0.65-14.94
KBS 03	Gourock	KBS	-	12.83 x 12.46 x 19.90	5.52	0.84-9.45
FAS 12	Fairlie	FAS	-	12.50 x 10.27 x 8.82	11.48	3.88-18.16
SCK 20	Carmen Road	SCK	-	9.66 x 10.88 x 12.46	13.56	8.24-17.96
SCK 23	Dalreoch Quarry	SCK	-	12.18 x 10.60 x 9.60	11.21	6.55-14
SCK 24	Bonhill Quarry	SCK	-	12.62 x 9.76 x 10.19	10.22	7.15-14.59

The highest porosities are therefore present in aeolian samples of the Stockiemuir Sandstone Formation and the Knox Pulpit Formation, indicated by higher porosities present in the Glenburn and Kipperoch boreholes, and from outcrop samples in the Dumbarton area. If similar facies were present in the Upper Devonian sandstones beneath Glasgow, then they may be favourable targets for geothermal exploration, particularly if grain coatings were present and quartz and carbonate cementation were restricted, thus preserving porosity.

4.8. Synthesis of Petrographic Thin Section, XRD and X-CT Results

4.8.1. Timing of Diagenetic Events

Detailed analysis of the diagenetic and burial history of the Upper Devonian sandstones of the MVS was outside the scope of this chapter, however, the results provide a preliminary insight to the possible timing of the dominant diagenetic processes which influence the properties of the sandstones.

The earliest diagenetic event was the formation of grain coating iron oxide in samples of the Kinnesswood Formation and Stockiemuir Sandstone Formation. In sample SCK 20 for example, grain coatings are present at grain contacts, which suggests that this diagenetic event took place prior to compaction (Figure 4.16a).

Mechanical compaction in both fluvial and aeolian deposits then followed. However, in both fluvial and aeolian samples, early carbonate cementation occurred at this time prior to compaction. This is shown by the presence of detrital grains which appear to float within the cement and point grain contacts which are preserved within the cement (Figures 4.D.14 and 4.D.15). Where dolomite cement is not present in samples, grains are well compacted with line, concave, and dissolution contacts.

Pressure dissolution at quartz grain contacts occurred as compaction increased due to the weight of overburden. Dissolution contacts were observed in fluvial and aeolian samples of both the Kinnesswood Formation and Stratheden Group, from outcrop and borehole core samples. The dissolution and breakdown of feldspar grains were also observed in numerous samples (e.g., Figures 4.12, 4.D.7, 4.D.13, 4.D.15). This may have generated authigenic kaolinite which was identified from the XRD analysis.

Pressure dissolution at quartz grain contacts and feldspar dissolution releases silica which form quartz overgrowths and syntaxial quartz cement (McBride, 1989). Feldspar dissolution was the major source of silica for the quartz overgrowth observed in fluvial samples of the Buchan Formation (Tang et al., 2020). The development of quartz cement and quartz overgrowths is usually suggested to occur in middle to late diagenetic stages (McBride, 1989; Paxton et al., 2002; Aagard and Jahren, 2010) at burial depths of c. 2 km and under formation temperatures of 60-100 °C, however, may occur earlier in the diagenetic history (Turner et al., 1993). Shown in Tables 4.D.1 and 4.D.2, quartz cementation or quartz overgrowths were observed in the majority of samples.

Indicators of late diagenetic events such as the illitization on kaolinite and smectite, and chloritization (e.g., Tang et al., 2018a, 2018b) were not examined in the present study.

By combining the results of the thin section petrography, XRD, and X-CT analyses, the diagenetic and depositional factors which preserve or restrict porosity in each sample were examined and the implications for geothermal energy exploration beneath Glasgow were assessed, as described in the following sections.

4.8.2. Effects of Diagenesis on Aquifer Properties

Tables 4.10 and 4.11 present syntheses of the analytical results, showing values of porosity and the properties of the samples which are influenced by the effects of deposition or diagenesis. The values of porosity shown were determined by the X-CT analysis, the mineralogical compositions of authigenic clay and carbonate cement were determined from the XRD analysis unless otherwise stated, and compaction and textural maturity were determined from the thin section observations. To further illustrate the effects of diagenesis and deposition on porosity, the porosity distribution within each scanned sample was plotted and compared with the related X-CT scan to correlate the presence of diagenetic and depositional characteristics with the preservation or reduction in porosity.

Table 4.10. Summary results for Kinnesswood Formation samples.

Sample	Φ (%)	Clay (%)	Cement (%)	Compaction	Textural Maturity
KNW 02	2.11	0	33	Low	Moderate
KNW 06	1.26	5	24	Moderate	Moderate
KNW 16	2.06	0	15*	Moderate-high	Low-moderate
KNW 19	7.08	0	0	Low-moderate	High
KNW 25	6.21	0	0	Moderate-high	Moderate-high
SSK 71377	4.38	0	12.8	Moderate	Moderate
SSK 71378	7.02	15	2*	Moderate-high	Low-moderate
SSK 71379	2.73	5	5*	Moderate	Low-moderate
SSK 71495	0.33	**	**	**	**
SSK 71496	2.92	0	35*	Moderate-high	Low
SSK 71497	6.85	2	5*	Moderate-high	Moderate
SSK 71504	1.88	0	0	Moderate-well	Moderate
SSK 71505	2.23	**	**	**	**
SSK 71506	-	5	30*	Moderate-high	Low
SSK 71507	5.85	5	2	Moderate	Low
SSK 71510	-	5	10*	Moderate-high	Moderate
SSK 71511	-	3	3*	Moderate-high	Low
SSK 71512	-	0	5*	Low-moderate	High
SSK 71513	-	3	15*	Moderate	Low
SSK 71514	-	0	3*	High	High
SSK 71516	-	3	15*	Moderate-high	Low
SSK 71517	-	3	30*	Low	Low-moderate
SSK 71519	1.8	3	10.1	Low-moderate	Moderate
SSK 71520	0.68	4	78.7	Low-moderate	Low
SSK 71521	0.09	9	5*	Moderate	Moderate

* Denotes values derived from thin section petrography in the absence of XRD results.

** Samples were classified as dolomitised wackestones and observations were not made.

Table 4.11. Summary results for Stratheden Group samples.

Sample	Φ (%)	Clay (%)	Cement (%)	Compaction	Textural Maturity
KBS 03	5.52	0	37.3	Moderate-high	Moderate-high
FAS 12	11.48	0	0	Moderate	Moderate-high
SCK 20	13.56	0	0	Low	High
SCK 23	11.21	0	1.2	Moderate	High
SCK 24	10.22	0	0	Moderate	Moderate
SSK 71380	12.34	5.6	6.8	High	High
SSK 71381	13.24	1.1	0	Low	High
SSK 71382	10.91	0.3	41.2	Moderate-high	High
SSK 71498	9.16	2.6	2.8	Low	Moderate-high
SSK 71499	9.59	1.6	14	Low-moderate	Low-moderate
SSK 71508	12.02	0	6.28	Moderate	Moderate-high
SSK 71509	10.69	0	24.7	Low	High
SSK 71518	5	0	20*	Low-moderate	Low-moderate
SSK 71522	1.01	0	5*	Moderate-high	Low-moderate
SSK 71523	7.61	0	0	Moderate	Moderate-high

* Denotes mineralogical composition derived from thin section petrography in the absence of XRD results.

Kinnesswood Formation

X-CT image processing and thin section petrography analysis demonstrated that both fluvial and cornstone samples of the Kinnesswood Formation analysed within this study lacked porosity (Table 4.10). Excluding a limited number of samples, the porosities determined for samples of the Kinnesswood Formation were significantly lower than those determined for samples of the Stratheden Group. The porosities of samples of the Kinnesswood Formation were controlled by the effects of compaction, cementation, and textural immaturity (Table 4.10). The influence of these controlling factors varied between samples and a combination of factors were often observed to restrict porosity.

The samples of the Kinnesswood Formation with the highest values of porosity determined by the X-CT image processing analysis were SSK 71378, SSK 71497, SSK 71507, KNW 19 and KNW 25 (Table 4.10). Thin section petrographic analysis also indicated that samples SSK 71511, SSK 71512 and SSK 71514 from the Barnhill borehole exhibited higher values of porosity in comparison to other samples of the Kinnesswood Formation (Table 4.D.1). Analysis of the mineralogical compositions of these higher-porosity samples showed that diagenetic dolomite or calcite cementation were either absent or minimal in each case (Table 4.10), and therefore the porosities of these samples were hindered by compaction, textural immaturity, and the presence of quartz cementation, to varying degrees.

For example, high textural maturity and the absence of carbonate cementation preserved higher values of porosity in samples KNW 19 and KNW 25. However, as evidenced by X-

CT imagery (Figure 4.19), porosity was restricted by compaction, the presence of concretionary structures, and possible syntaxial quartz cement. The presence of grain coating iron oxide on samples such as SSK 71378, SSK 71507, SSK 71514 and KNW 25 may have contributed to the preservation of porosity by inhibiting the development of more abundant quartz cementation.

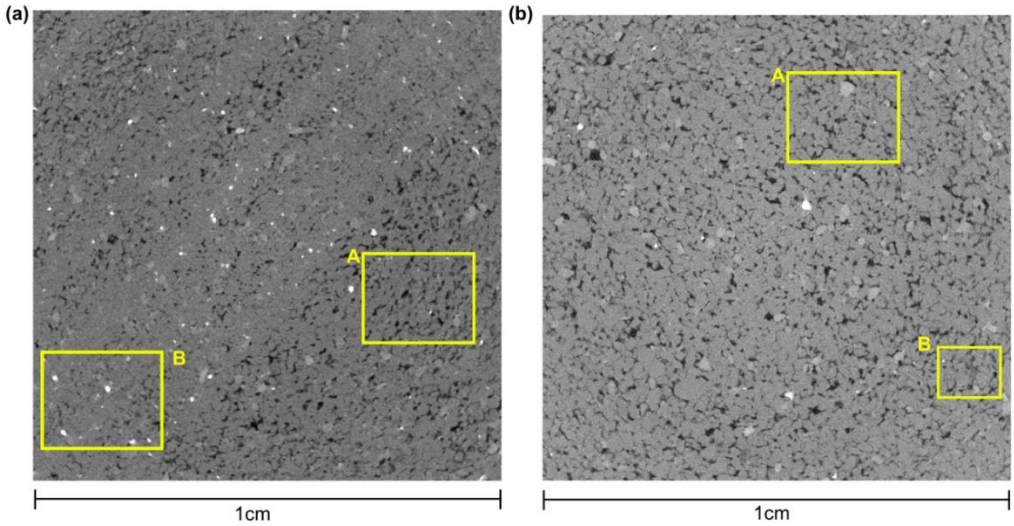

Figure 4.19. X-CT scan imagery of samples KNW 19 (a) and KNW 25 (b). Annotations: A: pores between compacted grains, and B: concretionary structures (KNW 19) and possible quartz cement (KNW 25) inhibiting porosity.

For a number of samples, the presence of dolomite or calcite cement was shown to have a significant impact on porosity. The correlation of carbonate cementation and low porosity was observed in around 50% of the samples of the Kinnesswood Formation, however in some cases the low porosities were caused by a combination of cementation, compaction, and textural immaturity. The effects of carbonate cementation on porosity are highlighted in Figures 4.20 and 4.21, which demonstrate the correlation between the presence of carbonate cementation and the reduction in porosity within samples SSK 71496 and SSK 71377.

Porosity was also restricted in samples of the Kinnesswood Formation by quartz cementation. Figure 4.21 indicates that another mineral phase occluded pore space within sample SSK 71377 in addition to carbonate cement. This supports the identification of quartz cement from thin section observations of this sample (Figure 4.D.1), and also highlights that those porosities determined by this study may be underestimated, as the micro-porosity present within the quartz cement was not segmented satisfactorily within the X-CT image processing analysis (see Appendix 4.H).

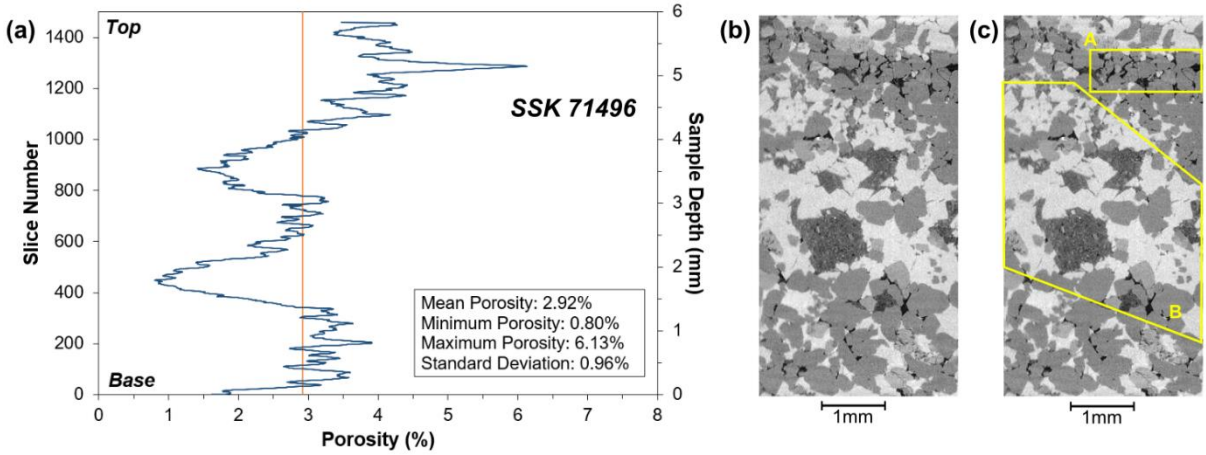

Figure 4.20. Comparison of porosity distribution and X-CT imagery for sample SSK 71496. Porosity distribution diagram plotted from X-CT image processing results (a), X-CT imagery of the sample (b), and the effects of diagenesis on porosity (c). Annotations: A: uncemented pore space, B: carbonate cement occluding pore space.

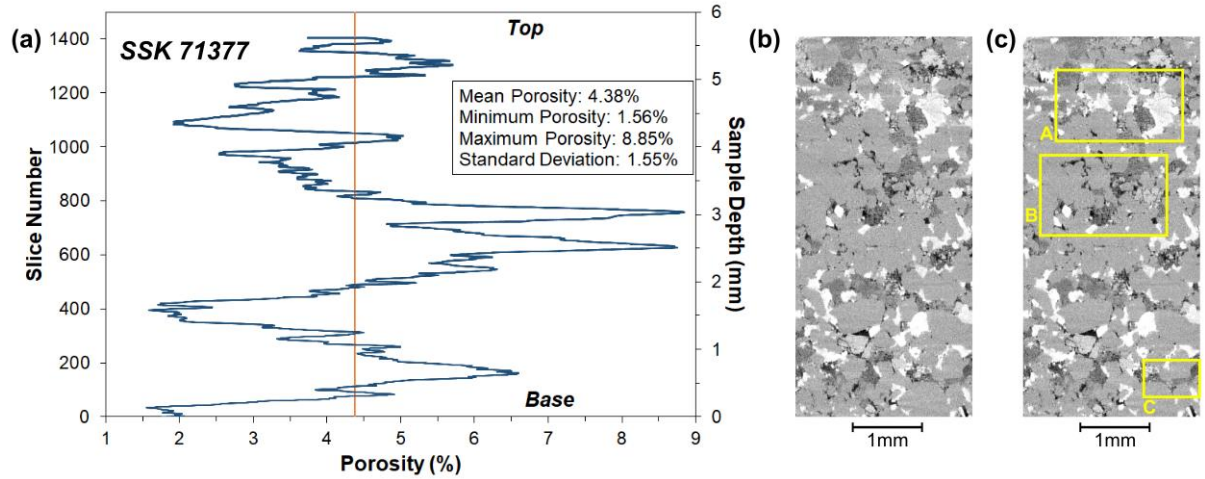

Figure 4.21. Comparison of porosity distribution and X-CT imagery for sample SSK 71377. Porosity distribution diagram plotted from X-CT image processing results (a), X-CT imagery of sample (b), and the effects of diagenesis on porosity (c). Annotations: A: carbonate cement, B: limited porosity, C: possible quartz cement.

Stratheden Group

Samples of the Stratheden Group sandstones analysed within this study were shown, predominately, to have significantly higher porosities than those determined in samples of the Kinnesswood Formation (Figure 4.22).

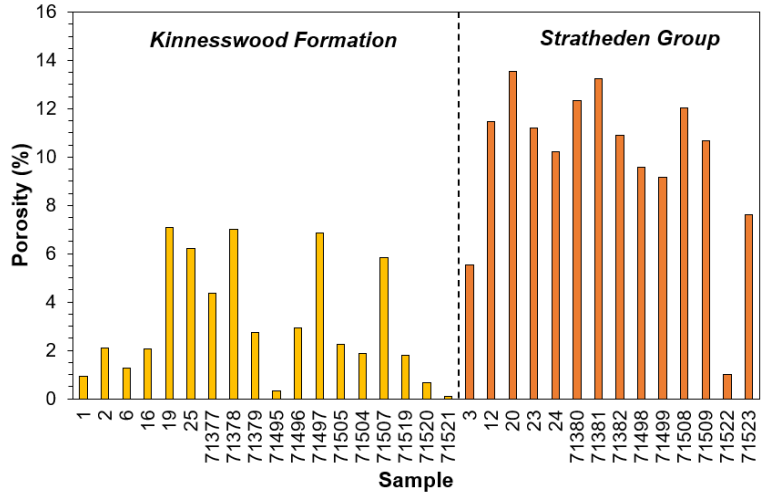

Figure 4.22. Comparison of porosities of the Kinnesswood Formation sandstones and Stratheden Group sandstones determined from X-CT image processing analysis.

Detailed in Table 4.11, aeolian samples of the Stockiemuir Sandstone, Knox Pulpit, and Fairlie Sandstone formations displayed higher porosities than fluvial samples of the Kelly Burn Sandstone Formation. The results signify that the porosities of both aeolian and fluvial sandstones of the Stratheden Group are restricted by compaction, cementation, and textural maturity, however these factors restrict the porosity to varying degrees, and with greater severity in fluvial samples. Most commonly the key controlling factor was compaction. Grain coatings and quartz cementation were also present in samples of the Stratheden Group sandstones, shown by thin section petrography and X-CT analyses.

XRD and thin section petrography analyses demonstrated that for a number of samples of the Stratheden Group, in particular those of aeolian origin, carbonate cementation was minimal or absent, and the sandstones were texturally and compositionally mature. Restriction in the porosity of these samples, therefore, was caused by compaction. This was the case for outcrop samples FAS 12, SCK 20, SCK 23, SCK 24, and core samples SSK 71381, SSK 71498, and SSK 71523. Figure 4.23 demonstrates the effect of compaction on porosity on samples of the Stockiemuir Sandstone Formation from outcrop sites, where sample SCK 20 exhibited low compaction and sample SCK 24 exhibited greater compaction and poorer grain sorting.

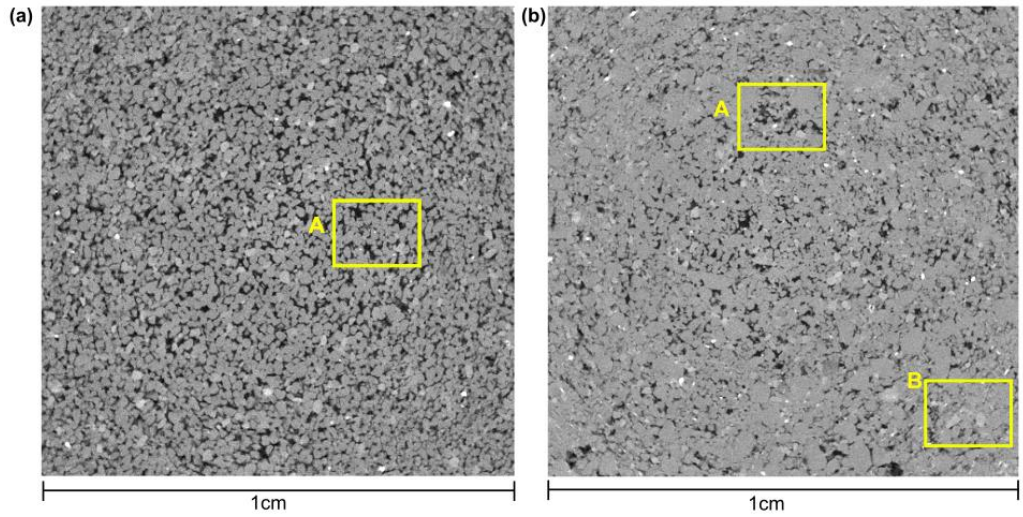

Figure 4.23. X-CT scan imagery of samples SCK 20 (a) and SCK 24 (b). Abbreviations: A: porosity, B: compaction.

Despite the absence of carbonate cement, syntaxial quartz cement and quartz overgrowths were observed to occlude pore space and reduce the overall porosity of many of these samples. This is shown in Figure 4.24, where X-CT scan imagery indicates the presence of a mineral phase occluding pore space which may represent quartz cement.

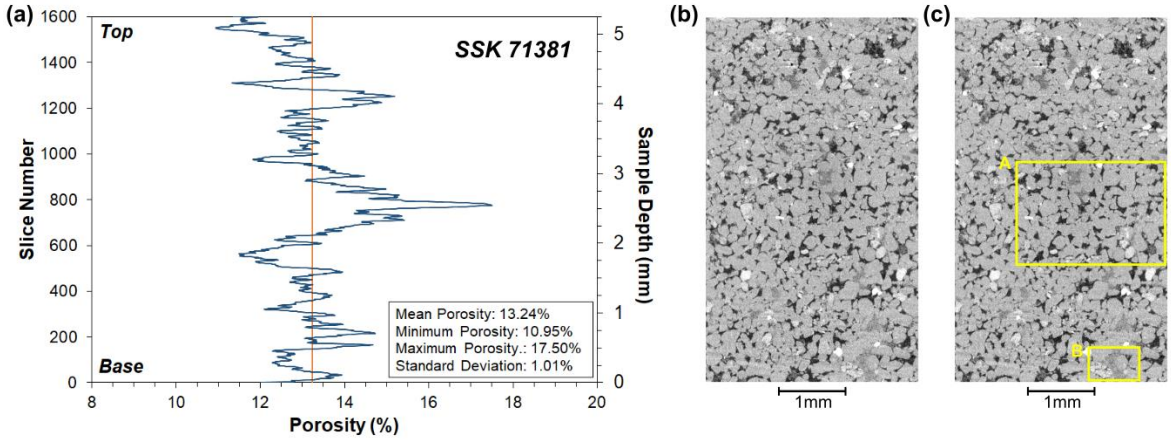

Figure 4.24. Comparison of porosity distribution and X-CT imagery for sample SSK 71381. Porosity distribution diagram plotted from X-CT image processing results (a), X-CT imagery of the sample (b), and the effects of diagenesis on porosity (c). Annotations: A: intergranular porosity, B: possible quartz cement.

XRD analysis determined that diagenetic dolomite or calcite cement were present in a number of Stratheden Group samples, including samples of both aeolian and fluvial origin. Illustrated by the results of X-CT image processing analysis, the presence of carbonate cementation restricted the porosity a number of samples. For example, samples SSK 71508 and SSK 71509 from the Kipperoch borehole exhibited moderate-high textural and

compositional maturity and low-moderate compaction, and as shown in Figure 4.25, the porosity within SSK 71508 was restricted by the presence of carbonate cement.

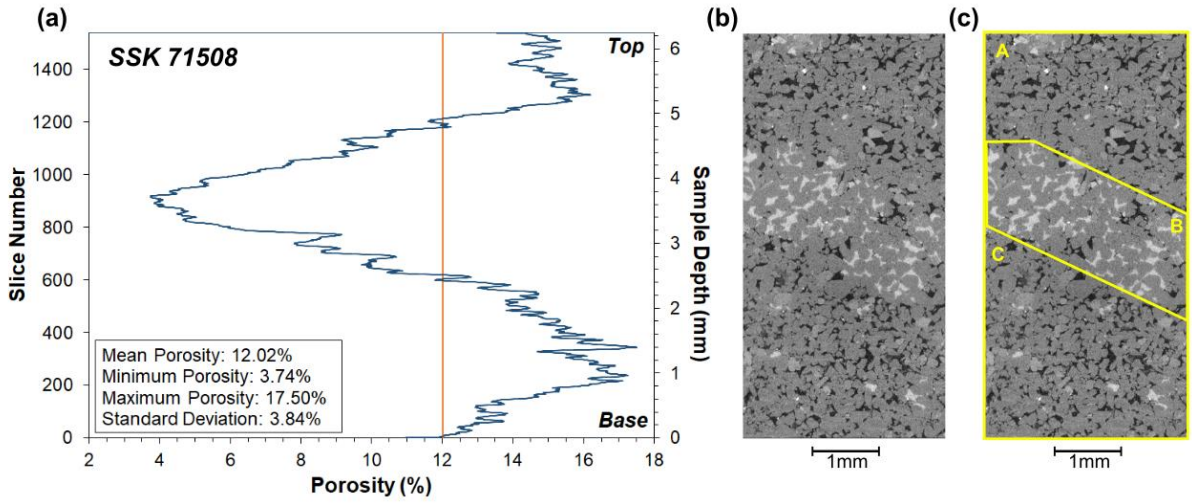

Figure 4.25. Comparison of porosity distribution and X-CT imagery for sample SSK 71508. Porosity distribution diagram plotted from X-CT image processing results (a), X-CT imagery of the sample (b), and the effects of diagenesis on porosity (c). Annotations: A, C: intergranular porosity, B: localised carbonate cement.

However, porosity was often also restricted by textural immaturity and compaction (Table 4.11). For instance, both compaction and cementation restricted porosity in samples KBS 3, SSK 71380, and SSK 7138, whereas the porosity of samples SCK 71499 and SCK 71518 were found to be controlled by both cementation and low textural maturity (Figure 4.26).

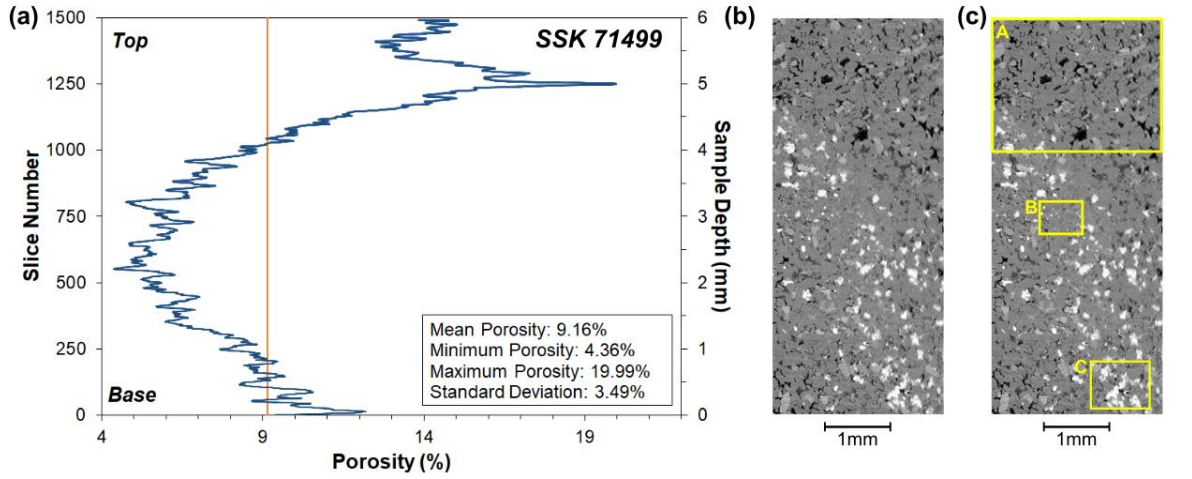

Figure 4.26. Comparison of porosity distribution and X-CT imagery for sample SSK 71499. Porosity distribution diagram plotted from X-CT image processing results (a), X-CT imagery of the sample (b), and the effects of diagenesis on porosity (c). Annotations: A: porosity, B: compaction, C: carbonate cement.

4.8.3. Implications for Geothermal Energy in Glasgow

The porosity of samples of the Kinnesswood Formation analysed within this study were significantly restricted by the effects of diagenesis and deposition. The findings of this study are consistent with the characteristics of fluvial sandstones of the Upper Devonian sandstones of the Buchan Formation (Tang et al., 2018a, 2018b), and demonstrate that low porosity was caused by the presence of carbonate and quartz cementation, compaction, and textural immaturity. The highest porosity was determined in sample KNW 19, which along with sample KNW 25 and samples from the Barnhill borehole, exhibited high textural maturity and low cementation. This has implications for geothermal exploration beneath Glasgow as these sandstones may be representative of the basal sequence of the Kinnesswood Formation which alongside the Knox Pulpit Formation, forms the productive aquifer in Fife and may therefore form part of the potential aquifer beneath Glasgow.

The effects of compaction and cementation on porosity were less severe in samples of aeolian sandstones of the Stratheden Group in comparison to the fluvial sandstones of the Kinnesswood Formation and the Kelly Burn Sandstone Formation. The highest values of porosity were determined in aeolian samples which had higher textural and compositional maturity, lower cementation, and lower compaction, and which contained grain coating iron oxides around quartz grains; similar to the characteristics of the aeolian sandstones of the Buchan Formation (Table 4.1). Whereas lower values of porosity were observed in fluvial samples which were influenced by high compaction, textural immaturity or the presence of carbonate or quartz cement.

The most promising porosities are therefore present in aeolian samples of the Stockiemuir Sandstone Formation and the Knox Pulpit Formation, indicated by higher porosities present in the Glenburn and Kipperoch boreholes, and from outcrop samples in the Dumbarton area. If these properties are present at depth beneath Glasgow, then the aeolian sandstones of the upper Stratheden Group may have sufficient permeabilities to support significant geothermal heat production and are viable targets for geothermal exploration.

However, quartz overgrowths and quartz cementation were observed in the majority of samples of both the Kinnesswood Formation and Stratheden Group formations. In general, grain coatings which inhibited the quartz overgrowths in the aeolian sandstones were less prevalent in samples of the Stratheden Group compared to those observed in the Buchan Formation (Tang et al., 2018a, 2018b).

Therefore, if the Kinnesswood Formation and Stratheden Group sandstones buried at c. 1400-2000 m depth beneath eastern Glasgow also lack grain coatings and are heavily cemented, either by early carbonate cementation or late-quartz cementation, then intergranular porosity will be significantly reduced and poorly interconnected. This will have an adverse impact on the permeability of the Upper Devonian sandstones and the potential for geothermal heat production from the aquifer.

Whether favourable aquifer properties would be preserved at burial depths of c. 1400-2000 m in eastern Glasgow is an open question which cannot be fully resolved prior to deep drilling. However, if the favourable properties of the aeolian sandstones in the upper Stratheden Group, such as those equivalent to the Knox Pulpit Formation, Stockiemuir Sandstone Formation and Fairlie Sandstone Formation, are maintained at greater burial depths beneath Glasgow then these formations could be viable targets for geothermal exploration. This is particularly true, if as discussed in Chapter 3, post-cementation fracturing has occurred in the damage zone associated with the Dechmont Fault which may either open fractures at depth or re-connect previously cemented and disconnected porosity, offering scope for significant fluid flow and geothermal heat production. However, as indicated by the present study, diagenetic effects such as compaction and cementation have had a considerable influence on the aquifer properties of the Upper Devonian sandstones in the western MVS and may restrict the porosity and permeability of deeply buried sandstones in the potential geothermal resource beneath Glasgow.

4.9. Conclusion

This chapter investigated the diagenetic and depositional factors which preserve or restrict porosity in samples of Upper Devonian sandstone in the western MVS. Fieldwork was conducted by the author to collect representative samples of the Kinnesswood Formation and underlying Stratheden Group samples from outcrop sites surrounding Glasgow and from borehole core archived by the British Geological Survey in Keyworth. Thin section petrography, X-CT and XRD analyses were then carried out to determine the effects of diagenesis and deposition on the porosity and properties of each sample.

This study found that diagenetic effects such as compaction and cementation have had a considerable influence on the aquifer properties of the Upper Devonian sandstones in the western MVS and may restrict the porosity and permeability of analogous deeply buried sandstones in the potential geothermal resource beneath Glasgow.

The effects of compaction and cementation on porosity were less severe in samples of aeolian sandstones of the Stratheden Group in comparison to the fluvial sandstones of the Kinnesswood Formation and the Kelly Burn Sandstone Formation. The most promising porosities were present in aeolian samples of the Stockiemuir Sandstone Formation and the Knox Pulpit Formation which had higher textural and compositional maturity, lower cementation, and lower compaction.

Quartz overgrowths and quartz cementation were observed in the majority of samples of both the Kinnesswood Formation and Stratheden Group formations. In general, grain coatings which inhibited the quartz overgrowths in the aeolian sandstones were less prevalent in samples of the Stratheden Group compared to those observed in the Buchan Formation. Therefore, if the Kinnesswood Formation and Stratheden Group sandstones buried at c. 1400-2000 m depth beneath eastern Glasgow also lack grain coatings and are heavily cemented, either by early carbonate cementation or late-quartz cementation, then intergranular porosity will be significantly reduced and poorly interconnected.

The results of this analysis showed that the outcrop and borehole samples had already been buried to significant depths, due to the presence of quartz cementation, dissolution contacts, and breakdown of detrital grains. The sandstones may therefore have already experienced the maximum effects of compaction, and deeper sandstones beneath Glasgow, despite having a greater maximum burial depth, will not have been compacted significantly more. The results from this outcrop and borehole study, in terms of compaction, are therefore comparable with the sandstones at depth beneath Glasgow. The uncertainty is whether cementation has occurred in the deeply buried sandstones and occluded pore space, reducing both intergranular porosity and permeability of the aquifer.

Whether favourable aquifer properties would be preserved at burial depths of c. 1400-2000 m in eastern Glasgow is thus an open question which cannot be fully resolved prior to deep drilling. However, if the favourable properties of the aeolian sandstones in the upper Stratheden Group, such as those equivalent to the Knox Pulpit Formation, Stockiemuir Sandstone Formation and Fairlie Sandstone Formation, are maintained at greater burial depths beneath Glasgow then these formations may have sufficient permeabilities to support significant geothermal heat production and could be viable targets for geothermal exploration.

Chapter 5. Appraisal and Revaluation of Glasgow's Geothermal Datasets

5.1. Introduction

Having established the extent and depth of the Upper Devonian sandstone sequence beneath eastern Glasgow in Chapter 3 and examined the aquifer properties from the outcrop and borehole analogue study in Chapter 4, the next step was to quantify the temperature of the geothermal resource. Reliably calculating the temperature of the geothermal resource beneath Glasgow was reliant on applying rigorous corrections to values of heat flow and geothermal gradient to account for the effects of palaeoclimate and topography. As a precursor to this, values of uncorrected heat flow, geothermal gradient, thermal conductivity, and thermal diffusivity were re-calculated in this chapter for sixteen boreholes across the western MVS. Factors which influence the accuracy of the geothermal dataset, such as perturbations to the subsurface thermal state caused by historic mining were then identified, thus creating a reliable dataset for use as input criteria to the palaeoclimate and topographic correction analysis of Chapter 6.

5.2. Chapter Aim and Rationale

Past investigations of geothermal energy in Britain have utilised inventories of measurements of temperature, heat flow and thermal conductivity from boreholes to assess the magnitude of resource across the country (e.g., Burley et al., 1984; Rollin, 1995).

There are sixteen boreholes in the western MVS from within which, measurements of heat flow, temperature and thermal conductivity have been observed (Table 5.1). However, none of these boreholes are sufficiently deep enough to encounter the Upper Devonian sandstones beneath Glasgow, and thus the temperature within the geothermal resource and the possible applications for the use of the geothermal heat must therefore be determined by extrapolation of measurements of geothermal gradient made within the shallower boreholes in the city.

The extent and quality of geothermal data used to calculate values of geothermal gradient in these boreholes is limited and varies from site to site. Measurements of subsurface temperature are available from thirteen of the sixteen boreholes in the region, however five of these datasets are limited to bottom hole temperature (BHT) measurements. Likewise, heat flow has been previously determined in eight of the sixteen boreholes, and thermal conductivity measurements made in five of the sixteen boreholes. The overall geothermal dataset is therefore variable and inconsistent, with values of temperature or heat flow absent from several of the boreholes.

Furthermore, these existing values of heat flow and geothermal gradient have not been corrected to account for the effects of palaeoclimate. This has been shown to increase heat flow significantly in boreholes across Britain which were otherwise previously underestimated (e.g., Westaway and Younger, 2013) and is therefore a critical step towards estimating the 'true' temperature within the geothermal resource beneath Glasgow. Analysis has been undertaken to apply palaeoclimate corrections to heat flow and geothermal gradient in boreholes in the western MVS in Chapter 6 of this thesis. However, this analysis relied on the utilisation of a suite of geothermal data as input criteria to calculation procedures. The required inputs include raw, uncorrected heat flow and temperature measurements for each borehole, and the thermal properties of the lithologies encountered in each borehole, such as thermal conductivity and thermal diffusivity.

The aim of this chapter, therefore, was to re-calculate each of these parameters as a pre-cursor for applying corrections to heat flow and geothermal gradient to account for the effects of palaeoclimate and topography in Chapter 6. Then, based upon the revised geothermal dataset for each borehole, the reliability of the data was appraised by identifying factors which perturb the subsurface thermal state, such as the influence of historic mining.

5.3. Borehole Analysis

This section first details the history of each borehole investigated within this chapter and the extent of the geothermal data available in each case. Then based upon these existing datasets, the calculations and results of harmonic mean thermal conductivity, harmonic mean thermal diffusivity, heat flow, and geothermal gradient are presented for each borehole. This includes new values of heat flow for eight boreholes as well as the recalculation of heat flow for the Blythswood, Maryhill and South Balgray boreholes. Furthermore, new subsurface temperature profiles are calculated for the Barnhill, Clachie Bridge, Hurlet and Kipperoch boreholes which were previously absent. The results of the sensitivity analysis on the effect of varying thermal properties on the resulting heat flow are also outlined. Finally, the reliability of the dataset was appraised by identifying factors which perturb the subsurface thermal state, such as the influence of historic mining (Watson et al., 2019).

5.3.1. Borehole History and Existing Data

The sixteen boreholes examined within this chapter are shown in Table 5.1 and their locations illustrated in Figure 5.1. The boreholes are located across the western MVS and vary stratigraphically (with summaries of each borehole stratigraphy shown in Appendix 5.A).

Table 5.1. Geothermal boreholes in the western MVS.

Name[1]	NGR[2]	Date[3]	Height[4] (m)	Z[5] (m)	Interval[6] (m)	T[7] (°C)	Q[8] (m Wm^{-2})	Type[9]	Ref[10]
Blythswood -1 [Bl]	NS 50030 68230	1868.01	2	117.4	18-105	12.05	52	EQM	A,B
South Balgray [SB]	NS 55780 67810	1869.07.13	30	320.61	0-137	14.52	64	EQM	A,B
Queenslie – 4 [Q]	NS 64640 65975	1952	77.6	732.58	0-691	36	-	BHT	A,C
Rashiehill [R]	NS 83860 73005	1952	153	1176.5	0-964	35.8	-	LOG	C
Slatehole [S]	NS 49070 23430	1954	80.68	1024	0-1024	40	-	BHT	D
Salsburgh - 1A [S1]	NS 81660 64869	1964.07.03	223.4	1300.5	0-898	34	-	DST	D,E
Hallside [Ha]	NS 66930 59740	1976.04.26	54.22	351.65	0-350	11.8	-	LOG	D
Kipperoch [K]	NS 37270 77420	1978.12.08	85.34	300.57	40-300	-	53.40±2.07	-	F
Barnhill [B]	NS 42690 75710	1978.12.18	100.3	356.4	25-355	-	48.91±4.42	-	F
Clachie Bridge [CB]	NS 64475 83680	1978.12.21	269.4	300.3	30-300	13.2	57.68±1.69	LOG	F
Hurlet [Hu]	NS 51110 61230	1979.5.18	30.31	304.3	95-295	-	61.75±1.32	-	F
Craighead – 1 [C]	NS 82670 62120	1981.11.23	244.1	909.8	0-910	35	-	LOG	D,E
Maryhill [M]	NS 57178 68558	1983.12.18	40	306.5	100-303	20.03	63	EQM	G
Salsburgh – 2 [S2]	NS 82110 63850	1986.01.26	225.2	1102.1	0-1102	44	-	BHT	E,H
Bargeddie -1 [Ba]	NS 69318 64649	1989.08.13	78	1036.5	0-979	38.7	-	DST	E
GGC01 [G]	NS 60915 63109	2018.12.12	9.66	199	0-197	14	28-33	LOG	I

(1) Name and abbreviation corresponding to Figure 5.1. (2) British National Grid Reference. (3) Date of last temperature measurement or the conclusion of drilling. (4) Height above sea level of the site. (5) Depth of the borehole. (6) Depth interval over which heat flow Q is calculated or temperature measured. (7) Deepest temperature measurement. (8) Heat flow measurement ± standard error of the mean, where available. Range of values for GGC01 depends on input parameters detailed in Watson and Westaway (2020). (9) Type of temperature measurement. BHT: bottom hole temperature measurement; DST: drill stem test; EQM: equilibrium measurement; LOG: log temperature. (10) References denote: A: Thomson et al. (1869); B: Benfield (1939); C: Anderson (1963); D: Burley et al. (1984); E: UK Onshore Geophysical Library, F: Previously unpublished data from Oxburgh (1982) provided from BGS within the BritGeothermal research partnership, now published in Busby (2019); G Wheildon et al. (1985); H: Rollin (1987); I: Watson and Westaway (2020).

Eight boreholes are located in the Glasgow or Greater Glasgow area, and are drilled through successions of Westphalian, Namurian and Dinantian aged sediments. These include Blythswood-1 and Hurlet to the south-west of Glasgow, Maryhill and South Balgray in the west-end of the city, and Bargeddie-1, GGC-01, Hallside, and Queenslie-4 in the east and south-east of the city (Figure 5.1). A further four boreholes are located to the east of Glasgow in North Lanarkshire and West Lothian (Figure 5.1). These include Craighead-1, Rashiehill, Salsburgh-1A, and Salsburgh-2, which are amongst the deepest boreholes examined within this chapter, and drilled through successions of Westphalian, Namurian and Dinantian sediments, with three of the boreholes terminating in Dinantian or Devonian aged lavas. Three boreholes examined within this chapter were also examined within Chapter 4 of this thesis: Barnhill, Clachie Bridge and Kipperoch. These boreholes are located to the north and west of Glasgow (Figure 5.1) and encounter the CPV, and sediments of Lower Carboniferous and Upper Devonian age, including the Upper Devonian sandstones of the Kinnesswood Formation and Stratheden Group (Appendix 5.A). The remaining borehole, Slatehole, is located in the Mauchline Basin in Ayrshire (Figure 5.1) and drilled through Permian sandstones and lavas, before encountering Scottish Coal Measures strata.

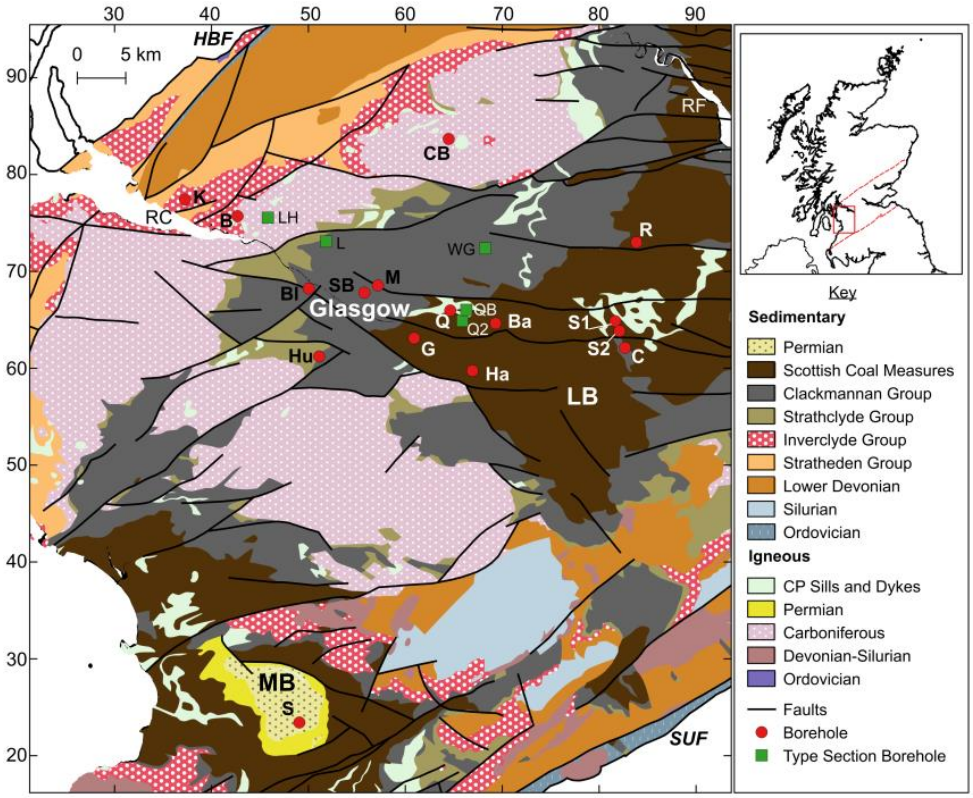

Figure 5.1. Simplified solid geology, structure and locations of boreholes studied in Glasgow and the surrounding conurbation. The co-ordinates (north and east) are in kilometres within British National Grid 100 km quadrangle NS. Abbreviations: LB: Lanarkshire Basin, MB: Mauchline Basin. Geological Map Data BGS © UKRI 2021.

The geothermal data available from each borehole is summarised in the following section. The stratigraphy of each borehole was also examined, and Figures 5.2-5.7 were produced by the author to depict the lithology and thickness of each rock layer encountered within each borehole. These figures were produced using the recorded strata from the drilling log of each borehole (BGS, 2021). This borehole log data was then used by within the calculations of harmonic mean thermal conductivity and diffusivity, heat flow, and temperature.

Blythswood-1 and South Balgray Boreholes

The Blythswood-1 and South Balgray boreholes (Figure 5.2) were drilled in 1863 and 1864, respectively, to prospect for coal and ironstone (Watson et al., 2019). Both boreholes were used by Lord Kelvin to conduct subsurface temperature measurements, providing the oldest records of geothermal data in the western MVS (Thomson et al., 1868, 1869). Benfield (1939) and Anderson (1940) determined values of heat flow in these boreholes using geothermal gradients calculated from Lord Kelvin's measurements and values of thermal conductivity which were measured in the Boreland borehole in Fife. Previously published reports (Burley et al., 1984) have mistakenly stated the location of the South Balgray borehole as NS 50 75. This was corrected in Watson et al. (2019), showing that the South Balgray borehole log as described by Thomson et al. (1868, 1869) is actually that of the No. 3 Gartnavel borehole at NS 55780 67810, located in Hyndland in Glasgow's west end.

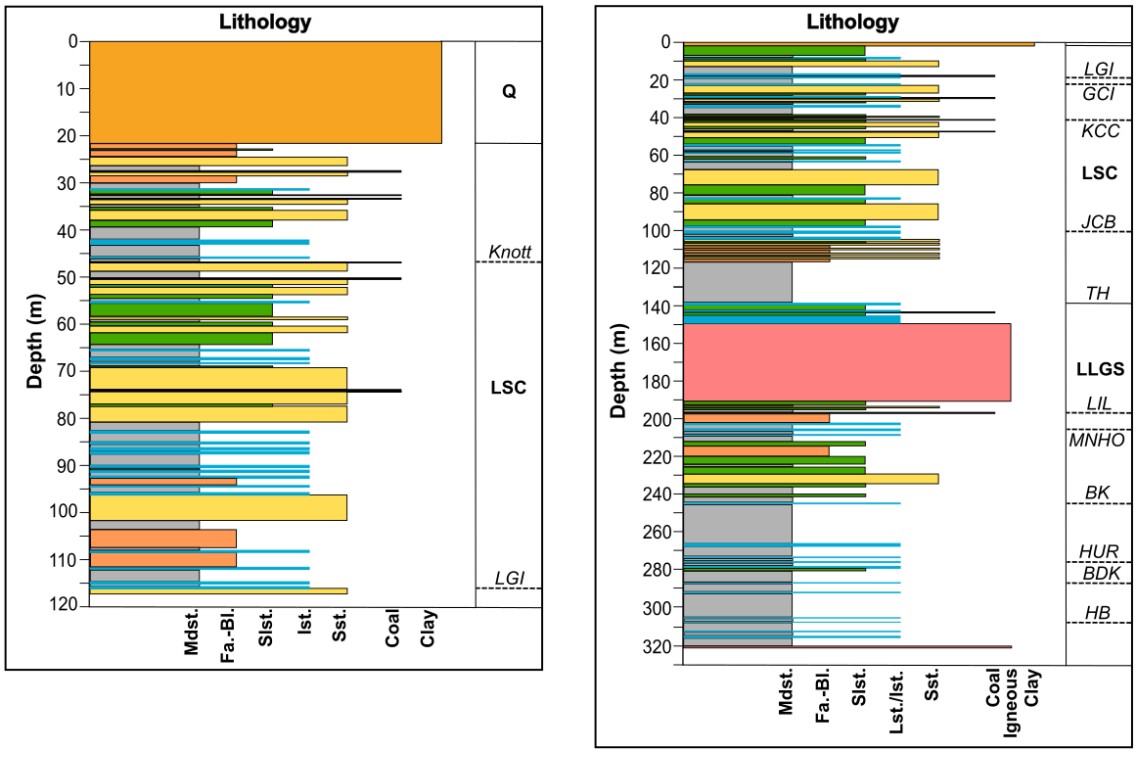

Figure 5.2. Stratigraphic columns for Blythswood-1 (Left) and South Balgray (Right). Based upon records provided by British Geological Survey (UKRI).

Queenslie-4 and Slatehole NCB Boreholes

The Queenslie-4 borehole (Figure 5.3) was drilled in 1952–53 as one of a series of National Coal Board (NCB) boreholes in eastern Glasgow. Three of the boreholes were cored throughout (Nos 1, 2, and 6) and have since provided valuable sections through the Lower Coal Measures (Forsyth, 1979). The Queenslie-4 borehole was 'open hole' to a depth of 441 m, meaning that this section of the borehole was not cored (Figure 5.3).

The Slatehole borehole (Figure 5.3) was drilled in 1954 by the NCB within the Permian aged Mauchline Basin, in Ayrshire. Beneath the Permian outcrop in the Mauchline Basin is a "Concealed Coalfield" (Eyles et al., 1930). While unconfirmed, it was likely that this borehole was drilled to investigate the stratigraphy of the Permian Basin, and the depth of workable coal seams to assess the economic feasibility of working the seams in this area. BHT measurements were recorded in both the Queenslie-4 and Slatehole boreholes.

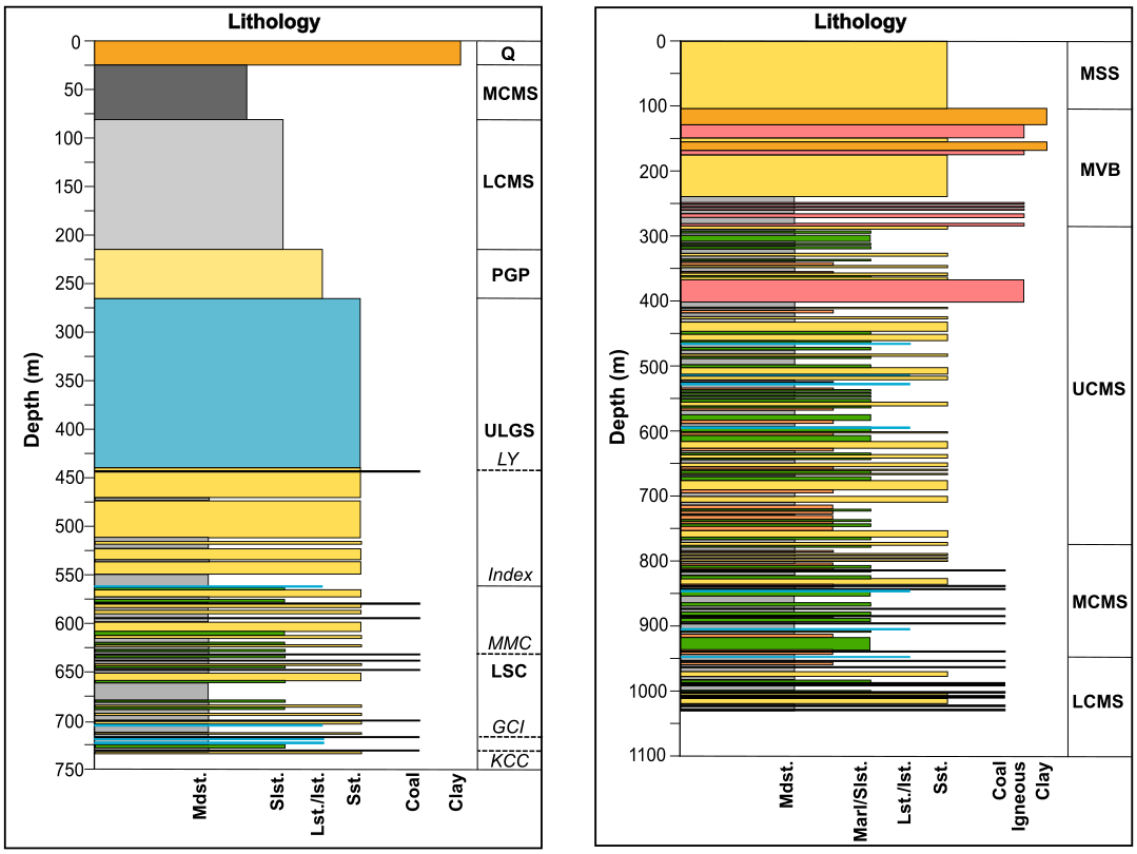

Figure 5.3. Stratigraphic columns for Queenslie-4 (Left) and Slatehole (Right). Based upon records provided by British Geological Survey (UKRI).

Rashiehill and Salsburgh Boreholes

The Salsburgh-1 borehole (Figure 5.4) was the first of five boreholes drilled to the east of Glasgow to prospect for hydrocarbon reservoirs within the West Lothian Oil Shale Formation (WLOS). This exploration well was drilled by the D'Arcy Exploration Company in 1944 and a re-entry of this well, Salsburgh-1A, was completed by BP in 1964. Well completion reports state that a BHT of 34°C was measured in Salsburgh-1 in 1945 and another of 30°C was measured in Salsburgh-1A in 1964.

The Rashiehill borehole (Figure 5.4) was drilled in 1951 in the Slamannan Coalfield, north-east of Glasgow. The borehole was drilled to investigate the presence and extent of the WLOS (Anderson, 1963). The WLOS was not encountered in the borehole, and it was terminated within a thick succession of Dinantian aged lavas (Figure 5.4) (Hall, 1971). A temperature log was recorded in the borehole to a depth of 964 m.

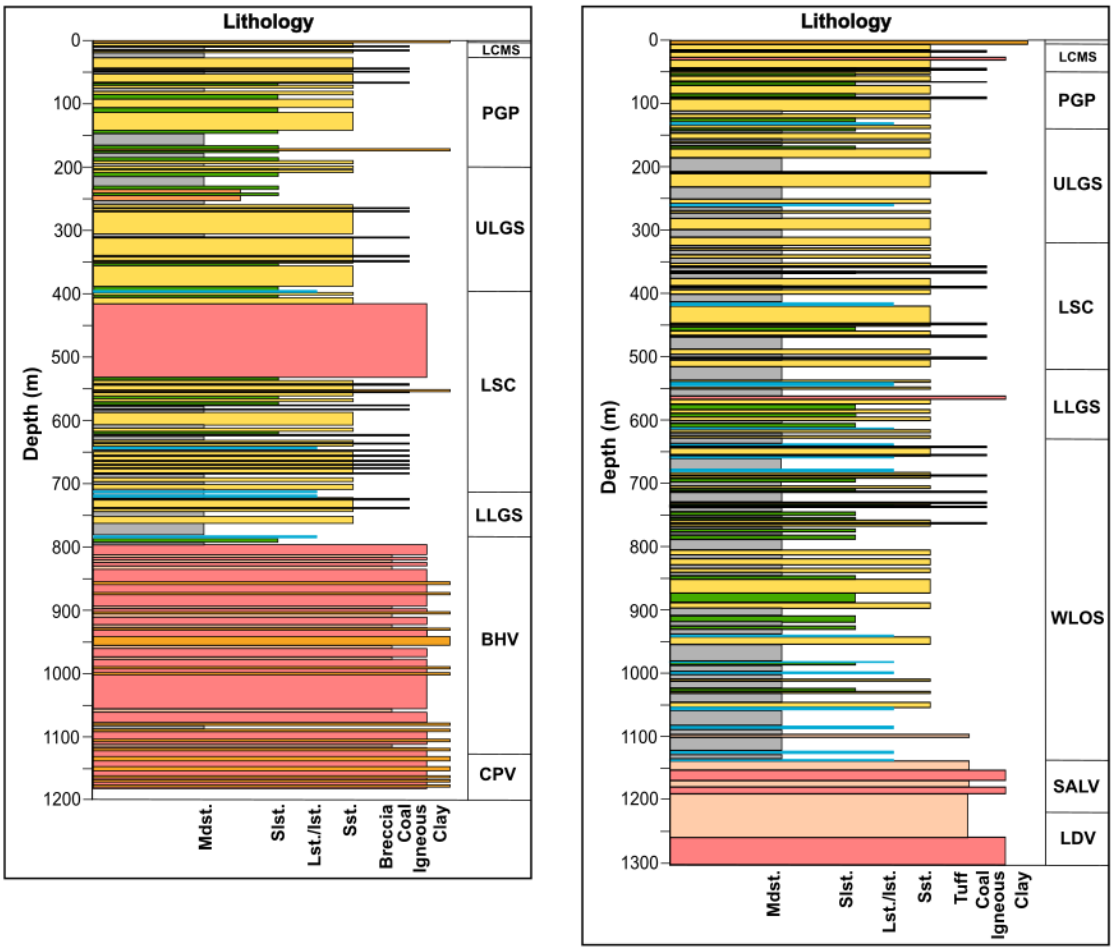

Figure 5.4. Stratigraphic columns for Rashiehill (Left) and Salsburgh-1 (Right). Based upon records provided by British Geological Survey (UKRI).

Bargeddie-1, Craighead-1, and Salsburgh-2 Boreholes

A further three boreholes were drilled to prospect for hydrocarbon reservoirs within the WLOS to the east of Glasgow (Appendix 5.A). The Craighead-1 borehole was drilled by Taylor Woodrow in 1981 and the Salsburgh-2 borehole was drilled by Candecca in 1985 (OGA, 2021). The Bargeddie-1 borehole was drilled by Marinex in 1989 to test for hydrocarbons in a laterally equivalent formation, the Upper Oil Shale Group (Teredo Petroleum PLC, 2000). Drill stem tests indicated poor reservoir conditions and each of these boreholes were plugged and abandoned (OGA, 2021). Measurements of temperature were recorded in each borehole, providing some of the deepest measurements in the region.

Barnhill, Clachie Bridge, Hurlet and Kipperoch IGS Boreholes

The Clachie Bridge, Barnhill, Hurlet and Kipperoch boreholes were drilled to investigate the Carboniferous and Devonian stratigraphy to the west, south-west and north of Glasgow (Figures 5.5 and 5.6) (IGS, 1976; 1978; 1980). Measurements of geothermal gradient, thermal conductivity and heat flow were recorded in each of these boreholes by the Oxford University Heat Flow Group (Oxburgh, 1982). A BHT measurement was also recorded in Burley et al. (1984) and a temperature log produced in Busby (2019) for the Clachie Bridge borehole.

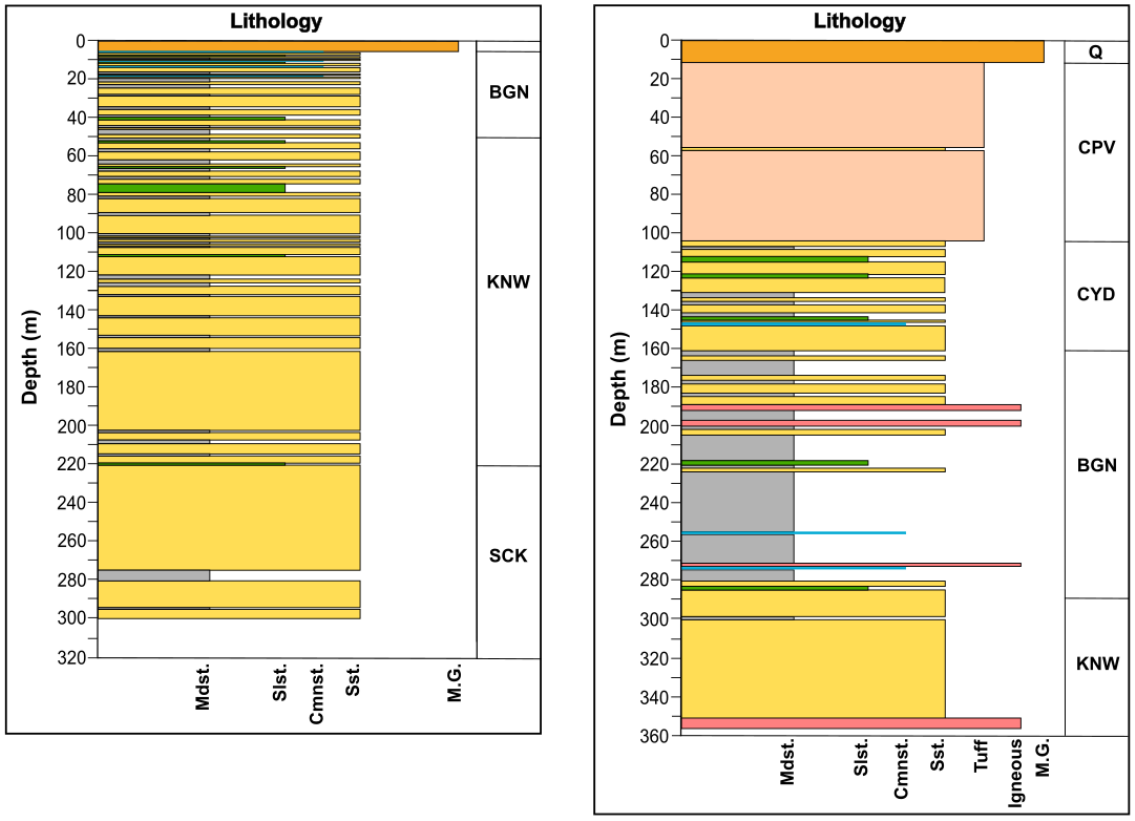

Figure 5.5. Stratigraphic columns for Kipperoch (Left) and Barnhill (Right). Based upon records provided by British Geological Survey (UKRI).

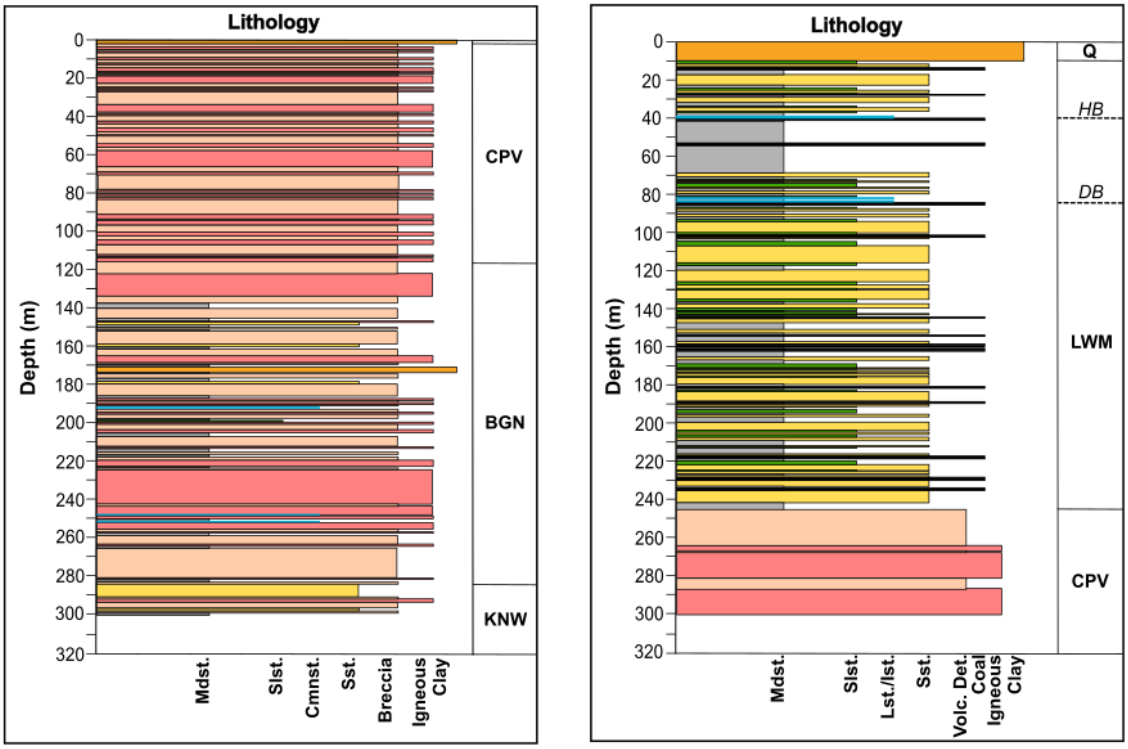

Figure 5.6. Stratigraphic columns for Clachie Bridge (Left) and Hurlet (Right). Based upon records provided by British Geological Survey (UKRI).

In each of the boreholes, the mean uncorrected and corrected heat flows were calculated from measurements observed across a limited range of depths, rather than the full extent of the borehole. At both Hurlet and Barnhill this was due to disintegration of fine-grained samples which limited the number of possible thermal conductivity measurements. A further issue occurred at Barnhill where the presence of flowing water was observed which may have perturbed the measurements.

Hallside Borehole

The Hallside borehole was drilled in 1976 to investigate the Carboniferous stratigraphy in the south-east of Glasgow (Figure 5.7) (IGS, 1978; Forsyth and Brand, 1986). The borehole was logged, and temperature was measured 60 hours post-circulation of drilling mud in the borehole (Burley et al., 1984).

Maryhill Borehole

The Maryhill borehole (Figure 5.7) was drilled by BGS in 1983 to collect geothermal data in Glasgow (Wheildon et al. 1985). This borehole was sited to give a 300 m sequence of rock, free of old mine workings, with a minimum thickness of porous sandstones, the objective being to record accurate measurements of the geothermal gradient, undisturbed by moving groundwater (Monro, 1983; Wheildon et al., 1985). Temperature was measured at

99 depths between 100 and 303 m depth, and together with 82 thermal conductivity measurements on borehole core, was used to calculate a value of heat flow for the borehole (Table 5.1) (Browne et al., 1987).

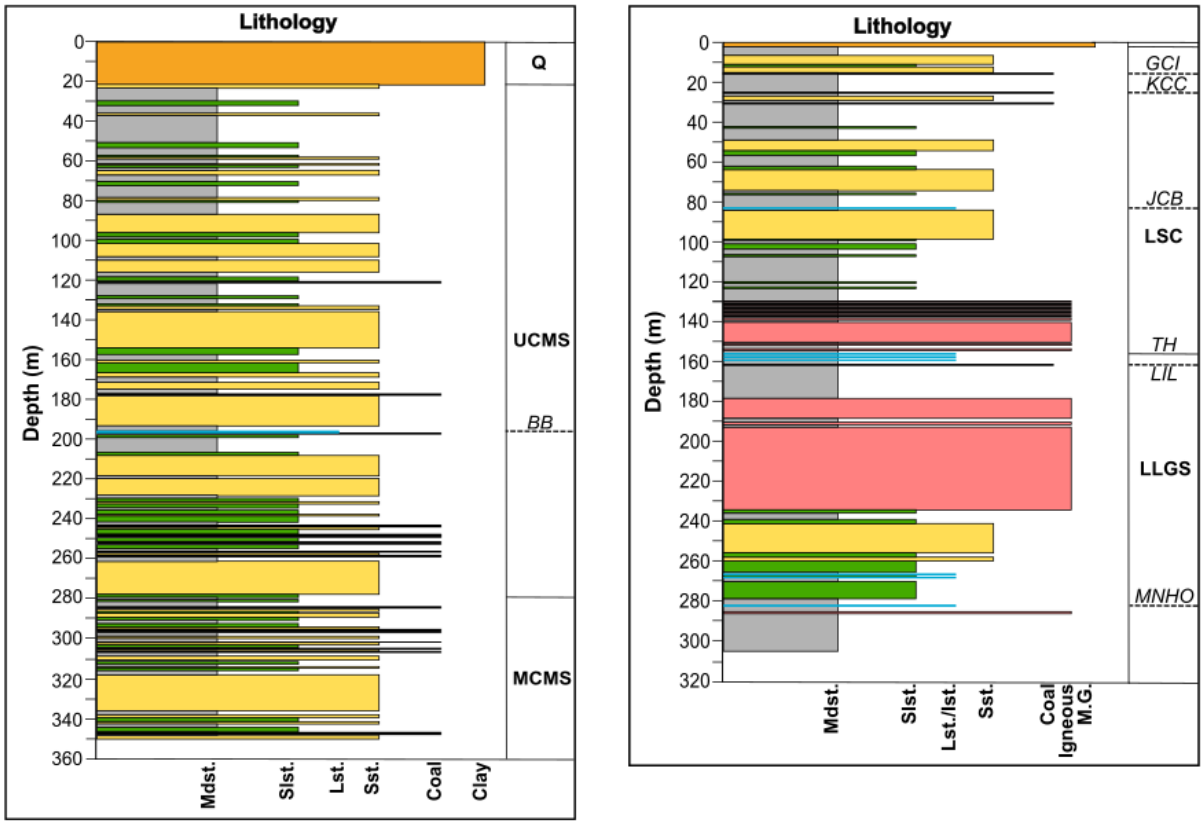

Figure 5.7. Stratigraphic columns for Hallside (Left) and Maryhill (Right). Based upon records provided by British Geological Survey (UKRI).

GGC01 Borehole

The GGC01 borehole was drilled between 19 November and 12 December 2018 as one of 12 boreholes at the UKGEOS GGERFS in the Clyde Gateway Redevelopment area in Dalmarnock, in the east end of Glasgow. The borehole was wireline logged in December 2018, providing temperature measurements to a depth of 196.8 m (Starcher et al., 2019).

Synthesis of Borehole Data

As discussed in section 5.2, the overall geothermal dataset for the western MVS from data measured in these sixteen boreholes is variable in quality and is inconsistent, with values of temperature or heat flow absent from several of the boreholes. Detailed in the following sections of this chapter, these borehole datasets have been appraised and re-evaluated by the author and new values of harmonic mean thermal conductivity, harmonic mean thermal diffusivity, temperature, and heat flow were calculated.

5.3.2. Calculation of Harmonic Mean Thermal Conductivity

According to Fourier's Law (Equation 2.1), a value of thermal conductivity is required to calculate heat flow from subsurface temperature measurements, or vice versa. An established procedure (e.g., Bott et al., 1972; Westaway and Younger, 2013) was adopted in this chapter to determine the harmonic mean thermal conductivity of the geological sequence over which heat flow or temperature was measured in each borehole.

The calculation of harmonic mean thermal conductivity accounts for small, frequent changes in lithology by considering the thermal resistance of each layer of rock encountered in a borehole. This approach was particularly relevant for this thesis as the boreholes studied contain rapid and recurring changes in lithology, typical of Carboniferous stratigraphy in Britain, as illustrated in Figures 5.2-5.7. The harmonic mean thermal conductivity of the geological sequence over which heat flow or temperature was measured in each borehole was calculated using Equation 5.1.

$$k = \frac{1}{\sum R / z_2 - z_1}$$

Equation 5.1

Where k is the harmonic mean thermal conductivity (W m^{-1} °C^{-1}), $z_2 - z_1$ is the depth interval over which the heat flow or temperature was measured (m), and ΣR is sum of the thermal resistance of each layer of rock encountered in the borehole over this interval.

Calculation Procedure

To calculate the harmonic mean thermal conductivity, the thermal resistance of each layer of rock in each borehole was first calculated by dividing the thickness of the layer by a value of thermal conductivity representative of the type of rock. The lithologies present in each borehole, and the thickness of each layer, were obtained from original drillers logs of each borehole (BGS, 2021) and are digitised in Figures 5.2-5.7.

The values of thermal conductivity assigned to each lithology were derived from two sources; (1) values were determined from existing measurements of thermal conductivity made in boreholes in the western MVS, and (2) values were obtained from literature if there were no pre-existing measurements for a particular lithology.

Measurements of thermal conductivity were reported by Oxburgh (1982) and Wheildon et al. (1985) for five boreholes in the western MVS; Barnhill, Clachie Bridge, Hurlet, Kipperoch and Maryhill. In each case, the divided bar method was used by these authors to measure the thermal conductivity of rock cuttings retrieved from each borehole. The raw data was provided by Dr. Jon Busby of BGS for re-examination in this chapter.

Using this data, the mean thermal conductivity, sample variation, sample standard deviation and standard error of the mean were calculated by the author for each measured lithology in each borehole. The results of these calculations are shown in Tables 5.2-5.6, where k is the mean thermal conductivity, N is the number of samples measured, σ is the sample variation, S is the sample standard deviation, and σ_x is the standard error of the mean.

Table 5.2. Maryhill thermal conductivity measurements (Wheildon et al. 1985).

Lithology	N	σ	S	$k \pm \sigma_x$ (W m^{-1} $°C^{-1}$)
Dolerite	9	0.07	0.26	1.81 ± 0.086
Mudstone	25	0.13	0.37	1.41 ± 0.073
Sandstone	17	0.16	0.40	4.54 ± 0.098
Siltstone	10	0.18	0.42	1.84 ± 0.133
Teschenite	13	0.01	0.11	2.16 ± 0.031

Table 5.3. Barnhill thermal conductivity measurements (Oxburgh, 1982).

Lithology	N	σ	S	$k \pm \sigma_x$ (W m^{-1} $°C^{-1}$)
Cementstone	1	0.00	0.00	3.83 ± 0.000
Cornstone	1	0.00	0.00	4.69 ± 0.000
Dyke	2	0.01	0.09	1.76 ± 0.067
Mudstone	2	0.01	0.12	2.46 ± 0.085
Sandstone	20	0.26	0.51	4.31 ± 0.113
Tuff	10	0.10	0.31	2.10 ± 0.099

Table 5.4. Kipperoch thermal conductivity measurements (Oxburgh, 1982).

Lithology	N	σ	S	$k \pm \sigma_x$ (W m^{-1} $°C^{-1}$)
Conglomerate	1	0.00	0.00	5.19 ± 0.000
Cornstone	2	0.24	0.49	4.10 ± 0.343
Mudstone	2	0.00	0.04	3.75 ± 0.028
Sandstone	41	0.37	0.61	3.59 ± 0.096
Siltstone	1	0.00	0.00	2.17 ± 0.000

Table 5.5. Hurlet thermal conductivity measurements (Oxburgh, 1982).

Lithology	N	$k \pm \sigma_x$ (W m^{-1} °C^{-1})
Basalt	6	2.00 ± 0.370
Sandstone	27	4.71 ± 0.520
Siltstone	4	3.02 ± 0.220
Volcanic Detritus	3	2.35 ± 0.130

Table 5.6. Clachie Bridge thermal conductivity measurements (Oxburgh, 1982).

Lithology	N	k (W m^{-1} °C^{-1})
Basalt	4	2.13
Breccia	12	2.63
Cementstone	2	2.64
Dolerite	1	2.13
Felsite	4	2.79
Mudstone	2	2.68
Sandstone	1	3.51

By comparison of Tables 5.2-5.6 and Figures 5.2-5.7, not all lithologies encountered in the boreholes in this study have existing, measured values of thermal conductivity. A literature review was therefore carried out to find appropriate values of thermal conductivity for lithologies such as coal, limestone, ironstone, marl, fireclay, and the Quaternary deposits encountered in the boreholes. Appropriate values of thermal conductivity were then assigned to each lithology in each borehole, tabulated in Appendix 5.B. In each case this was a combination of the mean values calculated from pre-existing measurements and appropriate values from literature.

One complication within this procedure concerned the Bargeddie-1, Craighead-1 and Salsburgh-2 boreholes which were drilled as commercial hydrocarbon exploration wells and therefore their borehole logs could not be accessed. Furthermore, a full cored log of the Queenslie-4 borehole was also absent as the top 441 m of the borehole was open hole and the lithologies encountered were not recorded. As result, there was a scarcity of information available on the exact lithologies and thicknesses of rock layers in each of these boreholes, prohibiting the calculation of thermal resistance and harmonic mean thermal conductivity using the same method as before.

To resolve this, the study was expanded to include boreholes which encounter known type sections of stratigraphic units in the western MVS (Table 5.7; Figure 5.A.3) (Forsyth et al., 1996; Hall et al., 1998). The harmonic mean thermal conductivity was calculated across each stratigraphic unit encountered in the boreholes detailed in Table 5.7 and, where possible, in

Table 5.1. As multiple boreholes encountered the same stratigraphic unit, a mean value was calculated to give an overall harmonic mean thermal conductivity for each respective stratigraphic unit (Table 5D.19). Since the general stratigraphy of the Bargeddie-1, Craighead-1, Salsburgh-2, and Queenslie-4 boreholes were known (e.g., Appendix 5.A, Figure 5.A.1), and as representative values of harmonic mean thermal conductivity of each of these stratigraphic units were now also known, the overall harmonic mean thermal conductivity of each of the aforementioned boreholes was thus determined.

Table 5.7. Boreholes in the western MVS which encounter type sections of stratigraphic units.

Borehole	NGR	Year	Height (m)	z (m)
Wester Gartshore [WG]	NS 68235 72390	1934	75	310.26
Queenslie 2 [Q2]	NS 65895 64900	1952	36.27	764.44
Queenslie Bridge [QB]	NS 66300 66030	1952	77.4	682.96
Lawmuir [L]	NS 51825 73095	1978	90.83	286.5
Loch Humphrey [LH]	NS 45820 75550	1978	351	423.48

Results

The results of the calculations of harmonic mean thermal conductivity are shown in Table 5.8.

Table 5.8. Harmonic mean thermal conductivity for each borehole.

Borehole	Interval (m)	k_H (W m^{-1} °C $^{-1}$)
Blythswood-1	18-105	2.00
South Balgray	0-137	1.64
Queenslie-4	0-691	2.13
Rashiehill	0-964	2.14
Slatehole	0-1024	2.10
Salsburgh-1A	0-898	1.96
Hallside	0-350	2.16
Kipperoch	40-300	3.57
Barnhill	320-355	3.67
Barnhill	25-355	2.67
Clachie Bridge	30-300	2.53
Hurlet	95-295	2.87
Craighead-1	0-909.8	2.03
Maryhill	100-303	1.80
Salsburgh-2	0-1102	2.03
Bargeddie-1	0-978.9	2.08
GGC01	0-197	1.60

5.3.3. Calculation of Harmonic Mean Thermal Diffusivity

Thermal diffusivity describes the rate at which heat is conducted through a medium. Thermal diffusivity is related to thermal conductivity, specific heat capacity, and density:

$$\kappa = \frac{k}{C_p \rho}$$

(Equation 5.2)

Where κ is the thermal diffusivity ($mm^2\ s^{-1}$), k is the thermal conductivity ($W\ m^{-1}\ °C^{-1}$), C_p is the specific heat capacity ($J\ kg^{-1}\ K^{-1}$) and ρ is the density ($kg\ m^{-3}$).

As there are no measured values of thermal diffusivity within boreholes in the western MVS, thermal diffusivity was calculated by the author for each lithology using Equation 5.2. A literature review was conducted to obtain representative values of specific heat capacity and density for each lithology and using these values alongside the assigned value of thermal conductivity, the thermal diffusivity was calculated for each lithology encountered in each borehole (Appendix 5.B; Tables 5B.1-B.18). Then, following the same procedure as in section 5.3.2, values of harmonic mean thermal diffusivity were calculated for each borehole. The results of these calculations are shown in Table 5.9.

Table 5.9. Harmonic mean thermal diffusivity for each borehole.

Borehole	Interval (m)	Mean κ ($mm^2\ s^{-1}$)
Blythswood-1	18-105	0.937
South Balgray	0-137	0.765
Queenslie-4	0-691	0.987
Rashiehill	0-964	0.959
Slatehole	0-1024	0.951
Salsburgh-1A	0-898	0.941
Hallside	0-350	1.018
Kipperoch	40-300	1.569
Barnhill	320-355	1.574
Barnhill	25-355	1.099
Clachie Bridge	30-300	0.961
Hurlet	95-295	1.198
Craighead-1	0-909.8	0.938
Maryhill	100-303	0.813
Salsburgh-2	0-1102	0.928
Bargeddie-1	0-978.9	0.954
GGC01	0-197	0.770

5.3.4. Calculation of Heat Flow

The heat flow dataset for the western MVS is limited to values determined in eight of the sixteen boreholes shown in Table 5.1. However, as described in section 5.3.1, subsurface temperature measurements were recorded in each of the eight remaining boreholes. New values of heat flow (Q) were therefore calculated for each of these boreholes by the author, expanding the existing heat flow dataset for the region. Furthermore, the values of heat flow determined in the Blythswood-1 and South Balgray boreholes by Benfield (1939) (Table 5.1) warranted re-calculation due to the availability of more appropriate thermal conductivity datasets. A new value of heat flow was also calculated for the Maryhill borehole as the calculation procedure adopted by Wheildon et al. (1985) was unclear to the author.

Heat flow was calculated using Fourier's Law (Equation 2.1), utilising the geothermal gradient (dT/dz) within each borehole and the newly calculated harmonic mean thermal conductivity (k), with results shown in Table 5.10.

Table 5.10. Newly calculated heat flow values for boreholes in the western MVS.

Name	Interval (z_1-z_2) (m)	T_1 (°C)	T_2 (°C)	k (W m^{-1} °C^{-1})	dT/dz (°C km^{-1})	Q (mW m^{-2})
Blythswood-1	18-105	8.86	12.05	2.00	36.47	72.84 ± 2.58
South Balgray	0-137	8.76	14.52	1.64	41.99	68.92 ± 6.7
Queenslie-4	0-691	8.39	36.00	2.13	39.96	85.28
Rashiehill	0-964	10.00	35.80	2.14	26.76	57.35 ± 6.81
Slatehole	0-1024	8.61	40.00	2.10	30.65	64.30
Salsburgh-1A	0-898	7.75	34.00	1.96	29.23	57.23
Hallside	0-350	8.50	11.80	2.16	9.43	20.34 ± 5.47
Craighead-1	0-909.8	6.95	35.00	2.03	30.83	62.54
Maryhill	100-303	12.29	20.03	1.80	38.28	69.08 ± 2.04
Salsburgh-2	0-1102.1	6.73	44.00	2.03	33.82	68.58
Bargeddie-1	0-978.9	9.30	38.70	2.08	30.03	62.52 ± 7.03

The geothermal gradient was calculated between the surface temperature (T_1) and deepest (T_2) temperature observations made within each borehole, or in the case of Blythswood-1 and Maryhill between 18-105 m and 100-300 m, respectively, to allow for direct comparisons to the Benfield (1939) and Wheildon et al. (1985) analyses.

Surface temperatures were reported during temperature logging at the Hallside and Rashiehill boreholes and were used, here, to calculate the geothermal gradient and thus heat flow. Excluding Blythswood-1 and Maryhill, for all other boreholes, the annual mean surface temperature was determined for the year in which borehole temperature measurements were

made and taken to be T_1 within these calculations. For this, historic air temperature data was obtained from meteorological stations at Paisley and Salsburgh (Met Office, 2021a; 2021b) and corrected for a regional lapse rate of 8 °C km^{-1} and a regional lateral variation in air temperature to give the annual mean surface air temperature at each borehole site. This procedure is detailed extensively in Chapter 6 and Appendix 6.E.

The standard error of the mean is presented in Table 5.10 for boreholes which contain multiple subsurface temperature measurements, such as Blythswood-1, Maryhill, South Balgray, Rashiehill, Hallside, and Bargeddie-1. Using Equation 2.1, values of heat flow were calculated at intervals throughout each borehole, based on the geothermal gradient and harmonic mean thermal conductivity of the intervals between the subsurface temperature measurements. The sample variation, standard deviation, and standard error of the mean were then determined. As the Queenslie-4, Slatehole, Salsburgh-1A, Craighead-1 and Salsburgh-2 boreholes consisted of only one bottom hole temperature measurement, the standard error in the mean could not be calculated.

5.3.5. Calculation of Subsurface Temperature Profiles

Measurements of thermal conductivity, geothermal gradient and heat flow were reported at 5 m intervals at the Barnhill, Clachie Bridge, Hurlet and Kipperoch boreholes by the Oxford University Heat Flow Group (Oxburgh, 1982), however measurements of raw temperature data were either not reported or observed in these boreholes. New subsurface temperature profiles were therefore calculated by the author using the existing data measured in each of these boreholes.

As a starting point to calculate the subsurface temperature profile from these existing borehole datasets, the annual mean surface temperature (T_o) was derived for each borehole, following the same process described in section 5.3.4. Then, using Equation 2.1, the geothermal gradient was calculated for each borehole by dividing the mean uncorrected heat flow (see Table 5.1) by the harmonic mean thermal conductivity (see Table 5.8). The geothermal gradient was then used to extrapolate the surface temperature to estimate the temperature (T_z) at the depth of first measurement interval in each borehole (Table 5.11).

Table 5.11. Oxburgh (1982) heat flow boreholes

Borehole	Interval (m)	T_o (°)	Q (mW m^{-2})	k (W m^{-1} °C $^{-1}$)	dT/dz (°C km^{-1})	T_z (°)	T_B (°)
Kipperoch	40-300	7.47	53.4	3.57	14.95	8.07	11.92
Barnhill	25-355	8.6	48.91	2.67	18.32	9.06	14.90
Clachie Bridge	30-300	6.46	57.68	2.53	22.81	7.14	13.19
Hurlet	95-295	9.16	61.75	2.87	21.55	11.20	15.51

In Table 5.11, "Interval" is the depth range over which measurements were recorded by Oxburgh (1982), "T_o" is the annual mean surface temperature at each borehole site, "Q" is the uncorrected mean heat flow (Oxburgh 1982), "k" is the harmonic mean thermal conductivity for the geological sequence encountered within the measurement interval in the borehole, "dT/dz" is the geothermal gradient calculated from the mean heat flow and the harmonic mean thermal conductivity, "T_z" is the estimated temperature at the depth of the first measurement in the borehole, and "T_B" is the estimated BHT.

Finally, with T_z as a starting point in each borehole, the incremental increases in temperature throughout the remainder of the borehole were calculated using the geothermal gradients measured at each 5 m interval by Oxburgh (1982), giving a reconstructed temperature profile for each of these boreholes. These temperature profiles are shown in Figure 5.8 and provide new subsurface temperature datasets for each of these boreholes. For comparison, the subsurface temperature profiles measured in the remainder of the boreholes in this study are presented in Figures 5.9 and 5.10. These datasets are important to the present study as the raw temperature profiles are (1) used to identify perturbations to the subsurface thermal state caused by anthropogenic industrial processes (Watson and Westaway, 2020) and historic mine workings (Watson et al., 2019), and (2) used within palaeoclimate correction modelling in Chapter 6 to determine the corrected heat flow and geothermal gradient for the region and thus the 'true' temperature within the geothermal resource beneath Glasgow.

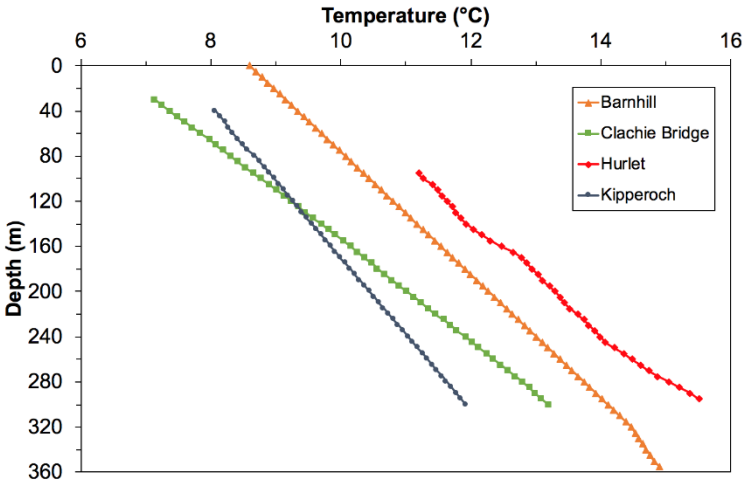

Figure 5.8. Borehole temperature measurements for the Oxburgh (1982) borehole datasets.

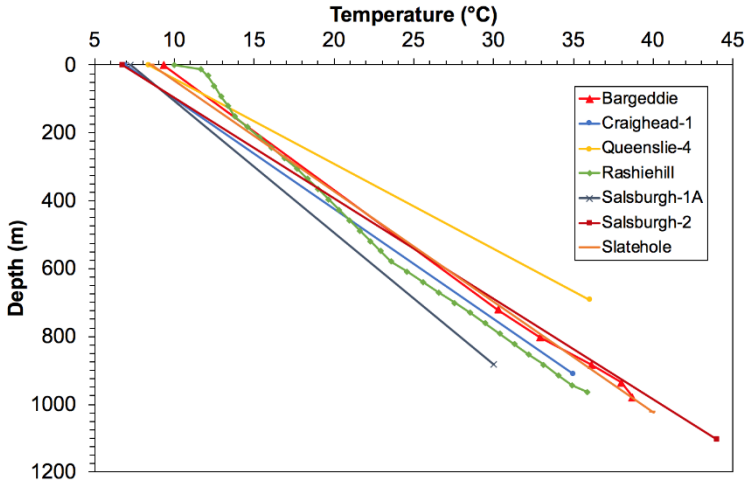

Figure 5.9. Borehole temperature measurements for the boreholes >500 m depth included in this study.

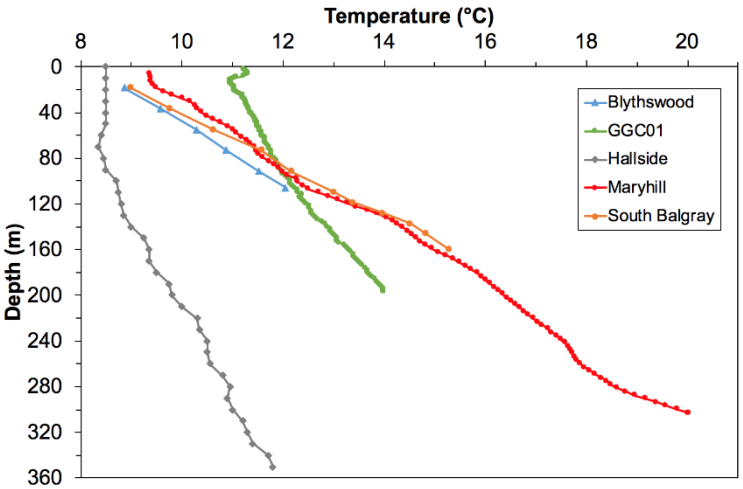

Figure 5.10. Borehole temperature measurements for the boreholes <500 m depth included in this study.

5.3.6. Thermal Properties Sensitivity Analysis

A sensitivity analysis was then conducted to determine lower and upper ranges of thermal conductivity and to show the resulting variation in the calculated heat flow. Mean and standard error of the mean values of thermal conductivity from measurements from the Barnhill, Clachie Bridge, Hurlet, Kipperoch and Maryhill boreholes were used to determine lower (i.e., the mean – the standard error of the mean) and upper (i.e., the mean + the standard error of the mean) sets of values of thermal conductivity (Appendix 5.C). These were assigned to lithologies in each borehole and the resulting harmonic mean thermal conductivity calculated. Using these lower and upper suites of thermal conductivity, and values of specific heat capacity and density obtained from literature, corresponding values of harmonic mean thermal diffusivity were calculated for each borehole (Appendix 5.D and 5.E). Finally, the lower and upper values of harmonic mean thermal conductivity were used to calculate corresponding values of heat flow in each of the boreholes. The variation in harmonic mean thermal conductivity for each borehole is shown in Table 5.12, and the resulting lower and upper estimates of heat flow is shown in Table 5.13.

As detailed in Appendix 5.C, some lithologies remained unchanged between the lower, mean, or upper sets of values. In these cases, the lithology was not frequently encountered in the borehole, or accounted for a small proportion of the total stratigraphy, and as such any changes to the thermal conductivity of these lithologies were deemed to have a negligible effect on the resulting heat flow. Examples of such lithologies are limestone, ironstone, coal, and Quaternary deposits.

Table 5.12. Lower and upper values of harmonic mean thermal conductivity (k) and diffusivity (κ).

Borehole	Interval	k_{Lower}	k_{Upper}	κ_{Lower}	κ_{Upper}
	(m)	(W m^{-1} °C^{-1})	(W m^{-1} °C^{-1})	(mm^2 s^{-1})	(mm^2 s^{-1})
Blythswood-1	18-105	1.92	2.07	0.900	0.971
South Balgray	0-137	1.58	1.71	0.735	0.797
Queenslie-4	0-691	1.99	2.27	0.919	1.049
Rashiehill	0-964	1.89	2.27	0.844	1.015
Slatehole	0-1024	1.83	2.19	0.829	0.991
Salsburgh-1A	0-898	1.83	2.08	0.876	1.002
Hallside	0-350	2.03	2.27	0.960	1.072
Kipperoch	40-300	3.48	3.66	1.528	1.610
Barnhill	25-355	2.57	2.76	1.058	1.137
Clachie Bridge	30-300	2.41	2.62	0.920	0.990
Hurlet	95-295	2.62	3.09	1.092	1.295
Craighead-1	0-909.8	1.88	2.16	0.869	0.998
Maryhill	100-303	1.70	1.88	0.768	0.845
Salsburgh-2	0-1102	1.88	2.16	0.856	0.989
Bargeddie-1	0-978.9	1.92	2.23	0.876	1.025

Table 5.13. Results of lower and upper values of heat flow (Q) for each borehole.

Name	k_{Lower} (W m^{-1} °C $^{-1}$)	Q_{Lower} (mW m^{-2})	k_{Upper} (W m^{-1} °C $^{-1}$)	Q_{Upper} (mW m^{-2})
Blythswood-1	1.92	70.01	2.07	75.48
South Balgray	1.58	66.35	1.71	71.81
Queenslie-4	1.99	79.53	2.27	90.70
Rashiehill	1.89	50.58	2.27	60.75
Slatehole	1.83	56.10	2.19	67.13
Salsburgh-1A	1.83	53.49	2.08	60.80
Hallside	2.03	19.14	2.27	21.40
Kipperoch	3.48	51.53	3.66	54.20
Barnhill	2.57	45.48	2.76	48.84
Clachie Bridge	2.41	54.00	2.62	58.71
Hurlet	2.62	56.46	3.09	66.59
Craighead-1	1.88	57.96	2.16	66.59
Maryhill	1.70	65.08	1.88	71.98
Salsburgh-2	1.88	63.58	2.16	73.05
Bargeddie-1	1.92	57.66	2.23	66.98

The boreholes in which heat flow was least affected by changes in thermal conductivity are Hallside, Kipperoch, Barnhill and Clachie Bridge. The standard error of the mean calculated from Barnhill and Kipperoch datasets for each lithology were well constrained and as such there was no significant change in thermal conductivity and thus no significant change in the resulting heat flow. At Hallside, the only lithologies for which thermal conductivity were altered were mudstone, sandstone, and siltstone and in each case the change was not significant, hence the minimal change in heat flow.

The standard error of the mean calculated for each lithology in the Maryhill borehole was, in general, greater than those of the Kipperoch and Barnhill boreholes. As expected, the variation in heat flow for the Maryhill borehole was also greater. Similar variations in heat flow were observed at the Blythswood-1 and South Balgray boreholes, which were expected due to the similarity in stratigraphy between each of the boreholes. The small differences between the results calculated for each borehole are explained by the differences in the proportions of siltstone and igneous rocks encountered in each borehole. The lithology with the greatest variation in the standard error of the mean from the Maryhill borehole dataset was siltstone. As shown in Appendix 5.B, the Maryhill and South Balgray boreholes both encountered a larger proportion of fakes or siltstone in comparison to Blythswood-1. As a result, the magnitude of the change in heat flow was greater for Maryhill and South Balgray compared to Blythswood-1. Another difference between the boreholes was the presence of approximately 80 m of igneous rocks within the interval in which heat flow was calculated at Maryhill. This igneous intrusion was absent at Blythswood-1; however, it was

encountered in the South Balgray borehole but at depths greater than those which affect the heat flow calculations. The variation in thermal conductivity of these igneous rocks, such as teschenite, dolorite and white trap, also contributes to the difference in results of the Maryhill, South Balgray, and Blythswood-1 boreholes.

Other than the measurements of thermal conductivity of cornstone made within the Kipperoch borehole, the largest values of standard error of the mean were calculated for lithologies in the Hurlet borehole. In comparison to measurements made on similar lithologies in the Maryhill borehole, i.e., sandstone, siltstone and basalt, the standard error of the mean calculated from measurements at Hurlet were considerably higher. As was expected, this greater variation in thermal conductivity results in a greater variation in heat flow at Hurlet. It was also shown that the heat flow of boreholes which utilise the values of thermal conductivity measured at Hurlet are more greatly affected by the changes in thermal conductivity. This is illustrated in the results calculated for the Craighead-1, Salsburgh-1A, Salsburgh-2, and Bargeddie-1 boreholes. Each of these boreholes encountered thick sequences of the WLOS, laterally equivalent to the Lawmuir Formation of the Hurlet borehole, and thus the same lower and upper values of thermal conductivity were applied to this formation.

In addition to Hurlet, two of the boreholes within which heat flow was most affected by changes in thermal conductivity are Rashiehill and Slatehole. There are similarities between these boreholes, despite the significant difference in geography and local geology. Both boreholes encountered cyclic successions of sedimentary rocks and significant thicknesses of igneous rocks. The dominant lithologies encountered at Slatehole were blaes, fakes, igneous rocks and sandstone, and similarly at Rashiehill the dominant lithologies were blaes, fireclay, igneous rocks and sandstone. The heat flow calculated in each borehole was therefore influenced by a number of the same features. These include the variation in the thermal conductivity of Coal Measures sandstone, mudstone and siltstone, the variation in thermal conductivity of igneous rocks, and the uncertainty in the choice of thermal properties for lithologies such as fakes and fireclay.

These results detailed in Tables 5.12 and 5.13 have been utilised within the analysis of palaeoclimate and topographic corrections to heat flow in Chapter 6 of this thesis, to determine upper and lower corrected values of heat flow for each borehole. The significance of the results of the sensitivity analysis and implications for quantifying the temperature within the geothermal resource beneath Glasgow are discussed in Chapter 6.

5.4. Implications for Geothermal Energy in Glasgow

The results from the sixteen boreholes examined in this chapter (Figure 5.1, Figure 5.10) were used to assess trends in heat flow across the region (section 5.4.1); to identify anomalous measurements of thermal conductivity, subsurface temperature, or heat flow, and to highlight any discrepancies or uncertainties within previously published work (section 5.4.2 and 5.4.3). Then, based upon these results, an examination of the influence of historic mining on Glasgow's subsurface thermal state was conducted (Watson et al., 2019; Watson and Westaway, 2020) and the principal findings are detailed in section 5.4.4.

Thus, the results of this chapter produced a robust and accurate dataset of geothermal gradient, heat flow, and thermal properties for boreholes in the western MVS for use within Chapter 6 to determine palaeoclimate and topographic corrections to heat flow, unveiling the 'true' heat flow of the Glasgow area.

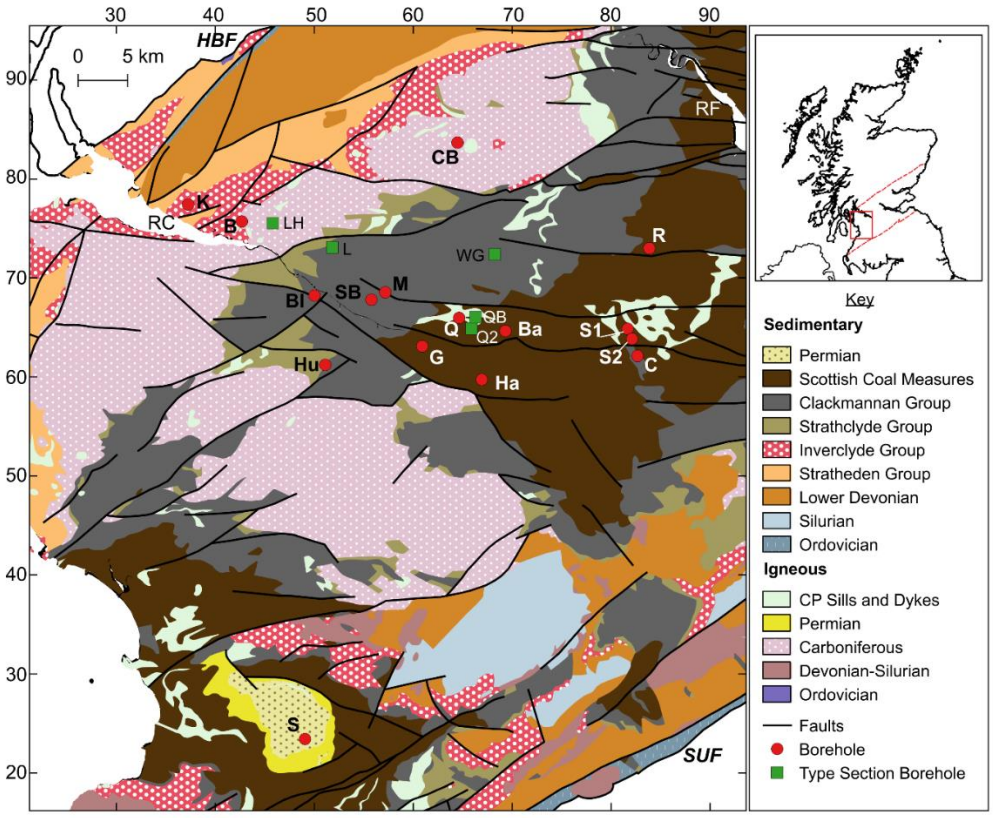

Figure 5.11. Simplified solid geology, structure and locations of boreholes studied in Glasgow and the surrounding conurbation. The co-ordinates (north and east) are in kilometres within British National Grid 100 km quadrangle NS. Geological Map Data BGS © UKRI 2021.

5.4.1. Regional Overview of Heat Flow

The regional mean heat flow and geothermal gradient from the sixteen boreholes examined in this chapter were 58.66 mW m^{-2} and 27.67 °C km^{-1} respectively. The lowest values of heat flow occur in the Hallside and GGC01 boreholes. These values are considerably lower than the regional mean heat flow, at 20 mW m^{-2} and 28-33 mW m^{-2}, respectively, and imply that the subsurface thermal state is perturbed at these locations (see section 5.4.4). The highest heat flow was determined in the Queenslie-4 borehole in eastern Glasgow. At 85 mW m^{-2}, this value of heat flow is higher than the regional mean heat flow and may be due to errors in measuring the bottom hole temperature or incorrectly assumed values of thermal conductivity (see section 5.4.3). Excluding the results of Hallside, GGC01 and Queenslie-4, the regional mean heat flow and geothermal gradient were calculated as 61.92 mW m^{-2} and 28.90 °C km^{-1}.

The most distinctive trend observed from these new results is that, in general, values of heat flow are higher in boreholes located in the Renfrewshire, Lanarkshire, and Mauchline Basins, compared to those located to the north and west of Glasgow in outcrops of Lower Carboniferous sedimentary and igneous rocks. The mean heat flow and geothermal gradient of Barnhill and Kipperoch, in the west, and Clachie Bridge, in the north of Glasgow, were calculated as 53.33 mW m^{-2} and 18.69 °C km^{-1}. Each of these boreholes were dominated by thick sequences of sandstone, mudstone, or breccia; in which high values of thermal conductivity were measured. The presence of these lithologies mean that the Barnhill, Clachie Bridge, and Kipperoch boreholes have a higher harmonic mean thermal conductivity, but lower geothermal gradient and heat flow compared to those boreholes located in younger Carboniferous stratigraphic formations.

The thirteen remaining boreholes encountered frequent variations of sediments between those of low and high thermal conductivity resulting in a lower overall harmonic mean thermal conductivity and higher heat flow (Figures 5.2-5.7). Excluding the results of the Hallside, GGC01 and Queenslie-4 boreholes, the mean heat flow and geothermal gradient of the remaining ten boreholes were calculated as 64.49 mW m^{-2} and 31.96 °C km^{-1}. In western parts of Glasgow, the mean heat flow and geothermal gradient of the Blythswood-1, Hurlet, Maryhill and South Balgray boreholes was found to be 68.10 mW m^{-2} and 34.57 °C km^{-1}. Of these boreholes, the highest heat flows were calculated at Blythswood-1 and South Balgray. To the east of Glasgow, the hydrocarbon exploration boreholes have a mean heat flow of 61.64 mW m^{-2} and mean geothermal gradient of 30.14 °C km^{-1}. Of these, the highest value of heat flow was calculated at the Salsburgh-2 borehole due to the high bottom

hole temperature and geothermal gradient measured in the borehole. Indeed, Salsburgh-2 has the highest bottom hole temperature of 44 °C of all sixteen boreholes analysed, which was to be expected as it is the deepest borehole of those analysed at 1102.1 m depth.

5.4.2. Increase in Heat Flow of Blythswood-1 and South Balgray

In the present study, the heat flow of the Blythswood-1 and South Balgray boreholes were re-calculated using measured thermal conductivity data from the nearby Maryhill borehole (Table 5.2). This differs from previous analyses of Benfield (1939) and Anderson (1940) which applied values of thermal conductivity measured on samples from the Boreland borehole in Fife, in the east of the MVS, to the lithologies encountered at Blythswood-1 and South Balgray (Tables 5C.1 and 5C.2 in Appendix 5.C). These samples of sandstone, fakes, blaes and fireclay were from depths of 509-631 m within the Upper Limestone Formation in the Boreland borehole. Given the difference in location, depth, and stratigraphy between the Boreland borehole and the Blythswood-1 and South Balgray boreholes, the thermal conductivity and heat flow were re-evaluated in this present study using analogous data from the nearby Maryhill borehole instead.

The Blythswood-1 borehole was located 7.5 km to the south-west of the Maryhill borehole (Figure 5.11), and like the Maryhill borehole, encountered the Limestone Coal Formation (Appendix 5.A). The South Balgray borehole was located less than 2 km to the west of the Maryhill borehole (Figure 5.11) and encountered a very similar stratigraphic succession through the Limestone Coal and Lower Limestone formations (Appendix 5.A). Detailed in Appendix 5.C, Tables 5.C.1 and 5.C.2, mean and standard error of the mean values calculated from measurements at Maryhill were assigned to the Blythswood-1 and South Balgray boreholes. Given the greater similarity in stratigraphy and proximity of location between the South Balgray and Maryhill boreholes, mean and standard error of the mean values of thermal conductivity were calculated between 0-137 m depth in the Maryhill borehole and assigned to equivalent lithologies in the South Balgray borehole. This was predicated on the assumption that these values of thermal conductivity would be typical of those in the South Balgray borehole between 0-137 m, the depth range over which temperature was measured and heat flow calculated. These values were then used to calculate the harmonic mean thermal conductivity of the Blythswood-1 and South Balgray boreholes and the resulting heat flow.

This recalculation resulted in an increase in heat flow at both boreholes, at Blythswood-1 from 52 mW m^{-2} to 73 mW m^{-2}, and at South Balgray from 64 mW m^{-2} to 69 mW m^{-2}. As shown in Appendix 5.B, sandstone, mudstone, and siltstone dominate both the Blythswood-1 and South Balgray boreholes and a substantive increase in the thermal conductivity of these lithologies, as detailed in Appendix 5.C, resulted in the increase in heat flow. By using values of thermal conductivity measured in the Boreland borehole to calculate heat flow at Blythswood-1 and South Balgray, Benfield (1939) underestimated the magnitude of heat flow at both boreholes, particularly in the case of the Blythswood-1 borehole.

The new results are therefore more representative of the true uncorrected heat flow in these boreholes as they take into consideration measured values of thermal conductivity from an analogous stratigraphic succession in the nearby Maryhill borehole. The new results form the basis of more reliable palaoeclimate corrections to heat flow in Chapter 6, and the resulting extrapolation of geothermal gradients to estimate the temperature of the geothermal resource beneath Glasgow.

5.4.3. Anomalous Heat Flow at Queenslie-4

The mean heat flow calculated for the Queenslie-4 borehole was considerably higher than the regional mean value. One explanation for this is that the measured bottom hole temperature was not at equilibrium with the surrounding rock and is an overestimate. This measurement is higher than subsurface temperature measurements made at greater depths within boreholes such as Craighead-1, Rashiehill and Salsburgh-1A, and is higher than the mean equilibrium mine water temperature of 32.2 °C at 700 m depth reported by the Coal Authority (2020).

Another contributing factor to the high heat flow calculated at this borehole was the high harmonic mean thermal conductivity. For comparison, the heat flow at Queenslie-4 was recalculated using the harmonic mean thermal conductivity from the nearby Queenslie-2 and Queenslie Bridge boreholes. Using a harmonic mean thermal conductivity of 1.82 W m^{-1} $°C^{-1}$ from the Queenslie-2 borehole, the heat flow at Queenslie-4 was recalculated as 73 mW m^{-2}. Then, using a slightly higher harmonic mean thermal conductivity of 1.88 W m^{-1} $°C^{-1}$ from the Queenslie Bridge borehole, the heat flow at Queenslie-4 was recalculated as 75 mW m^{-2}. These values are more comparable with the regional mean values of heat flow compared to the original value calculated for Queenslie-4 and suggest that the harmonic mean thermal conductivity calculated for the Queenslie-4 borehole may be too high. Two uncertainties which arose in the analysis of the Queenslie-4 borehole relate to the choice of appropriate

thermal properties for fakes and fireclay. Further analysis was conducted using lower values of thermal conductivity of these lithologies. In this case, it was assumed that the thermal conductivity of both fakes and fireclay were 1.35 W m^{-1} °C^{-1}. This reduced the heat flow of Queenslie-4 to 78 mW m^{-2}. Again, whilst this reduction in heat flow aligns Queenslie-4 closer to the remainder of the boreholes, it is still considerably greater than the regional mean heat flow for the western MVS.

5.4.4. The Influence of Historic Mining on Glasgow's Subsurface Thermal State

The heat flow of the Hallside borehole shown in Table 5.10 is considerably lower than the remainder of the boreholes examined in this chapter. This prompted an investigation of possible causes of the low bottom hole temperatures and resulting low heat flow calculated for each borehole.

Westaway and Younger (2016) observed that the entrainment and lateral dispersion of heat through abandoned mine workings contributes to subsurface thermal energy flows and influences measurements recorded in boreholes at depths shallower than the mine workings. There is also the possibility that upward or downward groundwater flow through connected mine workings influences subsurface heat flow. Either of these mechanisms may mean that subsurface temperature measurements may not be representative of the conductive heat flow in the locality. These factors were found to be prevalent in Tyneside and are likewise possible beneath the Glasgow area given the similar history of coal mining in these areas.

A chronology of mining activity in the vicinity of each of the boreholes in Table 5.1 was established using material from the Glasgow Archives in the Mitchell Library of the City of Glasgow, the Renfrewshire Archives, and the National Records of Scotland. The material examined included: mine entry data obtained from the Coal Authority's Online Interactive Map (Coal Authority, 2020) and the Northern Mine Research Society Online Interactive Map (Northern Mine Research Society, 2020); mine abandonment plans; borehole records held by the British Geological Survey (BGS); geological and mining memoirs; and historical maps.

The results of this investigation were published in Watson et al. (2019) and Watson and Westaway (2020) and are summarised here.

Hallside Case Study: History of Coal Mining

The Hallside borehole was located on the site of the former Hallside Colliery (Figure 5.12). The village of Hallside was originally built to serve the nearby Hallside Colliery and expanded when the Hallside Steelworks opened in 1872 (Hall, 2012). The Hallside Steelworks was one of the major steel-producing centres in Scotland until its closure in 1979 (Shepherd, 1996). Hallside Colliery opened in 1873 and closed in 1921 (Mines Department, 1931). The closure of the colliery was due to flooding of the mine workings as a result of the cessation of mining and pumping of groundwater during the 1921 General Strike (Findlay et al., 2020).

Until closure in 1921, pits at Hallside Colliery worked seams of Upper Coal, Ell Coal, Pyotshaw Coal, Main Coal, Splint Coal and Virgin Coal (Watson et al., 2019). After the closure of Hallside Colliery, neighbouring collieries continued to work these seams to varying extents across the local area, and beneath the location of the Hallside borehole (National Coal Board, 1961a; 1961b). Those collieries which remained active at this time were Newton, Bardykes and Blantyreferme (National Coal Board 1961a; Oglethorpe, 2006; Findlay et al., 2020). For example, seams of Upper and Ell Coal were worked beneath Hallside Colliery from Blantyreferme Colliery (National Coal Board, 1961a; 1961b) and Newton (Findlay et al., 2020); and the Blackband seam from Blantyreferme (National Coal Board, 1961a; 1961b) and Bardykes (Findlay et al., 2020). National Coal Board (1961b) plans shows the extent and timescale in which each seam of coal was worked at the Hallside and Blantyreferme pits. The plans show Main Coal workings dated January 1890 and January 1892, Virgin Coal workings dated 04 October 1910, Pyotshaw Coal workings dated 18 January 1915, Humph Coal workings dated April 1920, Upper Coal workings dated 17 June 1932 and Ell Coal workings dated 21 March 1944. All but a few of the plans show worked seams that are either in close proximity to or lie directly beneath the location of the Hallside borehole (Figure 5.13).

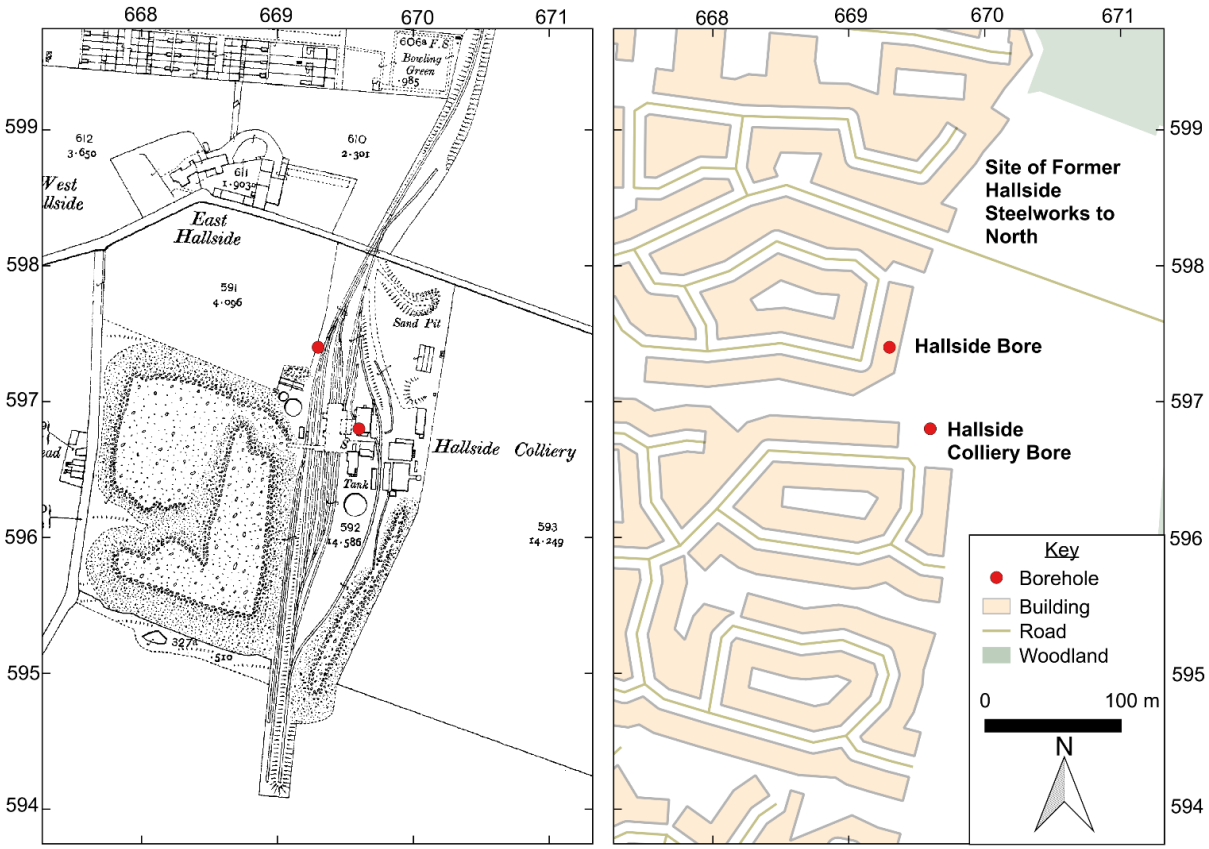

Figure 5.12. Historical map and present-day land-use map at the locality of the Hallside BGS borehole, showing proximity of the former Hallside Colliery (closed in 1921). The coordinates are in 100 m intervals within British National Grid 100 km quadrangle NS. Historical data: © Crown Copyright and Landmark Information Group Limited (2021). All rights reserved. (1914). © Crown copyright and database rights 2021 Ordnance Survey (100025252).

Attempts were made to develop the deeper workings in Main, Pyotshaw, Splint and Virgin coal seams beneath Hallside by neighbouring collieries but these flooded, former Hallside Colliery workings could not be pumped dry (Findlay et al., 2020). Numerous attempts were made to dewater Hallside Colliery from Bardykes Colliery however these failed. Flooding of Hallside Colliery and the inability to mine deeper seams contributed to the cessation of mining activity in the local area, with Bardykes Colliery closing in 1962 and Blantyreferme and Newton Colliery in 1964 (Findlay et al., 2020).

In the Hallside borehole, the base of the Upper Coal Measures was encountered at c. 279 m depth, with the borehole terminating at a depth of c. 352 m (Appendix 5.A). Another borehole, named the ‘Hallside Colliery’ borehole, was sunk from within the mine workings at c. 265 m depth to a depth of c. 451 m to give a section of the stratigraphy at the colliery (Figure 5.12 and 5.13). Clough et al. (1920) state that at Hallside Colliery, the Middle Coal Measures were overlain by around 293 m of Upper Coal Measures. This aligns relatively

well with the boundary of the Upper Coal and Middle Coal Measures observed in the Hallside borehole, indicating that there is close alignment between the depths of seams in the Hallside borehole and those worked in the Hallside Colliery. For the purpose of this analysis, it was assumed that the depth of each seam was the same in the 'Hallside Colliery' borehole as in the Hallside borehole (Figure 5.13). The depth of the worked seams, described above, in the Hallside Colliery borehole were all deeper than the base of the Hallside borehole (Figure 5.13), and a number of the deeper seams were known to have been flooded. This suggests that there was an influence from this legacy of mining on the flow of heat in the subsurface and explains why a low geothermal gradient, and associated heat flow, were observed in the Hallside borehole. The Hallside dataset, therefore, provides strong evidence that the conductive heat flow at depths overlying flooded mine workings has been altered by the existence of these workings and is therefore unrepresentative of the heat flow from the Earth's interior.

Hallside Case Study: Implications for Heat Flow

Two potential hypotheses are therefore considered at Hallside: (1) upward conductive heat flow is greatly reduced above the mine voids as heat is dispersed laterally through the workings (Figure 5.13) and/or, (2) downward flow of groundwater through the connected workings is partly cancelling the upward flow of heat. In both cases, the result is a reduced bottom-hole temperature in comparison to the regional average temperature gradient.

While the conductive heat flow and associated geothermal gradient have been significantly reduced, it may be the case that heat is moving horizontally, carried by groundwater flow, from the workings beneath the borehole to increase temperatures in the mines below other areas of Glasgow. Care must therefore be taken to consider such an effect as this when attempting to quantify the potential geothermal resource in abandoned, flooded mine workings in the future.

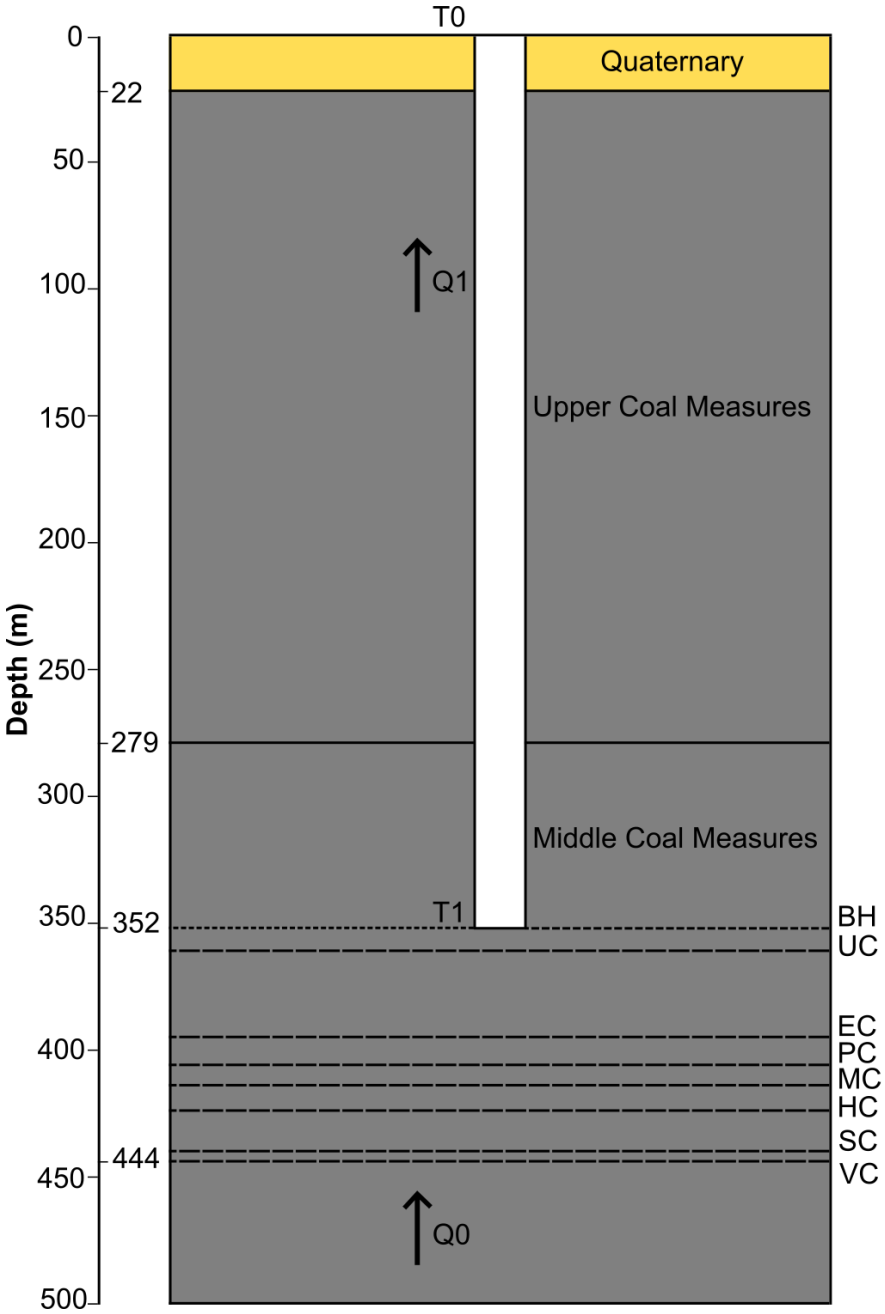

Figure 5.13. Schematic log of the Hallside Borehole [NS 66930 59740]. Showing summary stratigraphy including seams worked at the Hallside Colliery (depths from the log of the Hallside Colliery bore [NS 66960 59680]). BH, Bottom Hole; EC, Ell Coal; HC, Humph Coal; MC, Main Coal; PC, Pyotshaw Coal; SC, Splint Coal; UC, Upper Coal and VC, Virgin Coal. Yellow ornament denotes Quaternary deposits. Q0 denotes the heat flow below mine workings, Q1 denotes the heat flow above mine workings, T1 denotes the deepest temperature measurement in the borehole and T0 denotes the surface air temperature. Based upon records provided by British Geological Survey (UKRI).

As a first-order calculation, the heat flow passing into the flooded mine workings beneath the Hallside borehole was quantified. Detailed in Table 5.10, the harmonic mean thermal

conductivity at Hallside was calculated as 2.16 W m^{-1} $°C^{-1}$. The surface temperature observed in the temperature log at Hallside was 8.5 °C and the deepest temperature measurement in the log was 11.8 °C, giving a geothermal gradient of 9.43 °C km^{-1}. From Equation 2.1, this gives a heat flow of 20.34 mW m^{-2}. If the regional heat flow for Glasgow is taken as 61.91 mW m^{-2}, then c. 40-45 mW m^{-2} of heat flow is escaping laterally into the workings below the base of the Hallside borehole. If the effect of palaeoclimate is accounted for then the regional surface heat flow for Glasgow will increase, implying that a considerably higher magnitude of heat flow is entering the mine workings at Hallside on the order of 60-65 mW m^{-2}.

GGC01 Case Study

Another example of anthropogenic perturbations to the subsurface thermal state in Glasgow was observed in the GGC01 borehole dataset. This borehole was drilled in Dalmarnock, Glasgow, an area with a long history of coal mining and industrial development. First identified in Watson et al. (2019), and then extensively studied in Watson and Westaway (2020), the GGC01 temperature record was found to be significantly perturbed away from its natural state, in part because of the permeabilizing effect of past nearby coal mining and in part due to surface warming as a result of the combination of anthropogenic climate change and creation of a subsurface urban heat island by local urban development. The background upward heat flow through the shallow subsurface at this site was estimated as c. 28-33 mW m^{-2}, depending on the choice of model parameters, well below the regional mean heat flow of the Glasgow area. Similar to Hallside, it was therefore inferred that the 'missing' geothermal heat flow was entrained by horizontal flow at depth beyond the reach of the c. 200 m deep GGC01 borehole, possibly increasing temperatures in the mines below adjacent localities. (Watson and Westaway, 2020).

Influence of Historic Mining on Glasgow's Geothermal Dataset: Synthesis

The entrainment of heat flow into mine workings affects both the quantification of the geothermal resource in the mine workings themselves, and of greater significance to this thesis, the quantification of deeper geothermal resources, such as that in the Upper Devonian sandstone aquifer beneath Glasgow. In localities where this effect is present then the extrapolation of the shallow temperature gradient above mine workings would underestimate the temperature at depth in a deeper geothermal resource. This is particularly relevant for this thesis, considering that the temperature of the aquifer is determined by extrapolation of geothermal gradients from shallow boreholes in the Glasgow area. It is therefore necessary to acknowledge the influence of historic mining on the subsurface thermal state in order to

obtain realistic estimates of thermal performance, drilling costs and optimal locations for drilling, when appraising future geothermal developments in Glasgow.

The investigations undertaken in this chapter and those detailed in Watson et al. (2019) and Watson and Westaway (2020) established that the temperature measurements made within the Blythswood-1, South Balgray, Queenslie-4, Rashiehill, Slatehole, Salsburgh-1A, Hurlet, Barnhill, Kipperoch, Clachie Bridge, Maryhill, Craighead-1, Salsburgh-2 and Bargeddie-1 boreholes are not affected by the presence of mine workings. These measurements are therefore suitable for further analysis such as determining the necessary corrections to heat flow to account for the influence of palaeoclimate and topography, as detailed in Chapter 6, and estimating the temperature within the Upper Devonian aquifer beneath Glasgow. Whereas the results at Hallside and GGC01 indicate a significant proportion of the Earth's heat flow is being entrained within the mine workings, which is encouraging from the perspective of targeting the geothermal resource in flooded, abandoned mine workings in Glasgow. However, this geothermal data should not be used within estimations of deeper temperatures in the Upper Devonian sandstone aquifer given the perturbations to the borehole measurements caused by the presence of mine workings.

5.5. Conclusion

This chapter has re-appraised all existing geothermal data from boreholes in the western MVS, corrected outstanding inaccuracies within the geothermal dataset, and identified case studies where historic mining has perturbed the subsurface thermal state beneath Glasgow.

By assigning measured thermal conductivity values and representative thermal properties from literature to each lithology encountered in the respective boreholes, values of harmonic mean thermal conductivity, density, specific heat capacity, and thermal diffusivity were calculated for each borehole in this study. Then, using the harmonic mean thermal conductivity, and where available the existing heat flow and/or temperature data, the absent heat flow and temperature values were calculated.

Excluding anomalous results of GGC01, Hallside and Queenslie-4, the regional mean heat flow and geothermal gradient were calculated as 61.9 mW m^{-2} and 28.9 °C km^{-1} respectively. These results require corrections for the effects of palaeoclimate and topography, addressed in Chapter 6, to fully evaluate the potential heat resource beneath Glasgow. However, they indicate that promising temperatures may be encountered within the Carboniferous-Devonian basin beneath Glasgow and to the east in the Lanarkshire Basin.

New subsurface temperature profiles were calculated for the Barnhill, Clachie Bridge, Hurlet and Kipperoch boreholes, and new values of heat flow were calculated for a number of the boreholes. This included a revaluation of the heat flow of the Blythswood-1 and South Balgray boreholes by using more representative values of thermal conductivity than those utilised within previous analyses.

Based upon the newly calculated heat flow and geothermal gradient results for each of the boreholes, an examination of the influence of historic mining on Glasgow's subsurface thermal state was conducted. Whilst extensive mining was undertaken across much of Glasgow and the surrounding conurbation, the temperature datasets measured at the Blythswood-1, South Balgray, Queenslie-4, Rashiehill, Slatehole, Salsburgh-1A, Hurlet, Barnhill, Kipperoch, Clachie Bridge, Maryhill, Craighead-1, Salsburgh-2 and Bargeddie-1 boreholes are largely unaffected by the presence of mine workings. The measurements in these boreholes are reliable and therefore suitable for further analysis.

However, in the Hallside and GGC01 boreholes, the temperature datasets were influenced by the legacy of historic mining. At Hallside, the heat flow was calculated as c. 20 mW m^{-2} and for the GGC01 borehole, the heat flow was calculated as 28-33 mW m^{-2}. The difference relative to the expected regional heat flow suggests a significant component of horizontal heat flow into surrounding flooded mine workings. This is encouraging from the perspective of targeting the geothermal resource in flooded, abandoned mine workings. However, the results show that an examination of the 'true' geothermal resource beneath the city of Glasgow is reliant on understanding heat transport mechanisms in the subsurface and care must therefore be taken to consider such an effect as this when attempting to quantify the potential geothermal resource in both mine workings and HSAs in the future.

The results of this chapter are significant in terms of the investigation of Glasgow's deep geothermal resource for three reasons: (1) the calculations of temperature, heat flow, and rock thermal property data contributed new data to the overall geothermal dataset in the western MVS, (2) investigation of archive documentation on historic coal and ironstone mining in Glasgow, coupled with the revised geothermal dataset, examined for the first time, perturbations to Glasgow's geothermal dataset caused by historic mining, and (3) the resulting revised geothermal dataset enabled the palaeoclimate corrections to heat flow and geothermal gradient to be conducted, in Chapter 6 and hence the temperature in the geothermal resource within the Upper Devonian sandstones beneath Glasgow to be reliably estimated.

Chapter 6. Palaeoclimate and Topographic Corrections to Heat Flow and the Implications for Geothermal Resource Quantification in Glasgow

6.1. Introduction

In this chapter, the heat flow values derived from boreholes in the western MVS were corrected for the effects of palaeoclimate and topography. In the absence of obtaining temperature measurements from deep in the subsurface, this work is crucial in producing a corrected regional heat flow dataset, and thus reliably quantifying the temperature in the HSA geothermal resource beneath Glasgow. This chapter first outlines the aims and rationale of this study, emphasising the significance of palaeoclimate and topographic corrections to heat flow in western Scotland. Then, the methodology and results for the palaeoclimate corrections are described, followed by the those for the topographic corrections. The results were then combined to determine the corrected regional heat flow and geothermal gradient for the Glasgow area. Then, the thermal power output from geothermal doublet wells in eastern Glasgow were calculated and compared to local heat demand.

6.2. Chapter Aim

The aim of this chapter was to apply rigorous corrections to heat flow for the boreholes examined in Chapter 5 to account for the effects of both palaeoclimate and topography, thus determining the corrected regional heat flow for the Glasgow area and allowing the ‘true’ temperature within the Upper Devonian sandstones beneath Glasgow to be estimated. Then, combining these results with those from Chapters 3-5, DoubletCalc software was used to calculate the thermal power output from geothermal doublet wells located at candidate drilling sites in eastern Glasgow. The contribution that geothermal heat could make to local heat demand was then assessed.

As discussed in Westaway and Younger (2013), combining the palaeoclimate and topographic corrections is simply an additive process, and typically topographic corrections are considerably smaller in magnitude than palaeoclimate corrections. This chapter, therefore, first describes the methodology and results of the palaeoclimate corrections to heat flow in section 6.4, followed by the topographic corrections in section 6.5. The results are then combined to determine the corrected regional heat flow and geothermal gradient and used to quantify the geothermal resource beneath eastern Glasgow.

6.3. Rationale

The significance of the effect of palaeoclimate on heat flow in Britain was first recognised decades ago (e.g., Benfield, 1939; Jessop, 1971; Beck, 1977). However, in subsequent investigations of heat flow, many authors have either omitted, downplayed, or not fully explained any corrections for the effect of palaeoclimate. This systematic neglection or under-appreciation of the effect of palaeoclimate has resulted in values of heat flow being widely underestimated across Britain.

Over the past decade, various studies have been conducted to apply palaeoclimate corrections to heat flow across Britain. Westaway and Younger (2013) presented corrected values of heat flow for boreholes in south-west England, the Cairngorms, the Lake District and in north-east England, and found that accounting for the effects of palaeoclimate results in a positive correction to heat flow of up to 27 mW m^{-2}. Further localised and regional assessments of the effect of palaeoclimate on heat flow were conducted in south-west England (Beamish and Busby, 2016); Tyneside (Westaway and Younger, 2016); and the Cairngorms (Busby et al., 2015). As was the case in Westaway and Younger (2013) the revised heat flow values dramatically increased in these studies.

It has been established that variations in topography also affect heat flow, particularly in the case of heat flow measurements in shallow boreholes (Westaway and Younger, 2013). Like palaeoclimate corrections, resolving the effect of topography on heat flow is necessary when an accurate value of heat flow is required to calculate and extrapolate subsurface temperatures. Heat preferentially diffuses into valleys resulting in an overestimate of heat flow, whilst the opposite is true for hills and mountains, where heat flow is underestimated.

The combination of shallow temperature measurements in the existing geothermal dataset, the location of Britain in relation to the Gulf Stream, and the severity of cooling during Pleistocene cold stages, means that there is an acute need to comprehensively apply corrections for palaeoclimate and topography to heat flow in Britain (Westaway and Younger, 2013). It is anticipated that these effects are particularly influential in western Scotland. Until this present study, the heat flow and temperature datasets from boreholes in the western MVS have not been corrected for the effect of palaeoclimate despite this being one of the key recommendations of Gillespie et al. (2013). Topographic corrections have been made to a number of the boreholes in the region however these calculations are unclear, and a revision of these corrections is justified.

Without applying corrections for these effects, values of heat flow are significantly underestimated in the region, and any extrapolation of shallow geothermal gradient to greater depths underestimates the temperature at depth. Therefore, to enable a true quantification of the geothermal resource beneath Glasgow, it is necessary to conduct detailed palaeoclimate and topographic corrections to heat flow.

6.4. Paleoclimate Corrections to Heat Flow and Geothermal Gradient

6.4.1. Palaeoclimate Correction Methodology

The procedure and theory for applying palaeoclimate corrections to heat flow have been widely documented in both scholarly articles and textbooks (e.g., Birch, 1948, Beck, 1977; Turcotte and Schubert, 1982; Westaway and Younger, 2013). In summary, past variations in surface temperature ΔT_o relative to its present-day value are approximated as a series of step changes that propagate into the ground, each starting at a particular time *t'* before the present day. Each of these step changes has a specific timescale and a ΔT value representing the difference in surface temperature between that of the respective time period and that of the present day. The overall perturbation to the geotherm $\delta T(z)$ due to the effect of palaeoclimate, at each depth *z*, at the present day, is determined by adding the contributions of each of these step changes. The account of the theory from first principles by Westaway and Younger (2013) is detailed in Appendix 6.A, with an analytic formula for $\delta T(z)$ as a result of *n* past step changes ΔT_{oi} (i =1 to *n*) in surface temperature, given in Equation 6.A.9. The perturbation to the geothermal gradient, $\partial\delta T/\partial z$, is found analytically by term-by-term differentiation of Equation 6.A.9 and is given as Equation 6.A.10. Applying Fourier's Law, the perturbation to the geothermal gradient is scaled by the thermal conductivity of the bedrock, *k*, to determine the perturbation to the heat flow at depth z, $\delta Q(z)$. The assumed history of surface temperature variation therefore determines the present-day perturbation to the geothermal gradient, and the resulting heat flow perturbation scales in proportion to *k*.

Westaway and Younger (2013) developed Microsoft Excel spreadsheets which evaluate Equation 6.A.10 to determine $\partial\delta T/\partial z$ and δQ as functions of depth *z*. The solution for $\partial\delta T/\partial z$ is numerically integrated using Simpson's rule to determine the associated perturbation to temperature $\delta T(z)$. This methodology was used within this chapter to correct for the effect of palaeoclimate on heat flow in boreholes in the western MVS.

The following parameters were required as input to the palaeoclimate correction modelling: (1) the depth interval Δz over which heat flow was calculated in each borehole, (2) the thermal conductivity k and the associated thermal diffusivity κ, (3) temperature data measured in the borehole, and (4) a time-series of variations in surface temperature.

6.4.2. Thermal Properties, Geothermal Gradient and Heat Flow

Chapter 5 presented the results of calculations of harmonic mean thermal conductivity, harmonic mean thermal diffusivity, subsurface temperature profiles, and the uncorrected heat flow of each borehole studied in the western MVS. These parameters are utilised as input to the paleoclimate correction modelling, addressing points (1-3) above. In Chapter 5, a sensitivity analysis was conducted to determine lower and upper values of the harmonic mean thermal conductivity and thermal diffusivity, and the corresponding lower and upper values of heat flow for each borehole. To account for uncertainty in the thermal properties of the bedrock, the palaeoclimate corrections to heat flow were determined for the mean, lower and upper values of the harmonic mean thermal conductivity and thermal diffusivity.

6.4.3. Palaeoclimate Conditions in the Western Midland Valley of Scotland

To address point (4) above, a model palaeoclimate history of the western MVS was established by the author. Detailed in Tables 6.B.4 and 6.B.5, this temperature history was constructed from a combination of data sources, including marine and terrestrial ice core; palaeotemperature data from terrestrial sedimentary and bio-stratigraphic records across Scotland; literature on the timing, extent, and magnitude of Pleistocene palaeoclimatic conditions in Scotland; and meteorological data from the 18th century to the present day. An explanation of how this data was utilised is given in Appendix 6.B-6.E, and summarised here.

The primary data source used was the North Greenland Ice Core Project (NGRIP) stable oxygen isotope record ($\delta^{18}O$) (Rasmussen et al., 2014; Seierstad et al., 2014). This data series was converted by the author to show the temperature differences relative to the present day from the Ipswichian Interglacial at 125 ka BP to the Holocene (Appendix 6.B). The NGRIP record was chosen due to its use in modelling of British and Irish Ice Sheet (BIIS) chronology and dynamics (Hubbard et al., 2009) and the general similarity of the record with climatic events in Scotland (Lang et al., 2010; Brooks et al., 2012). From this data, a 5000-year average trend was calculated and calibrated with palaeotemperature observations recorded from sites in western Scotland (Tables 6.B.1-6.B.3). The NGRIP ΔT record was then approximated as a series of step changes relative to the present day shown in Figure 6.1.

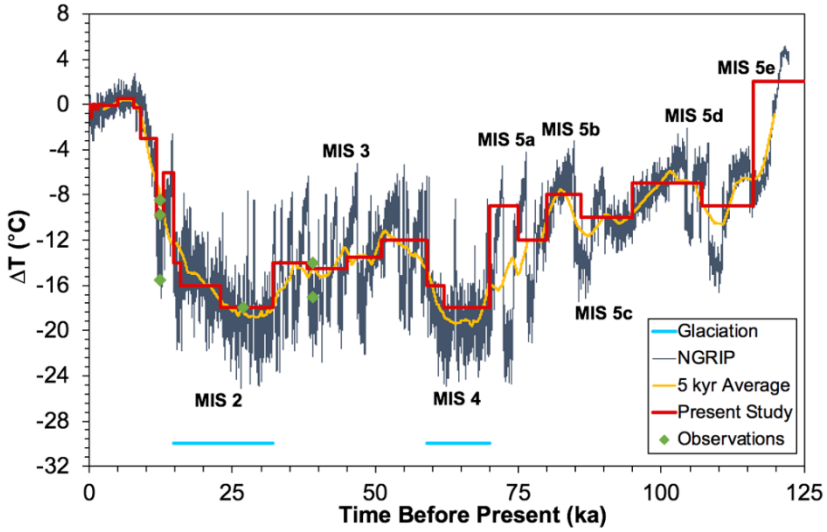

Figure 6.1. NGRIP $\delta^{18}O$ stable isotope dataset scaled to model surface temperature change over time relative to the present day. Plotted as a series of step changes (ΔTo) to facilitate palaeoclimate correction modelling. Data from Rasmussen et al. (2014) and plotted by the author. X-axis shows the time before present in thousands of years (ka).

To satisfy local conditions in the western MVS, a necessary amendment to the NGRIP record was made to alter ΔT to account for the insulating effect of glaciation on the ground surface temperature. Although the presence of an ice sheet indicates very cold conditions, depending on the thickness, ice cover will insulate the underlying ground surface from the prevailing arctic climate. Glasser and Siegert (2002) and Hall and Glasser (2008) found that complex feedbacks between ice movement and meltwater maintained the temperature at the base of an ice sheet at the melting point of ice, i.e., warm based, dynamic ice. However, where ice divides exist, the temperature at the base of the ice sheet was below the melting point of ice, i.e., cold based, static, ice frozen to the bedrock. Hall and Glasser (2008) showed that during basal freezing conditions, basal temperatures can range from -12 to -6 °C. However, when basal melting occurs, basal temperatures are more likely to be in the range of -1 to +1 °C.

The insulating effect of ice cover in the western MVS was accounted for in the NGRIP record using the chronology of Scottish Ice Sheet (SIS) dynamics (Figure 6.B.3), and the amended NGRIP interpretation is shown in Figure 6.2. Assuming an ice sheet thickness of ~2000 m (Kuchar et al., 2012), for those time periods when the ice sheet was dynamic it was assumed that the temperature at the base of the ice sheet was 0 or -1°C (Westaway and Younger, 2013), whereas for those time periods when the ice sheet was static, it was assumed that the temperature at the base of the ice sheet was -3°C (Busby et al., 2016).

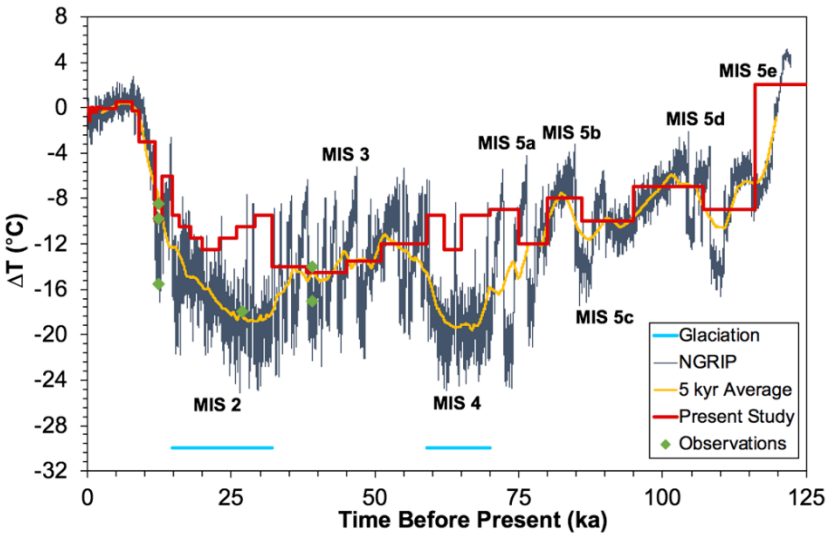

Figure 6.2. Temperature history adjusted to account for insulating effects of glaciation on the surface temperature.

The palaeoclimate history of the Early Quaternary period (prior to 125 ka BP) was established by following the approach of Hall et al. (2019), whereby values of $\delta^{18}O$ derived from the DSDP 607 marine core during the MIS 2 glaciation were compared with $\delta^{18}O$ values in earlier history (Figure 6.B.1) and if the value was similar, then it was assumed that similar climatic conditions prevailed during the respective time period.

By integrating these datasets of past climate change in the western MVS, a time-series of variations in surface temperature was established by the author for use within the palaeoclimate correction analysis, as detailed in Tables 6.B.4 and 6.B.5. Times t_1 and t_2 represent the start and end of each time phase, for which the surface temperature, relative to the present-day value, was assumed to have been ΔT.

Then, using meteorological data measured from the 18th century to the present day, a continuous temperature record from the pre-industrial period until the present day was compiled for the western MVS. From this record, accounting for the effects of lapse rate and lateral variation in temperature, the annual mean temperature was calculated for each year in which geothermal data was measured in each borehole. This allowed anthropogenic temperature change and any significant fluctuations in temperature in the years prior to the borehole measurements to be accounted for.

Following the same approach as the Quaternary palaeoclimate history, for each borehole, the surface temperature record from the pre-industrial period to the present day was approximated as a series of step changes (ΔT_0) relative to the annual mean temperature of the year in which temperature or heat flow was measured in the borehole (Figure 6.3), with time intervals t_1 and t_2 determined in relation to the year of the borehole measurement (Appendix 6.D).

The temperature record from the pre-industrial period to the present day was combined with that from the Quaternary period to the Little Ice Age, to give a continuous record of temperature history for the western MVS for use in the palaeoclimate correction modelling.

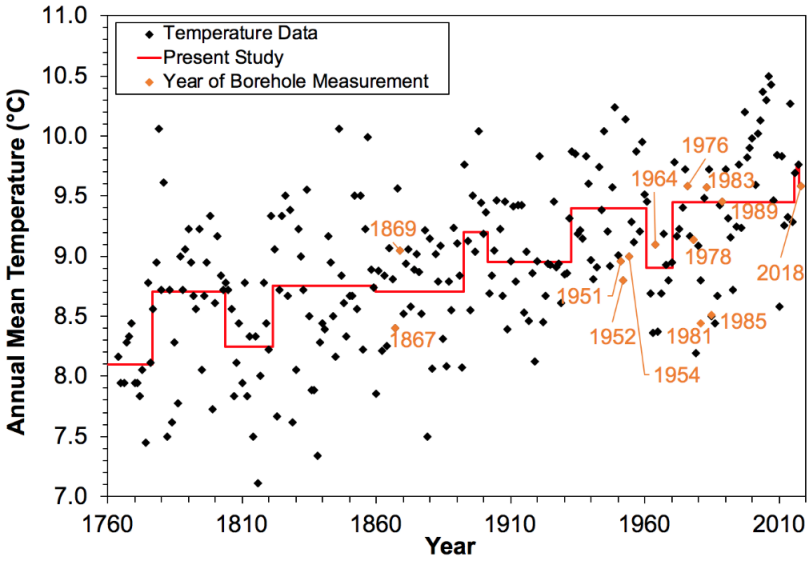

Figure 6.3. Temperature record for the western MVS from 1764 to the present day plotted as a series of step changes (ΔTo). Annual mean surface temperature data derived from Mossman, University of Glasgow Dowanhill Observatory, and the Paisley Coats Observatory.

6.4.4. Palaeoclimate Correction Results

The results of the palaeoclimate correction modelling are detailed in Table 6.1. Here, the corrected values of heat flow are shown for each borehole supplemented by the modelled input data. These results are accompanied by Figures 6.4-6.17 (a) which illustrate: the raw temperature measurements made within each borehole, the prediction of how the geotherm has been perturbed by palaeoclimate (*model prediction for temperature*), the prediction of what the steady state geotherm would be if there had been no palaeoclimate fluctuations (*uniform temperature gradient*), the depth intervals over which heat flow was calculated (Z_1 *to* Z_2), and key stratigraphic boundaries and markers within each borehole.

Table 6.1. Results of the palaeoclimate corrections to heat flow.

Name	Interval	T_o	k	κ	Q_o	Q_c	ΔQ
	(m)	(°C)	(W m^{-1} °C^{-1})	(mm^2 s^{-1})	(mW m^{-2})	(mW m^{-2})	(mW m^{-2})
Blythswood-1	18-105	7.95	2.00	0.937	72.84	83.00	10.16
South Balgray	0-137	8.65	1.64	0.765	68.92	81.00	12.08
Queenslie-4	0-691	8.39	2.13	0.987	85.28	98.00	12.72
Rashiehill	0-964	10.00	2.14	0.959	57.35	70.00	12.65
Slatehole	0-1024	8.61	2.10	0.951	64.30	76.50	12.20
Salsburgh-1A	0-898	7.75	1.96	0.941	57.23	70.00	12.77
Kipperoch	40-300	7.47	3.57	1.569	53.40	75.00	21.60
Barnhill	25-355	8.60	2.67	1.099	48.91	66.00	17.09
Clachie Bridge	30-300	6.46	2.53	0.961	57.68	75.50	17.82
Hurlet	95-295	9.16	2.87	1.198	61.75	81.00	19.25
Craighead-1	0-909.8	6.95	2.03	0.938	62.54	75.00	12.46
Maryhill	100-303	9.45	1.80	0.813	69.08	80.00	10.92
Salsburgh-2	0-1102.1	6.73	2.03	0.928	68.58	79.00	10.42
Bargeddie-1	0-978.9	9.30	2.08	0.954	62.52	75.00	12.48

where T_o: surface temperature, k: thermal conductivity, κ: thermal diffusivity, Q_o: heat flow from Table 5.1 or Table 5.10 with no palaeoclimate correction, Q_c: palaeoclimate corrected heat flow, and ΔQ: palaeoclimate correction.

The magnitude of the palaeoclimate corrected heat flow was dependent on achieving a suitable model solution whereby the model prediction for temperature matched the raw temperature measurements made within the borehole, thereby proving what the true heat flow would have to be to account for perturbations due to palaeoclimate. For each borehole, the palaeoclimate correction to heat flow was calculated using the respective value of thermal diffusivity (Table 6.1) and the steady state geotherm was calculated for the respective surface temperature, thermal conductivity, and corrected heat flow (Table 6.1).

The modelled prediction of the perturbed geotherm accounts for the seasonal variation of temperature, which was determined by the near surface thermal diffusivity and the month of

the year in which subsurface temperature measurements were made. This theory is detailed in Appendix 6.F.

The perturbations to temperature, geothermal gradient, and heat flow due to palaeoclimate, and how this varies with depth, are also illustrated for each borehole in Figures 6.4-6.17 (b).

Maryhill, Blythswood-1 and South Balgray

The palaeoclimate corrected heat flow for the Maryhill borehole was calculated as 80 mW m^{-2}. The correction increased the heat flow by 16% in comparison to the uncorrected value of 69.08 mW m^{-2}. Illustrated in Figure 6.4a, the model prediction matched the raw temperatures relatively well, however, there are disparities between the raw data and the model prediction. These disparities were caused by the fact that the thermal conductivity is consistently higher over some ranges of depth in the borehole and lower in others. For example, the higher geothermal gradients at c. 100-120 m and c. 280-300 m are present within a sequence of mudstone, with a low thermal conductivity, whereas the lower geothermal gradients at c. 240-260 m are present in sandstone, with high thermal conductivity. As uniform thermal properties were assumed throughout the model these mismatches could not be improved upon.

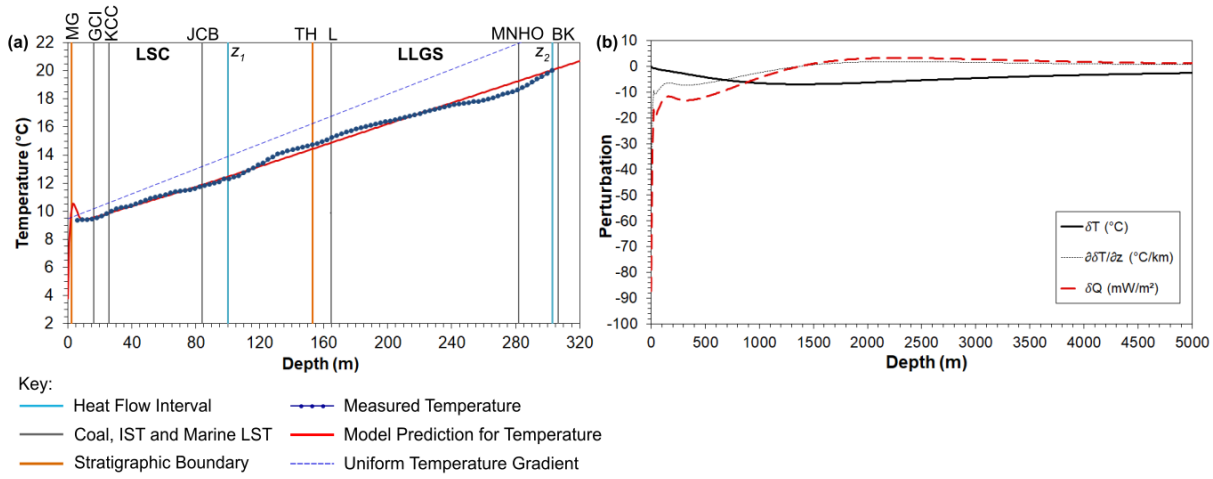

Figure 6.4. Maryhill palaeoclimate correction modelling (a) and output of the resulting perturbations to the present-day geotherm, geothermal gradient, and heat flow (b).

The palaeoclimate corrected heat flow for the Blythswood-1 borehole was calculated as 83 mW m^{-2}, with the heat flow rising by 14% in comparison to the uncorrected value. As an alternative solution, the thermal properties of Benfield (1939) were modelled which resulted in significantly lower uncorrected and corrected values of heat flow, of 52 and 59 mW m^{-2}, respectively. This was due to the use of the greatly reduced thermal diffusivity of 0.670 mm^2

and thermal conductivity of 1.43 W m^{-1} $°C^{-1}$. Figure 6.5a shows that the model prediction matched the Thomson et al. (1868) raw temperature measurements well, however an improved solution was achieved with the use of a cooler surface temperature of 7.95 °C instead of 8.35 °C derived from the meteorological data.

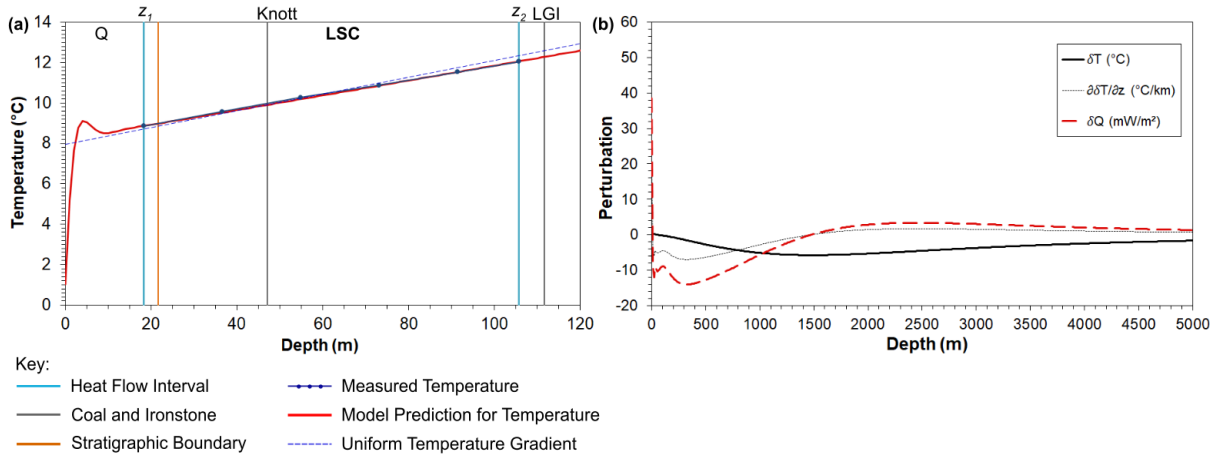

Figure 6.5. Blythswood-1 palaeoclimate correction modelling (a) and output of the resulting perturbations to the present-day geotherm, geothermal gradient, and heat flow (b).

The palaeoclimate corrected heat flow for the South Balgray borehole was calculated as 81 mW m^{-2}. This was an increase of 18% from the uncorrected heat flow. Like Blythswood-1, lower uncorrected and corrected values of heat flow, of 64 and 69 mW m^{-2} were calculated using the thermal properties of Benfield (1939). Again, similar to the Blythswood-1 model, the model prediction was well matched to the Thomson et al. (1869) raw temperature measurements, however an improvement was made by reducing the surface temperature from 8.75 °C to 8.65 °C (Figure 6.6a)

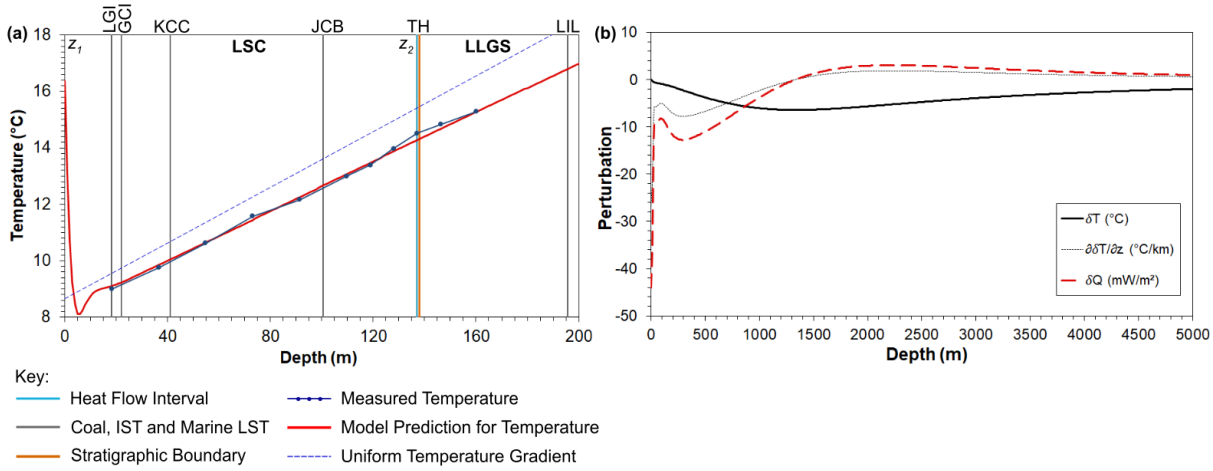

Figure 6.6. South Balgray palaeoclimate correction modelling (a) and output of the resulting perturbations to the present-day geotherm, geothermal gradient, and heat flow (b).

Barnhill, Clachie Bridge Hurlet and Kipperoch

For the Barnhill borehole the corrected heat flow was calculated as 66 mW m^{-2} across the depth interval of 25-355 m. This was an increase of 35%, from the uncorrected heat flow of 48.91 mW m^{-2}. The palaeoclimate corrected heat flow for the Clachie Bridge borehole was calculated as 75.5 mW m^{-2}, which was an increase of 31% compared to the uncorrected value of 57.68 mW m^{-2}. A similar corrected heat flow was calculated for the Kipperoch borehole, of 75 mW m^{-2}, which gave a 41% increase in comparison to the uncorrected value of 53.40 mW m^{-2}.

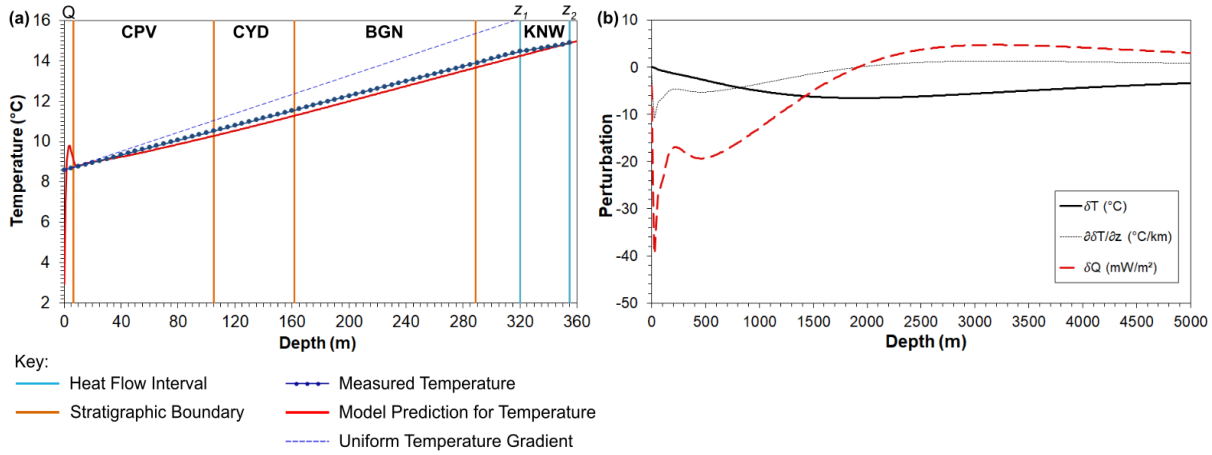

Figure 6.7. Barnhill palaeoclimate correction modelling (a) and output of the resulting perturbations to the present-day geotherm, geothermal gradient, and heat flow (b).

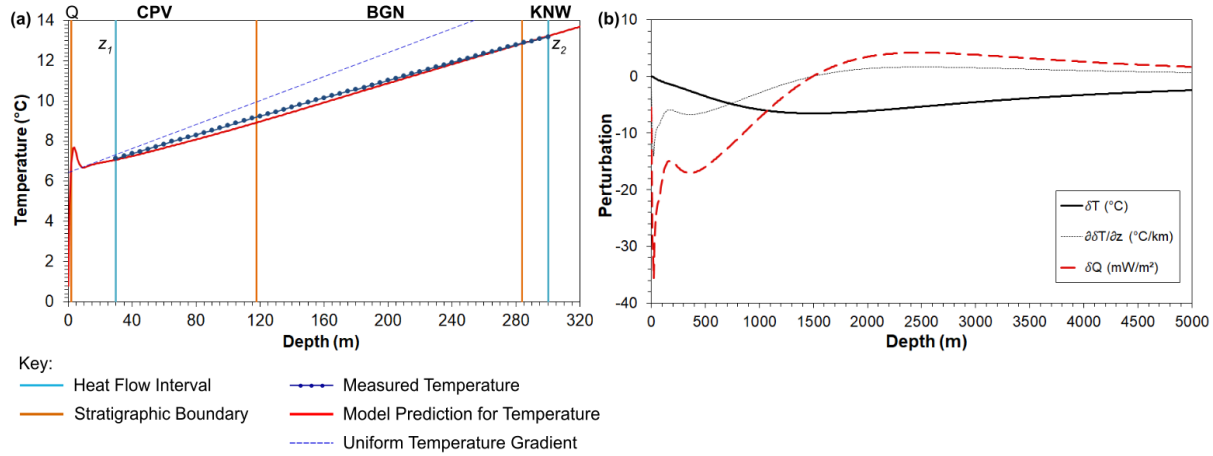

Figure 6.8. Clachie Bridge palaeoclimate correction modelling (a) and output of the resulting perturbations to the present-day geotherm, geothermal gradient, and heat flow (b).

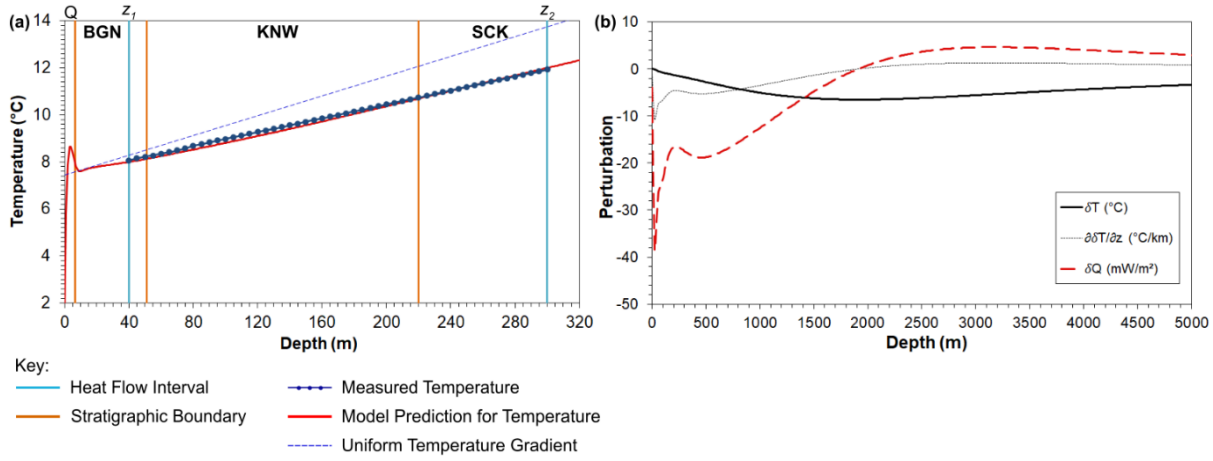

Figure 6.9. Kipperoch palaeoclimate correction modelling (a) and output of the resulting perturbations to the present-day geotherm, geothermal gradient, and heat flow (b).

The palaeoclimate corrected heat flow of the Hurlet borehole was calculated as 81 mW m^{-2}, representing a 31% increase from the uncorrected value. This was the highest corrected value of the Oxburgh (1982) datasets and provided comparable results with the corrected heat flows of Blythswood-1, Maryhill, and South Balgray, indicating a range of 80-83 mW m^{-2} for the palaeoclimate corrected heat flow for boreholes in Namurian and Visean sediments in the west and south-west of Glasgow.

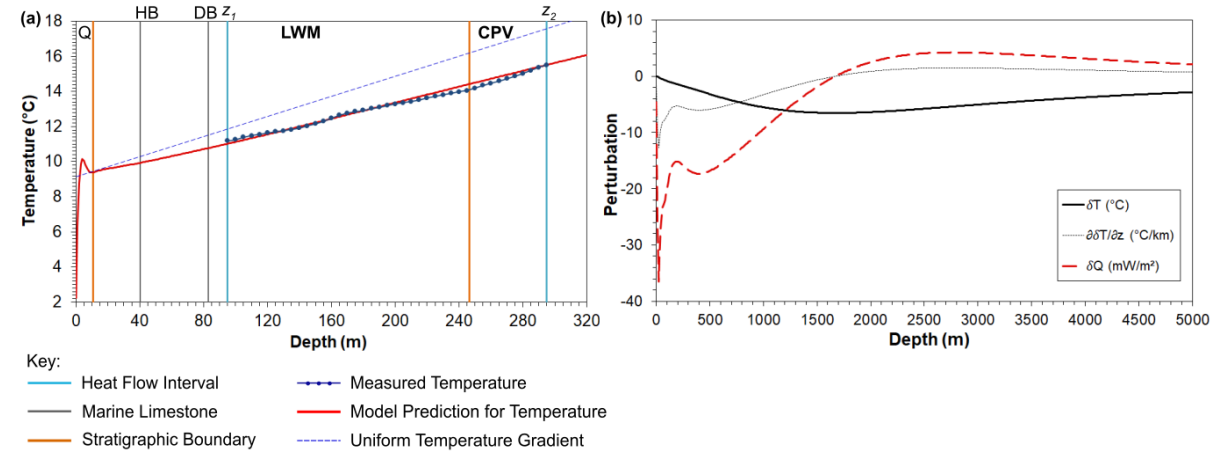

Figure 6.10. Hurlet palaeoclimate correction modelling (a) and output of the resulting perturbations to the present-day geotherm, geothermal gradient, and heat flow (b).

Queenslie-4 and Slatehole

The palaeoclimate corrected heat flow for the Queenslie-4 borehole was calculated as 98 mW m^{-2}, representing an increase of 15% from the uncorrected value. The magnitude of the palaeoclimate correction was consistent with other boreholes across Glasgow, however due to the high uncorrected heat flow, the corrected heat flow was similarly high. For comparison, using a thermal conductivity of 1.82 W m^{-1} °C^{-1} and thermal diffusivity of 0.820 mm^2 s^{-1} from the Queenslie-2 borehole, the corrected heat flow at Queenslie-4 was 85 mW m^{-2}. Similarly, using a slightly higher thermal conductivity of 1.88 W m^{-1} °C^{-1} and thermal diffusivity of 0.850 mm^2 s^{-1} from the Queenslie Bridge borehole, the corrected heat flow at Queenslie-4 was 87 mW m^{-2}. Whilst still higher, these results are more comparable to those elsewhere in Glasgow. For the Slatehole borehole the palaeoclimate corrected heat flow was calculated as 76.5 mW m^{-2}, an increase of 19% from the uncorrected value.

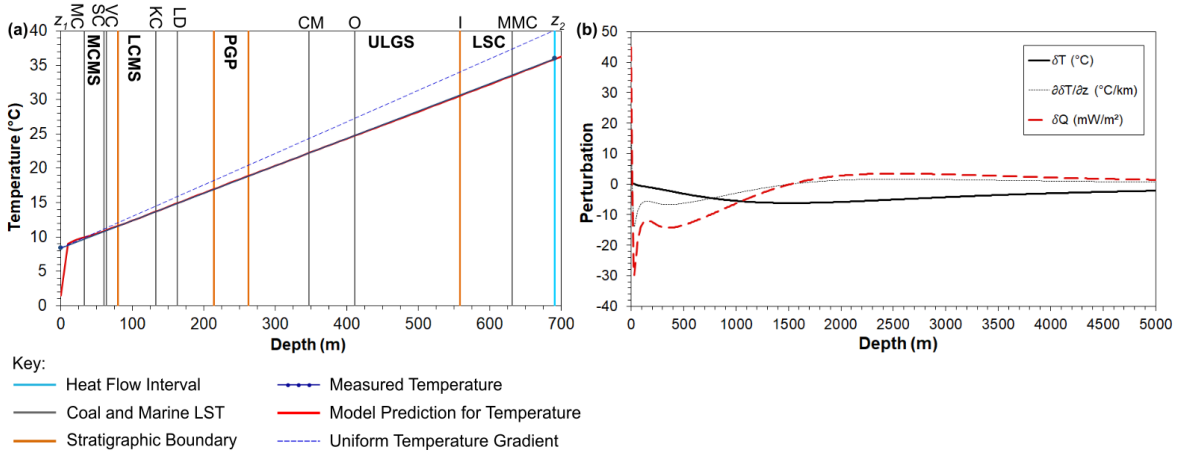

Figure 6.11. Queenslie palaeoclimate correction modelling (a) and output of the resulting perturbations to the present-day geotherm, geothermal gradient, and heat flow (b).

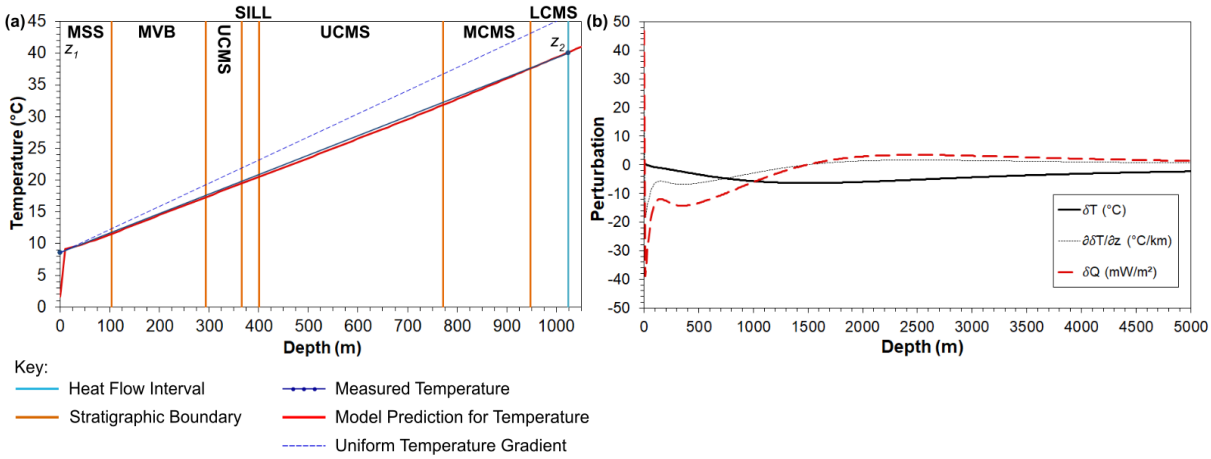

Figure 6.12. Slatehole palaeoclimate correction modelling (a) and output of the resulting perturbations to the present-day geotherm, geothermal gradient, and heat flow (b).

Bargeddie-1, Craighead-1, Rashiehill, Salsburgh-1 and Salsburgh-2

The palaeoclimate corrected heat flows of Bargeddie-1, Craighead-1 and Salsburgh-2 were broadly in agreement, which was anticipated given that the boreholes were drilled to a similar depth, encountered a similar stratigraphy, and were modelled using similar thermal properties. The palaeoclimate corrected heat flow was calculated as 75 mW m^{-2} for both the Bargeddie-1 and Craighead-1 boreholes. This was a 20% increase in heat flow compared to the uncorrected heat flow of each borehole. At Salsburgh-2, a palaeoclimate corrected heat flow of 79 mW m^{-2} was determined. This was a more modest increase of 15%, compared to both Bargeddie-1 and Craighead-1, however the uncorrected heat flow was greater at Salsburgh-2 due to the high bottom hole temperature measured in the borehole.

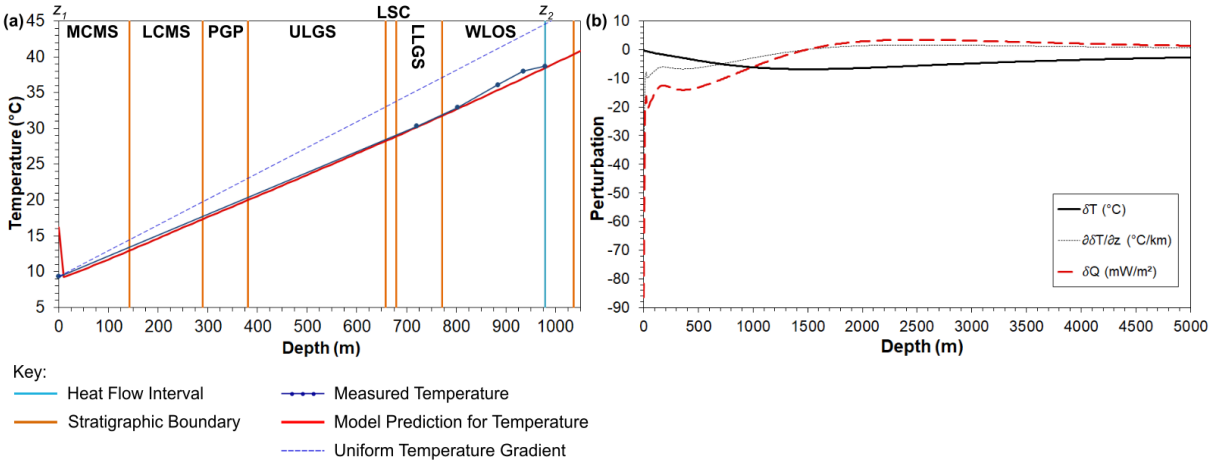

Figure 6.13. Bargeddie palaeoclimate correction modelling (a) and output of the resulting perturbations to the present-day geotherm, geothermal gradient, and heat flow (b).

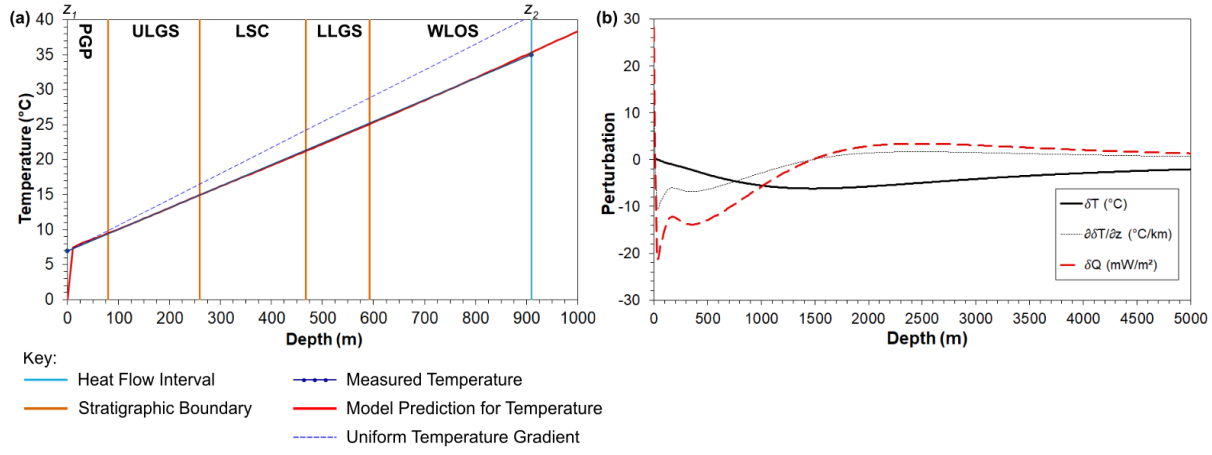

Figure 6.14. Craighead palaeoclimate correction modelling (a) and output of the resulting perturbations to the present-day geotherm, geothermal gradient, and heat flow (b).

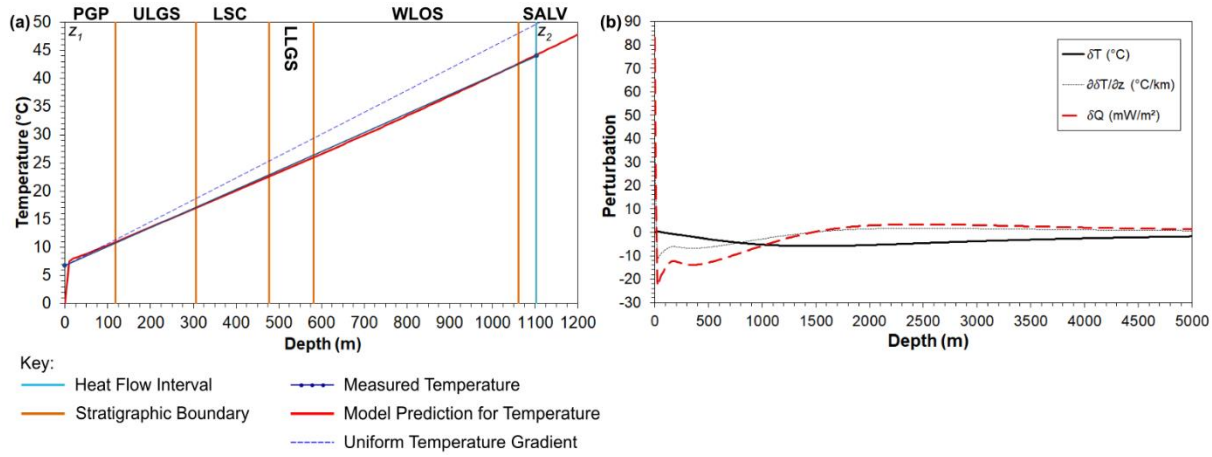

Figure 6.15. Salsburgh 2 palaeoclimate correction modelling (a) and output of the resulting perturbations to the present-day geotherm, geothermal gradient, and heat flow (b).

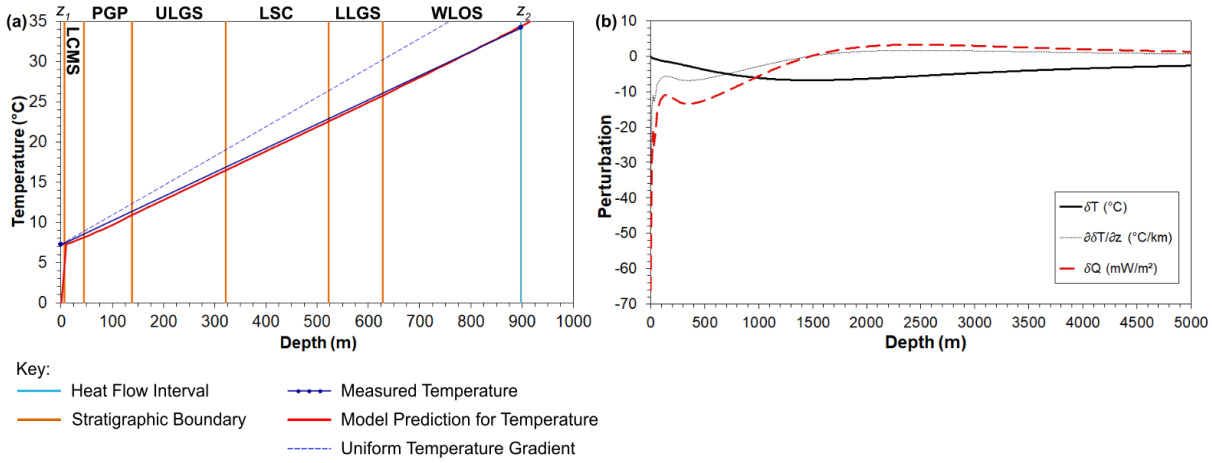

Figure 6.16. Salsburgh 1 palaeoclimate correction modelling (a) and output of the resulting perturbations to the present-day geotherm, geothermal gradient, and heat flow (b).

The palaeoclimate corrected heat flow for the Salsburgh-1 borehole was calculated as 70 mW m^{-2}, which was an increase of 22% from the uncorrected value. Similarly, the palaeoclimate corrected heat flow for the Rashiehill borehole was calculated as 70 mW m^{-2}, which was an increase of 22%, from the uncorrected heat flow. For comparison, the palaeoclimate correction for Rashiehill was remodelled for a surface temperature of 7.9°C. In this case the corrected heat flow was computed as 74.5 mW m^{-2}. By using the surface temperature calculated from meteorological data instead of that reported by Anderson (1963), the corrected heat flow was more comparable to those values determined for Bargeddie-1 and Craighead-1.

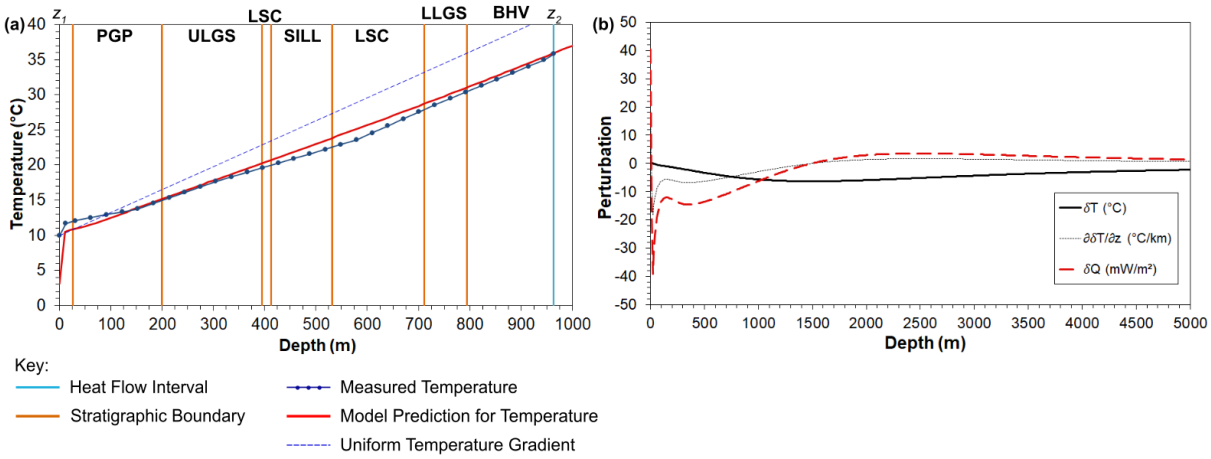

Figure 6.17. Rashiehill palaeoclimate correction modelling (a) and output of the resulting perturbations to the present-day geotherm, geothermal gradient, and heat flow (b).

6.4.5. Discussion of Results and Refinements to the Modelling

The magnitude of the palaeoclimate corrections to heat flow clearly illustrate that omission of these corrections in previous analyses significantly underestimated the heat flow and geothermal gradient measured in the boreholes, and therefore underestimated the magnitude of the geothermal resource beneath Glasgow. However, there are several areas where the present study could be refined further which may have an effect on the 'true' estimation of temperature within the geothermal resource beneath Glasgow.

Thermal Conductivity

In general, the palaeoclimate corrected heat flows determined for the deeper boreholes in the western MVS, are lower than those calculated for shallower boreholes such as Blythswood-1, Hurlet, Maryhill or South Balgray.

One reason for this is that the thermal properties adopted for the deeper boreholes may be unrepresentative of true subsurface conditions as they do not account for the increase in thermal conductivity with depth. Norden et al. (2020) demonstrated that the thermal conductivity of a sedimentary rock increased by approximately by 0.2 W m^{-1} $°C^{-1}$ over a depth of 1 km due to the effects of increasing pressure and temperature.

If, for example, the thermal conductivity of the Rashiehill borehole was increased from 2.14 to 2.34 W m^{-1} $°C^{-1}$, the thermal diffusivity correspondingly increased to 1.037 mm^2 s^{-1}, and the surface temperature kept constant at 7.9 °C the corrected heat flow increases to 81 mW m^{-2}. This corrected heat flow is more consistent with the corrected heat flow determined for the shallower boreholes.

To demonstrate the effect of varying the modelled thermal properties on the resulting palaeoclimate corrected heat flow, the results of a sensitivity analysis are shown in Tables 6.2 and 6.3. These results are based upon palaeoclimate correction modelling using the lower and upper suites of thermal properties outlined in Chapter 5 for each borehole.

Table 6.2. Palaeoclimate corrections using the lower range of thermal properties from Chapter 5.

Name	Interval	T_o	k	κ	Q_o	Q_c	ΔQ
	(m)	(°C)	(W m^{-1} °C^{-1})	(mm^2 s^{-1})	(mW m^{-2})	(mW m^{-2})	(mW m^{-2})
Blythswood-1	18-105	7.95	1.92	0.900	70.07	80.00	9.93
South Balgray	0-137	8.65	1.58	0.735	66.35	79.00	12.65
Queenslie-4	0-691	8.39	1.99	0.919	79.53	92.00	12.47
Rashiehill	0-964	10.00	1.89	0.844	50.58	62.00	11.42
Slatehole	0-1024	8.61	1.83	0.829	56.10	67.00	10.90
Salsburgh-1A	0-898	7.75	1.83	0.876	53.49	67.00	13.51
Kipperoch	40-300	7.47	3.48	1.528	51.53	75.00	23.47
Barnhill	25-355	8.60	2.57	1.058	45.48	66.00	20.52
Clachie Bridge	30-300	6.46	2.41	0.920	54.00	74.00	20.00
Hurlet	95-295	9.16	2.62	1.092	56.46	78.00	21.54
Craighead-1	0-909.8	6.95	1.88	0.869	57.96	70.00	12.04
Maryhill	100-303	9.45	1.7	0.768	65.08	76.00	10.92
Salsburgh-2	0-1102.1	6.73	1.88	0.856	63.58	73.00	9.42
Bargeddie-1	0-978.9	9.30	1.92	0.876	57.66	70.00	12.34

Table 6.3. Palaeoclimate corrections using the upper range of thermal properties from Chapter 5.

Name	Interval	T_o	k	κ	Q_o	Q_c	ΔQ
	(m)	(°C)	(W m^{-1} °C^{-1})	(mm^2 s^{-1})	(mW m^{-2})	(mW m^{-2})	(mW m^{-2})
Blythswood-1	18-105	7.95	2.07	0.971	75.48	85.00	9.52
South Balgray	0-137	8.65	1.71	0.797	71.81	85.00	13.19
Queenslie-4	0-691	8.39	2.27	1.049	90.70	104.00	13.30
Rashiehill	0-964	10.00	2.27	1.015	60.75	74.00	13.25
Slatehole	0-1024	8.61	2.19	0.991	67.13	80.00	12.87
Salsburgh-1A	0-898	7.75	2.08	1.002	60.80	76.00	15.20
Kipperoch	40-300	7.47	3.66	1.61	54.20	75.00	20.80
Barnhill	25-355	8.60	2.76	1.137	48.84	67.00	18.16
Clachie Bridge	30-300	6.46	2.62	0.99	58.71	76.00	17.29
Hurlet	95-295	9.16	3.09	1.295	66.59	84.00	17.41
Craighead-1	0-909.8	6.95	2.16	0.998	66.59	79.00	12.41
Maryhill	100-303	9.45	1.86	0.836	71.98	83.00	11.02
Salsburgh-2	0-1102.1	6.73	2.16	0.989	73.05	84.00	10.95
Bargeddie-1	0-978.9	9.30	2.23	1.025	66.98	81.00	14.02

where T_o: surface temperature, k: thermal conductivity, κ: thermal diffusivity, Q_o: uncorrected heat flow, Q_c: corrected heat flow, and ΔQ: palaeoclimate correction for Tables 6.2 and 6.3.

The results show that increasing the modelled thermal conductivity and thermal diffusivity of each borehole results in a greater corrected heat flow. Table 6.3 shows that the corrected heat flows of the deeper boreholes, using the upper suite of thermal property values, are similar to the corrected heat flows of the shallower boreholes in Table 6.1. This suggests that increasing the thermal conductivity of the deeper boreholes may produce more representative values of heat flow which account for the effects of both palaeoclimate and the increase in thermal conductivity with depth (e.g., Norden et al., 2020).

Alternative Temperature Histories

The palaeoclimate correction analysis showed that periods of colder climate from the Pleistocene control the magnitude of the perturbations to temperature, heat flow, and geothermal gradient caused by the effects of palaeoclimate (Figures 6.4-6.17b), and that the effects of more recent climatic events decrease with depth. For example, at Maryhill, at 30 m depth there was a greater influence on the perturbations from cooling during the Little Ice Age, and by 100-300 m depth the perturbations are caused by the periods of severe arctic climate and glaciation during the Dimlington Stadial, MIS 3 and MIS 6.

Furthermore, it was initially anticipated that the magnitude of the palaeoclimate correction to heat flow would be much less for deeper boreholes in comparison to corrections to shallower boreholes. However, significant corrections were still required due to the perturbations in temperature in the deeper boreholes caused by periods of colder climate during the early-mid Pleistocene. To illustrate this, at 100 and 300 m depth in these boreholes the perturbations were caused by the periods of glaciation and arctic climate during the Dimlington Stadial, MIS 3 and MIS 6, similar to that of the shallower boreholes, whereas at 1000 m depth, MIS 6, MIS 8, and MIS 30 had more of an influence on the perturbations, as well as a greater influence from the MIS 3 stage.

The assumed temperature history for the Pleistocene cold stages therefore has an influence on the magnitude of the palaeoclimate corrections, and thus may overestimate or underestimate the resulting corrections. A number of alternative temperature histories were therefore examined to assess the differences in results (Appendix 6.G). The most significant results are described here, with further results detailed in Appendix 6.H.

First, a comparison was made between the present study and the temperature histories adopted by Westaway and Younger (2013) and Busby et al. (2016). The temperature history used within Westaway and Younger (2013) is shown in Figure 6.18, and that used by Busby

et al. (2016) shown in Figure 6.19, and both are tabulated in Appendix 6.G. Both of these temperature histories were adapted for use in the present study for the Maryhill borehole. By adopting the temperature history of Westaway and Younger (2013), the corrected heat flow was found to be 85 mW m^{-2}, whereas it was found to be 82 mW m^{-2} using the temperature history of Busby et al. (2016). The larger increase in palaeoclimate correction using the Westaway and Younger (2013) temperature history, was due to the larger temperature differences assumed between the present day and MIS 2 and MIS 4 glacial periods. The climate model of Busby et al. (2016) was more comparable to that adopted in this study.

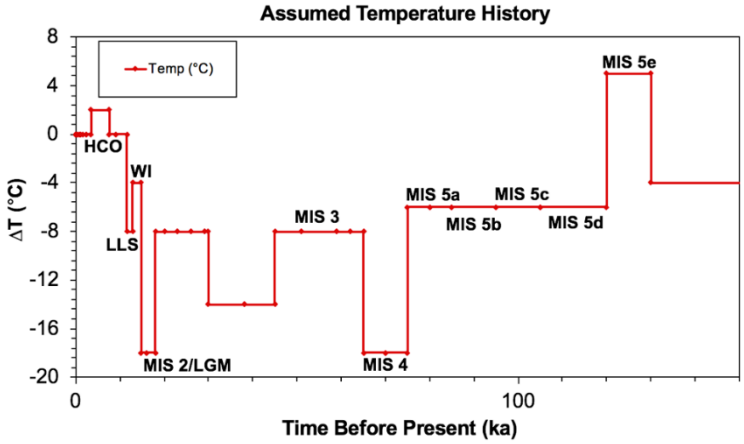

Figure 6.18. Temperature history from Westaway and Younger (2013). Present day surface temperature assumed to be 8 ºC.

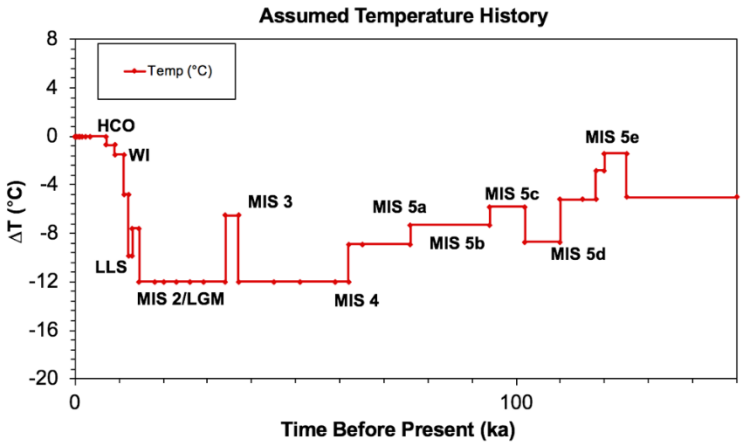

Figure 6.19. Temperature history from Busby et al. (2016). Present day surface temperature assumed to be 9 ºC). Periods of ice cover were assumed for 62-37 and 34-14.5 ka.

Insulating Effects of Glaciation

One important feature of the temperature history adopted in the present study was the higher temperatures assumed during periods of glaciation to account for the insulating effect of glaciation on the ground surface. This was particularly relevant to the study areas as it has been established that localities that were covered in ice during the Dimlington Stadial require a smaller palaeoclimate correction to heat flow than localities that experienced no glaciation (Jessop, 1971; Westaway and Younger, 2013). However, by accounting for this effect, the palaeoclimate correction may be underestimated. The impact of this was assessed by replacing the insulating effect of glaciation with much colder temperatures for these periods consistent with the NGRIP data series. During MIS 2, the absolute temperature from 14.7-16 ka BP was assumed to be -4.5 °C, from 16-23 ka BP it was assumed to be -6.5 °C, and from 23-32 ka BP it was assumed to be -8.5 °C. In addition, during MIS 4, the absolute temperature from 59-62 ka BP was assumed to be -6.5 °C and from 62-70 ka BP was assumed to be -8.5 °C. The modelled temperature histories are detailed in Appendix 6.G (Tables 6.G.3 and 6.G.4). This revised, colder temperature history was applied to both the Maryhill and Rashiehill boreholes in order to compare the effect on a shallow and deep borehole. For the Maryhill borehole, this change in temperature history increases the corrected heat flow from 80 to 83 mW m^{-2} due to the much colder climate assumed during the MIS 2 and MIS 4 glacial periods. A similar effect was observed at Rashiehill, with the corrected heat flow increasing from 70 to 73 mW m^{-2}.

Synthesis of Model Refinements

The most significant influence on the resulting palaeoclimate correction is the assumed thermal conductivity of the deep boreholes assessed within this study. The results indicate that the upper values of thermal conductivity may be more appropriate for the deeper boreholes to account for the increase in thermal conductivity with depth.

The results also show that individual details of the assumed temperature history may be contested, but it is apparent that for any plausible history, palaeoclimate corrections to heat flow are large for boreholes in the western MVS. The magnitude of the corrections emphasises the importance of correcting heat flow for the effects of palaeoclimate and indicates the extent to which it was previously underestimated.

6.5. Topographic Corrections to Heat Flow and Geothermal Gradient

6.5.1. Topographic Correction Methodology

To determine topographic corrections to heat flow in boreholes located in valleys in Britain, Westaway and Younger (2013) adopted the Lees Valley method (cf. Lees, 1910; Appendix 6.I). A Lees Valley is an analytic two-dimensional profile of topography which approximates the cross-sections of valleys, with the dependence of surface topography z_s against horizontal position *x* defined by Equation 6.I.8. The associated subsurface temperature distribution T(x,z) for depth $z \geq z_s$ is given by Equation 6.I.5 and that for the vertical component of the geothermal gradient by Equation 6.I.9. Similar to the palaeoclimate correction procedure, the assumed topographic profile determines the present-day perturbation to the geothermal gradient, and the resulting heat flow perturbation scales in proportion to *k*, in accordance with Fourier's Law.

Westaway and Younger (2013) developed Microsoft Excel spreadsheets to calculate corrections to the geothermal gradient and heat flow using the Lees Valley method, subject to the assumption that the Lees Valley solution fits the observed local topography. The Lees Valley solution is specified by the following parameters: (1) H is the depth of the valley floor at x=0, measured below the reference level z_0 (itself measured relative to sea-level) that specifies the height of top of the flanking valley walls; and (2) B is a measure of the half-width of the valley, the depth below z_0 of the model valley floor decreasing to H/2 at $x=\pm B$.

The topographic correction also depends upon the unperturbed near-surface geothermal gradient *u* (i.e., the geothermal gradient at z=0), the vertical temperature gradient at the bedrock surface *u'*, the latter being equal, for a subaerial bedrock surface, to the atmospheric lapse rate, and the radioactive heat production, Y, in the bedrock. Finally, the perturbation to vertical heat flow scales in proportion to the thermal conductivity of the bedrock, *k*.

The Westaway and Younger (2013) Microsoft Excel spreadsheets were used within the present study to determine topographic corrections to heat flow and geothermal gradient. The boreholes which required topographic corrections were Barnhill, Clachie Bridge and Hurlet. The local topography surrounding the remainder of the boreholes in the region was deemed to either be flat or a poor fit to the Lees Valley solution and were not included in these corrections. The elevation and depth of the boreholes are detailed in Table 5.1, and the atmospheric lapse rate was assumed to be 8 °C.

To conduct the topographic correction using the Lees Valley solution, a topographic profile sub-perpendicular to the valley in which each borehole is located was digitised using Ordnance Survey 5m and 50m Terrain Contours mapped using QGIS software. The topographic landscape within which each borehole is located, and the Lees Valley solution are shown in Figures 6.20-6.23.

The Barnhill borehole is located in farmland in the foothills of the Kilpatrick Hills, between the steep cliffs of Lang Craigs and a volcanic plug named Dumbowie (Figure 6.20a).

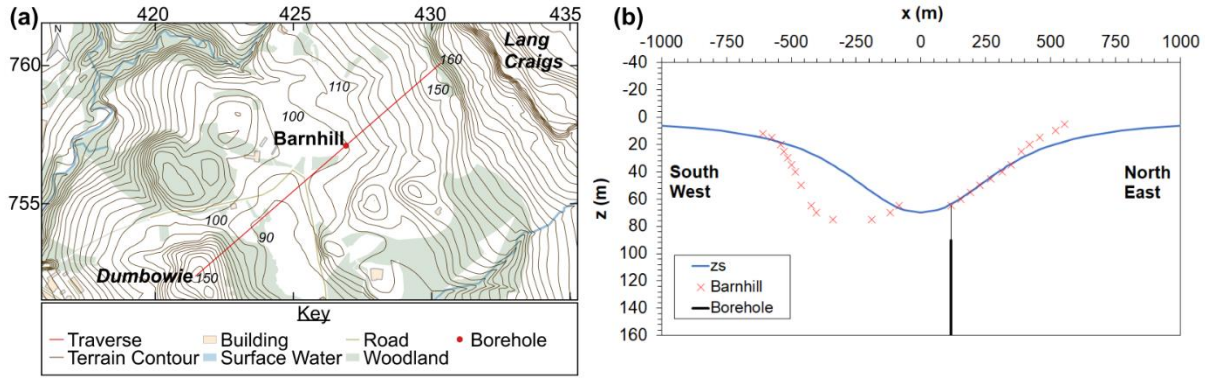

Figure 6.20. Barnhill topography (a) and Lees Valley analytical solution (b). The coordinates (north and east) are in 100 m intervals within British National Grid 100 km quadrangle NS. © Crown copyright and database rights 2021 Ordnance Survey (100025252).

The Clachie Bridge borehole is located between Leckett Hill to the south and the Fintry Hills to the north (Figure 6.21). While the borehole is located in lower ground between these hills, it is not located on the valley floor. The Lees Valley solution was fitted to the valley floor and in doing so, the borehole was located on the elevated flank of the Lees Valley profile.

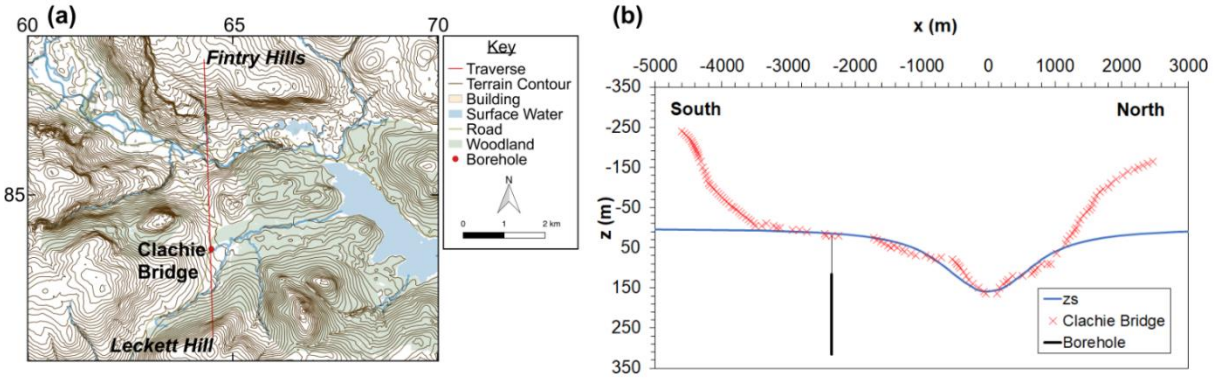

Figure 6.21. Clachie Bridge topography (a) and Lees Valley analytical solution (b). The coordinates (north and east) are in kilometres within British National Grid 100 km quadrangle NS. © Crown copyright and database rights 2021 Ordnance Survey (100025252).

The Hurlet borehole is located between Oldbar Hill and Hurlet Hill (Figure 6.22). Hurlet Hill is higher than Oldbar Hill and it was therefore difficult to find a suitable Lees Valley fit. Two solutions are shown which fit the borehole in the valley floor of the Oldbar Hill to the west, and then separately to Hurlet Hill to the east (Figure 6.23). The mean topographic corrections to heat flow and geothermal gradient were calculated from these two solutions.

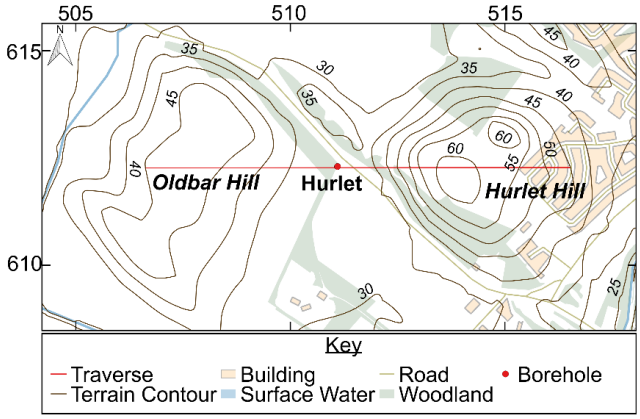

Figure 6.22. Topography surrounding the Hurlet borehole. The coordinates (north and east) are in 100 m intervals within British National Grid 100 km quadrangle NS. © Crown copyright and database rights 2021 Ordnance Survey (100025252).

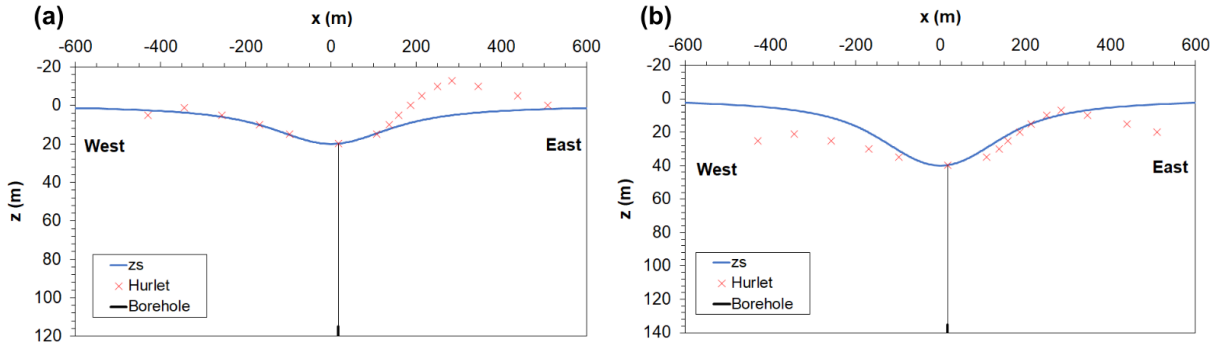

Figure 6.23. Lees Valley analytical solution for the topography west of the Hurlet borehole (a) and east of the Hurlet borehole (b). © Crown copyright and database rights 2021 Ordnance Survey (100025252).

Table 6.I.1 details the input parameters which determine the Lees Valley fit for each of the boreholes, where H is the depth of the valley floor; B is the half-width of the valley; D_z is the vertical distance between the valley floor and the base of the borehole; D is the depth of the borehole; and x is the horizontal distance from the valley axis to the borehole.

6.5.2. Topographic Corrections Results

The topographic corrections to heat flow for the Barnhill, Clachie Bridge, and Hurlet boreholes are presented in Table 6.4, and detailed as follows.

Barnhill

A Lees Valley was fitted through the cross-sectional profile of the local topography surrounding the Barnhill borehole from Dumbowie to the Lang Craigs cliff faces (Figure 6.20). Using Equation 6.I.5, with the borehole at x = 116 m (i.e., offset by 116 m from the valley axis) and its top at 100.3 m O.D modelled at a depth of z = H – 10 m, this Lees Valley solution predicts temperature perturbations due to the topography of 0.58°C and 0.30 °C at 25 and 355 m. The resulting geothermal gradient and heat flow are perturbed by 0.73 °C km^{-1} and 1.93 mW m^{-2} respectively over this depth interval, making the estimate for the topographically corrected heat flow in this borehole 46.98 mW m^{-2}. Oxburgh (1982) calculated a topographically corrected heat flow of 47.94 mW m^{-2} for the 25-355 m interval in the Barnhill borehole. The correction applied during the present study is greater, however, given the lack of transparency of the Oxburgh (1982) approach, it is unclear as to whether one analysis underestimates or overestimates the effect of topography in this locality.

Clachie Bridge

Illustrated in Figure 6.21, a Lees Valley was fitted through the cross-sectional profile from Lecket Hill in the south to the Fintry Hills in the north, however an unsatisfactory fit was achieved as the borehole was not located on the valley floor. Using Equation 6.I.5, with the borehole at x = 2353 m (i.e., offset by 2353 m from the valley axis) and its top at 269.4 m O.D modelled at a depth of z = H – 145 m, the Lees Valley solution predicts temperature perturbations due to the topography of 0.22 °C and 0.27 °C at 30 and 300 m. This results in a positive perturbation to the geothermal gradient and heat flow over this depth range by 0.18 °C km^{-1} and 0.44 mW m^{-2} respectively, making the estimate for the topographically corrected heat flow in this borehole 58.12 mW m^{-2}. In this case, the off-axis location of the borehole influences the topographic correction significantly. Keeping other parameters constant but moving the borehole to x = 0 with its top at z = H causes a negative perturbation, giving a topographic correction of 4.49 mW m^{-2} and reduces the estimate of the corrected heat flow to 53.19 mW m^{-2}. Oxburgh (1982) calculated a topographically corrected heat flow of 55.18 mW m^{-2} for Clachie Bridge, which was a more significant topographic correction in comparison to the present study. This is likely caused by differences in the topographic profile chosen for the analysis and the inadequate Lees Valley fit modelled for the location of the Clachie Bridge borehole in the present study.

Hurlet

Two Lees Valley solutions were fitted through the cross-sectional profile of the local topography to the west and east of the Hurlet borehole (Figure 6.23). For the west section, using Equation 6.I.5, with the borehole at x = 17 m (i.e., offset by 17 m from the valley axis) and its top at 30.03 m O.D modelled at a depth of z = H m, the Lees Valley solution predicts temperature perturbations due to the topography of 0.16 °C and 0.10 °C at 95 and 295 m. The resulting geothermal gradient and heat flow are perturbed over this depth range by 0.36 °C km^{-1} and 1.02 mW m^{-2} respectively, making the preferred estimate for the topographically corrected heat flow in this borehole 60.73 mW m^{-2}. For the east section, using Equation 6.I.5, with the borehole at x = 17 m (i.e., offset by 17 m from the valley axis) and its top at 30.03 m O.D modelled at a depth of z = H m, this solution predicts temperature perturbations due to the topography of 0.32 °C and 0.18 °C at 95 and 295 m. The geothermal gradient and heat flow are perturbed over this depth range by 0.68 °C km^{-1} and 1.96 mW m^{-2} respectively, making the preferred estimate for the topographically corrected heat flow in this borehole 59.79 mW m^{-2}. The mean of both these east and west corrections give an overall topographic correction for Hurlet of -1.49 mW m^{-2} and a corrected heat flow of 60.26 mW m^{-2}. Oxburgh (1982) calculated a topographically corrected heat flow of 60.37 mW m^{-2} for Hurlet, which is consistent with the topographic correction calculated in the present study.

Table 6.4. Results of the topographic corrections to heat flow for Barnhill, Clachie Bridge and Hurlet boreholes.

Borehole	Interval	Q_o	k	u_o	u_t	Δu_s	Δu_b	Δu_m	ΔQ_m	Q_f	ΔQ_T	Q_{fx}
	(m)	(mW m^{-2})	(W m^{-1} °C^{-1})	(°C km^{-1})	(°C km^{-1})	(°C km^{-1})	(°C km^{-1})	(°C km^{-1})	(mW m^{-2})	(mW m^{-2})	(mW m^{-2})	(mW m^{-2})
Barnhill	25-355	48.91	2.67	18.32	16.9	-1.82	-0.44	-0.89	-2.39	46.52	-1.93	46.98
Clachie Bridge	30-300	57.68	2.53	22.80	20.7	-2.53	-1.34	-1.84	-4.66	53.02	0.44	58.12
Hurlet (East)	95-295	61.75	2.87	21.52	20.5	-2.92	-0.39	-1.07	-3.07	58.61	-1.96	59.79
Hurlet (West)	95-295	61.75	2.87	21.52	21	-1.53	-0.20	-0.56	-1.60	60.15	-1.02	60.73
Hurlet (Mean)	95-295	61.75	2.87	21.52	20.75	-2.22	-0.30	-0.82	-2.34	59.38	-1.58	60.26

Q_o is the measured, uncorrected heat flow calculated in Chapter 5; u_o is the corresponding geothermal gradient and k is the corresponding harmonic mean thermal conductivity measured over the interval (with $Q_o = u_o \times k$). u_t is the 'target' geothermal gradient, the estimate of the regional geothermal gradient relative to which the topographic correction is derived. Interval is the depth interval over which the geothermal gradient, harmonic mean thermal conductivity and heat flow were measured in the borehole. u' is the atmospheric lapse rate, assumed to be 8 °C. Δu_s is the topographic correction to the geothermal gradient at the Earth's surface on the axis of the Lees Valley (i.e., at x=0, $z=z_s=H$), derived from Equation 6.I.10. Δu_b is the topographic correction to the geothermal gradient at the bottom of the borehole on the axis of the Lees Valley (i.e., at x=0, z=H+D), also derived from Equation 6.I.10. Δu_m and ΔQ_m are the perturbations to the mean geothermal gradient and mean heat flow, beneath the axis of the Lees Valley, spatially averaged between $z=z_s=H$ and z=H+D, calculated using Equation 6.I.15. Q_f is the corrected mean heat flow, calculated as $Q_o + \Delta Q_m$. ΔQ_T is the perturbation to the heat flow at x, the position of the borehole in relation to the valley axis, and Q_{fx} is the corrected heat flow, calculated as $Q_o + \Delta Q_T$, calculated at the position of the borehole.

6.6. Combined Palaeoclimate and Topographic Corrections

The palaeoclimate corrections (ΔQ_P) and topographic corrections (ΔQ_T) to heat flow for each borehole are shown in Table 6.5 and in Figure 6.24. The combined corrections increase the uncorrected heat flow (Q_o) significantly and present the "true" corrected heat flow of each borehole (Q_c). Excluding the anomalous value of Queenslie-4, the mean regional corrected heat flow was calculated as 75.7 mW m-2, an increase of 13.8 mW m^{-2} from the uncorrected value of 61.9 mW m^{-2}. This is a 23% increase in heat flow which highlights the importance of correcting for the effects of both palaeoclimate and topography and indicates the extent to which it was previously underestimated.

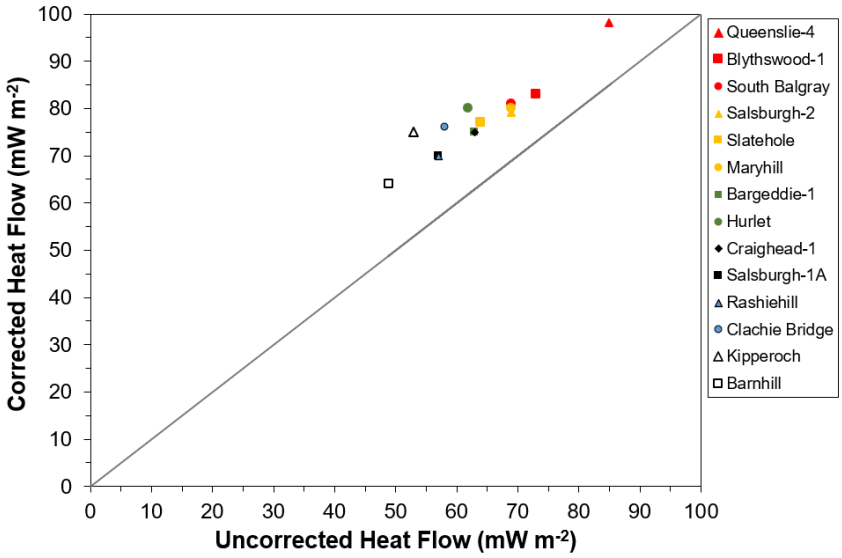

Figure 6.24. Combined palaeoclimate and topographic corrections to heat flow. For each site, the markers show the corrected heat flow; the diagonal line corresponds to both the corrected and uncorrected values being equal.

Table 6.5. Combined palaeoclimate and topographic corrections to heat flow.

Name	Interval	Q_o	ΔQ_P	ΔQ_T	Q_c
	(m)	(mW m^{-2})	(mW m^{-2})	(mW m^{-2})	(mW m^{-2})
Blythswood-1	18-105	72.84	10.16	0	83.00
South Balgray	0-137	68.92	12.08	0	81.00
Queenslie-4	0-691	85.28	12.72	0	98.00
Rashiehill	0-964	57.35	12.65	0	70.00
Slatehole	0-1024	64.3	12.20	0	76.50
Salsburgh-1A	0-898	57.23	12.77	0	70.00
Kipperoch	40-300	53.40	21.60	0	75.00
Barnhill	25-355	48.91	17.09	-1.93	64.07
Clachie Bridge	30-300	57.68	17.82	0.44	75.94
Hurlet	95-295	61.75	19.25	-1.49	79.51
Craighead-1	0-909.8	62.54	12.46	0	75.00
Maryhill	100-303	69.08	10.92	0	80.00
Salsburgh-2	0-1102.1	68.58	10.42	0	79.00
Bargeddie-1	0-978.9	62.52	12.48	0	75.00

6.7. Implications for Geothermal Energy in Glasgow

6.7.1. Extrapolation of the Corrected Geothermal Gradient

Having determined the corrected heat flow for each of the boreholes, the corrected geothermal gradients were extrapolated to calculate the temperature of the potential geothermal resource at each of the borehole sites. Assuming conduction as the main heat transfer process, these subsurface temperatures were modelled one-dimensionally with the corrected heat flow using Equation 6.1:

$$T = T_0 + \sum_{i=z_0}^{z} {Q_i}/{k_i}$$

Equation 6.1.

Where T is the temperature (°C) at depth z_i (m) and T_0 is the temperature at the Earth's surface, Q is the corrected heat flow (mW m^{-2}) and, k is the harmonic mean thermal conductivity (W m^{-1} °C^{-1}).

The boreholes examined in this chapter are located out with the gravity survey area of Chapter 3 and therefore the extent and depth of the Upper Devonian sandstone aquifer could not be constrained by the associated structural geological model. However, for the purpose of this calculation, the stratigraphy of the structural geological model alongside the stratigraphy of each borehole (see Chapter 5) were used to estimate the depth to the top of the Stratheden Group at each of the borehole sites and the temperature within the geothermal resource was calculated accordingly.

As the Barnhill, Clachie Bridge, and Kipperoch boreholes already intercept the Kinnesswood Formation or the Stratheden Group, temperatures at a nominal 2000 m depth were calculated beneath each borehole. The same approach was taken for the Rashiehill, Slatehole, Salsburgh-1, Salsburgh-2, and Craighead-1 boreholes due to uncertainty over the presence of deeply buried Upper Devonian sandstones in these areas of the MVS.

The results are shown in Table 6.6 and 6.7, with estimates of the temperature of the geothermal resource calculated for those boreholes located within Glasgow and the surrounding conurbation (Table 6.6), and for those boreholes located elsewhere in the western MVS (Table 6.7).

Table 6.6. Temperature of the geothermal resource based on boreholes in Glasgow.

Name	z	T_o	k	Q_o	Q_c	T_u	T_c	ΔT
	(m)	(°C)	(W m^{-1} $°C^{-1}$)	(mW m^{-2})	(mW m^{-2})	(°C)	(°C)	(°C)
Blythswood-1	1319	7.95	2.31	72.84	83.00	49.54	55.34	5.80
South Balgray	1298	8.65	2.26	68.92	81.00	48.23	55.17	6.94
Queenslie-4	1886	8.39	2.26	85.28	98.00	79.56	90.17	10.62
Hurlet	996	9.16	2.55	61.75	79.51	33.28	40.22	6.94
Maryhill	1361	9.45	2.31	69.08	80.00	50.15	56.58	6.43
Bargeddie-1	1787	9.30	2.20	62.52	75.00	60.08	70.22	10.14

Table 6.7. Temperature of the geothermal resource based on boreholes out with Glasgow.

Name	z	T_o	k	Q_o	Q_c	T_u	T_c	ΔT
	(m)	(°C)	(W m^{-1} $°C^{-1}$)	(mW m^{-2})	(mW m^{-2})	(°C)	(°C)	(°C)
Rashiehill	2000	10.00	2.29	57.35	70.00	60.09	71.14	11.05
Slatehole	2000	8.61	2.21	64.30	76.50	66.80	77.84	11.04
Salsburgh-1A	2000	7.75	2.19	57.23	70.00	60.01	71.68	11.66
Kipperoch	2000	7.47	3.55	53.40	75.00	37.55	49.72	12.17
Barnhill	2000	8.60	3.34	48.91	64.07	37.89	46.97	9.08
Clachie Bridge	2000	6.46	3.37	57.68	75.94	40.69	51.53	10.84
Craighead-1	2000	6.95	2.36	62.54	75.00	59.95	70.51	10.56
Salsburgh-2	2000	6.73	2.29	68.58	79.00	66.63	75.73	9.10

Tables 6.6 and 6.7 show the estimated depth to the geothermal resource at each borehole site (z); the surface temperature of the borehole site at the year of subsurface temperature measurement (T_o); the harmonic mean thermal conductivity (k) of the geological sequence from the surface to the geothermal resource calculated using the same method described in Chapter 5; the uncorrected heat flow (Q_o), the heat flow corrected for the effects of palaeoclimate and topography (Q_c); the temperature of the geothermal resource estimated from the uncorrected geothermal gradient (T_u); the temperature of the geothermal resource estimated from the corrected geothermal gradient (T_c), and the difference between the uncorrected and corrected temperature estimates (ΔT).

Excluding the anomalous results of the Queenslie-4 borehole, Table 6.6 shows that the most favourable temperatures were calculated where the Upper Devonian sandstone sequence is deepest in the east of Glasgow, as indicated by the results for the Bargeddie-1 borehole. Favourable temperatures are also present where the Upper Devonian sandstones are shallower in the west of the city, demonstrated by the Maryhill, South Balgray and Blythswood-1 results.

These corrected temperature estimations range from c. 40-70 °C, which are suitable for a variety of the direct heat applications such as district heating, the provision of heat to swimming pools or for horticulture or industrial uses (Figure 2.3).

Furthermore, promising temperatures were predicted beneath boreholes located in the Lanarkshire Basin to the east of Glasgow and in the Mauchline Basin in Ayrshire (Table 6.7). Despite the uncertainty surrounding the presence of the Upper Devonian sandstone aquifer at these locations, temperatures of c. 70-78 °C at 2 km depth are encouraging for geothermal exploration and warrant further investigation.

More modest temperatures were estimated at 2000 m depth beneath the Barnhill, Clachie Bridge, and Kipperoch boreholes in comparison to temperatures at equivalent depths elsewhere in the MVS (Table 6.7). Nonetheless, these results indicate that there may be scope for geothermal exploration in permeable horizons within the Strathmore Basin to the north of the MVS as postulated by Brown et al. (1985). Given that there are large areas of agricultural land in the northern and western MVS, there is the potential to utilise the geothermal heat for the development of greenhouses.

These results also indicate that the potential geothermal resource in flooded abandoned mine workings is significant. With reference to the Hallside and GGC01 case studies (Watson et al., 2019; Watson and Westaway, 2020), up to c. 60 mW m^{-2} of heat flow may be entrained within mine workings in east-southeast Glasgow.

This analysis therefore shows that by correcting for the effects of palaeoclimate and topography, higher temperatures are present in the geothermal resource beneath Glasgow than previously anticipated. This is particularly true in the east of the city, where the available geothermal heat could be utilised for a variety of direct heat use applications.

To assess the implications of this analysis on the magnitude of the geothermal resource and the scope for developing geothermal energy in Glasgow, the thermal power outputs of geothermal doublet wells located in Glasgow's East End were calculated and the contribution to local heat demand was examined. The results are detailed in the case study in the following section of this chapter.

6.7.2. Geothermal Resource Quantification: A Case Study in Glasgow's East End

Glasgow City Council's Energy and Carbon Masterplan (GCC ECM) (2015) outlined the city's strategy to reduce carbon emissions and fuel poverty by installing district heating infrastructure to supply low-carbon heating to areas of high heat demand and fuel poverty.

The East End of Glasgow was recognised as a priority target for investment in energy infrastructure in the GCC ECM due to the presence of high rates of fuel poverty coinciding with some of the most deprived areas of the city (Figure 6.J.1 and 6.J.2). The primary driver for energy consumption in the East End of Glasgow is the provision of space heating and hot water for buildings (Glasgow City Council, 2015). This, coupled with the high concentration of thermal loads from residential housing and 'anchor loads' from large energy consumers, makes the East End of Glasgow an attractive candidate for the development of low-carbon district heating. Indeed, since 2014, a 1.68 MW Combined Heat and Power (CHP) energy centre located in the Commonwealth Games Athletes Village has supplied heat and hot water via a district heating network to 704 homes, the Emirates Arena, and the Sir Chris Hoy Velodrome (Figure 6.25a) (Vital Energi, 2021). The GCC ECM illustrated further areas which are potential targets for the development of district heating networks such as Dalmarnock, Bridgeton, Carmyle, and Shettleston (Glasgow City Council, 2015), where there are large areas of vacant and derelict land suitable for developing low-carbon technologies and building energy centres associated to district heating networks.

These priority areas of high fuel poverty and high heat demand in Glasgow's East End coincide with areas of the city examined in this thesis, where the extent and depth of the geothermal resource has been established and the estimated aquifer temperature is the most encouraging. There is, therefore, an opportunity for direct heat use applications of the deep geothermal heat to contribute to meeting some local heat demand from residential housing and anchor loads from large energy consumers in the East End of Glasgow.

To quantify the geothermal resource in the Upper Devonian sandstone sequence, DoubletCalc software (version 1.4.3) was used to calculate the indicative thermal power of geothermal doublet wells located in the East End of Glasgow. Having addressed the need to correct heat flow for the effects of palaeoclimate and topography, and by combining the results of Chapters 3-6 of this thesis, for the first time the magnitude of the geothermal resource beneath Glasgow was quantified.

DoubletCalc Modelling

The depth of the geothermal aquifer modelled in DoubletCalc was derived from the 'Upper' and 'Lower' structural geological models developed in Chapter 3. Shown in Figure 6.25, from the 'Upper' and 'Lower' structural geological models, there are four alternative depths to the Stratheden Group sequence within the modelled area, and thus four alternative model scenarios:

1) An upper estimate of the depth from the UCMS to the Stratheden Group of 1994 m.
2) An upper estimate of the depth from the MCMS to the Stratheden Group of 1894 m.
3) A lower estimate of the depth from the UCMS to the Stratheden Group of 1629 m.
4) A lower estimate of the depth from the UCMS to the Stratheden Group of 1529 m.

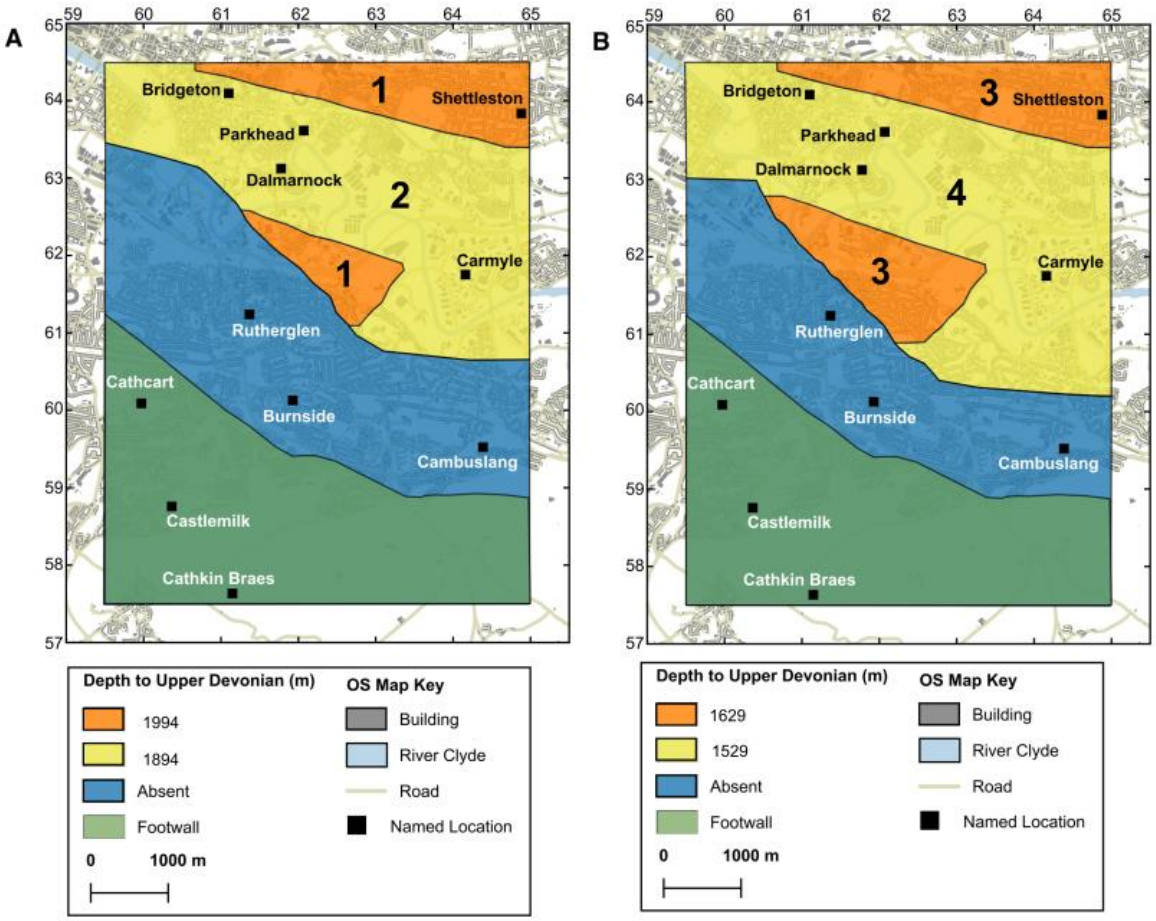

Figure 6.25. Extent and depth of the Stratheden Group derived from the 'Upper' model (a) and the 'Lower' model (b).

Using the thermal conductivities calculated for each stratigraphic formation in Chapter 5 (Table 5.D.19), and the modelled formation thicknesses (Table 6.J.2), the harmonic mean thermal conductivity was calculated for the stratigraphy from the ground surface to the

geothermal resource for each of the four model scenarios described above (Table 6.J.3). The corrected regional geothermal gradient was then calculated (Table 6.J.3) using the harmonic mean thermal conductivity and the corrected regional heat flow calculated in section 6.6. The aquifer properties were informed by the results of Chapter 4. As a 'base case' scenario, the aquifer permeability was assumed to be 40.64 mD, which was the mean permeability of the aeolian Stratheden Group sequence in the Glenburn borehole (Table 6.J.4). A series of other input parameters, such as the salinity of the geothermal brine, as well as engineering parameters pertaining to the design of the doublet system and the well casing were informed by precedents of geothermal projects located in similar geological conditions (Appendix 6.J).

Using this input data, the indicative thermal power outputs produced by geothermal doublet wells located in Glasgow's East End were calculated using DoubletCalc for the four alternative model scenarios described previously. The results are shown in Table 6.8, with Models 1 to 4 representing the four alternative aquifer depths for the areas illustrated in Figure 6.25.

Table 6.8. DoubletCalc results using the corrected dT/dz and 'base case' permeability.

Parameter	Model 1	Model 2	Model 3	Model 4
Depth (m)	1994	1894	1629	1529
dT/dz (°C/km)	33.25	33.15	33.46	33.36
Permeability (mD)	40.64	40.64	40.64	40.64
Geothermal Power (MW)	2.08	1.89	1.47	1.31
Aquifer Temperature (°C)	78.79	75.27	67.02	63.51
Temperature at Heat Exchanger (°C)	72.37	69.28	62.14	59.07
No. of Houses Heated	1518	1379	1072	956

The results of these calculations are encouraging, with thermal power outputs exceeding 1 MW in each of the four model scenarios and aquifer temperatures ranging from 64-79 °C. The upper estimates of the depth to the Stratheden Group (Model 1 and Model 2) yield the most favourable results, however high thermal outputs of c. 1.3-1.5 MW were also achieved based upon the shallower aquifer depths (Model 3 and Model 4).

The ‘base case’ permeability of 40.64 mD may however be an optimistic choice if intergranular porosity is significantly reduced by cementation and quartz overgrowths in the Upper Devonian sandstones beneath eastern Glasgow, as shown in fluvial sandstone samples from the Glenburn and Everton boreholes (Table 6.J.4). Indeed, Browne et al. (1987) stated that the permeability of the most deeply buried Upper Devonian sandstones beneath the MVS is likely to be of the order of 10 mD, perhaps attaining 100 mD within isolated zones. To examine the influence of permeability on the resulting thermal power output, the results were re-calculated using a permeability of 10 mD (Table 6.9) and 100 mD (Table 6.10).

Table 6.9. DoubletCalc results for permeability of 10 mD.

Parameter	Model 1	Model 2	Model 3	Model 4
Depth (m)	1994	1894	1629	1529
dT/dz (°C/km)	33.25	33.15	33.46	33.36
Permeability (mD)	10	10	10	10
Geothermal Power (MW)	0.39	0.35	0.27	0.23
Aquifer Temperature (°C)	78.79	75.27	67.02	63.51
Temperature at Heat Exchanger (°C)	58.26	55.96	50.94	48.70
No. of Houses Heated	284	255	197	167

Table 6.10. DoubletCalc results for permeability of 100 mD.

Parameter	Model 1	Model 2	Model 3	Model 4
Depth (m)	1994	1894	1629	1529
dT/dz (°C/km)	33.25	33.15	33.46	33.36
Permeability (mD)	100	100	100	100
Geothermal Power (MW)	5.19	4.74	3.74	3.35
Aquifer Temperature (°C)	78.79	75.27	67.02	63.51
Temperature at Heat Exchanger (°C)	75.93	72.61	64.88	61.58
No. of Houses Heated	3788	3459	2729	2445

The reduction of aquifer permeability from 40.64 mD to 10 mD results in a substantial reduction in thermal power output from the geothermal doublet well on the order of c. 1-1.6 MW. On the other hand, if post-cementation fracturing has occurred or if open permeable apertures in the Dechmont Fault zone were present, the results show that an increase in aquifer permeability from 40.64 to 100 mD increases the thermal power output dramatically, on the order of c. 2-3 MW. This crucial aspect of the geothermal resource, however, cannot be fully understood without deep exploratory drilling and testing to investigate the aquifer properties of the deeply buried sandstones.

To examine the contribution of the estimated thermal power output towards local heat demand, Scotland's Heat Map (SHM) data was first mapped across the area encompassed by the structural geological model (Figure 6.26b). Based upon this data candidate end-users of the geothermal heat were identified. This includes both thermal loads from residential housing and energy intensive buildings which are suitable as anchor loads for district heating networks, as suggested by the GCC ECM (Figure 6.26a).

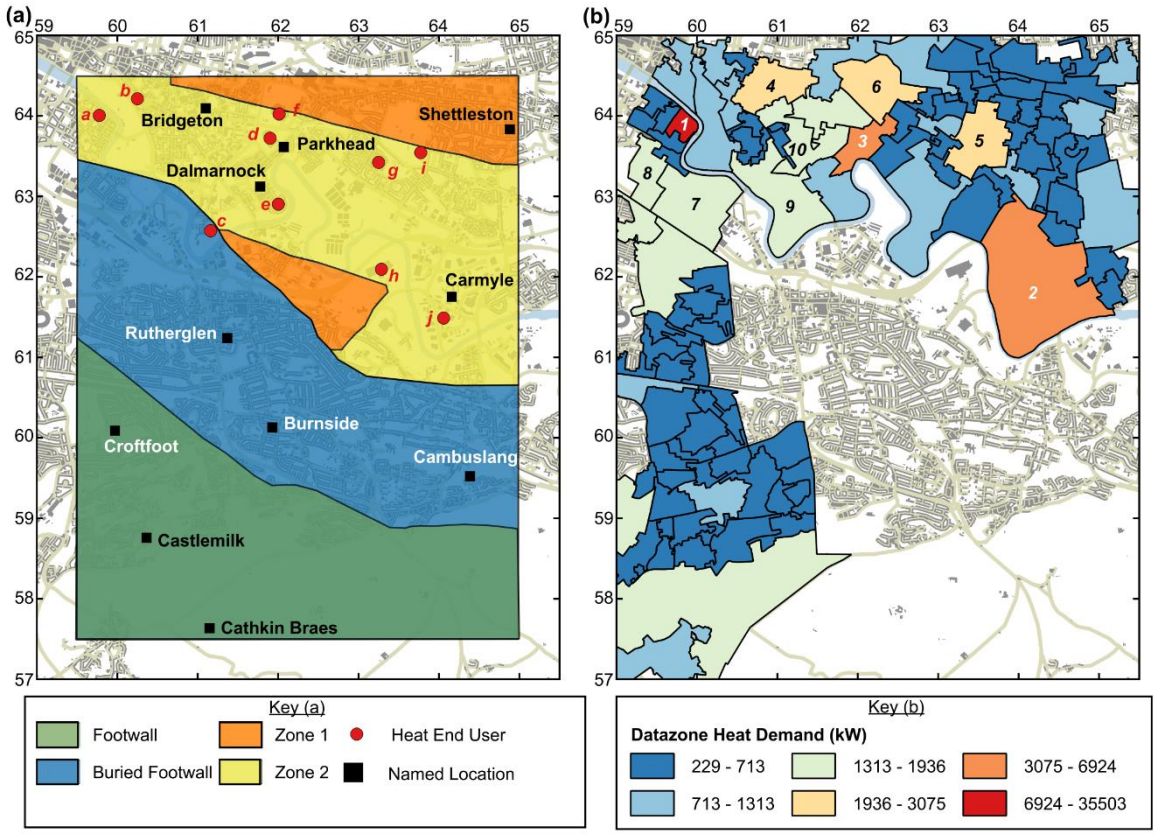

Figure 6.26. Candidate locations for locating a geothermal doublet in the gravity survey area based on the presence of the Upper Devonian from the 'Upper' model (a). Datazone heat demand from Scotland's Heat Map showing the ten datazones with the highest heat demand (b). Annotations in (a): a: Strathclyde Distillery, b: West Brewery, c: Dalmarnock Wastewater Treatment Works, d: Sir Chris Hoy Velodrome and Emirates Arena, e: Commonwealth Games Athletes Village, f: Cardowan Creameries, g: McVities Victoria Biscuit Works, h: Liberty Steel Clyde Bridge Steel Works, i: Tollcross Leisure Centre, and j: Clydesmill Industrial Estate. Numbered datazones in (b) correlate to Table 6.J.9.

Assuming an annual typical domestic gas consumption value of 12,000 kWh, equivalent to 1.37 kW (Ofgem, 2020), the number of households which could be heated by a geothermal doublet well was calculated. The results are shown in Tables 6.8-6.10 for each of the

modelled DoubletCalc scenarios. For the ‘base case’ aquifer permeability of 40.64 mD, the annual heat demand of 1379-1518 households in the East End of Glasgow could be met by the thermal power output of a geothermal well doublet if the aquifer is present at 1894-1994 m depth. Whereas, if the aquifer is present at a shallower depth of 1529-1629 m, the annual heat demand of 956-1072 households could be met.

As an example of the heat demand of an anchor load which could be met by geothermal heating, a preliminary assessment of the Tollcross Leisure Centre was conducted. This building is a large energy consumer in the East End of Glasgow, as it contains the Tollcross International Swimming Centre, as well as a sauna, steam room, spa, and gym and sports facilities. Swimming pools such as this are ideal candidate end-users of geothermal heat as demonstrated by feasibility studies (Barbato et al., 2018; Watson et al., 2020) and operational geothermal-heated pools (e.g., Jubilee Pool, 2021). The upper estimate of the depth of the aquifer at Tollcross Leisure Centre is 1894 m, and the lower estimate is 1529 m. Assuming the ‘base case’ scenario, the upper estimate of the thermal power output of a geothermal doublet in this area of the East End is calculated as 1890 kW and the lower estimate is 1310 kW. By comparison to Table 6.11, for either modelled scenario, the geothermal doublet would match the entirety of the annual heat demand of the building with excess output available for alternative direct heat use applications.

Table 6.11. Tollcross Leisure Centre annual heat demand (data provided by Glasgow Life).

Year	Heat Demand (kW)
2015-16	1129.53
2016-17	851.08
2017-18	627.94
2018-19	913.80
2019-20	842.95

This analysis has shown that, if there is sufficient permeability in the aquifer, the geothermal resource beneath Glasgow’s East End is capable of supporting a variety of direct heat use applications of geothermal heating and could contribute to meeting some of the local heat demand. Whether favourable aquifer conditions are present, however, cannot be fully understood without deep exploratory drilling.

6.8. Conclusion

By utilising the results of Chapters 5 and establishing a palaeoclimate history for the western MVS, rigorous corrections to account for the effects of palaeoclimate and topography on heat flow were calculated for the Blythswood-1, South Balgray, Queenslie-4, Slatehole, Rashiehill, Salsburgh-1, Hurlet, Barnhill, Clachie Bridge, Kipperoch, Craighead-1, Maryhill, Salsburgh-2, and Bargeddie-1 boreholes. This analysis was critical in investigating fully the geothermal resource beneath Glasgow, as until this present study, corrections for the effects of palaeoclimate and topography have not been applied to boreholes in the western MVS.

Overall, the combined corrections increase the heat flow significantly and present the "true" heat flow of each borehole. Excluding the anomalous value of Queenslie-4, the mean regional corrected heat flow was calculated as 75.7 mW m^{-2}, an increase of 13.8 mW m^{-2} from the uncorrected value of 61.9 mW m^{-2}. This is a 23% increase in heat flow which highlights the importance of correcting for the effects of both palaeoclimate and topography and emphasises the extent to which it was previously underestimated.

The corrected geothermal gradients were then extrapolated to the depth of the geothermal resource at each borehole location. These calculations indicate that higher temperatures are present in the geothermal resource than were previously anticipated. Excluding the anomalous results of the Queenslie-4 borehole, these temperature estimations range from c. 40-78 °C, and are particularly encouraging in eastern Glasgow due to the greater burial depth of the geothermal resource.

To assess the implications of this analysis on the magnitude of the geothermal resource and the scope for developing geothermal energy in Glasgow, the thermal power outputs of geothermal doublet wells located in Glasgow's East End were calculated using DoubletCalc software and the contribution to local heat demand was examined. If suitable permeability is present within the deeply buried sandstone aquifer, then the resulting thermal power outputs are encouraging, with values ranging from 1.31-2.08 MW dependent upon the depth of the aquifer. Based upon these results, the geothermal resource is capable of supporting a variety of direct heat use applications of geothermal heating which can contribute to meeting some of the local heat demand, including the provision of heating for 956-1518 households or for large energy consumers such as Tollcross Leisure Centre. However, if the aquifer permeability is restricted due to the effects of diagenesis, then the resulting thermal power outputs and contribution towards meeting local heat demand are greatly reduced.

Chapter 7. Conclusion

7.1. Scope of Research

The research objectives of this thesis were formed in recognition of the growing awareness of the need to increase renewable heating generating capacity as an essential step towards meeting statutory emissions targets and resolving the 'energy trilemma' in Scotland.

The Scottish Government have acknowledged that, as part of a diverse energy supply strategy, geothermal energy has a role in the decarbonisation of heat supply in Scotland, particularly when utilised for direct heat use applications. In 2013, the Scottish Government commissioned a study into the potential for deep geothermal energy in Scotland (Gillespie et al., 2013). This study outlined barriers to the development of the geothermal sector in Scotland and recommended policy options and the research required to overcome these challenges. In terms of characterising the geothermal resource, two key recommendations of Gillespie et al. (2013) were that palaeoclimate corrections to heat flow should be conducted, and that a National Geothermal Exploration Programme should be implemented, first as a research programme to identify deep geothermal prospects, and second as a physical exploration programme, consisting of a geophysical survey to identify target resources followed by deep exploratory drilling.

Precedents of operational geothermal projects in the Netherlands and France have shown that the success of low-mid enthalpy geothermal projects is reliant on the proximity of the geothermal resource to end-users of the heat, enabling local heat demand to be met by geothermal heating (e.g., Boissavy et al., 2019; Smith, 2019). This is pertinent for Glasgow, where the urban development of the city is a consequence of its economic development, in part fuelled by local coalfields which exploited rocks in the same sedimentary basin within which the prospective deep geothermal resource is present. This therefore creates an opportunity to provide geothermal heating to areas of dense urban population with high heat demand. This, coupled with Scotland's energy context and the recommendations by Gillespie et al. (2013), shaped the direction of this thesis.

7.2. Summary of Research and Unique Contributions of Thesis

This thesis quantified the deep geothermal resource in the Upper Devonian sandstone aquifer beneath eastern Glasgow and identified candidate locations where geothermal wells may be drilled to match local heat demand. The key achievements of this thesis are as follows:

1) Development of a Structural Geological Model of Eastern Glasgow

A high-density gravity survey was conducted over a 29 km^2 area of eastern Glasgow, measuring 161 new gravity points in the footwall and hanging wall of the Dechmont Fault. Constrained by this new gravity data and depth-converted seismic data, gravity forward modelling was carried out to develop a 3-D structural geological model of the survey area. This analysis was significant as it, (1) determined the extent and depth of the Upper Devonian sandstones beneath eastern Glasgow, and (2) identified possible locations where the Dechmont Fault may increase the porosity and permeability of the Upper Devonian sandstone sequence. Candidate areas were then selected for deep geothermal exploration to take place in Glasgow's East End. This encompassed areas such as Bridgeton, Dalmarnock, Parkhead, Carmyle, Tollcross and Shettleston, where the lower estimated depth of the Stratheden Group ranged from 1529-1629 m and the upper estimated depth from 1894-1994 m.

2) Examination of the Properties of Upper Devonian Sandstones

Thin section petrography, X-CT and XRD analyses were carried out on newly collected samples of Upper Devonian sandstone from borehole core and outcrop sites in the western MVS. This analysis found that diagenetic effects such as compaction and cementation have had a considerable influence on the properties of these sandstones and may restrict the porosity and permeability of analogous deeply buried sandstones beneath Glasgow. The highest porosities were present in aeolian samples of the Stratheden Group which had high textural and compositional maturity, low cementation, and low compaction. However, quartz overgrowths and quartz cementation were observed in the majority of samples and grain coatings which inhibited quartz overgrowths in aeolian sandstones of the analogous Buchan Formation were less prevalent in samples of the Stratheden Group. Therefore, if the Stratheden Group sandstones beneath eastern Glasgow also lack grain coatings and are heavily cemented, either by early carbonate cementation or late-quartz cementation, then intergranular porosity will be significantly reduced and poorly interconnected. Whether favourable aquifer properties would be preserved at burial depths of c. 1500-2000 m in eastern Glasgow is, however, an open question which cannot be fully resolved prior to exploratory drilling.

3) Identification of Perturbations to Glasgow's Subsurface Thermal State

Existing geothermal datasets from sixteen boreholes in the western MVS were re-evaluated and new values of heat flow, subsurface temperature, harmonic mean thermal conductivity, and harmonic mean thermal diffusivity were calculated. Based upon the newly calculated heat flow and geothermal gradient results, an examination of the influence of historic mining on Glasgow's subsurface thermal state was conducted. This found that the Hallside and GGC01 borehole temperature datasets were influenced by the legacy of historic mining. The heat flow of the Hallside borehole was calculated as c. 20 mW m^{-2} and the heat flow of the GGC01 borehole was calculated as 28-33 mW m^{-2}. The difference relative to the mean regional heat flow suggests a significant component of horizontal heat flow into surrounding flooded mine workings in the vicinity of these boreholes. This is encouraging from the perspective of targeting the geothermal resource in flooded, abandoned mine workings. The results also demonstrate that care must be taken to consider such an effect as this when attempting to extrapolate geothermal gradients from shallow boreholes to quantify the geothermal resource in deeper HSA settings.

4) Palaeoclimate and Topographic Corrections to Heat Flow

Rigorous corrections to account for the effects of palaeoclimate and topography on heat flow were applied to the Blythswood-1, South Balgray, Queenslie-4, Slatehole, Rashiehill, Salsburgh-1, Hurlet, Barnhill, Clachie Bridge, Kipperoch, Craighead-1, Maryhill, Salsburgh-2, and Bargeddie-1 borehole datasets. Until this present study, corrections for these effects had not been applied to boreholes in the western MVS and values of heat flow were underestimated. Overall, the combined corrections increase the heat flow significantly and present the "true" heat flow of each borehole. Excluding the anomalous value of Queenslie-4, the mean regional corrected heat flow was calculated as 75.7 mW m^{-2}, an increase of 13.8 mW m^{-2} from the uncorrected value of 61.9 mW m^{-2}. This is a 23% increase in heat flow which highlights the importance of correcting for the effects of both palaeoclimate and topography and emphasises the extent to which it was previously underestimated. The corrected geothermal gradients were then extrapolated to estimate the temperature at the depth of the potential geothermal resource at each borehole site. The results demonstrate that higher temperatures are likely to be present in the aquifer than were previously anticipated. These temperature estimations range from c. 40-78 °C and are particularly encouraging in eastern Glasgow due to the greater burial depth of the Upper Devonian sandstone sequence.

5) Geothermal Resource Quantification

Combining the results of Chapters 3-6 of this thesis, the thermal power outputs of geothermal doublet wells located in the East End of Glasgow were calculated using DoubletCalc software. In doing so, the magnitude of the geothermal resource in the Upper Devonian sandstone sequence beneath Glasgow was quantified for the first time. The estimated thermal power outputs are encouraging, with values ranging from 1.31-2.08 MW dependent upon the depth of the aquifer. This, however, is predicated upon a 'base case' aquifer permeability of 40.64 mD. If this is reduced to 10 mD due to the effects of diagenesis, then the resulting thermal power outputs reduce significantly to 230-390 kW. Using data from Scotland's Heat Map, candidate end-users of the geothermal heat were then identified. This includes both thermal loads from residential housing and energy intensive buildings which are suitable as anchor loads for district heating networks. For the 'base case' aquifer permeability of 40.64 mD, the annual heat demand of 956-1518 households in the East End of Glasgow could be matched by geothermal heat, dependent upon the location of the well and depth of the aquifer. As an alternative, geothermal heat could be utilised to meet the c. 900 kW annual heat demand of the Tollcross Leisure Centre. However, the estimated thermal power outputs and contribution to local heat demand are significantly less promising if the aquifer permeability is reduced due to the effects of diagenesis.

7.3. Scope for Geothermal Energy in Glasgow

Based upon the magnitude of the resource and the potential contribution that geothermal heat could make towards meeting local heat demand, this thesis has shown that there is scope for targeting the HSA resource in the Upper Devonian sandstones beneath Glasgow. This is reliant, however, on the presence of sufficient matrix permeability or fracture networks in the sandstone sequence. This crucial aspect cannot be fully understood without deep exploratory drilling.

The Science Central geothermal project in Newcastle upon Tyne is an example of the risks involved in geothermal projects in sedimentary basins in the UK. Research done prior to drilling the Science Central borehole highlighted the fact that the target aquifer, the Fell Sandstone Formation, was a prolific, transmissive aquifer near its outcrop. Therefore, there was good reason to expect that, if present beneath Tyneside, the Fell Sandstone Formation might indeed be productive. This was not the case, and one hypothesis for the lack of flow was that cementation (by carbonate in the upper part of the formation, and by quartz in the lower part) had occluded pore necks so that much of the remnant porosity was poorly

interconnected (Younger et al., 2016). As shown in Chapter 4, similar diagenetic effects on porosity could likewise be present in the Upper Devonian sandstones beneath Glasgow.

That said, the original concept of the Science Central project was to exploit fracture permeability in the Fell Sandstone Formation in the vicinity of the Ninety Fathom Fault. Drilling, however, took place in the footwall of the fault some 1.6 km from its footwall cut-off, being determined by the location of the Science Central redevelopment site in Newcastle upon Tyne city centre rather than the most likely location to encounter fault-induced groundwater flow (Westaway et al., 2019).

The drilling of the Science Central borehole was not preceded by any research process relating to the structural geology of the site, analogous to that described in Chapter 3. Demonstrated by the workflow and results of Chapter 3, collection and modelling of new gravity data identified target geological horizons and locations for geothermal developments to take place, which can reduce project risks.

Therefore, despite the failure of the project, the original concept of the Science Central borehole to intersect faults and their damage zones may be a reasonable avenue of enquiry for future geothermal exploration beneath Glasgow, and the work of this thesis has identified locations in the city where this may be possible. Given the orientation of the Dechmont Fault to the maximum horizontal compressive stress axis, there may be permeably open apertures in the associated fault zone. Furthermore, where post-cementation fracturing has occurred, intergranular porosity within the Upper Devonian sandstone aquifer (which was previously lost due to cementation) may well have re-interconnected (Younger et al., 2016). This would offer scope for significant fluid flow and thus geothermal production.

Nonetheless, the lack of certainty regarding the porosity and permeability of the Upper Devonian sandstone sequence beneath eastern Glasgow poses a risk for any proposed geothermal project due to the high capital cost of exploratory drilling. Based upon the geothermal project costing model used in the Netherlands (van Wees et al., 2010), a 2000 m deep geothermal well doublet located in Glasgow's East End would cost c. £3.1 million for the initial exploration well, and c. £6.2 million for the doublet. The van Wees et al. (2010) costing model predicts much higher costs than would be expected in the UK, reflecting different local conditions (the c. 1.8 km deep Science Central borehole was drilled with a budget of £1.2 million (Westaway, 2018)). Regardless, both these estimations and precedents of geothermal drilling in sedimentary basins in the UK emphasise the high capital

costs required for geothermal drilling projects. Thus, the lack of assured project-success, given the uncertainties surrounding the aquifer properties at depth, coupled with the high capital costs of drilling, pose barriers to the development of deep geothermal energy in the HSA setting beneath Glasgow.

However, if an exploratory borehole drilled in Glasgow's East End found that the matrix permeability of the Upper Devonian sandstone sequence was too tight, or if fractures were not present, then a potential solution would be to drill the well to greater depths, thus encountering greater temperatures, re-completing the well as a DGSW (e.g., Alimonti et al., 2018; 2021). Analytical modelling established that DGSW heat production was found to be cost-effective under the former RHI subsidy regime for deep geothermal heat in the UK, provided that boreholes were deep enough and in localities where the geothermal gradient is high enough (Westaway, 2018). This technology also has potential applications linked to seasonal thermal storage which may contribute further added value to such an exploratory borehole. The corrected regional heat flow and geothermal gradient for the Glasgow established in Chapter 6, demonstrated that temperatures of >90° C may be present at depths of 3 km. This may make the DGSW technology economic and sustainable, generating sufficient thermal energy output to justify its use. An exploratory geothermal well located in Glasgow's East End could, therefore, be designed in such a way as to be utilised for alternative means, creating value for the project even if the primary geothermal target of matrix permeability in the deeply buried Upper Devonian sandstone aquifer is absent.

Another consideration is whether the high capital costs of drilling a deep geothermal doublet well in Glasgow's East End is a justifiable option, given the magnitude of the resource available compared to alternative low carbon heat solutions. First the heat resource available from a geothermal doublet well located in eastern Glasgow is compared to those available from other low-mid enthalpy geothermal heat projects. Then, a comparison is made to an alternative low carbon heat resource established in Glasgow and the surrounding conurbation.

Table 7.1 details the thermal power output of both operational and potential low-mid enthalpy geothermal projects from the UK, and worldwide.

Table 7.1. Comparison of low-mid enthalpy geothermal sites. Adapted from Watson et al. (2020).

Site	Country	T_z (°C)	T_o (°C)	Q (MWth)	Type
Operational Sites					
Agriport	NL	92	9	28	Doublet
Trias Westland	NL	85	10	20	Doublet
Vogelaer	NL	85	10	18	Doublet
Heerlen	NL	28	10	9.63	Minewater
The Hague	NL	76	10	7	Doublet
Issy-Les-Moulineaux	F	30	10	4.7	Single Well
Jonzac	F	65	14	3.1	Single Well
Southampton	UK	76	10	2.2	Single Well
Mieres	ES	23	13	2.2	Minewater
Dawdon	UK	19	9	2	Minewater
Dannenbaum	D	37	10	0.6	Minewater
Springhill	CA	18	7	0.111	Minewater
Potential Sites					
Meerbrook Sough	UK	15	8	20	Minewater
Kibblesworth	UK	15	9	7.5	Minewater
Glasgow (100 mD)	UK	78	10	5.2	Doublet
Polkemmet	UK	17	10	2.2	Minewater
Glasgow (40.64 mD)	UK	78	10	2.08	Doublet
Glasgow (10 mD)	UK	78	10	0.39	Doublet

Note: Sites in each group are listed in order of thermal power output, Q. T_z is the source temperature of the produced water; T_o is the annual mean air temperature at the sites obtained from meteorological data. Countries where projects are located are denoted as: CA, Canada; D, Germany; F, France; ES, Spain; NL, the Netherlands; and UK, the United Kingdom. Table adapted from Watson et al. (2020), Table 8. References and notes for each project except the Glasgow (10, 40.64, 100 mD) entries are provided in Watson et al. (2020). For simplicity, the Glasgow results are shown for Model 1.

The list of operational projects includes four examples of modern geothermal doublets in the Netherlands: Agriport, Trias Westland, and Vogelaer for horticulture, and the Leyweg scheme for district heating in The Hague (Geothermie Nederland, 2021). Next are mine water geothermal schemes, at Heerlen (Verhoeven et al., 2014), Mieres (GRC, 2019), Dannenbaum (Bussmann et al., 2019), Springhill (Jessop et al., 1995), and Dawdon (Evans, 2020; TCA, 2020).

Example single well projects are also shown from Southampton in southern England (Gluyas et al., 2018), Issy-les-Moulineaux in the Paris Basin, and Jonzac in the Aquitine Basin of south-west France (Boissavy et al., 2019).

The list of potential projects includes Meerbrook Sough, a drainage adit created for historic lead mining in the Peak District of northern England, the Kibblesworth mine dewatering scheme in north-east England (Westaway and Younger, 2016), and the hypothetical mine water geothermal scheme at Polkemmet in central Scotland (Watson and Westaway, 2020).

Table 7.1 shows that the estimated thermal power output of a geothermal doublet located in Glasgow's East End, with an aquifer permeability of 40.64 mD or 100 mD, is comparable to the thermal power output of the single well projects at Southampton, Jonzac, and Issy-Les-Moulineaux, and mine water geothermal projects at Mieres and Dawdon, as well as the estimated output at Polkemmet. However, if the aquifer permeability is reduced to 10 mD, then the thermal power output of 390 kW is comparable to mid-scale mine water geothermal projects such as Dannenbaum and Springhill.

If heat outputs can be harnessed from mine workings beneath Glasgow comparable to those at Dannenbaum, Dawdon, or indeed those estimated at Polkemmet, then geothermal heat abstraction from flooded, abandoned mine workings may be a more viable first step in developing geothermal energy in Glasgow than targeting the deeper HSA resource. This would avoid the high capital costs of drilling to the deeply buried aquifer, and the project-risk of encountering a highly cemented or unfractured sandstone sequence.

This thesis has shown that the geothermal resource within flooded abandoned mine-workings beneath areas of Glasgow is likely to be significant, with an estimated c. 60 mW m^{-2} of heat entrained in flooded mine-workings beneath the Hallside borehole in the south-east of the city (Watson et al., 2019; Watson and Westaway, 2020).

Watson and Westaway (2020) suggested that mine water geothermal heat extraction projects should focus on deeper mine workings, in part because of the greater potential heat outputs due to their higher temperatures and in part due to the resource at these depths being renewable, as a result of basal heat flow from the Earth's interior, and thus capable of sustainable development. A candidate location for the development of a mine water geothermal project in Glasgow is Stepps, in the north-east of the city. This area is host to the deepest mine workings in Glasgow, associated with the former Cardowan Colliery, which extend to depths of c. 600 m (Oglethorpe, 2006).

The UK mine water geothermal energy resource is substantial, reported by Adams et al. (2019) as 2.2 million GWh, and given the proximity of former coalfields to areas of high

urban density and heat demand, flooded, abandoned mine workings present a “low hanging fruit” for the development of geothermal energy sector in the UK (Banks et al., 2019; Farr et al., 2020). Developing mine water geothermal projects could, thus, make a significant contribution to decarbonising heat supply in Glasgow, and across the UK.

Another opportunity for the development of renewable heat generating capacity in Glasgow is the recovery of heat from the River Clyde using Water Source Heat Pumps (WSHP). This technology has already been established on the River Clyde in the town of Clydebank, to the west of Glasgow. Here, on the site of the former John Brown’s Shipyard, two 2.65 MW WSHP’s upgrade residual heat from the River Clyde to 75 °C which is circulated through the Queens Quay district heating network (Vital Energi, 2021). This project supplies heat to over 1000 homes, commercial buildings, a health centre, and care home, and costed £20 million (Queens Quay, 2020).

Watson and Westaway (2020) noted that the River Clyde in Glasgow’s East End is a significant source of heat. The mean flow rate can be taken as 47.22 $m^3 s^{-1}$, at the Daldowie gauging station (at NS 672 616), as reported by Marsh and Hannaford (2008), and at Glasgow Green, between Dalmarnock and Glasgow City Centre, the water temperature in the Clyde is typically c. 10 °C, fluctuating between c. 16 °C in the summer and c. 4 °C in the winter (Burt et al., 2017). If all of this flow could be cooled by 1 °C, the thermal power output would be c. 200 MW (Watson and Westaway, 2020).

Due to the magnitude of the heat resource available from the River Clyde, and the established use of WSHP’s on the river already, this potentially significant heat output might be developed as a more effective local option for heat supply than deep geothermal energy in Glasgow.

7.4. Wider Implications of Research and Recommendations

The research process undertaken in this thesis to quantify the deep geothermal resource beneath Glasgow can be followed to investigate prospective geothermal resources in sedimentary basins elsewhere in the MVS, and across the UK. This is particularly true for areas of the country, like Glasgow and the western MVS, where there is an absence of deep boreholes (> 1.5-2 km depth) and the existing geothermal data is of variable quality.

To build upon the work of this thesis, the following steps are recommended to develop deep geothermal energy resources in sedimentary basins in the MVS and elsewhere in the UK:

Recommendation 1: Collect and Analyse New Geophysical Data

Analogous to the research process and results of Chapter 3, collection and modelling of new geophysical data will validate aspects of structural geology which are critical to any proposed geothermal development in sedimentary basins in the MVS, and the UK.

Recommendation 2: Apply Palaeoclimate Corrections to Heat Flow

Applying palaeoclimate corrections to heat flow will determine the true heat flow measured in boreholes across the country. Past failure to apply palaeoclimate corrections vastly underestimates the magnitude of heat flow, and thus the geothermal resource. As proven in this thesis, applying palaeoclimate corrections to heat flow and geothermal gradient is a critical step to reliably estimate the temperature of a geothermal resource in the absence of deep temperature measurements.

Recommendation 3: Examine Hydrocarbon Well Core

To supplement the outcrop and borehole analogue study conducted in Chapter 4, further analysis of samples from the Inch of Ferryton borehole will provide an insight to the effects of diagenesis on the aquifer properties of deeply buried (c. 2km) Upper Devonian sandstones beneath the MVS. Furthermore, permeability and fluid flow modelling will provide insight to the intergranular porosity and permeability of the sandstones at this depth, and the likelihood of supporting geothermal heat production.

Recommendation 4: Develop a Geothermal Resource Mapping Tool

Integration of data on the extent and magnitude of Glasgow's geothermal resource with socio-economic data and Scotland's Heat Map data, will create a GIS-based tool to be used by stakeholders to determine candidate locations for exploratory drilling. This could then be scaled, incorporating data from across Scotland and the UK, creating a nationwide GIS-based mapping tool, similar to Thermo-GIS in the Netherlands, to assess the country's geothermal resource base and its proximity to heat-users.

Recommendation 5: Appraisal of DGSW Heat Production in Glasgow

A technical and economic feasibility study of DGSW heat production from a borehole located in Glasgow would confirm whether there is scope for utilisation of this technology if suitable aquifer properties are not present in the Upper Devonian sandstone sequence. The economic risk associated with drilling an exploratory borehole in Glasgow would be reduced if it were proven that the borehole could be successfully repurposed for DGSW heat production. Furthermore, after a duration of use, if the technology is no longer economic, then the infrastructure might be easily repurposed for seasonal heat storage, offering the potential of making a significant long-term contribution to sustainable future heat supply.

Recommendation 6: Exploratory Drilling

Exploratory drilling in Glasgow will provide critical data on the temperature and properties of the deeply buried Upper Devonian sandstones beneath the city. This could then be used to inform the design of, and de-risk, further geothermal projects located in similar geological settings across the MVS, and in sedimentary basins in the UK.

7.5. Summary

This research has ultimately proven the three hypotheses of this thesis. First, the deep geothermal resource beneath Glasgow has been underestimated due to a previous lack of consideration for the effects of palaeoclimate and topography on shallow measurements of temperature and heat flow. Second, Upper Devonian sandstones of the Stratheden Group are present at depths ranging from c. 1500-2000 m beneath eastern Glasgow, with estimated aquifer temperatures ranging from c. 60-80 °C. Third, the abstraction of geothermal heat from a geothermal doublet well may contribute to meeting some local heat demand in residential housing or public or commercial buildings if suitable aquifer properties are present.

The results of this thesis demonstrate that the geothermal resource in the Upper Devonian sandstones beneath eastern Glasgow may be capable of supporting a wide variety of direct heat use applications. However, the presence of favourable aquifer properties in the deeply buried sandstone sequence is uncertain and cannot be fully understood without deep exploratory drilling.

The lack of assured project-success, given uncertainties related to the aquifer properties at depth, coupled with the high capital costs of drilling, pose barriers to the development of deep geothermal energy in the HSA setting beneath Glasgow. These technical and economic risks could, however, be mitigated by examining the scope for repurposing an exploratory borehole for DGSW heat production and seasonal thermal energy storage. Further investigation of the economic viability of deep geothermal exploration, and alternative technological solutions is therefore required.

However, if sufficient matrix permeability or fracture networks are present at depth in the Upper Devonian sandstone sequence, and temperatures of c. 60-80 °C can be harnessed, then the potential contribution that geothermal energy could make to meeting local heat demand, reducing greenhouse gas emissions, and addressing the ‘energy trilemma’ in Glasgow is significant.